Study on Parametric Optimization of Fused Deposition Modelling (FDM) Process

A THESIS SUBMITTED IN FULFILLMENT OF

THE REQUIREMENT FOR THE AWARD OF THE DEGREE

OF

DOCTOR OF PHILOSOPHY

IN

MECHANICAL ENGINEERING

BY

ANOOP KUMAR SOOD

(ROLL NO. 507ME012)

NATIONAL INSTITUTE OF TECHNOLOGY
ROURKELA - 769008, INDIA

May – 2011

CERTIFICATE

This to certify that the thesis entitled "**Study on Parametric Optimization of Fused Deposition Modelling (FDM) Process**" being submitted by **Anoop Kumar Sood** for the award of the degree of Doctor of Philosophy (Mechanical Engineering) of NIT Rourkela, is a record of bonafide research work carried out by him under our supervision and guidance. Mr. Anoop Kumar Sood has worked for more than two and half years on the above problem at the Department of Mechanical Engineering, National Institute of Technology, Rourkela and this has reached the standard fulfilling the requirements and the regulation relating to the degree. The contents of this thesis, in full or part, have not been submitted to any other university or institution for the award of any degree or diploma.

Dr. Siba Shankar Mahapatra
Professor
Department of Mechanical Engineering
NIT, Rourkela

Dr. RajKumar Ohdar
Associate Professor
Department of Forge Technology
NIFFT, Ranchi

Place: Rourkela

Date:

ACKNOWLEDGEMENT

This thesis is a result of research that has been carried out at **National Institute of Technology, Rourkela**. During this period, I came across with a great number of people whose contributions in various ways helped my field of research and they deserve special thanks. It is a pleasure to convey my gratitude to all of them.

In the first place, I would like to express my deep sense of gratitude and indebtedness to my supervisors **Prof. S.S. Mahapatra** and **Dr. R. K. Ohdar** for their advice, and guidance from early stage of this research and providing me extraordinary experiences throughout the work. Above all, they provided me unflinching encouragement and support in various ways which exceptionally inspire and enrich my growth as a student, a researcher and a scientist.

I specially acknowledge **Prof. S.S. Mahapatra** for his advice, supervision, and crucial contribution, as and when required during this research. His involvement with originality has triggered and nourished my intellectual maturity that will help me for a long time to come. I am proud to record that I had opportunity to work with an exceptionally experienced scientist like him.

I am grateful to **Prof. P.C. Panda**, Director, **Prof. S.K. Sarangi**, ex-Director, **Prof. R.K. Sahoo**, Head of Mechanical Engineering Department, and **Prof. B.K. Nanda,** former Head of Mechanical Engineering Department, National Institute of Technology, Rourkela, for their kind support and concern regarding my academic requirements.

I express my thankfulness to the faculty and staff members of the Mechanical Engineering Department for their continuous encouragement and suggestions. Among them, **Sri P. K. Pal** deserves special thanks for his kind cooperation in non-academic matters during the research work.

I am indebted to **Dr. Saurav Dutta** and **Mr. Gouri Shankar Beriha** for their support and co-operation which is difficult to express in words. The time spent with them will remain in my memory for years to come.

Thanks are also due to my colleagues at **National Institute of Foundry and Forge Technology, Ranchi**, for their whole hearted support and cooperation during the course of this work.

My parents deserve special mention for their inseparable support and prayers. They are the persons who show me the joy of intellectual pursuit ever since I was a child. I thank them for sincerely bringing up me with care and love.

The completion of this work came at the expense of my long days of absence from home. Words fail me to express my appreciation to my wife **Himani** and my little angel **Mannat** for their understanding, patience and active cooperation throughout the course of my doctoral dissertation. I thank them for being supportive and caring.

Last, but not the least, I thank the one above all of us, the omnipresent **God**, for giving me the strength during the course of this research work.

Anoop Kumar Sood

ABSTRACT

Rapid prototyping (RP) is a generic term for a number of technologies that enable fabrication of physical objects directly from CAD data sources. In contrast to classical methods of manufacturing such as milling and forging which are based on subtractive and formative principles respectively, these processes are based on additive principle for part fabrication. The biggest advantage of RP processes is that an entire 3-D (three-dimensional) consolidated assembly can be fabricated in a single setup without any tooling or human intervention; further, the part fabrication methodology is independent of the complexity of the part geometry. Due to several advantages, RP has attracted the considerable attention of manufacturing industries to meet the customer demands for incorporating continuous and rapid changes in manufacturing in shortest possible time and gain edge over competitors. Out of all commercially available RP processes, fused deposition modelling (FDM) uses heated thermoplastic filament which are extruded from the tip of nozzle in a prescribed manner in a temperature controlled environment for building the part through a layer by layer deposition method. Simplicity of operation together with the ability to fabricate parts with locally controlled properties resulted in its wide spread application not only for prototyping but also for making functional parts. However, FDM process has its own demerits related with accuracy, surface finish, strength etc. Hence, it is absolutely necessary to understand the shortcomings of the process and identify the controllable factors for improvement of part quality. In this direction, present study focuses on the improvement of part build methodology by properly controlling the process parameters. The thesis deals with various part quality measures such as improvement in dimensional accuracy, minimization of surface roughness, and improvement in mechanical properties measured in terms of tensile, compressive, flexural, impact strength and sliding wear. The understanding generated in this work not only explain the complex build mechanism but also present in detail the influence of processing parameters such as layer thickness, orientation, raster angle, raster width and air gap on studied responses with the help of statistically

validated models, microphotographs and non-traditional optimization methods.

For improving dimensional accuracy of the part, Taguchi's experimental design is adopted and it is found that measured dimension is oversized along the thickness direction and undersized along the length, width and diameter of the hole. It is observed that different factors and interactions control the part dimensions along different directions. Shrinkage of semi molten material extruding out from deposition nozzle is the major cause of part dimension reduction. The oversized dimension is attributed to uneven layer surfaces generation and slicing constraints. For recommending optimal factor setting for improving overall dimension of the part, grey Taguchi method is used. Prediction models based on artificial neural network and fuzzy inference principle are also proposed and compared with Taguchi predictive model. The model based on fuzzy inference system shows better prediction capability in comparison to artificial neural network model.

In order to minimize the surface roughness, a process improvement strategy through effective control of process parameters based on central composite design (CCD) is employed. Empirical models relating response and process parameters are developed. The validity of the models is established using analysis of variance (ANOVA) and residual analysis. Experimental results indicate that process parameters and their interactions are different for minimization of roughness in different surfaces. The surface roughness responses along three surfaces are combined into a single response known as multi-response performance index (*MPI*) using principal component analysis. Bacterial foraging optimisation algorithm (BFOA), a latest evolutionary approach, has been adopted to find out best process parameter setting which maximizes *MPI*.

Assessment of process parameters on mechanical properties viz. tensile, flexural, impact and compressive strength of part fabricated using FDM technology is done using CCD. The effect of each process parameter on mechanical property is analyzed. The major reason for weak strength is attributed to distortion within or between the layers. In actual practice, the parts are subjected to various types of loadings and it is necessary that the fabricated part must withhold more than one type of loading simultaneously.

To address this issue, all the studied strengths are combined into a single response known as composite desirability and then optimum parameter setting which will maximize composite desirability is determined using quantum behaved particle swarm optimization (QPSO).

Resistance to wear is an important consideration for enhancing service life of functional parts. Hence, present work also focuses on extensive study to understand the effect of process parameters on the sliding wear of test specimen. The study not only provides insight into complex dependency of wear on process parameters but also develop a statistically validated predictive equation. The equation can be used by the process planner for accurate wear prediction in practice. Finally, comparative evaluation of two swarm based optimization methods such as QPSO and BFOA are also presented. It is shown that BFOA, because of its biologically motivated structure, has better exploration and exploitation ability but require more time for convergence as compared to QPSO.

The methodology adopted in this study is quite general and can be used for other related or allied processes, especially in multi input, multi output systems. The proposed study can be used by industries like aerospace, automobile and medical for identifying the process capability and further improvement in FDM process or developing new processes based on similar principle.

Keywords: Rapid prototyping; Polymers; Extrusion; Quality control testing; Dimensional accuracy; Surface roughness; Mechanical strength; Wear; Design of experiment; Grey Taguchi; Principal component; Composite desirability; Artificial neural network; Fuzzy logic; QPSO; BFOA; Multi objective optimization.

CONTENTS

LIST OF TABLES

LIST OF FIGURES

GLOSSARY OF TERMS

2 ½	Two and a half dimension
3D	Three dimensional
3-DP	3D printing
ABS	Acrylonitrile butadiene styrene
AD	Anderson-Darling
AF	Automated fabrication
AHP	Analytic hierarchy process
AM	Additive manufacturing
ANN	Artificial neural network
ANSI	American national standards institute
ASCII	American standard code for information interchange
ASTM	American society of testing and materials
BFOA	Bacteria foraging optimisation algorithm
B-rep	Boundary representation
CAD	Computer Aided Design
CAGR	Compound annual growth rate
CAM	Computer aided manufacturing
CCD	Central composite design
CLI	Common layer interface
CNC	Computer numerical control
CSG	Constructive solid geometry
CT	Computed tomography
DFM	Design for manufacture
DLF	Directed light fabrication
DMD	Direct metal deposition
DMLS	Direct metal laser sintering
DOE	Design of experiment
DXF	Drawing exchange format
E. coli	Escherichia coli
EDM	Electrical discharge machining
EN	Electroless nickel
EOV	End of vector
FCCCD	Face centred central composite design
FDM	Fused deposition modelling
FDMet	Fused deposition of metals
FE	Finite element
FFF	Freeform fabrication
FIS	Fuzzy inference system
FSE	Fuzzy synthetic evaluation
GA	Genetic algorithm
GRA	Grey relational analysis
GRG	Grey relational grade
HPGL	Hewlett-Packard Graphics Language
IC	Investment casting

IGES	Initial Graphics Exchange Specification
ISO	International organization for standardization
LEAF	Layer exchange ASCII format
LENS	Laser engineered net shaping
LM	Layered manufacturing
LOM	Laminated object manufacturing
LV	Low vacuum
MADM	Multi attribute decision making
MJM	Multi jet modelling
MPI	Multi-response performance index
MSD	Mean square deviation
NCDS	Nano composite deposition
NRMS	Normalized root mean square
NURBS	Non-uniform rational B-spline
OA	Orthogonal array
PC	Polycarbonate
PSO	Particle swarm optimization
PTFE	Poly-tetra-fluoro-ethylene
QPSO	Quantum behaved particle swarm optimization
RBP	Resilient back propagation algorithm
RE	Reverse engineering
RM	Rapid manufacturing
RP	Rapid Prototyping
RPI	Rapid prototyping interface
RSM	Response surface methodology
RT	Rapid tooling
SEM	Scanning electron microscope
S/N	Signal to noise
SGC	Solid ground curing
SL	Stereolithography
SLC	Stereolithography contour
SLM	Selective laser melting
SLS	Selective laser sintering
STEP	Shape transfer exchange protocol
STL	Stereolithography file
TOPSIS	Technique of order preference by a similarity to ideal solution
UC	Ultrasonic consolidation
UV	Ultra violet

CHAPTER 1

BACKGROUND AND MOTIVATION

1.1 Introduction

Many exogenous factors lead to modify the way the products are being designed and exploited for sustenance of firms in a competitive environment. Among them the introduction of new materials, technologies for reducing design and manufacturing lead time, services and the attention paid to the end user requirements are critical to gain edge over competitors [1]. The emphasis on reduction of product development time has a profound influence on manufacturing processes and resulted in the birth of a new generation of production equipment which manufacture part directly from the its CAD (computer aided design) model on a layer by layer deposition principle without tools, dies, fixtures and human intervention. The method of such additive part generation processes is known as "**Rapid Prototyping**". The rapid prototyping (RP) technology enables quick and easy transition from concept generation in the form of computer images to the fabrication of physical models. Although RP is a cheap, flexible and fast way to create test parts prior to production, material availability has traditionally limited the technology for its widespread application. But now, with ongoing advances in material sciences and RP process itself, the opportunity has been opened for more applications. So no longer the technology is just used for prototyping but also for end products [2].

RP may trace back to the mid 1980s with the advent of stereolithography (SL). Over the ensuing years, a plethora of RP processes appeared including but not limited to selective laser sintering (SLS), laminated object manufacturing (LOM), fused deposition modelling (FDM) and 3D printing (3-DP). According to the report published by Wohelers associates in 2010, demand for products and services from RP technology has been felt strong over its 22-year history. The compound annual growth rate (CAGR) of revenues produced by all products and services over this period is 26.4%. Annual unit sales of RP systems worldwide grew by an estimated 13.9% [3]. The industry has applied these processes and their variations in novel ways to address a wide variety of problems in a diverse number of technical areas [4, 5, 6]. Further, with the advancement of the internet technologies, it has now been widely accepted that the future of manufacturing organizations will be information oriented, knowledge driven and much of their daily operations will be automated around the global information network that connects everyone together [7]. RP technique using the internet can further enhance the design and manufacturing productivity, speed, and economy. In addition, various RP machines are currently too expensive to be offered by a large number of small and medium size enterprises.

Web based RP systems, however, will let these types of companies make parts remotely without owning the expensive RP machines [8].

1.2 Rapid Prototyping

Methods and techniques of making three dimensional (3D) solid of predetermined shapes are well known. The desired part is initially drawn, either manually or automatically (utilizing CAD procedure), then the article being ultimately shaped by removing or forming material from a block of work piece to form the desired shape in a machine operation. Non-traditional machining techniques available to form the objects have their own limitations and are incapable of making complete shapes. Thermal molding by injection or other molding techniques requires expensive molds and is better adapted economically for large runs were reproducibility is required [9, 10].These operations may also be automated with the utilization of a CAM (computer aided manufacturing) processes. These costly and time consuming processes are repeated multiple times to perfect the final manufacturing of part, model or prototype. The designer's success is often dependent upon the interpretation or the skill of the machinist making the prototype or part.

Thus, the need exists for relatively simple and effective process and apparatus by means of which designers may design and create three dimensional objects at office workstation with the same ease and simplicity of using desktop computer and printer in a timely and cost effective manner. Advent of desktop computers and resulting developments in the field of CAD, CAM and computer numerical control (CNC) with growth and availability of industrial lasers together with materials result in emergence of new paradigm commonly known as RP to persuade the over stated need.

RP is a generic term for a number of technologies that enable fabrication of physical objects directly from CAD data sources. In all commercial RP processes, the part is fabricated by deposition of layers contoured in a plane (x-y) two dimensionally. The third dimension (z) results from single layers being stacked up on top of each other but not as a continuous z-coordinate [11,12]. RP methods are generally similar to each other in that they add and bond materials in layer-wise fashion to form the objects. This is directly opposite of what classical methods such as milling and forging do. In the former, objects are created by mechanically removing material whereas in later mechanical forces are applied to material to permanently deform into desired shape. RP is also known by the names of freeform fabrication (FFF), layered manufacturing (LM), additive manufacturing (AM), automated fabrication, and other

variants. Sometimes the names of the specific RP process are also used synonymously to denote the field as a whole [13].

The main process stages involved in fabricating parts are common to most RP systems but the mechanisms by which the individual layers are created depends on the specific system. The common process stages are shown in Figure 1.1 [13].

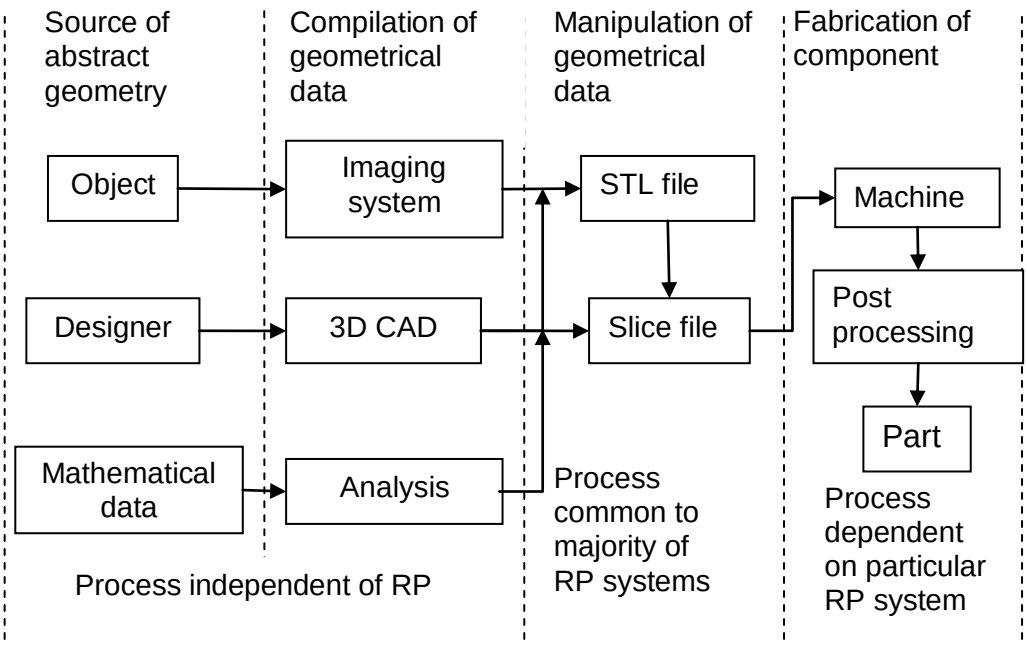

Figure 1.1 Main process stages common to most RP systems

The starting point for any RP process is the source of the abstract geometry of the object to be built. From this, a data set describing the geometry must then be compiled. The data must be manipulated to generate the instructions required to control the process in the final stage of actually fabricating the component. Input at the start of RP process can be a point cloud obtained from scanning methods (reverse engineering) or 3D CAD models generated from various solid modelers or mathematical data obtained by using analytical equations. The whole procedure of generating part by any RP method can be divided into two steps.

STEP 1: In this step, STL (Stereolithography) file is generated by tessellating 3D model, tessellated model is sliced and the generated data is stored in standard formats that could be interpreted by RP machines. This information is used in step 2. At this stage, choice of part orientation and slice thickness are the most important parameters as part building time,

surface quality, amount of support structures, cost etc. are influenced by them.

STEP 2: In this step, generation of physical model takes place. This step is different for different RP processes and depends on the basic deposition principle used in the RP machine The software that operates RP system generates laser-scanning paths (in processes like Stereolithography, Selective laser sintering etc.) or material deposition paths (in processes like Fused deposition modeling) from the slice information obtained in step 1. At this stage, various process related information like tolerance (surface finish), material, machine (like laser spot diameter, cutting speed, temperature etc.) are provided [13, 14].

There are several well known RP technologies available in the market and few of them are Stereolithography (SL), Selective laser sintering (SLS), Laminated object manufacturing (LOM), fused deposition modelling (FDM), 3D printing (3DP), Multi jet modelling (MJM), and Solid ground curing (SGC) [15]. An overview of various processes is provided below.

1.2.1 Stereolithography (SL)

It is the first commercial RP machine introduced in mid 1980s by 3D systems, California, USA. It fabricates part from a photo curable liquid resin that solidifies when sufficiently exposed to a laser beam that scans across the surface of resin. The solidified layer is then lowered into a vat so that another layer of liquid can be exposed to the laser. This process is repeated until all cross sections are built into a solid model of the original CAD model. When all the slices have been traced by the laser, the platform is removed from the vat and excess liquid polymer is cleaned off the completed part. The completed part is then finally cured in an ultraviolet oven.

1.2.2 Selective Laser Sintering (SLS)

It was developed and patented by the University of Texas at Austin and was initially commercialized by DTM corporation which was later on owned by 3D systems, USA. In this process, a thin layer of thermoplastic powder is spread by a roller over the surface of a build cylinder and heated to just below its melting point by infrared heating panels at the side of the cylinder. Then a laser beam traces out the cross-section of one slice of the part. Where the laser beam hits the powder, the affected particles fuse together (or sintered). The first fused slice descends one object layer, the roller spreads out another layer of powder, and the process continues until the part is built. The un-sintered material in each layer can act as a

support structure for the part itself. When the part is complete, the un-sintered material can simply be brushed off.

1.2.3 Laminated Object Manufacturing (LOM)

Helisys, California, USA, introduced the LOM technique which creates parts using a unique additive/subtractive process. A layer of material with an adhesive coating on one side is placed on a platform with adhesive side down. A heated roller passes over the material and sticks the material to the platform. A laser beam then traces the outline of one slice of the part and cutting through the layer of the material. The laser beam then crosshatches the material that does not form part of the cross-section again cutting through the layer. The platform is then lowered one layer thickness, another layer of material is stuck onto the previous layer and the procedure is repeated with the next cross section slice of the part. When all cross-section slices have been added, the solid block of material is removed from the platform. The crosshatched areas of the block are then broken away from the final part.

1.2.4 Fused Deposition Modelling (FDM)

FDM was introduced by Stratasys, Minnesota, USA. A filament of material is extruded out of a fine nozzle in a semi liquid state and deposited onto a platform. The nozzle moves in the X-Y plane so that the filament is laid down to form a thin cross-sectional slice of the part. As each layer is extruded, it bonds to the previous layer and solidify. The platform is then lowered relative to the nozzle and the next slice of the part is deposited on top of the previous slice. A second nozzle is used to extrude a different material in order to build-up support structures for the part where needed. Once the part is completed, the support structures are broken away from the part.

1.2.5 Three Dimensional Printing (3-DP)

3-DP process has invented and patented by the Massachusetts Institute of Technology (MIT), USA. The 3DP process uses ink jet technology to build parts in layers. Each layer begins with a thin distribution of powdered material over the surface of powder bed. Using the inkjet printing technology, a binder material selectively joins the particles where the object is formed. The bed is then lowered by a fixed distance. Powder is then deposited and spread evenly across the bed with a roller mechanism, and a second layer is built. This is repeated until the entire model is fabricated. The completed object is embedded inside unprocessed powders and is extracted by brushing away the loose powders.

1.2.6 Multi Jet Modelling (MJM)

A print head containing 96 tiny nozzles (or jets) in a linear array passes into the X-Y plane over a platform. A jet dispenses a droplet of a thermo-plastic polymer where material is to be deposited. Any number of the 96 jets can be activated simultaneously giving a rapid dispense rate when all jets are active. The hot droplets of material bond to the previous slice of the part that has just been printed. Thin support pillars must also be built-up slice by slice in the same material where they are needed. When the current slice of the part (plus slice of support pillars) is completed, the platform is lowered relative to the print head and the next slice is printed. When all the slices have been completed, the part is removed from the machine and the support structure is broken off.

1.2.7 Solid Ground Curing (SGC)

This system utilizes photo polymer resins and ultra-violet (UV) light. Data from the CAD model is used to produce a mask which is placed above the resin surface. When the layer has been cured, the excess resin is wiped away and spaces are filled with wax. The wax is cooled and the wax chips removed. A new layer of resin is applied and the process is repeated. The advantages of SGC are that the entire layer is solidified at once reducing the part creation time, especially for multi-part builds. Also, no post-curing is required. The disadvantages of this system are that it is noisy, large and needs to be constantly manned. It wastes a large amount of wax which cannot be recycled.

1.3 Need for the research

Design freedom, elimination of tooling and the subsequent removal of many design for manufacture (DFM) related constraints helps the designers to adjust their design intent to facilitate the component or assembly to be manufactured using the capability of RP. Manufacturing of different components simultaneously and sequentially, especially for low volume production, is possible. It is a fast and flexible manufacturing with reconfigurable capability. Consequently, its gains has benefited diverse fields like medical, aerospace, automobile, construction, tooling and die making [16]. In spite of these advantages, a number of key barriers still exist across many RP processes. For example, a new foundation for CAD systems is needed that overcomes the limitations of solid modelling in representing very complex geometries and multiple materials [17]. Most machines are designed in such a way that they have inherent trade-offs among part size, accuracy, strength, surface smoothness and speed [18]. There are significant variations in geometry and property among

identical parts built on different machines. There is a need for industrial standards for data transfer between dissimilar CAD-RP systems, testing and characterization of part properties [19, 20, 21]. Availability of processable materials is also limited [22]. Since most of the RP processes are patented, many of the best improvements to a particular process or machine is available to one manufacturer.

These limitations offer new opportunities for RP development and growth as follows:

- Goal based design tools are needed to integrate general design for RP rules with process specific capabilities to rapidly produce CAD geometry that meet specific design requirements. These tools should enable designers to better utilize preassembled and complex-geometry benefits of RP.
- There is a need to develop screening methodologies for RP processable materials or development of new materials or altering existing materials as per the process requirement.
- A much better understanding is needed for the basic physics and chemistry of RP processes to capture the complexity of the process and effect of various parameters in an interacting environment on responses.
- Technical and operation related advances are needed to ensure that RP processes are as reliable and predictable as conventional manufacturing processes.
- Control algorithms based on predictive models of system response to process changes are needed to maximize the performance of RP machines.
- Developments of formalized standards for the RP industry will help to achieve continued growth and further advancements of RP technologies.

1.4 Research objective

Though technological barriers exist, as in most technology areas, it is important to overcome them by developing proper understanding of process with related attributes. In this direction, next chapter (Chapter 2) explains the various efforts directed for improving the industrial feasibility of RP process. Exhaustive literature review reveals that FDM is least explored out of many RP processes. In this direction, present work emphasise on the FDM process functionality to understand the multiple interacting phenomena involved with this process and make it reliable and predictable as other RP or conventional manufacturing processes.

Based on these guiding principles, the objective of present research are as follows:

- Study on effect of fabrication parameters on part quality. Part quality is measured in terms of dimensional accuracy improvement, mechanical strength, wear and surface roughness.
- Analysis of experimental results using statistical methods.
- Determination of relationship between process parameters and properties studied.
- Optimum parameters selection for overall improvement in part quality.

Methodology adopted for achieving these objectives are quite general and can provide common methods for measuring the benefits and limitations of various RP processes.

1.5 Thesis outline

The remainder of this thesis is organized as follows:

- Chapter 2: Literature review

Includes a literature review to provide a summary of the base of knowledge already available involving the issues of interest.

- Chapter 3: Materials and methods

Include a description of the material, test procedures, and design of experiments methodology.

- Chapter 4: Improvement of dimensional accuracy

Study the effect of processing conditions on the dimensional accuracy of test specimen. Neural network and fuzzy predictions are compared and optimal parameter settings are obtained using grey Taguchi method.

- Chapter 5: Improvement of surface roughness

Optimum process conditions are determined for overall improvement of part surface roughness. Weighted principal component analysis is used to obtain uncorrelated responses from correlated data on surface roughness of a measured part. Latest evolutionary technique namely bacteria foraging optimisation algorithm (BFOA) has been adopted to determine the optimum parameter setting.

- Chapter 6: Improvement of mechanical strength

Effect of process parameters on part strength measured in terms of tensile, compressive, flexural and impact strength is studied in detail. In order to optimize process parameters for maximum strength, a quantum behaved particle swarm optimization (QPSO) is used.

- Chapter 7: A study on sliding wear

Comprehensive investigation on the effect of process parameters on sliding wear of FDM processed part is made. Finally, comparison between BFOA and QPSO is also presented.

- Chapter 8: Executive summary and conclusions

The conclusion and scope for future work are given in this part of thesis

1.6 Conclusions

Present chapter highlights the importance of RP as a new product development tool. The general attributes of RP can be put together as:

- A material additive process.
- Able to build complex 3D geometries including enclosed cavities.
- Process is automatic and based on a CAD model.
- Requires no part specific tools or fixtures.
- Require minimal or no human intervention to operate.

These characteristics open new opportunities for faster product development in a simplified and cost effective way. To overcome the limitations of RP processes in general and FDM in particular, research objective together with work outline is presented in this chapter.

In next chapter, the literature review is presented through exhaustive study.

CHAPTER 2

LITERATURE REVIEW

2.1 Introduction

One of the current challenges faced by manufacturing industries is the reduction of product development time through adoption of rapid prototyping (RP) technologies. In this direction, the current chapter highlights the development and problems associated with various aspects of RP with special relevance to FDM process. Having the concept of RP was introduced in mid 1980s, literature survey begins with papers published after 1990 with maximum attention paid to last ten years. The search was restricted on those articles for which full text was available. Table 2.1 provides the source and number of citations from each source. The majority of the citations were found in journals (89.2%). Two journals namely, "International Journal of Advance Manufacturing Technology" and "Journal of Materials Processing Technology" together account for 36.4% of total citations in journals.

Table 2.1 Summary of publications referred

Source	Citation
Acta Metallurgica	1
Advanced Engineering Materials	1
Advanced Materials Research	1
Archives of Orofacial Sciences	1
Biomaterials	1
CIRP Annals - Manufacturing Technology	6
Composites Part B	1
Computer Aided Design	8
Computer Aided Engineering	1
Computer Applications in Engineering Education	1
Computers & Industrial Engineering	1
Computers in Industry	7
European Journal of Operational Research	1
Image and Vision Computing	1
Industrial Engineering	1
International Journal of Advanced Manufacturing Technology	33
International Journal of Oral and Maxillofacial Surgery	1
International Journal of Precision Engineering and Manufacturing	1
International Journal of Production Economics	1
International Journal of Production Research	3
International Journal of Engineering Education	1
International Journal of Machine tools and Manufacture	6
Journal of the European Ceramic Society	4
Journal of Manufacturing Systems	1
Journal of Materials Processing Technology	27
Journal of Cranio-Maxillofacial Surgery	1
Journal of Industrial Technology	1
Journal of Intelligent Manufacturing	2

Journal of Manufacturing Processes	1
Journal of Manufacturing Science and Engineering	3
Journal of Manufacturing Technology Management	1
Journal of Material Science and Technology	1
Journal of Materials Science	1
Journal of the International Societies for Precision Engineering and Nanotechnology	1
Macromolecular Chemistry and Physics.	1
Materials and Design	6
Materials and Manufacturing Processes	1
Materials Science and Engineering C	2
Mathematica	1
Mechatronics	1
Medical Engineering & Physics	1
Precision Engineering	3
Proceedings of the Institution of Mechanical Engineers, Part B: Journal of Engineering Manufacture	5
Rapid Prototyping Journal	8
Robotics and Computer Integrated Manufacturing	6
Scripta Materialia	1
Tsinghua Science and Technology	3
Virtual and Physical Prototyping	2
Wear	1
Conference	13
Book	5
Web Site	2
Total	185

The literature is classified into an assortment of sections dealing with specific issues associated with RP as illustrated in Figure 2.1. Figure 2.2 provides the breakdown of the number of citations by research classification. Next sections provide brief discussion on these issues. Finally, chapter is concluded by summarizing the advancement taken place in RP technology and possible literature gap so that relevance of the present study can be emphasized.

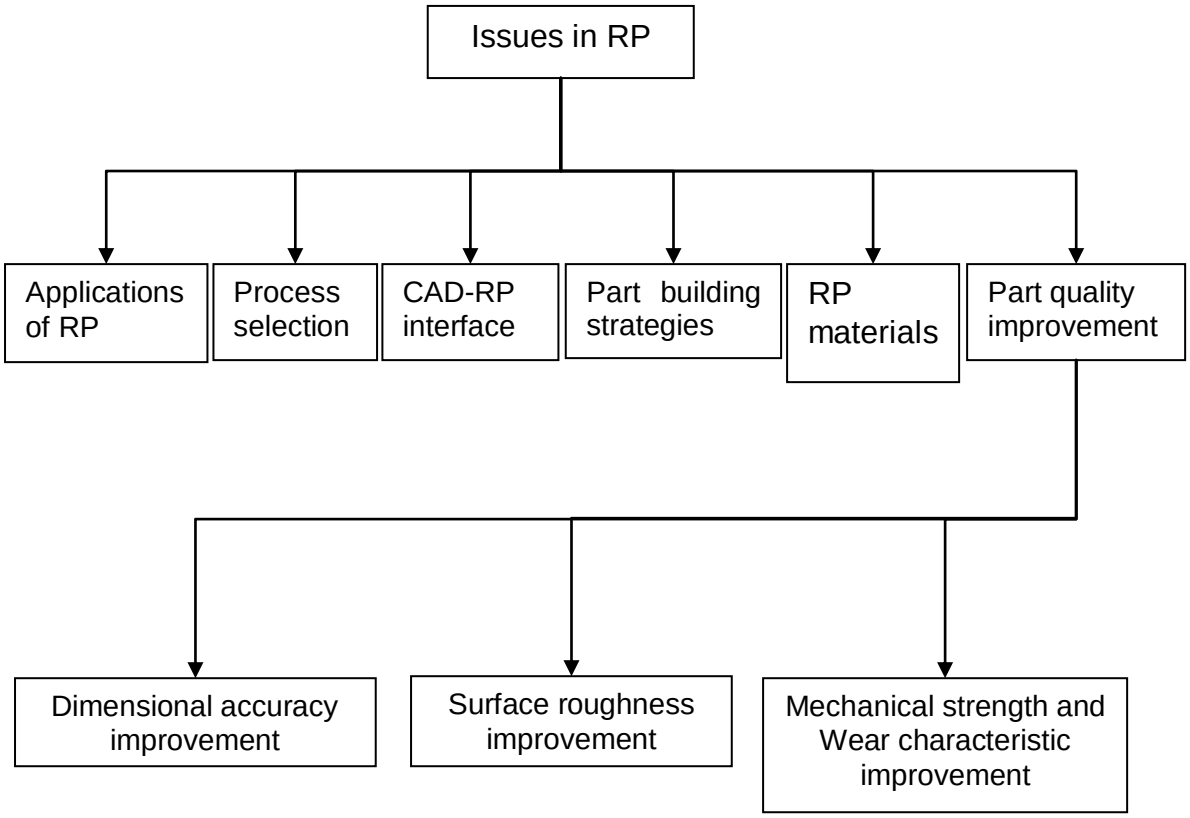

Figure 2.1 Research issues in RP

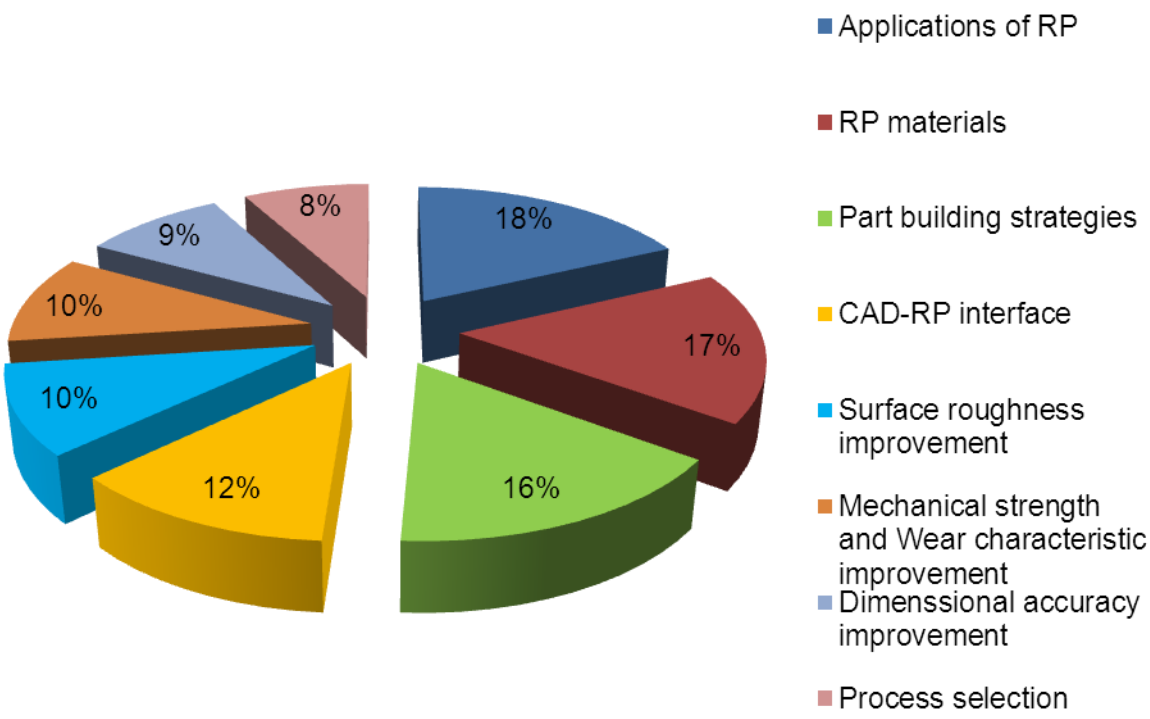

Figure 2.2 Percentage of paper surveyed

2.2 Applications of RP

Fast changing customer demand and increased competitiveness in marketplace forced the industries to rethink the way products are designed resulting in introduction of new technologies for part fabrication. Notable among them are rapid prototyping (RP) technologies which are able to conceive the complete product directly from its CAD (computer aided design) model without any tooling or human interference. The time and cost consideration favours prototype production using RP because more time is available for design iteration and optimization [23, 24, 25]. A case study provided by Wiedemann and Jantzen [26] for Daimler-Benz AG shows that complete engine mock-ups can be fabricated by RP technique at one fifth of the cost as compared to traditional methodologies. As an example of application in medical field, the possibility of viewing and physically handling the precise geometry before surgery enables the surgeon to obtain three dimensional anatomical information as well as a solid product on which the proposed surgery can be simulated [27, 28]. Many engineering assisted surgery related publications discuss the use of bio-models generated through RP for diagnostics operation planning [29] and preparation of implants [5, 30] in a virtual environment [31]. Some studies have been conducted integrating CAD, FE (Finite element) analysis and RP techniques for direct manufacturing of customized implant model [32]. These studies demonstrate that application of RP in surgery reduces the overall cost by reducing the theatre time and part preparation time. The inherent porosity of many products produced by RP is advantageous for construction of individual, patient-specific scaffolds [33].

Initially, RP systems have not been designed for the production of end use parts. However, design freedom and no tooling requirement with RP enables economically viable production [2, 4]. Manufacturing of end-use products using RP techniques directly from CAD model is now known as rapid manufacturing (RM) [34, 35]. RM is beneficial for the industry in terms of reducing the production equipment requirement and time period for fabrication. Multi layer printed circuit board (PCB) can be conveniently fabricated by RP technology like SGC (solid ground curring) [36].

Although direct manufacturing of metal parts with RP is not well developed, indirect methods have been found feasible through the combination of RP and metal casting. Such type of integration gives rise to new application of RP in generating tools which are capable of forming several thousand or even millions of parts before final wear out occurs is known as rapid tooling (RT). RT is considered as natural extension of RP and is typically used to describe a process which either uses a RP model as a pattern to create a mould quickly or uses the RP process directly to

fabricate a tool [37, 38, 39]. RT methods can be classified into direct and indirect tooling categories. Indirect RT requires some kind of master pattern which can be made by any RP process. Today, almost all commercialised RP processes, selective laser sintering (SLS), stereolithography (SL), fused deposition modelling (FDM), ink-jet plotting, 3D printing (3D-P), solid ground curing (SGC), multi-jet modelling (Actua) and laminated object manufacturing (LOM) have been employed to produce patterns with varying success [40-43]. Direct RT, as the name suggests, involves manufacturing a tool cavity directly by the use of RP system; hence, eliminates the intermediate step of generating a pattern [44, 45]. The outstanding manufacturing capabilities of FDM technology is exploited in investment casting (IC) process to produce ABS pattern for IC process [9, 46].

Electrical discharge machining (EDM) seems to be another interesting area in which rapid tooling finds a potential application. Some methods of making EDM electrodes based on RP technique have been developed such as abrading process, copper electroforming and spray metal deposition [47]. However, post processing of RP parts for EDM applications is necessary to meet the EDM specifications. For non conductive materials, metallization is required to change the conductivity [48]. Hsu et al. have proposed an effective method for manufacturing electrical discharge machining (EDM) electrodes using the Zcorp 402 3DP rapid prototyping system [49]. Test results indicate that no crack was found on the electrode and the performance of electrical discharge machining is quite promising. Zang et al. have proposed integration of RP and reverse engineering (RE) in die making for clutch house of diesel engine [50]. LOM is used for die making using RE data of clutch housing die.

The use of rapid prototyping (RP) technology for RT and RM has given rise to the development of application-oriented composites. The important processes employed for fabricating composites are Selective Laser Sintering/Melting (SLS/SLM), Laser Engineered Net Shaping (LENS), Laminated Object Manufacturing (LOM), Stereolithography (SL), Fused Deposition Modelling (FDM), Three Dimensional Printing (3DP) and Ultrasonic Consolidation (UC) [51, 52].

2.3 Process selection

Selection of an appropriate process requires addressing to various criteria such as cost, part quality, part properties, build envelope, build time (speed) and other concerns suiting to a particular situation. A number of studies have been carried out in this direction, predominantly concerning with development of decision support systems along with software tools for assisting RP users in selecting the most suitable RP process. Early attempts for selection of a conformable RP system

are based on benchmarking studies that compare different RP systems on the basis of working accuracy, strength and other information [53- 55].

Recently, Mahesh et al. have developed a database in which features of individual RP systems are stored [56]. The database structure facilitates the use of queries to decide on selection of a particular RP system. Comparison of RP systems through benchmarking trials have met with limited success because RP vendors hardly agree on a common benchmark part. Recent efforts in selection of RP system has been directed to the development of computer based selector programs. In this direction, analytic hierarchy process (AHP) has proved to be an effective tactical tool for selecting the RP technology that best fits the end user's needs [57, 58, 59]. Industrial Research Institute, Swinburne (IRIS) have proposed a rule based RP system selector that uses selection criteria such as the price of the machine, accuracy, surface finish, build envelope, type of material and building speed. The database also includes full specifications for each RP machine which is displayed when the program recommends the specific RP machine [60, 61]. The major limitation of the program is that it cannot take care of conditional statements. Byun and Lee [62] used a modified technique of order preference by a similarity to ideal solution (TOPSIS), a multi attribute decision making (MADM) approach, for ranking RP systems by means of ratings with respect to multiple attributes. The major attributes used for RP process selection include accuracy, surface roughness, strength, elongation, build time and cost of the part. The approach can handle both quantitative and qualitative data. However, assignment of relative importance to attributes is somewhat inconsistent. A method integrating the expert system and fuzzy synthetic evaluation (FSE) is proposed by Lan et al. [63] to select the most appropriate RP process according to users' specific requirements. The selection process is divided into two stages. In first stage, feasible alternatives are generated when executed under expert system environment. Subsequently, given those feasible alternatives, the FSE approach is employed to produce a ranking order of the alternatives. Chowdary employs back propagation artificial neural network for selection of a different types of SLA machines [64]. Laser configuration (type, wavelength and power), layer thickness, beam diameter, drawing speed, elevator configuration (resolution and repeatability), maximum part weight, capacity, maximum build envelope, operating system, size, weight and cost are chosen as SL machine selection parameters. Results demonstrate the suitability of method in selecting SL machines in a reasonable computation time. Rao and Padmanabhan presents a methodology for selection of a RP process using graph theory and matrix approach [65]. A rapid prototyping process selection index is proposed to rank the

RP processes for producing a given product or part. Subburaj et al. [66] presented a computer aided rapid tooling (RT) process selection and manufacturability evaluation methodology that not only helps in RT process selection but also facilitates identifying difficult-to-manufacture features of a part.

2.4 CAD-RP interface

RP process starts with the creation of solid or surface model of a part to be fabricated using any suitable CAD software. As current RP machines are not able to read the model data in its native CAD software format; so it has to be converted into other format which is accepted by RP machine. 3D Systems Inc., first set the de facto file-format standard for the RP industry in 1988 known as STL (Stereolithography) format. The STL format is a polyhedral representation of the part with triangular facets. It is generated from a precise CAD model using a process known as tessellation which generates triangles to approximate the CAD model. The STL file can either be in ASCII (American standard code for information interchange) or binary format. Important requirements of triangular facets in STL are that each triangular facet must share one and only one edge with each of its adjacent triangles and a vertex of one triangle cannot lie on the edge of another triangle. Vertices must be listed in counter clockwise order when looking at the object from outside and normal of triangle must point outward [17, 67]. Many CAD systems would generate incorrect STL files that disobey the above mentioned requirements specifically when the CAD models are very complex. As a result, errors like non-manifold facets, cracks, incorrect normal, overlapping facets etc. arises [13]. Most of current STL file repairing programs can repair only simple defects automatically such as incorrect normal, overlapping facets, and simple cracks that have all edges in a plane. Complex cracks which contain many edges that are not in a single plane and non-manifold facets are difficult to repair [68]. Other than these problems, STL format has inherent drawback like redundancy of information i.e. each vertex of a triangular facet is recorded at least four times. This brings extra computational memory occupation and time consumption. In STL format, 3D surfaces are represented by planer triangles. The number of triangles increases with increase in approximation accuracy for the shape of 3D CAD model, resulting in increase in STL file size. Also, STL format records only the geometry of object surface and lacks topological information and object attributes such as colours [69, 70].

Fortunately, in the last few years, many research efforts have been dedicated to determine better interface between CAD and RP technology. Two approaches were proposed. One approach is to use other existing data formats such as IGES

(Initial Graphics Exchange Specification), HPGL (Hewlett-Packard Graphics Language), and STEP (Shape Transfer Exchange Protocol) [71, 72]; the other is to develop a special new format [73-76]. Table 2.1 present the review of some of the CAD-RP data exchange format.

Table 2.2 RP-CAD interfaces

Interface	Brief description	Advantages	Disadvantages
IGES Initial Graphics Exchange Specification	Set up as an American National Standard in 1981. Precisely represents CSG and B-rep (boundary representation) solids. Many RP systems like DTM sinterstation 2000 and Stratsys 3D modeler series accept this format.	Implemented by almost every commercial CAD/CAM system. Provide the entities of points, lines, arcs, curves, curved surfaces and solid primitives to precisely represent CAD models.	Includes much redundant information. Does not support facet representation. The algorithms dealing with an IGES file are more complex than those dealing with the STL format. Supports must be created in CAD and converted to IGES.
HPGL Hewlett-Packard Graphics Language	Standard format for graphics plotter. Data types are all two dimensional.	Many commercial CAD systems have an interface to output this format. It can be directly passed to RP systems without being sliced.	Many small files are needed to represent a solid object. The support must be created in CAD before being converted to the HP/GL file.
STEP Shape Transfer Exchange Protocol	It is an international standard format (documented as ISO 10303) to exchange product data.	Supported by all CAD systems. Efficient in file size and Independent of hardware and software.	Carries much redundant information which is not necessary for RP systems.
CLI Common layer interface	Developed in Brite Euram project.	Geometry of a part is described by 2½-D layers, Each layer is defined by its thickness, and a set of contours and hatches, It is easily sliced, Error in the layer information is much easier to correct.	Straight lines used for contour construction reduce the accuracy of curve.
RPI Rapid prototyping interface	Design by Renselaer design research center.	It can be derived from the currently accepted STL format data, Gives the topological information of each facet instead of only	Slicing algorithm is complex, Surface patches suitable for solid approximation cannot be

		specifying the vertex coordinates for it.	identified.
LEAF Layer exchange ASCII format	Generated by Helsinki University of Technology.	It is human-readable unambiguous representation, Independent of CAD and RP process, Slices of CSG models can be represented almost directly in LEAF and the parts representing the support structures can be easily separated from the original part.	Structure is complicated and special interpreter is needed to transfer data to the RP systems.
SLC Stereolithog-raphy contour	It is '21/2-D' contour representation of a CAD model. Consist of successive cross sections taken at ascending Z intervals. Solid material is represented by interior and exterior boundary polylines.	It is a simple representation of the solid object, Directly accepted by 3D RP systems and need not necessarily be sliced in some cases.	Represent solid objects only approximately.

To overcome the limitations of STL formats, some researchers even suggested the direct integration of CAD models with RP machines to generate geometric data for rapid prototyping. These methods generate slicing data directly from the original CAD model without using the STL format. Guduri et al. [77] have proposed a direct slicing method that provides accurate laser beam paths by slicing the constructive solid geometry (CSG) representation of a part. Vuyyuru et al. [78] have directly sliced a solid model built by I-DEAS and segmented NURBS (non-uniform rational B-spline) based contour curves. Direct slicing of CAD models was implemented using parasolid CAD software along with user defined routines in C by Jamieson and Hacker [79] and parts were modelled using boundary representation. Chen et al. [80] proposed a direct slicing approach based on Power SHAPE models. Power SHAPE (Delcam International, Birmingham, UK) is a package for building models and it provides macro language and picture files for its secondary development work. In this approach, sliced layers are stored as picture file that uses lines, arcs and Bezier curves to describe the section contours. To meet the requirement of faster and precise slicing in RP, a direct slicing approach from AutoCAD solid models is proposed by Cao and Miyamoto [81]. The sliced layers are saved in ASCII-DXF (American standard code for information interchange - Drawing exchange format) files. In DXF files, the sliced planar data will be saved as lines, arcs

and circles. Unlike STL files, in addition to geometric information, material types are also included in DXF files. The material information can be used to calculate the centroid of the part to be fabricated and build a support when required. It is also possible to fabricate a part with different materials. Ma et al. [82] have adaptively sliced non-uniform rational B-spline (NURBS) surfaces to generate RP slice data. Further, a selective hatching strategy is employed to reduce the build time by solidifying the kernel regions of a part with the maximum allowable thick layers while solidifying the skin areas with adaptive thin layers to obtain the required surface accuracy. Xu et al. [83] have employed slicing function of Solid Works software to slice CAD models directly and stores the section image of 3D models as image format. Dynamic graphic masks for the SL system are created according to the cross-section images, and then 3D real prototypes are fabricated conveniently.

There are many practical situations where actual CAD model of part is not available or difficult to construct. In these situations, the physical model or sample must be reverse engineered to create or refine the CAD model. In reverse engineering, real parts are transformed into engineering models and concepts. For this purpose, contact type or non-contact type data acquiring devices can be used which capture the model geometrical information in terms of set of coordinate points called point cloud [84-86]. Generating physical part from RP process using point cloud data involves three approaches. In the first approach, surface model is generated from point cloud model and then tessellated model for RP layers is generated from surface model [87]. Error in this approach may arises while generating surface model from point cloud data, then converting surface model into STL and finally generating sliced model from STL model. As these errors are accumulated in each stage, it makes it difficult to control the error of the RP model. In the second approach, the STL file of a model is created directly from point clouds [88]. This link bypasses the creation of surface models, which involves tedious manual operations but the control of error in final RP model is still not straightforward as it involves generation of STL model from point cloud model and then generation of RP model from STL model. The third method considers the generation of RP layer model directly from point cloud without generating STL model and thus, it eliminates all intermediate errors mentioned in first and second approach [89].

2.5 Part building strategies

Another major issue for RP process improvement is concerned with the layer by layer generation of part itself. It is possible to construct accurately a part like a cube by properly stacking the layers. However, the same is not true with solid models

featuring curved or inclined surfaces. These surfaces when sliced will suffer an inevitable loss of information because RP machines deposit each layer in 2 1/2 (two and a half dimension) dimensional form resulting in stair like appearance to the layers (Figure 2.3). It is referred as the staircase effect that deteriorates the surface quality of manufactured part. However, near-vertical surfaces are less affected by stair step error than the near-horizontal surface. Therefore, it is desirable to orient a surface either along the direction of part build or perpendicular to it for maximization of surface accuracy [90]. Decreasing the layer thickness to a value allowed by the process can also reduce staircase error. But doing so, number of layers increases resulting in augmentation of build time and fabrication cost. Therefore, selection of proper orientation not only maximizes the surface accuracy but also minimizes the build time, support material requirement (if process requires support for overhanging or thin features), post processing operations and hence total fabrication cost [91, 92].

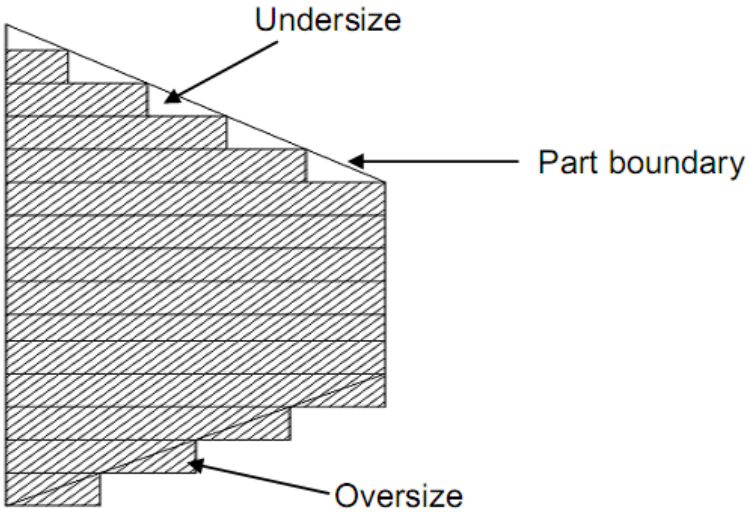

Figure 2.3 Slicing error

To determine the best orientation for improvement of surface accuracy, various measures are considered. In this direction, Hur and Lee [93] determined the slicing accuracy based on the user defined cusp height. Cusp height is the maximum deviation from layered part to the CAD surface measured in the direction normal to CAD surface. Part is sliced in different orientation and the orientation in which total numbers of layers are minimum is selected as optimum orientation. Taking single value of cusp height for entire part is suitable for simple part geometry. The complex shape part may not have uniform cusp height requirement everywhere. Some faces of the part are required to be smooth while other faces are relatively unimportant. To overcome this limitation, slicing using non-uniform cusp height is proposed [94, 95]. In this approach, user specifies different allowable cusp heights for different surfaces according to their importance; a small allowable cusp height for important faces that

are required to be smooth and a larger one for the other relatively unimportant faces. When multiple parts are manufactured at same setting, different features may coexist at the same height with different geometries such that each requires distinct layer thickness to meet the tolerance conditions. For such type of cases, three step local adaptive slicing procedure is proposed by Tyberg and Bohn [97]. In first step, tessellated CAD model is sliced into uniformly thick slabs using the maximum thickness available in a RP system. Then, the contours on the top and the bottom of each slab at a given height are grouped into sub-slabs that reflect that these contours would be physically connected by a surface even if only the sub-slabs at that particular height are fabricated. Finally, each sub-slab is sliced independently into some integral number of uniform thickness slices to satisfy the surface deviation tolerance measured in terms of cusp height of that particular sub-slab.

When the surface normal is nearly in the plane of the layer, the cusp height is a good representation of both volumetric difference (difference between CAD model and the slice volume) and surface smoothness. But if the normal of the CAD model is nearly perpendicular to the plane of the layer, the cusp height is not a good representative of the volumetric difference. To minimize the volumetric difference, Masood et al. [98], Masood and Rattanawong [99], Rattanawong [100], Yang et al. [101] presented the generic part orientation system for rapid prototyping of solid parts of any complexity, considering the volumetric error encountered in parts during the layer by layer building process. An algorithm is developed that slices the part with horizontal planes and computes the volumetric error of each layer using the complex shapes of the resulting contours of each layer.

In order to improve the efficiency of uniform slicing, a unilateral tolerance (positive tolerance or negative tolerance) slicing method was proposed by Liao et al. [102]. Instead of using slope of part as criteria for slicing, they use the dot product (D) between the normal direction of triangular facet (obtain from STL file) and the working direction (part build direction). Layers are added successively based on layer thickness starting from first layer. D is calculated for triangular facet that passes through layer plane. If $D \geq 0$, bottom up slicing for positive tolerance and top down slicing for negative tolerance is recommended. If $D<0$ top down slicing for positive and bottom up slicing for negative tolerance is used. This procedure aided the operator at the time of post processing as either complete part is oversized or undersize.

Pande and Kumar [103] presented a generative process planning system for parts produced by the RP process. The proposed process planning involves optimal selection of orientating the model with a proper support structure and then provides

an intelligent slicing methodology, such as direct or adaptive, to minimise the built time, keeping the geometry and cusp height errors in control. As an alternative to rectangular build edges, sloping build edges are also considered for the better approximation of surface of the part. The main advantage achieved is improved surface finish and decreased build time as thick layers can be used [104]. Thrimurthulu et al. [105] assumed a parabolic build edges for FDM build part and uses the concept of minimum surface roughness measured in terms of layer thickness and part build orientation for determining the optimum orientation of part. Byun and Lee [106, 107] considered three criteria that are the surface roughness, the build time, and the part cost to identify the optimal part orientation using the variable slicing method. Instead of considering sharp edge model for surface roughness determination they consider round edge model to compensate the presence of resin, powder or glue as residue in the corner between layers. Zhao et al. [108] presented a slicing method to compute accurate contour curves based on an STL model. First, the normal vector of a triangle facet to be sliced is calculated. An interpolation curve between two vertices is constructed in a normal section to approximate the original curve in the normal section in terms of the position of the two vertices and the tangent vector at the two vertices. The exact points of the slice contour are obtained by calculating the intersection points between the interpolation curve and the slice plane. Finally, accurate smooth contours are achieved by fitting the intersection points with a cubic B-Spline curve. The experimental results indicate that the presented slicing method improves the precision of cross contours.

Giannatsis and Dedoussis [109], Canellidis et al. [110] developed the decision support system that automates the build orientation selection in the SL process. The proposed methodology employs a genetic algorithm, to search the solution space using a multi-criteria objective function for evaluating feasible orientations. Hu et al. [111] determined the optimal orientation of part in hybrid-RP process considering both the CNC machining process attributes and the deposition process attributes. The main criteria for determining the build direction are the tool accessibility of the machining features, the build time, the number of bridges, and the number of supports. In addition, a method is presented to secure a part with bridges instead of using specially designed fixtures. Chen et al. [112] proposed a methodology to employ fuzzy set theory to select the preferred build orientation in hybrid-RP system. Part build orientation is considered as dependent on seven factors namely base plane size, skewness of centre of gravity, height of centre of gravity, inaccessible volume, support needed area, number of stock layers, and volume of removed material.

Significant savings in cost and time in RP can also be achieved by manufacturing multiple parts in a single setup to achieve efficient machine volume utilization. Obtaining this packing by hand or by a knowledgeable operator is a tedious process and does not guarantee the optimal placement of all parts. To solve this problem, a simple procedure is proposed by Nyaluke et al. [113]. In this procedure, all parts are arranged according to the volume that the part occupies in the work space. The work space is filled by placing the largest part at the extreme end of work table followed by second largest part. The process will continue until all the parts have been fitted into the work space or the work space has been filled. This method is based on the user placement selection and does not generate the alternative placement sequences and hence may not guarantee optimal layout configuration. Hur et al. [114] reported genetic algorithm (GA) based algorithm for the SLS process. Optimal part orientations are based on the build height of individual parts and the best packing sequence is obtained using the bottom-left (BL) approach. Part is modelled as a 3D 'voxel' structure for the purpose of interference checks. Zhang et al. [115] presented a layout optimization by considering part as enveloped by a rectangular box. Packing state of a model is determined by the location and the orientation of model's envelope. Simulated annealing search principles are used to find the best part layout which minimizes the packaging height and overlap between parts envelop. Pande and Gogate [116] developed a comprehensive methodology for optimal layout planning of parts for RP considering various constraints like build time, part quality and support structures requirement. First acceptable orientations for all the parts to be produced are obtained and rated them based on their desirability. Then, optimal placement of parts (in their chosen orientations) is subsequently obtained to achieve optimal part cost and quality using a GA based procedure.

As tracing of the cross sectional solid area in each layer is the most time consuming process, faster speed can be achieved by tracing the thin-shell solid that contains less solid material [117]. Hun et al. [118] used layer interior deposition planning approach, which not only speeds up the process but also ensure good layer quality for a specific set of deposition parameters. In their approach, neighbouring vector segments with similar lengths will be grouped together. Then, each group will be assigned an appropriate roller speed according to its group mean of vector segment lengths.

2.6 RP materials

RP is capable of using solid, liquid, and powder as a base material but the choice of material within each category is limited by the constraint offered by RP

process itself. For example, in FDM the raw material required for the process must have proper range of melting and solidification temperatures, low coefficient of thermal expansion, minimal shrinkage, low viscosity after filament is liquefied and the deposited material must be capable of solidifying in a relatively short time in order to achieve a good build speed. Generally, a part-building zone temperature of 70-100°C is preferred. The suitable solidification temperature range is preferably 5-10°C below the softening point. Thermoplastics such as acrylonitrile butadiene styrene (ABS), polycarbonate (PC), polyphenylsulfone etc. satisfy these requirements and are preferred as build materials [15, 16]. Based on such type of process specific constraints, each RP process is limited in the range of material available for processing. Table 2.3 list some of the RP processes with commonly used materials [13, 22].

Table 2.3 Materials in RP

Technology	Working Principle	Material
Stereolithography (SL)	UV laser is selectively scanned onto photo sensitive polymer	Liquid photopolymers like acrylates and epoxies
Fused Deposition modelling (FDM)	Plastic filament is extruded through heated nozzle	Wax, ABS, elastomers
Selective laser sintering (SLS)	Laser is used to sinter together powder particles	Polycarbonates, nylons, elastomers, ceramics, some metals
Laminated object manufacturing (LOM)	CO2 laser is used to cut cross sections out of layers of paper	Paper; similar to wood
Three dimensional printing (3-DP)	Printer head deposit molten wax onto bed of starch	Wax, starch
Multi jet modelling (MJM)	Similar to an inkjet printer, several print heads deposit beads of wax	Wax

With the advancement in material technology and RP machines, lot of activities in materials development have been observed over the past years. For example, Z Corporation introduced zp 140, a high-performance material, for its 3D printing process. The new powder material is engineered for simple, fast, and easy post processing [119]. In comparison to traditional powder systems used for 3D printing, polymer ionomers like zinc-poly acrylic acid ionomer has shown better options particularly in terms of mechanical strength [120].

Studies have shown that blending of ABS with fibres, small amount of plasticizer and compatibilizer will improve the strength, flexibility and durability of build parts [121]. Composite manufacturing using iron/nylon mixture consisting of iron metal particles in nylon matrix has also shown better mechanical properties for

producing functional parts and tooling directly on the FDM system [122]. Swinburne University of Technology, Australia, has also developed new composite materials involving acrylonitrile-butadiene-styrene (ABS) and iron [123]. A new high performance thermoplastic composite involving thermotropic liquid crystalline polymer (TLCP) fibre is developed for FDM system to fabricate prototype parts. The tensile modulus and strength of this material is approximately four times those of ABS [124]. For medical applications bio-resorbable and bio-compatible polymers [125, 126] are also found suitable for the production of tissues or implants using FDM. Calcium phosphate mineral are considered as promising materials to develop bio-mimetic porous scaffolds for bone replacement using SL [127].

Hinczewski et al. [128] and Greco et al. [129] have shown the applicability of SL process for processing ceramic slurry containing alumina powder. The study emphasized on the necessity of minimizing the organic concentration in the suspension, and keeping the viscosity of the suspension as low as possible to allow a good recoat of the liquid monomer on the polymerized layer. For ink-jet printing, Lejeune et al. [130] used lead zirconate titnate and titanium dioxide ceramic suspension respectively for fabricating different kinds of micro pillar array structures. Results reveal that main characteristics of the micro-pillar array structures (morphology, definition, compactity) strongly depend on the conditions of configuration of the deposit, driving parameters of the printing head, delay between two successive layers, ceramic loading, nature and content of binder and surfactant. Yen et al. [131] employed the ceramic slurry comprised of silica powder, clay, silica gel, water and inorganic binders to fabricate inter-connective porous structure having better surface quality and higher strength using SLS process. Liu et al. [132] combined SLS and gelation technique for fabricating ceramic–metal composite green parts. Unlike SLS process which sinter/fuse powder particles to form a solid part, they increase the concentration of the silica sol by evaporation using laser beam energy. In this process, sol yields the gel that links stainless steel powder particles together to form 3D networks and to bridge the gap between particles. Unlike previous research in this area, the silica sol is also a part of the finish sample rather than being removed in post-possessing. In comparison with other processes for making ceramic-metal composites, this approach features lower laser forming energy and faster fabrication speed. The feasibility of this process was demonstrated by manufacturing a composite prototype with a bending strength of 45 MPa, a surface finish of 32 μm, and a dimensional variation of 10% under a laser energy density of 0.4 J/mm^2. In order to overcome intrinsic difficulties such as high cost, poor shapability and machinability in forming and synthesising ceramics, Zhang et al. [133]

uses LOM for the fabrication of Al_2O_3 ceramic parts with complicated shapes. Adaptation of ceramic materials for generating 3D parts using FDM principle generated a new type of machines known as fused deposition of ceramics (FDC). In FDC, the ceramic powder is compounded with binder and solvent and the filament welds by diffusion. All the organic contents can be removed by sintering at a high temperature so that a pure ceramic lattice results [134-136].

With the advancement in material technology and RP technology, some RP machines are able to produce metal parts. The most evolving RP technology in this direction is SLS, which thermally bind the metal powders together [137]. For depositing metals directly by RP technology, other techniques have been tried including direct metal laser sintering (DMLS), laser engineered net shaping (LENS), direct metal deposition (DMD), ultrasonic consolidation (UC), selective laser melting (SLM) and directed light fabrication (DLF). These processes combine the developed technologies of powder metallurgy, solidification metallurgy, CAD/CAM and RP. Direct metal laser sintering (DMLS) from Electro optical system, Munich, Germany is an 'additive' technology that works by sintering very fine layers of metal powders layer-by-layer from the bottom up until the build is complete. Various materials are available to run in the DMLS technology including bronze-based alloy, low-carbon steel-based alloy, tool steel-based alloy [138]. In LENS, objects fabricated are near net shaped but generally require finishing operations. The strength of the process lies in its ability to fabricate fully dense metal parts with good metallurgical properties at reasonable speed. Generally, materials such as 316 and 304 stainless steel, nickel based super alloys such as Inconel 625, 690, and 718, H13 tool steel, tungsten, TI-6AL-4V titanium alloy, and nickel aluminides have been used in industry [139, 140]. DMD from POM Group Inc. is a laser-based fabrication process which produces fully dense metal products using tool steel alloys, stainless steel, cobalt-based alloys, and copper based alloys [141]. Researchers at the University of Kentucky have developed a dedicated control technology including slicing/planning, system implementation and post-processing for RP using gas metal arc welding as the deposition process. The metal transfer control system is used to control the size and frequency of the droplets in order to improve the deposition accuracy. The deposition parameters, including the travel speed, torch angle, welding current, and arc voltage are controlled to achieve the required density and three-dimensional geometry [142, 143]. Based on FDM process, a novel method known as fused deposition of metals (FDMet) is presented [144]. In FDMet process, filament was fabricated via extrusion process. For filament preparation, stainless steel powder 17-4 PH is compounded with binder after coating the powder with stearic acid by ball milling. The results show

that FDMet has good accuracy and reproducibility but optimization of process parameters is needed. Other perspective ways to build metal parts with RP is a combination of the benefits of material additive process with the advantages of material removal process [145]. Shape deposition manufacturing (SDM) is evolving in this direction. In SDM, a CAD model is first sliced into 3D layer structure. Layer segments are then deposited as near-net shape and then machined to net shape before additional material is deposited. The process shows great potential with higher precision and less inner stress [146].

2.7 Part quality improvement

Although RP offers advantages in terms of reduction in product build time for complex shaped parts and production of parts without use of tools, it has its own relative merits and demerits as far as part quality requirement is concerned. Hence, it is necessary to understand the shortcomings of a process before recommending for industrial application. Kim and Oh [18] compared various RP process based on tensile, compressive and impact strength, hardness, heat resistance, surface roughness, geometrical and dimensional accuracy, manufacturing speed and material cost. It was verified that SL process is advantageous in hardness, accuracy and surface roughness and poly jet process in tensile strength at room temperature. The SLS process was advantageous in compressive strength and manufacturing speed, the 3-DP process in speed and material costs, and LOM process in heat resistance. The FDM and LOM process are superior in impact strength in the scanning direction, but the change of building direction significantly reduce the tensile and impact strength. It has been proposed that improvement of surface quality, part strength, build time, accuracy, and repeatability are key issues to be addressed for successful implementation of RP technology. Following sections will illustrate the past studies employed in this direction.

2.7.1 Dimensional accuracy improvement

Ippolito et al. [21] studied the manufacturing accuracy of various rapid prototyping machines using the ISO-ANSI (International Organization for Standardization- American National Standards Institute) standards. The quality of parts produced by rapid prototyping typically lies between IT (International Tolerance) 14 and IT 16 and mostly influenced by the process parameter setting. Dao et al. [147] calculated shrinkage compensation factors for FDM parts with varying lengths. They observed that mean error after shrinkage compensation follows a linear trend i.e. error increases as nominal dimensions increases. Also, the residual errors are found

to be scattered due to lack of process stability. They attributed this trend to the noise shrinkage which is not compensated by the scaling factors used. Study on four RP process: SL, SLS, FDM, and LOM, through a benchmark part by Xu et al. [148] illustrated that the SL process gives the best dimensional accuracy for the majority of the measured dimensions followed by LOM, FDM, and SLS. In terms of the roundness of cylindrical features, SL and LOM produce the best results. SLS gives intermediate results, while FDM performs worst. Superior dimensional accuracy of SL is further established by Nizam et al. [149] while fabricating a human skull from Computed tomography (CT) images.

During part fabrication, errors arise due to process related attributes like machine path control accuracy, tool scan speed uniformity, platform control accuracy, material properties, material feed uniformity, and part thermal shrinkage and distortion [150]. While building a part, if the laser scan speed is adjusted dynamically according to the scan length which varies with geometric shape of the part, the geometrical accuracy can be significantly improved [151]. Senthilkumaran et al. [152-154] has shown that the beam offset, inertia of scanning mirror and positioning errors in hatch generations, exposure strategies and part orientation are found to influence the accuracy of the part to be produced by SLS. Hence, certain compensations other than shrinkage are needed to get accurate estimate of the shrinkage.

To control process related errors, Zhou et al. [155] proposed parameter tuning approach using Taguchi experimental design to improve the dimensional accuracy of SL part. A standard sample was developed to act as a benchmark for comparison of the total of twenty different dimensional, geometrical, and surface features. Analysis suggests that the best setting of control factors for each individual feature is different. For example, blade gap has the largest effect for horizontal dimension whereas overcure is more influencing in vertical direction for dimensional accuracy improvement.

Lehtihet et al. [156] consider errors in the coordinate of laser focus in SL machine as a function of errors along X, Y and Z-axis. Unknown coefficients in these functions are determined using measurement on test parts. Calculated values of error are compensated in the STL model. The resulting model shows feature position accuracy, and profile accuracy improvement. Huang and Lang [157, 158] proposed the finite element based simulation method to obtain the distortion data of part processed using SL. The volumetric shrinkage and curl distortion are considered as two important factors responsible for part inaccuracy. Calculated distortion of each node is added to its original coordinates and considered as static reveres compensation. Static reverse compensation results in oversize of the part. Due to

increase in size, the scanning length increases which again results in part inaccuracy. Hence dynamic reverse compensation is calculated using distortion data and added to the original scanning length. For generating new CAD model, original CAD model is divided into simpler regions. For each region, distorted surface model is generated from compensation data and finally they are merged together to form the solid model. This solid model is used for part fabrication. Comparison with experimental results shows that static reverse compensation is suitable for smaller dimension parts or small distortion data whereas dynamic reverse compensation gives better results for larger parts or large distortion data.

In DMLS process, two types of shrinkages namely thermal shrinkage and sintering shrinkage is quantified by Zhu et al. [159]. The sintering shrinkage is mainly caused by densification and is a kind of elastic compressive shortening. The thermal shrinkage caused by cyclic heating can be reduced by controlling process parameters such as laser power, scan speed and scan spacing. Wang et al. [160] studied the effect of process parameters on shrinkage characteristics in SLS process. They found that percentage shrinkage increases with increase in the scanning speed and hatch spacing, but decreases with increasing layer thickness, the laser power, part bed temperature and delay time.

Pandey and Raghunath [161] have shown that laser power and scan length are most influencing process variables along X direction, laser power and beam speed are significant along Y direction and beam speed, hatch spacing and part build temperature are significant along Z- direction while studying shrinkage phenomena in SLS part using Taguchi design of experiment. The developed relationship is applied to STL file to compensate the shrinkage effect and improve the part dimensional accuracy. Campanelli et al. [162] recommended that hatch overcure and border overcure must be set at their maximum level for improving part accuracy when layer thickness is high. If low layer thickness is desired then hatch overcure should be maintained at medium level and border overcure at maximum level. These process settings not only improve part accuracy but also eliminate the necessity for post curing the SLS part.

2.7.2 Surface roughness improvement

The surface finish of parts obtained through RP process is highly important, especially in cases where the parts come in contact with other elements or materials in their service life, for example moulds made up of components manufactured by RP processes.

Perez et al. [163, 164] have proposed a theoretical model for roughness of parts fabricated using stereolithography apparatus (SLA-350) in terms of layer thickness and horizontal space between layers. It has been recommended that layer thickness should be modified as a function of the slope of the exterior profile of the component to obtain good surface finish. Paul and Voorakarnam [165] have developed a hypothetical model to predict the roughness of laminated object manufacturing (LOM) processed parts considering layer thickness and part orientation as two process variables. Results indicate that the model can predict well for surfaces with moderate surface roughness but poorly perform for thickest paper at the largest orientation angle.

Anitha et al. [166] have used Taguchi method for assessment of influence of three process parameters such as layer thickness, road width and deposition speed on FDM processed parts. It has been observed that quality of parts is significantly affected by layer thickness as compared to road width and speed. It has been demonstrated through correlation analysis that inverse relation exist between layer thickness and surface roughness. Campbell et al. [19] compared the surface profiles of test samples made by various RP processes like SLA (SLA-350), Thermo Jet (Actua 2100), FDM (FDM 16500), LOM (LOM 1015) and 3D Printer (Z 402) with roughness prediction model proposed by Reeves and Cobb as shown in equation 2.1.

$$R_a = L_t \sin\theta / 4\tan\theta \qquad (2.1)$$

where R_a is average roughness, L_t is layer thickness and θ is the angle between the surface normal and vertical direction. It has been shown that surface roughness can be well predicted in a wide range of angles for majority of systems (SLA, Actua, FDM, and LOM). However, equation 2.1 estimates higher values of surface roughness for upward facing surface in parts built on Actua 2100, most surfaces of FDM and 3D printer built parts. The study clearly indicates that, there are other process parameters apart from layer thickness that influence surface roughness. Tay et al. [167] suggested the use of electro-less nickel (EN) plating over the semi bright nickel electroplating to improve the surface quality of the mould produced by DMLS technique to an industrial acceptance level. The surface finish has been improved from 17-19 µmm to 2-3 µmm by EN plating without losing any sort of dimensional accuracy. EN ions are found to penetrate inside the material through the pores and fill up the voids. Sui and Leu [168] studied the surface roughness of ice parts built by the rapid freeze prototyping (RFP) process. Through experimental analysis, the surface roughness of an ice part is shown as a function of water deposition rate, scanning speed, and contact angle. However, it is independent of slant angle of

vertical wall. Two different types of technologies based on multi jet modelling (Actua 2100 system and Thermojet system) have been considered in order to analyse the differences that exist when referring to the surface roughness by Luis et al. [169]. The results show that Thermojet system is having lower range of layer thickness values is better as compared to Actua 2100. However, there are some cases of angles in which Actua 2100 is better than Thermojet. In order to improve surface roughness of parts, Pandey et al. [170] proposed a hybrid FDM system in which materials deposition in a layer-by-layer fashion and machining of edges by hot cutter machining simultaneously. It is concluded that proposed machining method is able to produce surface finish of the order of 0.3µm with 87% of confidence level. The mould produced using DMLS is usually not suitable to produce parts because of the presence of to high surface roughness and open porosity. Considering these necessities, many surface treatments are analysed by Rossi et al. [171]. The most promising are the grinding and emery polishing, which produce a surface roughness lower than 1 µm. To guarantee the corrosion resistance of prototyped components, CrN/NbN layers, PTFE (poly-tetra-fluoro-ethylene) based coating and electroless nickel coatings with and without SiC (silicon carbide) and PTFE particles are considered. The nickel coating, applied after shot peening and polishing shows the best performance because coatings results in uniform thickness and guarantee a good corrosion protection.

Kim and Lee [172] have developed a multi-objective genetic algorithm approach for prediction of surface roughness of parts built by SL process. The results indicate that the algorithm can predict effectively for relatively difficult to post process parts of small, thin or complex shape. However, the model suggests that fabrication time of parts for long or flat parts invariably increases although post processing time is reduced.

Ahn and Lee [173] proposed a post machining technology combining coating and grinding processes to improve the surface quality of SL parts. Paraffin wax and pulp are used as the coating and grinding materials. By grinding the coating wax only up to the boundary of the part, the surface smoothness can be improved without damaging the surface. This post-machining, however, is also detrimental to the original geometry of the part and is time consuming. To minimize the required post-machining region in the RP, a genetic algorithm based methodology is proposed to determine the optimal fabrication direction [174]. Theoretical and actual characteristics of the surface roughness distributions of RP processed parts were investigated to represent the actual roughness, and an equation was introduced to express the surface roughness distribution in terms of the surface angle using

measured surface roughness data and interpolation. Also, a surface roughness prediction application was presented to verify the proposed methodology. The validity and effectiveness of the proposed approach were demonstrated through the calculated roughness error estimation and several application examples. Ahn et al. [175-177] have proposed a theoretical model for prediction of surface roughness involving surface angle, layer thickness and overlap interval between adjacent layers for FDM built parts using filament of elliptical cross section. But the control mechanism is difficult to implement in real practice. Further, the effect of FDM process parameters is not fully explained in terms of their role in controlling surface roughness. Galantucci et al. [178] apply the chemical treatment to FDM ABS part by immersing them in a volume of 90% di-methyl-ketone and 10% water for 300s. The results show that the chemical treatment cuts away material but the subtracted ABS is balanced by the absorption of the solution and the roughness of the specimens has been improved considerably by using the chemical process as compared to untreated specimen.

2.7.3 Mechanical strength and wear characteristic improvement

A factor of significant importance in the RP applications is the capability of producing components with adequate mechanical performance. Cheah et al. [179] studied the mechanical properties of specimens fabricated by the SL process using an acrylic-based photopolymer (De Solite SCR-300) and post-cured under intense UV (ultra violet) light. It was observed that the post cured specimens yielded higher measured values of elastic modulus, ultimate tensile strength, and elongation to fracture. It was also observed that these mechanical properties of the post-cured specimens were functions of the layer pitch and the laser exposure density used in generating its green state counterparts. By increasing the laser exposure density and decreasing the layer pitch, the mechanical properties of the post-cured prototype can be increased, leading to a post-processed prototype with higher mechanical strength.

A study made by Es Said et al. [180] shows that raster orientation causes alignment of polymer molecules along the direction of deposition during fabrication and affect tensile, flexural and impact strength. Since semi-molten filament is extruded from nozzle tip and solidified in a chamber maintained at certain temperature, change of phase is likely to occur. As a result, volumetric shrinkage takes place resulting in weak interlayer bonding and high porosity; hence, reduces load bearing area. Ahn et al. [181] have pointed out that process parameters such as air gap and raster orientation significantly affect the tensile strength of FDM processed part as compared to other parameters like raster width, model

temperature and colour through experimental design and analysis. In addition, built parts exhibit anisotropic properties as far as tensile strength is concerned depending on build orientation. Khan et al. [182] have concluded that layer thickness, raster angle and air gap influence the elastic performance of the compliant FDM ABS prototype. An effect of part-build orientation in the laser sintering process is presented by Ajoku et al. [183]. Results highlight the presence of anisotropy in tensile, compression and flexural tests. The test parts built in the direction of laser scanning showed the highest tensile and compressive strength. Flexural strength of test parts is highest along the direction perpendicular to laser scanning. Lee et al. [184] performed experiments on cylindrical parts made from three RP processes such as FDM, 3D printer and nano composite deposition (NCDS) to study the effect of build direction on the compressive strength. Experimental results show that compressive strength is 11.6% higher for axial FDM specimen as compared to transverse FDM specimen. In 3D printing, diagonal specimen possesses maximum compressive strength in comparison to axial specimen. For NCDS, axial specimen showed compressive strength 23.6% higher than that of transverse specimen. Out of three RP technologies, parts built by NCDS are severely affected by the build direction.

Wang et al. [185] utilized the mathematical model for warp deformation in FDM prototype. It has been observed that deformation is more in bottom layers than upper layers. Higher the stacking section lengths cause large deformations. If chamber temperature increases, deformation will gradually decrease and become zero when chamber temperature equals glass transition temperature of the material. It is proposed that material used for part fabrication must have lower glass transition temperature and linear shrinkage rate. Also the extruded fiber length must be small. Bellehumeur et al. [186] have experimentally demonstrated that bond quality between adjacent filaments depends on envelope temperature and variations in the convective conditions within the building part while testing flexural strength specimen. Temperature profiles reveal that temperature at bottom layers rises above the glass transition temperature and rapidly decreases in the direction of movement of extrusion head. The minimum temperature increases with the number of layers. Microphotographs indicate that diffusion phenomenon is more prominent for adjacent filaments in bottom layers as compared to upper layers. Simulation of FDM process using finite element analysis shows that distortion of parts is mainly caused due to accumulation of residual stresses at the bottom surface of the part during fabrication [187].

Chockalingam et al. [188] through Taguchi design of experiment has proposed that layer thickness, post curing time and part built orientation has significant influence on the strength of SL products. Using finite element analysis, Nickel et al. [189] has shown that raster pattern used to deposit an interior of layer has a significant effect on the resulting residual stresses and deformation of part generated using SDM (Shape Deposition Modelling). A raster deposited at a large angle with respect to long axis of part will produce a smaller distortion. Pandey et al. [190] improved the tensile strength of SLS processed part by experimentally optimizing the time difference for laser exposure between any two adjacent points on successive scanning lines on a layer. As this time difference depends on part build orientation, an algorithm has been developed and implemented to find out optimum part build orientation for improving tensile strength.

Wear is an important characteristic for the durability of part and little work is devoted to understand the wear characteristic of RP processed part. In relation to other RP processes, Ramesh and Shrinivas [191, 192] have shown that iron-silicon carbide metal matrix composites manufactured by direct metal laser sintering (DMLS) process exhibits higher micro-hardness, coefficient of friction and lower wear rates as compared with iron. Low laser speed results in high density, micro-hardness and wear resistance of the developed composites. Kumar and Kruth [193] has indicated that parts produced by selective laser sintering (SLS) process shows better wear performance as compared to parts built through selective laser melting (SLM) process.

2.8 Discussions

Ability to fabricate in virtually tool free environment and geometrically insensitive of the RP process has given it a distinct advantage in comparison to conventional metal forming or subtractive manufacturing processes. The present applications, not only limited to form, fit and functional testing but it is coming into increasingly widespread use in specialized technology applications where limited quantities of durable precision components are needed. Further, integrating these technologies with other secondary processes not only reduce the time to market but also give the cost benefit to the practitioners [37-42]. The most benefitted application areas include: medical, product design, aerospace and automotive industries [23-36]. With a growing interest of both industries and researchers towards RP, a number of new technologies are being introduced each year [11, 15, 16]. It is hard for a RP user to keep in track of all the systems available and get acquainted with their process capabilities. Second, a great number of factors or selection criteria (e.g. time, cost,

accuracy, building envelop, material type, surface roughness etc.), either qualitative or quantitative, must be synthetically considered when evaluating and selecting a proper RP system. Moreover, the descriptions and judgements on most of these criteria are usually linguistic and vague in nature. There is dearth of benchmark standards and industry experience with most of these systems. Therefore, it becomes an increasingly difficult task for many novices and inexperienced RP users to select quickly an adequate RP system to serve their needs. A number of studies have been carried out into the development of methodologies, decision support techniques and software tools for assisting RP users in selecting the most suitable RP process. Early attempts in selecting a conformable RP system were based on benchmarking studies that compared different RP systems [53-55]. This approach may be time consuming and quite expensive. More recent studies have concentrated on developing the knowledge-based expert systems for RP process selection [56-66]. However, biggest drawback with these approaches is the ranking method. It may be mentioned that the ranking depends upon the judgments of relative importance made by the decision maker.

Almost all of RP processes have inherent limitations. First and foremost is related to absence of suitable interface between CAD and RP machines and second one is related with the layer by layer part generation principle used by RP machines. As shown in Figure 2.4 to overcome the first limitation, three approaches were suggested viz. use of STL or other interfaces, direct slicing of CAD model and use of point cloud data generated using reverse engineering techniques.

The direct slicing of the original CAD model avoids the approximation errors resulting from tessellation. However, there are several constraints with direct integration. It can only be used for a specific set of CAD software and machine, and is not applicable to any other CAD-RP combinations. The execution of program for adding support configuration is not easy; CAD model is stored in the form of analytical surfaces or mathematical descriptions instead of coordinates of points as in the case of STL models results in difficulty to orient the model [77-83]. On the other hand, point cloud data can be fed to RP systems using three procedures. In the first procedure, surface model is generated from point cloud which is then converted to STL format. In second method STL files are directly generated from point cloud data. In the third third approach, sliced model is directly obtained from the point cloud data. The third approach is robust than other two approaches of integrating point cloud data and RP system as it eliminate the errors arising while generating surface and tessellated (STL) models. But, integration of a point cloud data with RP often calls for many steps such as use of correct method to capture geometry, pre-processing of

point cloud data, data segmentation, post processing of captured geometry by operations such as blending and stitching, and finally verification of captured model for accuracy [84-89]. Moreover, presence of actual part for data capturing is a pre-condition. Irrespective of its shortcomings, tessellated representation of CAD models (STL file) has several advantages like its availability with most of the CAD systems and supported by all the RP machines, implementation of slicing algorithm, better ability of orientation of the model and simple way of adding support structure [17, 67-70]. Some other types of interfaces are also proposed but they have their own inherent disadvantages as mention in Table 2.2. Some of these interfaces are still in development phase or are not supported by majority of CAD and RP systems vendors [71-76].

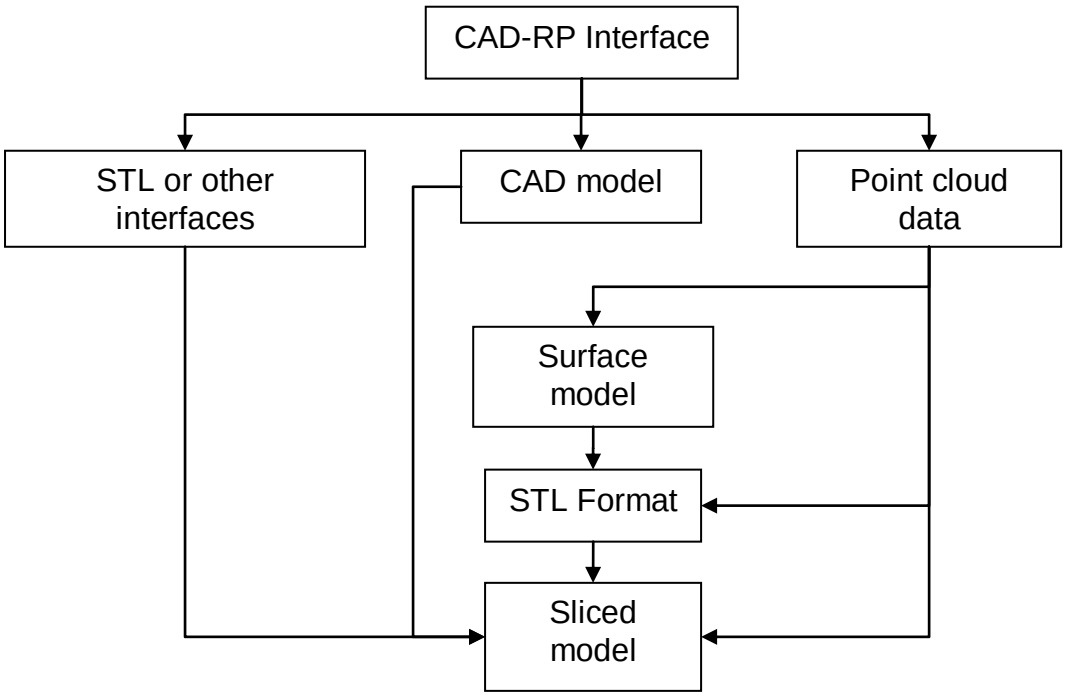

Figure 2.4 Approaches to generate sliced model from CAD model

Intrinsic nature of RP process to generate parts by layer by layer deposition results in staircase effect which will be dominating in those surfaces whose outward normal is inclined to the direction of build at an inclination other than zero or ninety degree. The staircase effect generally depends upon the slicing accuracy and builds orientation. Various procedures have been proposed to improve the slicing accuracy but none of them achieves the 100% efficiency [90-112]. For critical surfaces, the part orientation must be selected in such manner that staircase effect will be minimized. In addition, adaptive slicing is paramount in comparison to uniform slicing. It is difficult to change the thickness during the deposition with most of the commercial RP systems presently available. For example, in FDM Vantage SE

system the CAD model is sliced for a constant slice thickness, which depends upon the nozzle tip diameter. To change the slice thickness, the nozzle tip needs to be changed. To have this facility, there is a need for the development of hardware, which is capable of depositing variable slice thickness. Furthermore, orientation limits the maximum part size that can be built in fixed size build chamber, the support structure requirement, build time and time of post processing operation to smooth the part surface or remove the support material. As these requirements are also important considerations for evaluating part cost, it can be said that choice of proper orientation also control the part cost. It has been reported that significant saving in build time and cost can be achieved by optimum utilization of build chamber space and proper tool path generation [113-118].

Although RP is an efficient technology, full scale application has not gained much emphasis because of compatibility of presently available materials with RP technologies [13, 15, 16, 22]. The majority of RP technologies produce parts made of some certain and often proprietary materials. In addition to the state of the material used, the choice of materials is dependent on specifies of the process. Researchers tailored the RP materials by blending with other materials to improve the build part performance requirements [120-127]. RP has demonstrated the potential to produce unique ceramic parts and composites manufacturing. However, it can be used to explore ceramic processing allowing precise variation in properties of the powder compact [128-136]. Till this date, the biggest challenge for RP users is to build metal parts directly. Number of researchers around the word have developed or modified various RP processes to build metal parts with varied degree of success [137-146].

RP processes were initially used for rapid prototyping to help the designer verify part geometry, but are now increasingly used to make moulds for castings and manufacture of one-off and small batch production of parts. They may have inferior properties when compared with objects manufactured by other means, especially those related with fabricated part quality requirements measured in terms of dimensional inaccuracy, surface smoothness and part strength. Benchmark studies performed on RP fabricated parts [21, 148, 163, 164] shows that part quality differ not only between different rapid prototyping technologies, but also in different geometrical features and orientations of parts. The variation in properties can be seen as the result of the systematic errors and random errors existing in the RP building process. For a stable manufacturing process, the random errors should be small and evenly distributed among the positive and negative deviations. The systematic errors common in the RP processes may come from the shrinkage effect, positioning error of the motion control system, laser

overcuring or overheating effect, laser beam profile, distortion in the post processing stage, improper setting of process parameters, and so on [150-154]. To overcome the limitation RP processes, it is necessary to control the process related errors. In this direction, past studies employed for dimensional accuracy improvement can be divided into two categories. The first is related with determination of suitable scaling factors by experiments or simulations [147, 152-154, 156-158] and compensate it on CAD model before actual part fabrication. But this approach may introduce additional errors and may not be suitable for all size part. Also, due to the dynamic nature of the process, a realistic simulation of shrinkage occurring in the process using FEM is often difficult and unrealistic. Another approach is related with parameter tuning. Its basic advantage is that it can be achieved by operator or process planner without affecting the CAD file. Further, it also incorporates the process traits for dimensional accuracy improvement [155, 159-162]. Poor surface quality is sometimes overcome by performing finishing operations such as grinding or polishing after an object is built. These post-processing operations are however unfavourable to the original geometry of the component and are time consuming [167, 170, 171, 173, 174, 178]. Earlier attempts to improve this are related with slicing accuracy and part build orientation determination using empirical models. Later on, some attempts were made to understand the functional relationship between process related variables and surface roughness using experimental analysis [19, 163-166]. Most of the surface roughness models consider layer thickness and build orientation neglecting many other parameters involved during actual part building stage. However, Anitha et al. [166] pointed out that the influence of parameters other than layer thickness and orientation may not be as dominating as these two but certainly important for controlling for surface roughness of the part. Ahn et al. [175-177] proposed a good prediction model but the control mechanism is difficult to implement in real practice.

One of the major issues of concerning with RP is the mechanical strength of processed part. The mechanical strength of RP processed parts are usually less compared to conventional manufacturing process or to original material. Part of this drawback is due to processable material related constraints but major limitation is due to their own part build principles. For example, for the case of FDM process, build material in the form of a flexible filament is partially melted and extruded from a robotically controlled deposition nozzle onto a table in a temperature-controlled environment for building the 3-D part layer by layer. As the material is extruded out, there is a shearing effect that forces material to spread forward and sideward when the nozzle moves. The material will have sufficient residual heat energy to activate

the surfaces of the adjacent regions and the bonding between neighbouring filaments takes place via thermally driven diffusion welding [185]. Diffusion phenomenon is more prominent for adjacent filaments in bottom layers as compared to upper layers and bond quality depends on envelope temperature and variations in the convective conditions within the building part [186]. Once a layer is built, the platform goes down a distance of the layer thickness and the following layer is deposited on top of the previous one resulting in formation of 3-D part in a sequential manner. The 3-D part takes the form of a laminate composite with vertically stacked layers consisting of contiguous material filaments with interstitial voids. When semi molten filament is extruded from nozzle tip and solidified in a chamber maintained at certain temperature, change of phase is likely to occur. As a result, volumetric shrinkage takes place resulting in weak interlayer bonding, high porosity and hence reduces load bearing area [180]. Change in temperature of depositing material causes inner stresses to be developed due to uneven heating and cooling cycles resulting in inter layer and intra layer deformation that appear in the form of cracking, de-lamination, or even part fabrication failure [185]. Deformation in part is mainly caused due to accumulation of residual stresses at the bottom surface of the part during fabrication and increases with the increase in stacking section length [187]. These phenomena affect the part strength. RP literature suggests that improvement in strength of built part can be achieved if their processing conditions are properly controlled [155, 162, 165, 178, 188-190]. It is also observed that very little work has been performed to understand the wear nature of RP built parts [191-193].

The trend of current literature suggests that all RP technologies have some generic and exclusive common features, which convey a number of synergies among them. The main appeal is towards the novel possibilities and applications offered by these technologies. However, these technologies still differ greatly in terms of physical process, geometry, performance and materials that can be processed. Studies carried out worldwide have shown the significant variation in the part properties with changing process parameter conditions. This highlights the scope of improvement in them. Though much work has been reported on various RP technologies but the possibility of improvement in FDM process is not properly explored. Table 2.4 highlights some of the important contributions in this direction. Available literature did not fully explained process variables and their interaction effect for part quality improvement. Therefore, there is a need to develop a systematic approach to understand the influence of various process parameters in FDM and develop empirical model so that users can easily predict and control the functional requirement of the part. Therefore, it is felt that avenue exist for exhaustive

research on FDM process perfection. This is main concern of industries such as aerospace and bio-medical which would like to use FDM technology for producing directly usable products [3, 9, 11, 13, 16, 28, 34].

Table 2.4 Important contributions in the area of FDM process improvement

Year	Author	Title	Summary
1999	Dao et al. [147]	Calculation of shrinkage compensation factors for rapid prototyping (FDM 1650)	Calculate shrinkage compensation factors for FDM parts with varying lengths. Mean error after shrinkage compensation follows a linear trend and is increasing for increasing nominal dimensions. Also the residual errors are found to be scattered due to lack of process stability. They attributed this trend to the noise shrinkage which is not compensated by the scaling factors used.
2000	Said et al. [180]	Effect of layer orientation on mechanical properties of rapid prototyped samples.	Study shows that for FDM process semi-molten filament is extruded from nozzle tip and solidified in a chamber maintained at certain temperature, change of phase is likely to occur. As a result, volumetric shrinkage takes place resulting in weak interlayer bonding and high porosity; hence, reduces load bearing area.
2001	Anitha et al. [166]	Critical parameters influencing the qualities of prototype in fused deposition modelling.	It has been demonstrated through correlation analysis that inverse relation exist between layer thickness and surface roughness of FDM build part. Study pointed out that the influence of parameters other than layer thickness and orientation may not be as dominating as these two but certainly important for controlling for surface roughness of part
2002	Campbell et al. [19]	Surface roughness visualization for rapid prototype models.	Compared the surface profiles of test samples made by various RP processes including FDM with theoretical model based on part orientation and layer thickness. There study indicates that apart from stair stepping, there are other factors in FDM which also contribute to surface roughness.
2008	Bellehumeur et al. [186]	Effect of processing conditions on the bonding quality of FDM polymer filaments	Experimentally demonstrated that in FDM process bond quality between adjacent filaments depends on envelope temperature and variations in the convective conditions within the building part while testing flexural strength

			specimen. Temperature profiles reveal that temperature at bottom layers rises above the glass transition temperature and rapidly decreases in the direction of movement of extrusion head. The minimum temperature increases with the number of layers. Microphotographs indicate that diffusion phenomenon is more prominent for adjacent filaments in bottom layers as compared to upper layers.
2008	Chou et al. [187]	A parametric study of part distortion in fused deposition modelling using three dimensional element analysis.	Simulation of FDM process using finite element analysis shows that distortion of parts is mainly caused due to accumulation of residual stresses at the bottom surface of the part during fabrication

2.9 Conclusions

This chapter provide the insight into various past developments and improvements in the area of RP. For the sake of simplicity, it is divided into six main sections. In section 2.2, new opportunities and applications of RP as an appropriate manufacturing tasks has been discussed. Each RP process has its own strengths, limitations and application field. Users with reasonable RP experience find it difficult to select a suitable process In this direction section 2.3 reviews the literature on selection of a RP process suiting to a particular need taking into account quantitative and qualitative data. Survey of current and proposed data formats for communication between CAD to RP systems is presented in section 2.4. The advantages and disadvantages of various data transfer methods are discussed. However, despite its proprietary nature and associated problems, STL is currently almost universally used as a neutral format for CAD-RP interface. Section 2.5 reveals that appropriate orientation and accurate slicing methodology are important considerations for improving the surface accuracy of built part, reducing the build time and consequently cost of fabrication. It is further suggested that optimum utilization of build volume by manufacturing number of parts simultaneously and employing proper layer filling methodology helps to achieve cost reduction. In section 2.6 the issue of limitations of processable material with RP has been addressed. The material limitation is the key contributing factor why rapid prototyping has yet to make a major advance towards rapid manufacturing. It has been a goal of many researchers in the past years to overcome this limitation and create processable materials with an acceptable end performance. Section 2.7 deals with improvement of part quality measures as they are identified as key enabling factors for industrial viability of RP

process. To understand the past studies employed in this direction, the section is further divided into three sub- sections as follows. Sub-section 2.7.1 reviews various approaches for improving dimensional accuracy and sub-section 2.7.2 deals with surface roughness. Sub-section 2.7.3 relates to improvement of mechanical strength and wear characteristic of RP built parts. It is observed that parameter tuning is an appropriate and commonly used approach for improving part quality. In this direction, present work attempts to explain the effect of process parameters and their possible interaction, if any on the quality of FDM processed parts through experimental investigation. Also, attempt has been made to determine optimal parameter setting for best performance output.

CHAPTER 3

MATERIALS AND METHODS

3.1 Introduction

FDM has significant advantages in terms of the elimination of expensive tooling, the flexibility, and the possibility of producing very complex parts and shapes [22-25]. Existing examples tend to prove that this process offer time and cost advantages over conventional technologies [26, 33, 46]. One of the current challenges faced by FDM users is the quality of parts produced, which is allied with the accurate application of the specified performance [18, 21]. This makes it essential to understand the performance of FDM process parts with the variation of process parameters so make them reliable for industrial applications. To achieve this, the present chapter describes the materials and methods used for the testing of FDM processed part under investigation. It presents the details of the part fabrication methodology and various tests that the samples are subjected. Dimensional accuracy, surface roughness, part mechanical strength, and wear characteristics are considered as measure of part quality in accordance to industrial requirements. All tests are carried out at the temperature 23±2ºC and relative humidity 50±5% as per ISO R291:1977 (Plastics – Standard Atmospheres for Conditioning and Testing). The methodology related to the design of experiment technique based on Taguchi method and the response surface analyses are also presented in this part of the thesis.

3.2 Material

The material used for test specimen fabrication is acrylonitrile butadiene styrene (ABS P400). ABS (chemical formula $((C_8H_8 \cdot C_4H_6 \cdot C_3H_3N)_n$) is a carbon chain copolymer and belongs to styrene ter-polymer chemical family. ABS is derived from acrylonitrile, butadiene, and styrene (Figure 3.1). It contains 90-100% acrylonitrile/butadiene/styrene resin and may also contain mineral oil (0-2%), tallow (0-2%) and wax (0-2%). Acrylonitrile is a synthetic monomer produced from propylene and ammonia; butadiene is a petroleum hydrocarbon obtained from the C_4 fraction of steam cracking; styrene monomer is made by dehydrogenation of ethyl benzene - a hydrocarbon obtained in the reaction of ethylene and benzene. ABS is made by polymerizing styrene and acrylonitrile in the presence of poly-butadiene. The result is a long chain of poly-butadiene criss-crossed with shorter chains of poly (styrene-co-acrylonitrile). The nitrile groups from neighbouring chains, being polar, attract each other and bind the chains together, making ABS stronger than pure polystyrene. Its three structural units provide a balance of properties with the acrylonitrile providing heat resistance, butadiene imparting good impact strength and

the styrene gives the copolymer its rigidity [15]. Varying the proportion of constituents in the material or the conditions under which the material is being processed may vary the material properties. Table 3.1 list the properties of commercially available extruded and moulded ABS [194]. In the present study, the material supplied by the original equipment manufacturer is used.

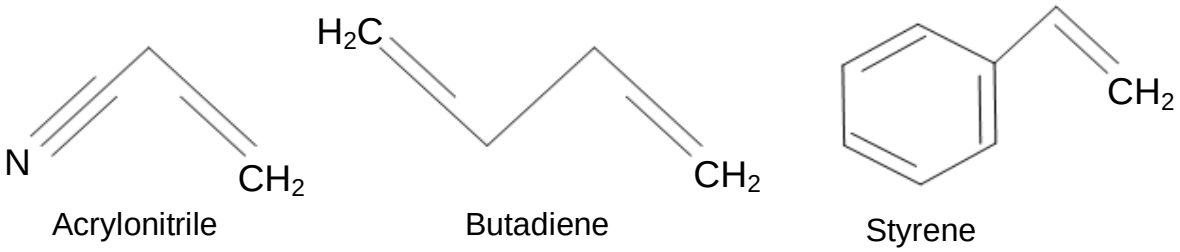

Figure 3.1 Monomers in ABS polymer

Table 3.1 Properties of ABS

Property	Extruded	Moulded	Unit
Physical property			
Density	0.350-1.26	1.02-1.17	g/cm3
Moisture Absorption at Equilibrium	0.150 - 0.200	0.000 - 0.200	%
Viscosity	155000 - 255000 (Temperature 240-260°C)	1.16e+6-1.52e+6 (Temperature 240-260°C)	cP
Linear Mould Shrinkage	0.00240 - 0.0120	0.00200 - 0.00900	cm/cm
Mechanical property			
Hardness Rockwell R	90.0 - 121	68.0 - 115	
Tensile Strength, Ultimate	27.0 - 52.0	28.0 - 49.0	MPa
Tensile Strength, Yield	20.0 - 62.0	13.0 - 65.0	MPa
Modulus of elasticity	1.52-6.10	1.00-2.65	GPa
Elongation at Yield	0.620 - 30.0	1.70 - 6.00	%
Flexural Modulus	1.20 - 5.50	1.61 - 5.90	GPa
Flexural Yield Strength	28.3 - 81.0	40.0 - 111	MPa
Charpy Impact, Notched	0.900 - 5.00	0.400 - 14.0	J/cm²
Izod Impact, Notched	0.380 - 5.87	0.100 - 6.40	J/cm
Thermal properties			
Thermal Conductivity	0.150 - 0.200	0.128 - 0.200	W/m-K
Coefficient of thermal expansion, linear	68.0 - 110	0.800 - 155	µm/m-°C
Glass Transition Temperature	108 - 109	105 - 109	°C

3.3 Specimen fabrication

Specimens are fabricated using FDM Vantage SE machine for respective characteristic measurement. This machine is developed and marketed by Stratasys Inc., 14950 Martin Drive, Eden Prairie, MN 55344-2020 U.S.A. As compared to other vantage series machines like vantage I, vantage X, and vantage S, vantage SE series machine has large build chamber volume (406x355x406mm). It incorporate

multiple materials like ABS, ABSi (high impact grade of ABS), PC (polycarbonate), PC-ABS and PC-ISO and uses Water Works soluble support for ABS, ABSi and PC-ABS, breakaway support for PC and PC-ISO (BASS^{TM}). Support material use can be easily breakaway by hand. It can build part in three available layer thicknesses that are 0.127mm, 0.178mm and 0.254mm. It has two auto load model material and two auto load support material canisters with 1510 cubic cm modelling material per canister. Vantage SE machine has automatic changeover facility between canisters [195].

The 3D models of specimens are generated using CATIA V5 solid modelling software and exported as STL (stereolithography) file to FDM software (Insight). Here, factors are set as per experiment plan. Software breaks the STL model into individual slices and generate tool path. After this, data is sent to the FDM hardware for modelling. The article forming material (ABS P400), in the form of a flexible strand of solid material is supplied from a supply source spool to the head of the machine (Figure 3.2). One pair of wheels or rollers having a nip in between are utilized as material advance mechanism to grip a flexible strand of modelling material and advance it into a heated dispensing or liquefier head (Figure 3.3). The material is heated above its solidification temperature by a heater (liquefier) on the dispensing head and extruded in a semi molten state on a previously deposited material onto the build platform following the designed tool path. The head is attached to the gantry that manoeuvres the head in the X and Y directions when building a part. The XY gantry assembly is located under the top hood of the machine. The entire gantry is outside of the build chamber. Only the bottom of the head protrudes into the build chamber. The build platform moves along the Z direction. The drive motion are provided to selectively move the build platform and dispensing head relative to each other in a predetermined pattern through drive signals input to the drive motors from CAD/CAM system. For material deposition FDM uses two nozzles, one for model material deposition and other for support material deposition. These two nozzles work alternately to each other. Figure 3.4 provides the schematic description of steps entailed during part fabrication in FDM machine. For each layer generation, contour is laid down first to generate boundary of the layer and then interior is filled through vector filling (known as raster), the raster angle is alternated by 90 degrees between consecutive layers to obtain adequate interlocking between layers through efficient bonding of rasters. The fabricated part takes the form of a laminate composite with vertically stacked layers, each of which consists of contiguous material fibres or raster with interstitial voids. Fibre-to-fibre bonding within and between layers occurs

by a thermally driven diffusion bonding process during solidification of the semi-liquid extruded fibre [14].

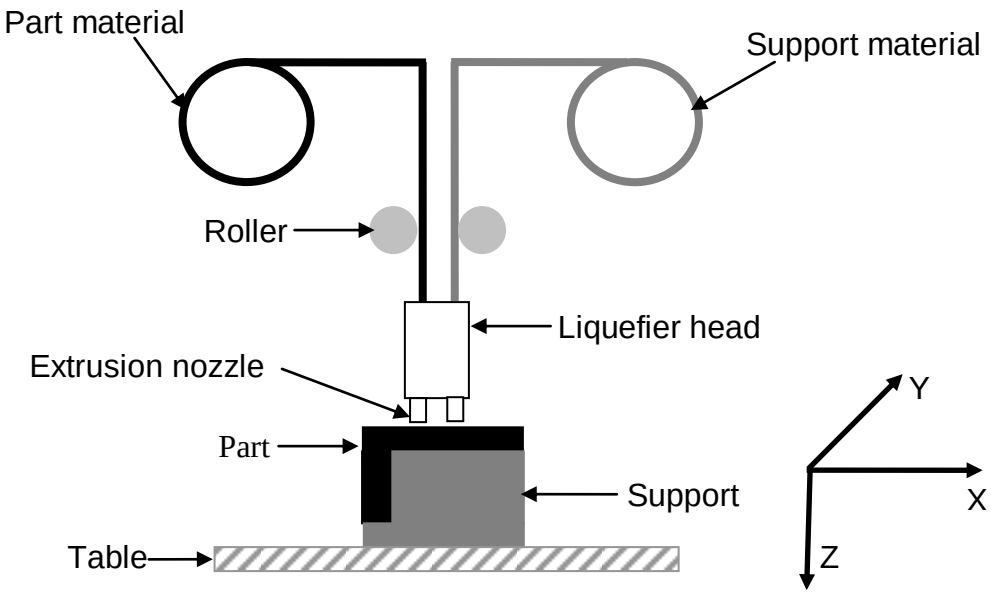

Figure 3.2 Schematic of fused deposition modelling

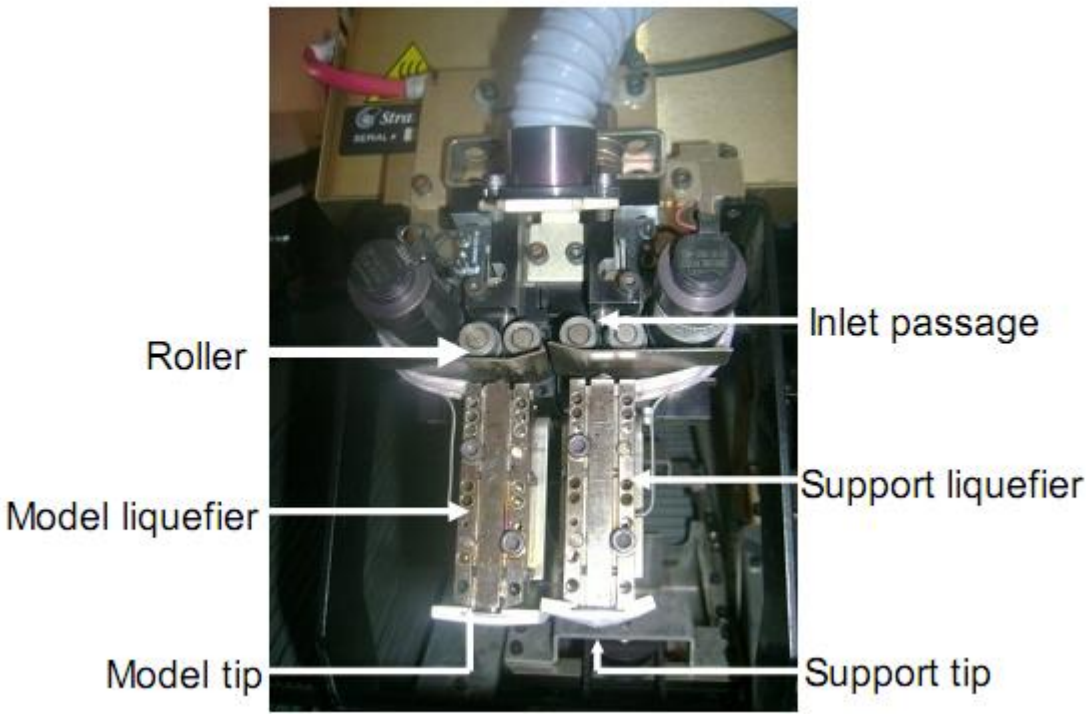

Figure 3.3 Head assembly

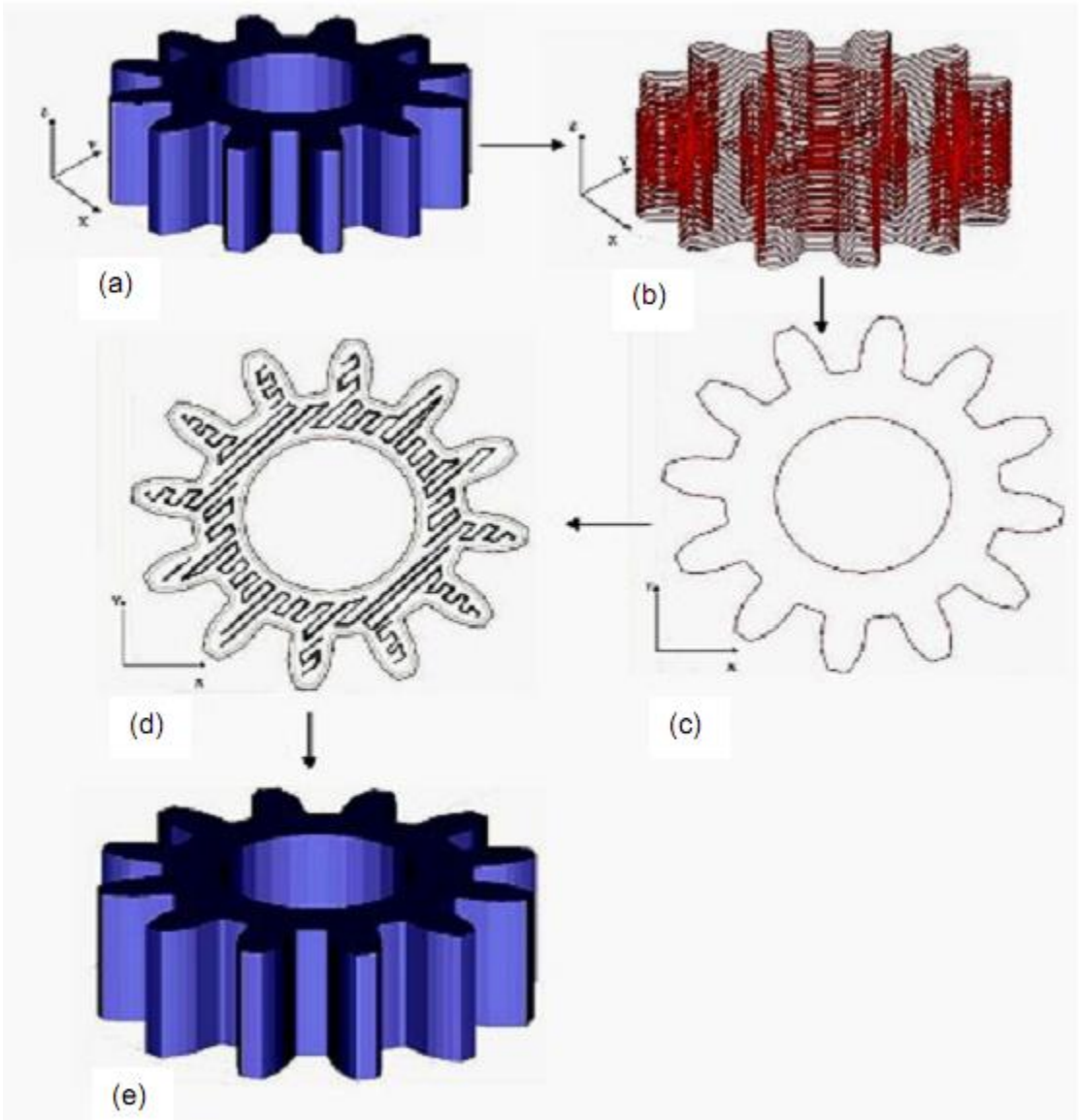

Figure 3.4 Steps involved in part fabrication (a) CAD model (STL format) (b) Sliced model (c) Outer contour generation (d) Raster filling of interior region (e) FDM part

3.4 Measurements

3.4.1 Dimensional accuracy

Test specimen employed for measuring dimensional accuracy is shown in Figure 3.5. Dimensions are measured using Mitutoyo vernier calliper having least count of 0.01mm. Vernier caliper is a precision instrument that can be used to measure internal and external distances accurately. For measurement purpose it has two jaws, external and internal jaws. External jaws are used to measure external dimensions like length, width and thickness. Internal jaws are used for measuring

internal dimensions of holes and cavities. Other then these two jaws there is depth measuring bar used for measuring the heights or depth. For measuring length (L), width (W) and thickness (T), the specimen to be measured is placed between external jaws and they are carefully brought together. For measuring hole diameter (d) internal jaws are adjusted carefully until they touch the internal surface of hole.

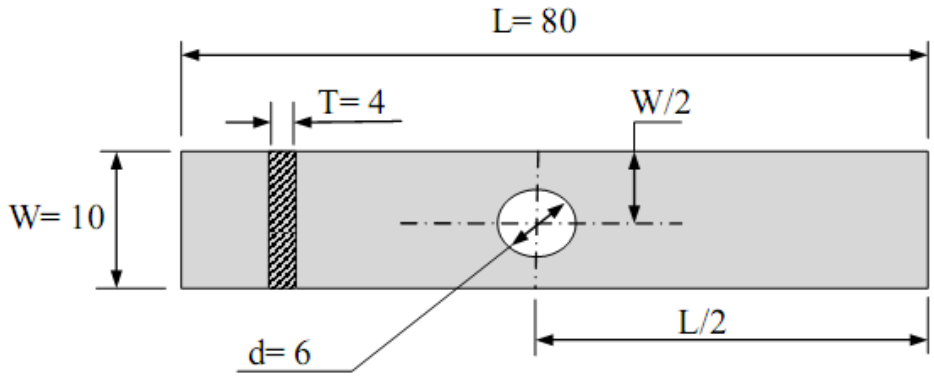

Figure 3.5 Test sample for dimensional analysis (all dimensions are in mm)

3.4.2 Surface roughness

Three readings of average surface roughness (R_a) on top, bottom and left side surface is taken for specimen shown in Figure 3.6. Mean of these three observations is taken as representative value of respective surface roughness. For measuring surface roughness, a contact type roughness tester, Hommel werke Turbo Wave V7.20 is used (Figure 3.7). The mechanical scanning of the surface roughness in the Hommel tester is based on the principle of an inductive distance sensor system. A diamond stylus mounted on a probe arm, which pivots perpendicular to the tracing level, is moved over the surface to be measured. There are two ferrite plates on the upper side of the probe arm. When the probe is in its neutral position, the distance between these plates and two coils in the probe housing is exactly defined. A sinus wave carrier voltage is applied to these coils. Deflection of the stylus due to movement over the rough surface causes change in the inductance of coils. The voltage changes are evaluated, transformed into a signal proportional to deflection, and displayed and logged as a surface dimension. The conditions used for roughness measurement are given in Table 3.2.

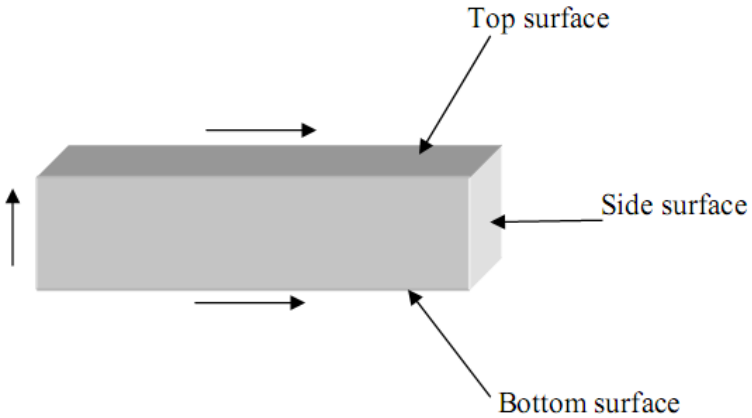

Figure 3.6 Test specimen for roughness measurement (arrow show direction of measurement of roughness)

Figure 3.7 Hommel Werke Turbo Wave V7.20 roughness tester

Table 3.2 Roughness measuring conditions

Condition	Value
Probe tip radius (TKU 300)	0.005 mm
Measuring range	80µm
Traverse length	4.8 mm
Speed	0.5 mm/s
Filter	ISO11562 [M1]

3.4.3 Tensile strength

Tensile strength at break is determined according to ISO R527:1966 (Plastics: Determination of tensile properties). Figure 3.8 shows the shape of the test specimen. The tensile tests were performed using Instron 1195 series IX automated material testing system (Figure 3.9) with crosshead speeds of 1mm/min.

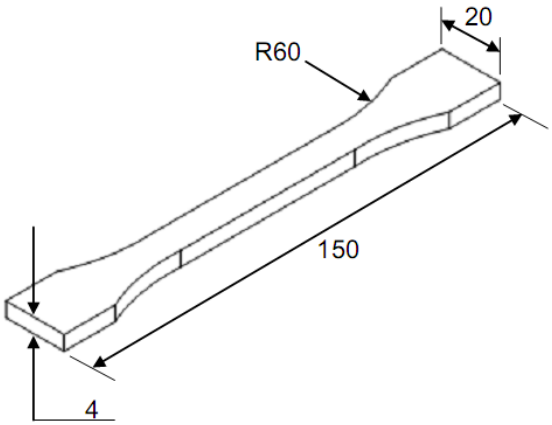

Figure 3.8 Tensile strength specimen (all dimensions are in mm)

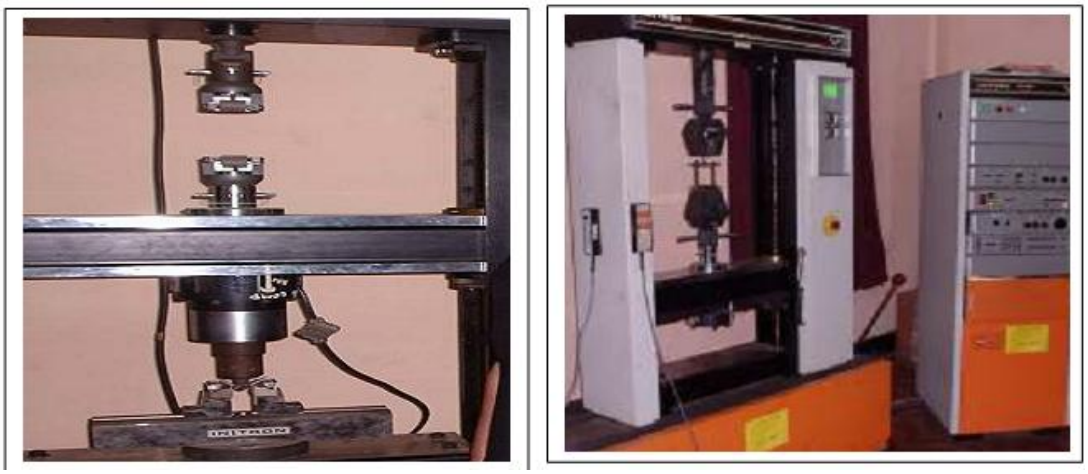
Figure 3.9 Photograph of Instron 1195 series IX machine

3.4.4 Flexural strength

Flexural strength at yield is determined as per ISO R178:1975 (Plastics – Determination of flexural properties of rigid plastics) standard for the specimen shown in Figure 3.10 using three-point bending test in Instron 1195 series IX automated material testing system (Figure 3.11) with crosshead speeds 2mm/min.

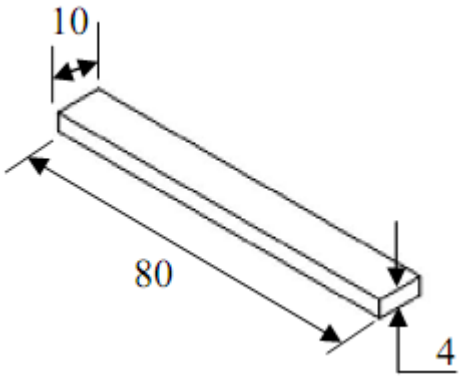

Figure 3.10 Flexural strength specimen (all dimensions are in mm)

Figure 3.11 Three point bend test

3.4.5 Impact strength

Charpy impact test performed in Instron Wolpert pendulum impact test machine (Figure 3.12) is used to determine the impact strength of specimen shown in Figure 3.13 in accordance with ISO 179:1982 (Plastics – Determination of charpy impact strength of rigid plastics). During impact testing, specimen is subjected to quick and intense blow by hammer pendulum striking the specimen with a speed of 3.8m/s. The impact energy absorbed is measure of the toughness of material and it is calculated by taking the difference in potential energy of initial and final position of

hammer. Impact energy is converted into impact strength using equation 3.1 for notched specimen.

$$\text{Impact strength} = \frac{A_K}{L1 \times L2} \tag{3.1}$$

where A_k is impact energy in joules, L1 and L2 are the dimensions of test specimen as explained in Figure 3.13.

Figure 3.12 Instron Wolpert pendulum impact test machine (arrow shows direction of impact)

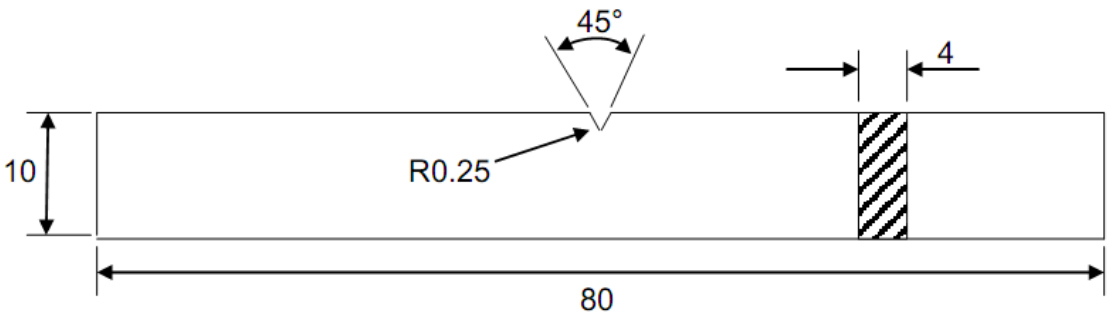

Figure 3.13 Impact strength specimen (all dimensions are in mm), Type A notch, L1=4, L2=0.8xL1

3.4.6 Compressive strength

Compressive strength at break is determined according to ISO604-1973 (Plastics-Determination of compressive properties) using Instron 1195 series IX automated material testing system with crosshead speed of 2mm/min and full scale load range of 50KN. Figure 3.14 shows the specimen for compressive strength.

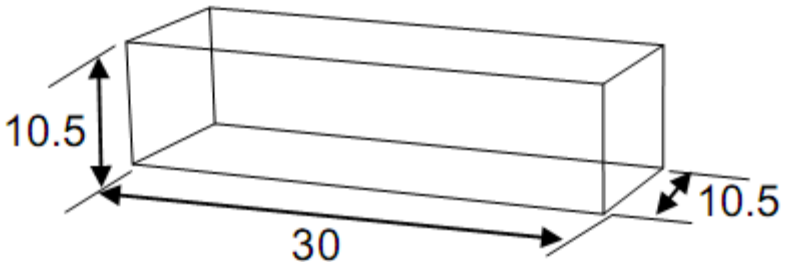

Figure 3.14 Compressive strength specimen (all dimensions are in mm)

3.47 Wear testing

For wear measurement sliding wear test is done using pin on disk apparatus (Ducom, TR-20LE-M5) shown in Figure 3.15 as per ASTM G99-04 (Standard test method for wear testing with pin on disk apparatus) standard. Test specimen for wear testing is shown in Figure 3.16. The material of disc is EN 31 hardened steel, hardness RC 62 and roughness (Ra) 0.32-0.35µm. For getting reliable and repeatable wear data, contact between the disc and the specimen is made 100% by the application of suitable load parallel to the axis of specimen and virgin material is exposed to the disc. The standard test parameters are given in Table 3.3.


Figure 3.15 Sliding wear test apparatus

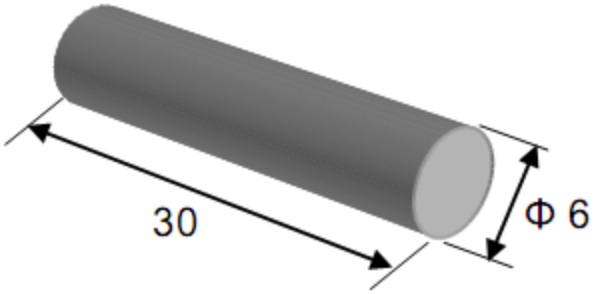

Figure 3.16 Test specimen for wear test (all dimensions are in mm)

Table 3.3 Wear test conditions

Test parameter	Value
Load	25N
Speed	1m/s
Contact path diameter	120mm
Test duration	25-30 minutes
Lubricant	Dry
Room temperature	23±2ºC
Relative humidity	50±5%
Atmosphere	Laboratory air

3.5 Scanning electron microscope

The surfaces of the specimens are examined directly by scanning electron microscope (SEM) JEOL JSM-6480LV as shown in Figure 3.17. The JEOL JSM-6480LV is a high-performance, scanning electron microscope with a high resolution of 3.0nm. The low vacuum (LV) mode (which can be accessed by the click of a mouse), allows for observation of specimens which cannot be viewed at high vacuum due to excessive water content or due to a non-conductive surface. Its asynchronous five-axis stage can accommodate a specimen of up to 8-inches in diameter.

Figure 3.17 Scanning Electron Microscope (SEM)

3.6 Design of Experiments

A commonly use approach in scientific and engineering investigation is to study one factor at a time or study several factors one at a time. This approach has inherent disadvantages like, more experimental runs are require for the precision in effect estimation, factor interaction effects cannot be studied, conclusions are not general and may miss the optimal settings of factor. To overcome this problem design of experiment (DOE) is a scientific approach to effectively plan and perform experiments, using statistics and are commonly used to improve the quality of a products or processes. Such methods enable the user to define and study the effect of every single condition possible in an experiment where numerous factors are involved [196, 197]. FDM is such a process in which a number of control factors collectively determine the performance output in other words the part quality. Hence, in the present work two statistical techniques called Taguchi method and response surface methodology are used to optimize the process parameters leading to the improvement in performance output of the part under study.

The most important stage in the DOE lies in the selection of the control factors and their levels. FDM process has large number of process related parameters which are defined in Table 3.4. Based on initial trials and exhaustive literature review [19, 21, 97-100, 147, 166, 175-178, 180-182, 186, 187] five parameters namely, layer thickness (A), orientation (B), raster angle (C), raster width (D), and air gap (E) are identified as significant factors and hence are selected to study their influence on output responses. The levels of factors are selected in accordance with the permissible minimum and maximum settings recommended by the equipment manufacturer, experience, and real industrial applications. The operating conditions under which tests are carried out are given in Table 3.5.

Table 3.4 Process parameters in FDM

Process parameter	Definition
Part fill style	Determines the fill pattern used to build a solid model. It is of two types: ➢ Perimeter/rasters: Creates a part fill consisting of a single outer contour and internal raster fill. ➢ Contours to depth: Fills the part with an outer contour, internal contours, and internal raster fills. The number of additional contours is determined by the depth of contours value
Contour width	The width of the contour tool path that surrounds each of the part curves. Every part curve is filled by using at least one contour.

Part interior style	Choose the manner in which part interior is filled. It is of three types: ➢ Solid normal: Fills the part completely. ➢ Sparse: Minimize the amount of material use. Utilizes a unidirectional rasters. ➢ Sparse double dense: minimizes the amount of model material used, but utilizes a crosshatch raster pattern (instead of uni-directional) for added strength.
Visible surface	The intent of this feature is to maintain part appearance while allowing for a coarser, faster fill. The default choice is Normal rasters.
Part XY shrinkage factor	The shrinkage factor applied in the XY plane.
Part Z shrinkage factor	The shrinkage factor applied in the Z direction.
Perimeter to raster air gap	The gap between the inner most contour and the edge of the raster fill inside of the contour.
Layer thickness	It is a thickness of layer deposited by nozzle and depends upon the type of nozzle used.
Orientation	Part build orientation or orientation refers to the inclination of part in a build platform with respect to X, Y, Z axis. X and Y-axis are considered parallel to build platform and Z-axis is along the direction of part build.
Raster angle	It is a direction of raster relative to the x-axis of build table.
Raster width	Width of raster pattern used to fill interior regions of part curves
Air gap	It is the gap between two adjacent rasters on same layer.

Table 3.5 Factors and their levels

Fixed Factors			Control Factors					
Factor	Value	Unit	Factor	Symbol	Level			Unit
					1	2	3	
					low level (-1)	centre level (0)	high level (+1)	
Part fill style	Perimeter Raster	-	Layer thickness	A	0.127	0.178*	0.254	mm
Contour width	0.4064	mm	Orientation	B	0	15	30	degree
Part interior	Solid normal	-	Raster angle	C	0	30	60	degree

style								
Visible surface	Normal raster	-	Raster width	D	0.4064	0.4564	0.5064	mm
XY & Z shrink factor	1.0038	-	Air gap	E	0	0.004	0.008	mm
Perimeter to raster air gap	0	mm						

* modified centre level value

3.6.1 Taguchi experimental design

Study of five factors at three levels requires 243 (3^5) experiments if classical DOE is used but same statistically valid results can be obtained if Taguchi method is adopted with lesser number of experiments [198, 199]. In Taguchi design, selection of orthogonal array is an important issue for obtaining valid conclusions. Since five factors each at three level and interaction of orientation with all the other factors are considered in this study, the total degree of freedom happens to be 26. The appropriate orthogonal array for this case is L_{27} (3^{13}). This array consists of 13 columns for assigning factors or interaction and 27 rows designating the trial or experiment conditions. To avoid the incorrect analysis, faulty conclusion and minimize the confounding effect of factors and interactions, assignment of factors and interactions is done as per the linear graph as shown in Figure 3.18.

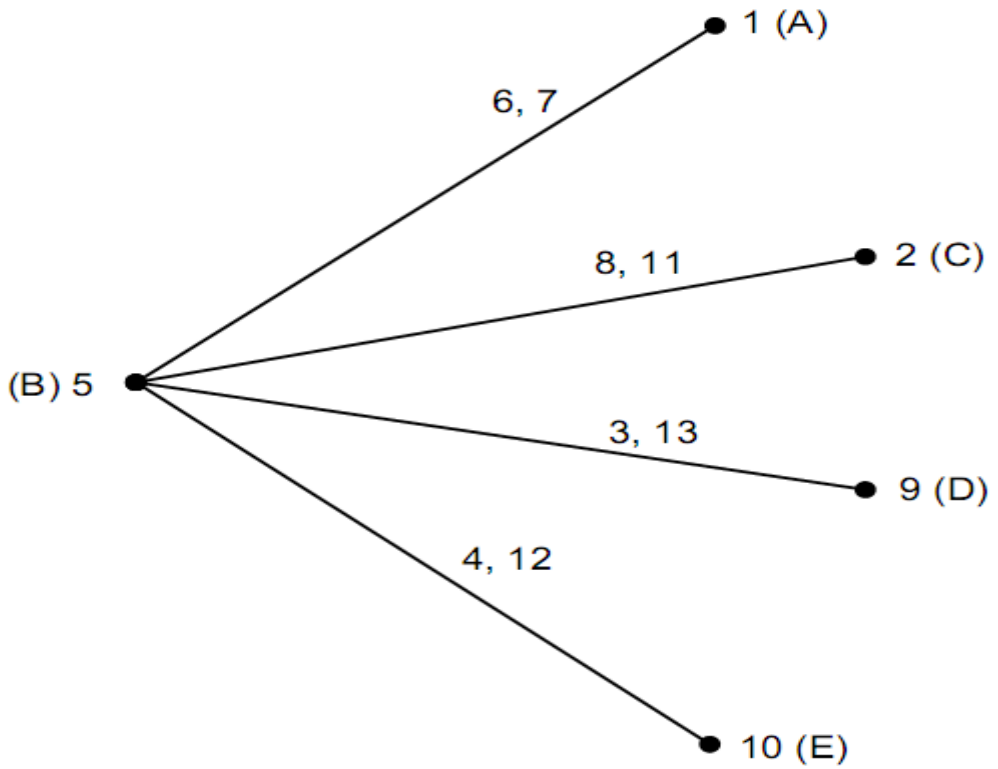

Figure 3.18 L_{27} Linear graph

Each dot in linear graph represents the factor column number and line joining two dots represents the interaction between the factors assigned to these columns.

Numbers on line shows the column number to which these interactions can be assigned. Interaction of orientation with all the other factors is considered so it is assign to column number 5. In order to change the layer thickness nozzle has to be changed. Frequent change of nozzles is time consuming and involves wastage of material. To prevent frequent change of nozzle, layer thickness is assigned to first column. Factor C is assigned to column 2, factor D is assigned to column 9 and factor E is assigned to column 10. The final L_{27} orthogonal array is shown in Table 3.6.

Table 3.6 L_{27} orthogonal array

Exp. No	Factors				
	A	B	C	D	E
1	1	1	1	1	1
2	1	2	1	2	2
3	1	3	1	3	3
4	1	1	2	2	2
5	1	2	2	3	3
6	1	3	2	1	1
7	1	1	3	3	3
8	1	2	3	1	1
9	1	3	3	2	2
10	2	1	1	2	3
11	2	2	1	3	1
12	2	3	1	1	2
13	2	1	2	3	1
14	2	2	2	1	2
15	2	3	2	2	3
16	2	1	3	1	2
17	2	2	3	2	3
18	2	3	3	3	1
19	3	1	1	3	2
20	3	2	1	1	3
21	3	3	1	2	1
22	3	1	2	1	3
23	3	2	2	2	1
24	3	3	2	3	2
25	3	1	3	2	1
26	3	2	3	3	2
27	3	3	3	1	3

3.6.2 Response surface experimental design

Response surface methodology (RSM) quantifies the relationship between the controllable input parameters and the obtained response. The goal is to find a suitable approximation for the true functional relationship between independent variables and the response. Usually a second-order model as given in equation 3.2 is utilized in response surface methodology.

$$y = \beta_0 + \sum_{i=1}^{k} \beta_i x_i + \sum_{i=1}^{k} \beta_{ii} x_i^2 + \sum_{i<j} \sum \beta_{ij} x_i x_j + \varepsilon \quad (3.2)$$

where ε is a random error. The β coefficients are obtained by the least square method.

A full factorial design would provide estimation of all the required regression parameters (β). However, full factorial designs are expensive to use as the number of runs increases rapidly with the number of factors. Therefore, for the purpose of analysis central composite design (CCD) is useful as it help to fit the second order model to the response with the use of a minimum number of runs [196, 197]. For k factors each at two level, the CCD consists of a 2^k factorial or fraction factorial with N runs, $2k$ axial or star runs and n_c centre runs. There are two variants of CCD available known as, spherical CCD and cubical CCD. Spherical CCD puts all the factorial and axial design points on the surface of sphere of radius $\alpha = \sqrt{k}$ and requires five levels of each factor. To reduce the number of levels due to machine constraints, well established cubical CCD known as face centred central composite design (FCCCD) in which α=1 is considered in present study. This design locates the axial points on the centres of the faces of cube and requires only three levels for each factor. Moreover, FCCCD does not require as many centre runs as spherical CCD. In practice, two or three centre runs are sufficient [196, 197]. In order to get a reasonable estimate of experimental error, six centre runs are chosen in the present work. To reduce the experiment run, half-factorial 2^k design (k factors each at two levels) is considered. Maximum and minimum value of each factor is coded into +1 and -1 respectively using equation 3.3 so that all input factors are represented in same range.

$$\begin{aligned} \xi_{ij} &= \left(\frac{x_{ij} - \bar{x}_i}{\Delta x_i}\right) \times 2 \\ \bar{x}_i &= \frac{\sum_{j=1}^{2} x_{ij}}{2} \\ \Delta x_i &= x_{i2} - x_{i1} \\ 1 \le i \le k,\ & 1 \le j \le 2 \end{aligned} \quad (3.3)$$

where ξ_{ij} and x_{ij} are coded and actual value of j^{th} level of i^{th} factor respectively and k is total number of factors.

Due to unavailability of nozzle corresponding to layer thickness value at centre level as indicated by equation 3.3, modified centre level value for layer thickness is taken. Half-factorial 2^5 unblocked design having sixteen experimental run, 10 ($2k$, where k=5) axial run and six centre run is shown in Table 3.7.

Table 3.7 Experimental plan for FCCCD runs

Run Order	Factor (Coded units)				
	A	B	C	D	E
1	-1	-1	-1	-1	+1
2	+1	-1	-1	-1	-1
3	-1	+1	-1	-1	-1
4	+1	+1	-1	-1	+1
5	-1	-1	+1	-1	-1
6	+1	-1	+1	-1	+1
7	-1	+1	+1	-1	+1
8	+1	+1	+1	-1	-1
9	-1	-1	-1	+1	-1
10	+1	-1	-1	+1	+1
11	-1	+1	-1	+1	+1
12	+1	+1	-1	+1	-1
13	-1	-1	+1	+1	+1
14	+1	-1	+1	+1	-1
15	-1	+1	+1	+1	-1
16	+1	+1	+1	+1	+1
17	-1	0	0	0	0
18	+1	0	0	0	0
19	0	-1	0	0	0
20	0	+1	0	0	0
21	0	0	-1	0	0
22	0	0	+1	0	0
23	0	0	0	-1	0
24	0	0	0	+1	0
25	0	0	0	0	-1
26	0	0	0	0	+1
27	0	0	0	0	0
28	0	0	0	0	0
29	0	0	0	0	0
30	0	0	0	0	0
31	0	0	0	0	0
32	0	0	0	0	0

The assumptions made in model building are listed as (i) Out of many FDM process related parameters, only five important parameters are considered (ii) There exist non-linear relation among parameters themselves and with responses (iii) Analysis of results is performed at 95% of confidence level (iv) Standard specimen and test conditions are used (v) Standard statistical procedure is adopted for model building. Standard statistical tests like analysis of variance (ANOVA), t-test and Anderson darling tests are performed to validate the test results [196, 197].

3.7 Conclusions

This chapter summarizes the material and methods uses in the present study. The next chapter outlines study on effect of processing parameters on dimensional accuracy of the test parts.

CHAPTER 4

IMPROVEMENT OF DIMENSIONAL ACCURACY

4.1 Introduction

This chapter presents experimental investigations on the influence of important process parameters such as layer thickness (A), part orientation (B), raster angle (C), air gap (D) and raster width (E) along with their interactions on dimensional accuracy of Fused Deposition Modelling (FDM) processed ABSP400 (acrylonitrile-butadiene-styrene) part. Taguchi's parameter design, being a simple and inexpensive method, is adopted to understand effect of process parameters and their interaction on accuracy of dimensions in different directions of FDM built parts with minimum experimental runs [196]. Conventional Taguchi method can effectively establish optimal parameter settings for a single performance characteristic. When multiple performance characteristics with conflicting goals are considered, the approach becomes unsuitable [200, 201]. The multiple performance measures considered in this work are relative change in length (ΔL), width (ΔW), thickness (ΔT) and diameter of hole (Δd). All of these dimensions can be combined together into a single representative unit that is volume and change in volume can be minimized. The main disadvantage of this approach is that it may be possible that some dimensions show large deviation and some may show small deviation from the desired values. The combined effect may decrease change in volume. But actual fabrication of part should be made in such a manner that all dimensions show minimum deviation from desired value simultaneously at a common factor level setting. Grey based Taguchi method has the ability to combine all the objectives into single representative unit and find the factor levels which satisfy all the considered objectives simultaneously [202, 203]. For this purpose, a grey based Taguchi method is exploited in this work to convert different performance characteristics into a single equivalent response known as grey relational grade (GRG). All the responses need to be individually minimized whereas overall GRG is maximized.

As FDM process involves large number of conflicting factors and complex phenomena for building parts, it is difficult to predict the output characteristics accurately through mathematical equations. Hence, there is a need for a better prediction tool to supplement the experiments. Over last two decades, different modeling methods like artificial neural networks (ANNs) [204, 205] and fuzzy inference system (FIS) [206, 207] have been used by many researchers for a variety of engineering applications. ANNs are a family of massively parallel architectures that solve difficult problems via cooperation of highly interconnected but simple computing elements (or artificial neurons) arranged in layers. This technique is especially valuable in processes where a complete understanding of the physical mechanisms

is difficult. On the other hand, theory of fuzzy logics, proposed by Zadeh in 1965, can be viewed as a prominent tool for handling types of uncertainty in decision making. It may be viewed as an attempt to converse, reason, and make rational decisions in an environment of imperfect information [208]. In the present study, predictive models based on fuzzy logic and artificial neural network have been presented for improving the dimensional accuracy of FDM built parts subjected to different operating conditions. Taguchi's orthogonal array (OA) used for experimental data collection in a systematic fashion helps not only to reduce experimental runs but also develop valid ANN and FIS models conveniently. The models are expected to perform better compared to additive models generated in Taguchi method because non-linearity is not considered in Taguchi's predictive model. Finally, a comparative study of effectiveness of both the models has been made.

4.2 Methodology

Specimens shown in Figure 3.5 are fabricated in FDM vantage SE machine as per Taguchi experimental plan as discussed in sub-section 3.6.1. Three readings of length (L), width (W), thickness (T) and diameter (d) of circular through hole are taken per sample and mean is taken as representative value for each of these dimensions. Relative change in dimensions is calculated as per equation 4.1.

$$\Delta X = \left| \frac{X - X_{CAD}}{X_{CAD}} \right| \tag{4.1}$$

where X represents measured value of dimension, X_{CAD} represents the respective CAD model value, ΔX represents relative change in X.

Signal to noise (S/N) ratio is used to determine the influence and variation caused by each factor and interaction relative to the total variation observed in the result. The advantage of using S/N ratio lies in the fact that it takes into account both the effect of change in mean and variation (variance) with equal priority using a single measure known as mean square deviation (MSD). Analysis using the S/N ratio provides guidelines to select the optimum factor level based on least variation around the target and also on the average value closest to the target [199]. Objective of experiment plan is to reduce the relative change in length (ΔL), width (ΔW), thickness (ΔT) and diameter (Δd) as small as possible. Therefore "smaller the better" quality characteristic is considered. For "smaller the better" quality characteristic, S/N ratio (η) is expressed by equation 4.2 [198].

$$\eta = 10\log_{10}(\text{MSD})$$
$$\text{MSD} = \sigma^2 + (Y_{avg} - Y_o)^2 \quad (4.2)$$

where σ^2 is called variance, Y_{avg} is average value for data points and Y_o is a target value (zero in this case).

Experiment analysis is made using Minitab R14 software. Main effect plot for S/N ratio is used to predict the optimum factor level. Relative influence of each factor and interaction is determined by ANOVA. Calculations needed for ANOVA are shown in equation 4.3-4.6 [198].

$$S_T = \sum_{i=1}^{N} (\eta_i - \bar{\eta})^2 \quad (4.3)$$

where S_T is a total sum of square, N is total number of observation and $\bar{\eta}$ is the overall mean of S/N ratio.

$$SS_j = \sum_{i=1}^{I} (\eta_{ji} - \bar{\eta})^2 \quad (4.4)$$

where SS_j is sum of square deviation of j^{th} factor, i is level of j^{th} factor.

$$V_j = \frac{SS_j}{f_j} \quad (4.5)$$

V_j and f_j is variance and degree of freedom respectively of j^{th} parameter.

$$F_j = \frac{V_j}{V_e} \quad (4.6)$$

F_j is F-statistic of j^{th} factor and V_e is variance of error.

If error degree of freedom becomes zero then it is not possible to calculate F-value and analysis of variance (ANOVA) cannot be carried out. In such cases, factors and interactions having small sum of squares are pooled together to represent error sum of squares [199]. Significance of factor and interaction is determined by comparing calculated F-value with standard F-value at a particular confidence level (95% in present study). Once the significant factors and interactions are identified, the final step is to predict and verify improvements in observed values through the use of factor level combination as given in equation 4.7 [198].

$$\eta_{pre} = \bar{\eta} + (\bar{A}_i - \bar{\eta}) + (\bar{B}_j - \bar{\eta}) + (\bar{C}_k - \bar{\eta}) + (\bar{D}_m - \bar{\eta}) + (\bar{E}_n - \bar{\eta})$$
$$+ [(\bar{A}_i \bar{B}_j - \bar{\eta}) - (\bar{A}_i - \bar{\eta}) - (\bar{B}_j - \bar{\eta})]$$
$$+ [(\bar{B}_j \bar{C}_k - \bar{\eta}) - (\bar{B}_j \quad \bar{\eta}) - (\bar{C}_k \quad \bar{\eta})] \qquad (4.7)$$
$$+ [(\bar{B}_j \bar{D}_m - \bar{\eta}) - (\bar{B}_j - \bar{\eta}) - (\bar{D}_m - \bar{\eta})]$$
$$+ [(\bar{B}_j \bar{E}_m - \bar{\eta}) - (\bar{B}_j \quad \bar{\eta}) - (\bar{E}_m \quad \bar{\eta})]$$

η_{pre} is predicted S/N ratio value of response, $\bar{\eta}$ is overall experimental average, $\bar{A}_i, \bar{B}_j, \bar{C}_k, \bar{D}_m, \bar{E}_n$ are average response for factor A, B, C, D, E at respective level *i*, *j*, *k*, *m*, *n* (*i*, *j*, *k*, *m*, *n* = 1, 2, 3) respectively. Factors and interactions which are insignificant are usually omitted from equation 4.7 [198, 199].

Four performance measures such as relative change in length, width, thickness and diameter of hole are considered with an aim to minimize all responses simultaneously at the single factor level setting. However, the Taguchi method is best suited for optimization of a single performance characteristic whereas grey based Taguchi (Grey Taguchi) combines all performance characteristics (objectives) considered in the study into a single value that can be used as the single characteristic in optimization problems. Grey Taguchi method is based on grey system theory proposed by Professor Deng Ju-long from China in the year 1980 and provides approaches for analysis and abstract modelling of systems for which the information is limited, incomplete and characterised by random uncertainty [209, 210]. Grey relational analysis (GRA) is an impacting measurement method in grey theory that analyzes uncertain relations among factors and interactions in a given system. It is actually a measurement of the absolute value of the data difference between sequences and it could be used to measure the approximate correlation between sequences. The steps involved in GRA are [202, 209, 210]:

4.2.1 Grey relational generation

When the units in which performances are measured are different for different attributes, the influence of some attributes may be neglected. This may also happen if performance measures of some attributes have a large range. In addition, if the goals and directions of these attributes are different, this will cause incorrect results in the analysis. It is thus necessary that all attributes must have the same measurement scale. Therefore, normalization of data is done so as to process all performance values for every alternative into a comparability sequence. This process is called grey relational generation. There are three different types of grey relational generation as discussed below.

4.2.1.1 Larger the better

If the target value of original sequence is infinitely large then it has a characteristic of the "the-larger-the-better". The normalized experimental results for the larger the better characteristic can be expressed as [202]:

$$x_{ij} = \frac{y_{ij} - min_j(y_{ij})}{max_j(y_{ij}) - min_j(y_{ij})} \tag{4.8}$$

4.2.1.2 Smaller the better

When the target value of original sequence is infinitely small then it has a characteristic of the "the-smaller-the better". The normalized smaller the better characteristic is expressed as [202]:

$$x_{ij} = \frac{max_j(y_{ij}) - y_{ij}}{max_j(y_{ij}) - min_j(y_{ij})} \tag{4.9}$$

4.2.1.3 Nominal the best

When the target value is closer to desired value the normalization is done as [202]:

$$x_{ij}=1-\frac{\left|y_{ij}-y_j^*\right|}{max\{[max_j(y_{ij})-y_j^*],[y_j^*-min_j(y_{ij})]\}} \tag{4.10}$$

y_{ij} is the original sequence for the i^{th} experimental results in the j^{th} experiment, x_{ij} is the sequence after the data pre-processing and y_j^* is target value, *max* and *min* stands for maximum and minimum values respectively.

Application of grey relational generation procedure to original data results in all performance values scaled into [0, 1].

4.2.2 Grey relational coefficient calculation

For an attribute *j* of alternative *i,* if the value of x_{ij} that has been found out to be equal to one or nearer to one during grey relational generation then alternative *i* is the best choice for attribute *j*. However, this kind of alternative does not usually exist. Thus, an ideal sequence known as, reference sequence with each element x_{ij}^o equal to one is assumed. The grey relational coefficient is used to determine how close x_{ij} is to x_{ij}^o. If grey relational coefficient is larger, x_{ij} is close to x_{ij}^o. The grey relational coefficients can be calculated as [202]

$$\begin{aligned}
&\gamma(x_j^o, x_{ij}) = \frac{\Delta_{min} + \zeta\Delta_{max}}{\Delta_{ij} + \zeta\Delta_{max}} \\
&\Delta_{ij} = \left|x_j^o - x_{ij}\right| \\
&\Delta_{min} = min\{\Delta_{ij},\ i = 1,2,...,m;\ \ j = 1,2,...,n\} \\
&\Delta_{max} = max\{\Delta_{ij},\ i = 1,2,...,m;\ \ j = 1,2,...,n\}
\end{aligned} \tag{4.11}$$

where $\gamma(x_j^o, x_{ij})$ is the grey relational coefficient between x_{ij} and x_j^o and $\zeta \in [0,1]$ is called distinguishing coefficient. The purpose of distinguishing coefficient is to expand or compress the range of the grey relational coefficient. The distinguishing coefficient can be selected by judgement of the decision maker and different distinguishing coefficients usually provide different results in grey relational analysis.

4.2.3 Grey relational grade (GRG) calculation

GRG represents the level of correlation between the reference sequence and the comparability sequence. After calculating the entire grey relation coefficients $\gamma(x_j^0, x_{ij})$, the GRG can be calculated using equation 4.12 [202].

$$\Gamma(x^o, x_i) = \sum_{j=1}^{n} w_j \gamma(x_j^o, x_{ij})$$
$$\sum_{j=1}^{n} w_j = 1 \qquad (4.12)$$

where Γ is the grey relational grade between x^0 and x_i . w_j is the weight of attribute j that usually depends on decision makers' judgments or the structure of the proposed problem. In this work, weights for relative change in length, width, thickness, and diameter of hole are taken as 0.25 (equal weights).

If a comparability sequence for an alternative gets the highest grey relational grade, it will be more similar to reference sequence and that alternative would be best choice. Once the multiple responses are converted to single response (GRG), it is maximized using standard Taguchi procedure. Figure 4.1 gives the flow chart of proposed Grey Taguchi method.

4.3 Results

Measured values show that there is shrinkage in length, width and diameter of hole but thickness is always more than the computer aided design (CAD) model value. Change in dimension is calculated as per equation 4.1 and results are shown in Table 4.1. Experimental data on change in dimension is converted into S/N ratio value as shown in Table 4.2 using equation 4.2 for "the-smaller-the-better" quality characteristic.

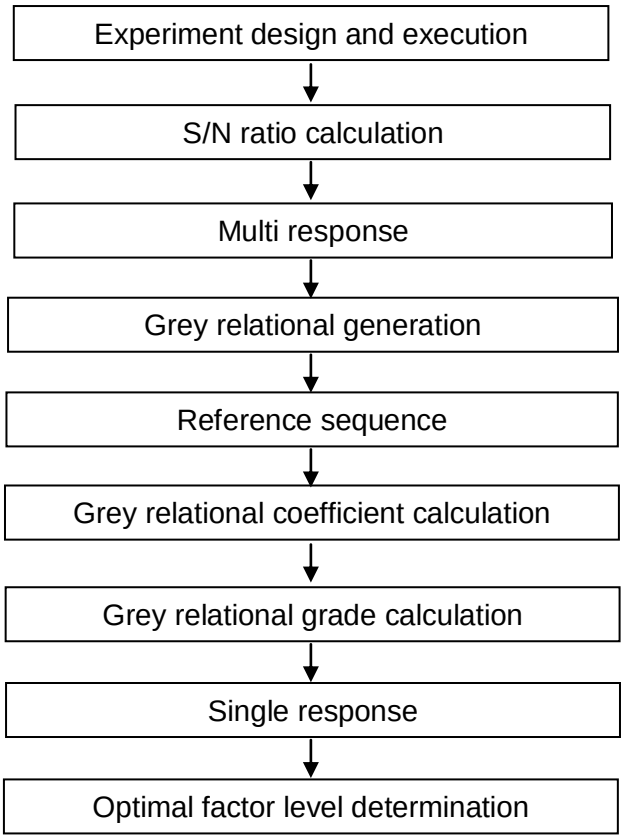

Figure 4.1 Procedure for Grey based Taguchi method

Table 4.1 L_{27} Orthogonal array with change in dimension

Exp. No	Factors					Change in dimension			
	A	B	C	D	E	ΔL	ΔW	ΔT	Δd
1	1	1	1	1	1	0.057500	0.600000	2.9167	0.990370
2	1	2	1	2	2	0.120000	0.433333	3.9167	0.993889
3	1	3	1	3	3	0.106667	0.833333	2.5833	0.991852
4	1	1	2	2	2	0.048333	0.733333	2.6667	0.989907
5	1	2	2	3	3	0.190833	0.500000	3.8333	0.991111
6	1	3	2	1	1	0.176667	0.433333	2.6667	0.989259
7	1	1	3	3	3	0.028333	0.533333	3.1667	0.989907
8	1	2	3	1	1	0.137500	0.666667	4.0000	0.989722
9	1	3	3	2	2	0.117500	0.633333	3.7500	0.988519
10	2	1	1	2	3	0.012500	0.200000	2.6667	0.991481
11	2	2	1	3	1	0.033333	0.766667	4.3333	0.989722
12	2	3	1	1	2	0.070000	0.500000	4.5000	0.991019
13	2	1	2	3	1	0.096667	0.366667	3.6667	0.989722
14	2	2	2	1	2	0.140833	0.433333	4.8333	0.989444
15	2	3	2	2	3	0.132500	0.366667	4.5000	0.991296
16	2	1	3	1	2	0.075833	0.366667	3.0000	0.992593
17	2	2	3	2	3	0.091667	0.666667	4.2500	0.991111
18	2	3	3	3	1	0.047500	0.366667	3.6667	0.992222
19	3	1	1	3	2	0.071667	0.120000	6.5833	0.997963
20	3	2	1	1	3	0.063333	0.420000	9.5833	0.992963
21	3	3	1	2	1	0.149167	0.240000	9.4167	0.988889
22	3	1	2	1	3	0.041667	0.180000	8.6667	0.996852
23	3	2	2	2	1	0.035833	0.400000	10.5000	0.994352
24	3	3	2	3	2	0.121667	0.300000	6.4167	0.990185
25	3	1	3	2	1	0.025000	0.280000	6.5833	0.993611
26	3	2	3	3	2	0.060833	0.400000	8.5833	0.996944
27	3	3	3	1	3	0.025833	0.400000	7.6667	0.988981

Table 4.2 L_{27} Orthogonal array with S/N ratio data

Exp. No	Factors					S/N ratio			
	A	B	C	D	E	ΔL	ΔW	ΔT	Δd
1	1	1	1	1	1	24.8066	4.4370	-9.29770	0.084047
2	1	2	1	2	2	18.4164	7.2636	-11.8583	0.053243
3	1	3	1	3	3	19.4394	1.5836	-8.24360	0.071064
4	1	1	2	2	2	26.3151	2.6940	-8.51940	0.088109
5	1	2	2	3	3	14.3869	6.0206	-11.6715	0.077553
6	1	3	2	1	1	15.0569	7.2636	-8.51940	0.093798
7	1	1	3	3	3	30.9540	5.4600	-10.0120	0.088109
8	1	2	3	1	1	17.2339	3.5218	-12.0412	0.089734
9	1	3	3	2	2	18.5992	3.9674	-11.4806	0.100304
10	2	1	1	2	3	38.0618	13.979	-8.51940	0.074308
11	2	2	1	3	1	29.5424	2.3079	-12.7364	0.089734
12	2	3	1	1	2	23.0980	6.0206	-13.0643	0.078365
13	2	1	2	3	1	20.2945	8.7146	-11.2854	0.089734
14	2	2	2	1	2	17.0259	7.2636	-13.6849	0.092172
15	2	3	2	2	3	17.5557	8.7146	-13.0643	0.075930
16	2	1	3	1	2	22.4028	8.7146	-9.5424	0.064579
17	2	2	3	2	3	20.7558	3.5218	-12.5678	0.077553
18	2	3	3	3	1	26.4661	8.7146	-11.2854	0.067821
19	3	1	1	3	2	22.8937	18.416	-16.3689	0.017712
20	3	2	1	1	3	23.9674	7.5350	-19.6303	0.061339
21	3	3	1	2	1	16.5266	12.396	-19.4779	0.097050
22	3	1	2	1	3	27.6042	14.894	-18.7570	0.027388
23	3	2	2	2	1	28.9143	7.9588	-20.4238	0.049198
24	3	3	2	3	2	18.2966	10.458	-16.1462	0.085672
25	3	1	3	2	1	32.0412	11.057	-16.3689	0.055671
26	3	2	3	3	2	24.3172	7.9588	-18.6731	0.026581
27	3	3	3	1	3	31.7564	7.9588	-17.6921	0.096237

Data analysis is made using Minitab R14 software at 95% of confidence level. Relative influence of factors and interactions is determined by ANOVA. The total degree of freedom of five factors each at three level and four interaction terms is twenty six which is same as experimental degree of freedom and hence F-value cannot be calculated as variance of error term is undefined. Therefore, percentage contribution of each term defined as ratio of sum of squares of the term to the total sum of square is calculated. The terms having small percentage contributions are considered as insignificant and are pooled from ANOVA table. ANOVA results are presented in Table 4.3, Table 4.4, Table 4.5 and Table 4.6 for ΔL, ΔW, ΔT and Δd respectively. For minimizing each response, main effect plot for S/N ratio (Figure 4.2) give different factor levels as shown in Table 4.7.

Table 4.3 ANOVA Table for ΔL

Source	Degree of freedom	Sum of square	Variance	F-value	Percentage contribution
A	2	100.486	50.243	2.762413	10.68
B	2	224.957	112.478	6.184159	23.91
C	2	95.084	47.542	2.613909	10.11
D[a]		12.152			
E[a]		61.578			
AXB[a]		68.18			
BXC[a]		76.347			
BXD	4	168.206	42.052	2.312063	17.88
BXE	4	133.928	33.482	1.840876	14.23
Error	12	218.257	18.18808		
Total	26	940.917			

[a] pooled

Table 4.4 ANOVA Table for ΔW

Source	Degree of freedom	Sum of square	Variance	F-value	Percentage contribution
A	2	177.304	88.652	22.73795	42.87
B	2	69.176	34.588	8.871318	16.73
C[a]		12.685			
D[a]		0.864			
E[a]		2.266			
AXB	4	65.842	16.46	4.22175	15.92
BXC[a]		29.816			
BXD[a]		8.953			
BXE	4	46.636	11.659	2.990363	11.28
Error	14	54.584	3.898857		
Total	26	413.541			

[a] pooled

Table 4.5 ANOVA Table for ΔT

Source	Degree of freedom	Sum of square	Variance	F-value	Percentage contribution
A	2	322.492	161.246	291.0578	83.19
B	2	33.962	16.981	30.6516	8.76
C[a]		0.529			
D[a]		2.520			
E[a]		0.248			
AXB	4	5.951	1.488	2.6859	1.54
BXC	4	5.645	1.488	2.6859	1.46
BXD	4	14.084	3.521	6.3556	3.63
BXE[a]		2.243			
Error	10	5.540	0.554		
Total	26	387.675			

[a] pooled

Table 4.6 ANOVA Table for Δd

Source	Degree of freedom	Sum of square	Variance	F-value	Percentage contribution
A	2	106.302	53.151	12.1749	28.93
B	2	50.156	25.078	5.7444	13.65
C[a]		4.477			
D[a]		14.665			
E	2	25.273	12.637	2.8946	6.88
A*B	4	109.169	27.292	6.2515	29.71
B*C[a]		15.783			
B*D	4	20.695	5.174	1.1851	5.63
B*E	4	20.974	5.244	1.2012	5.71
Error	8	34.925	4.366		
Total	26	367.494			

[a] pooled

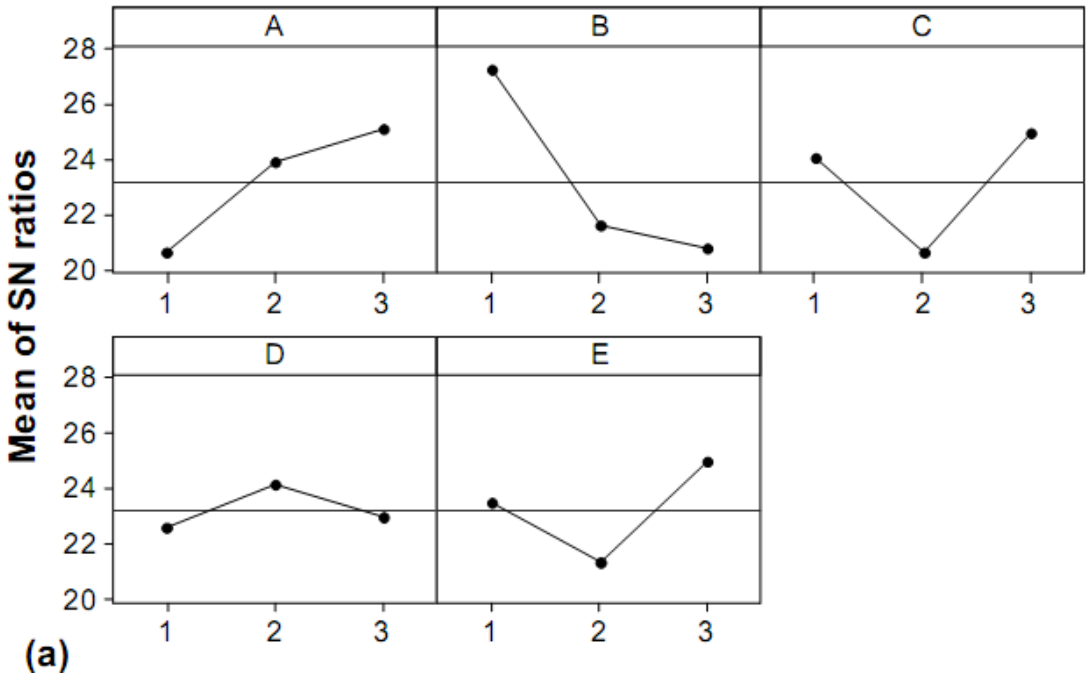

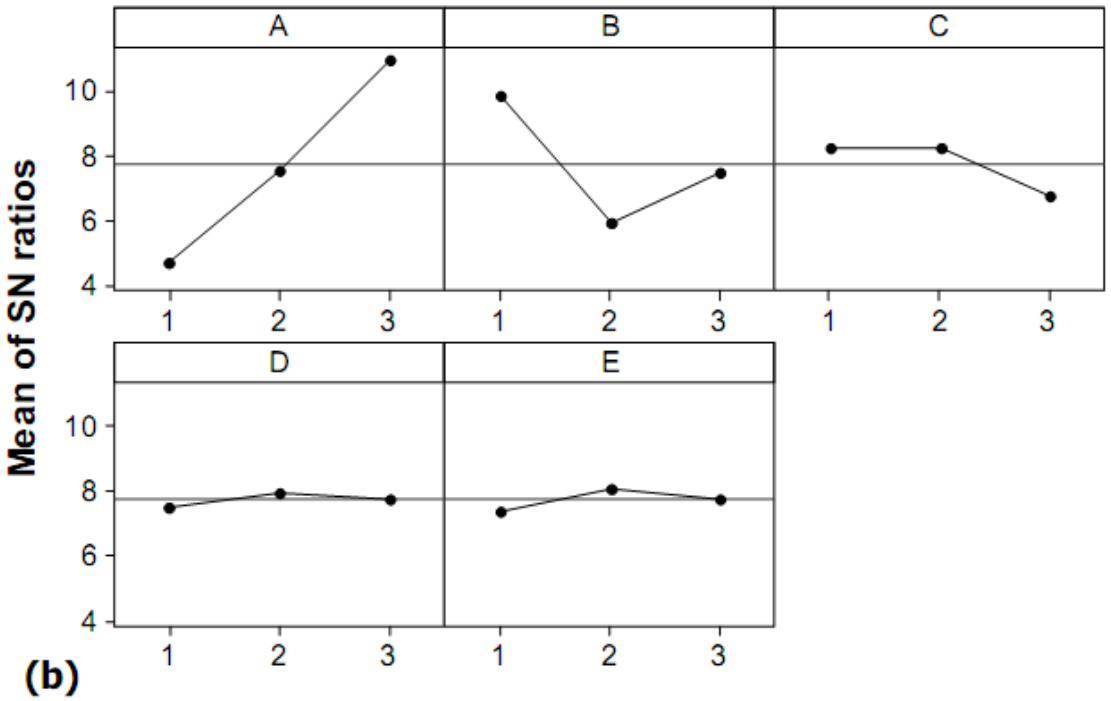
A
B
C
D
E
Mean of SN ratios
10
8
6
4
1
2
3

(b)

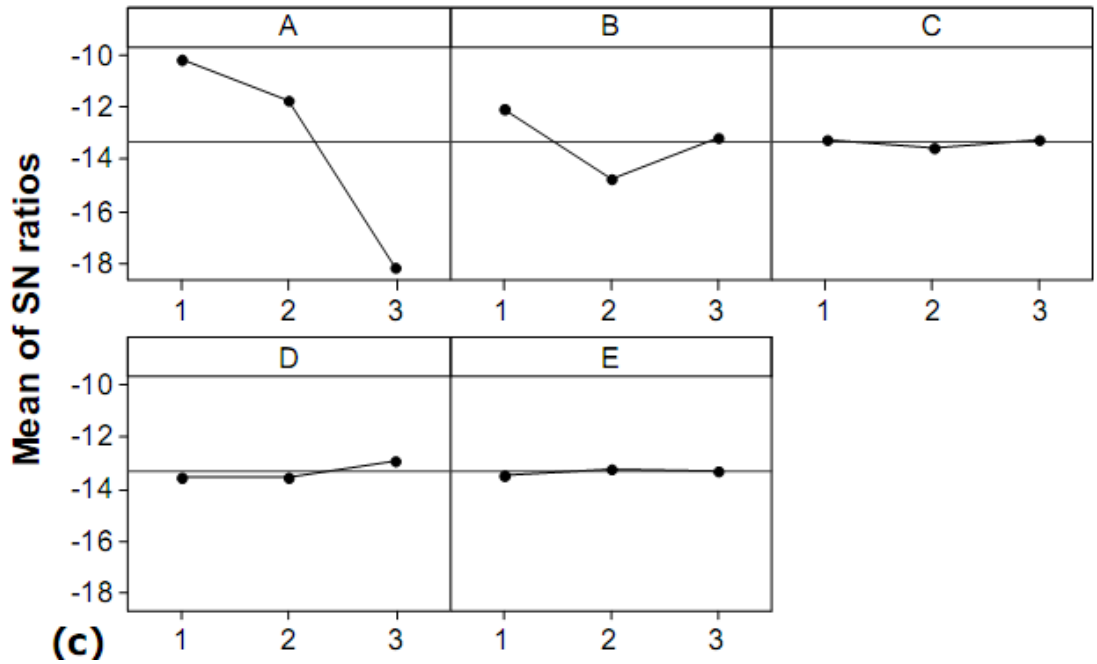
A
B
C
D
E
Mean of SN ratios
-10
-12
-14
-16
-18
1
2
3

(c)

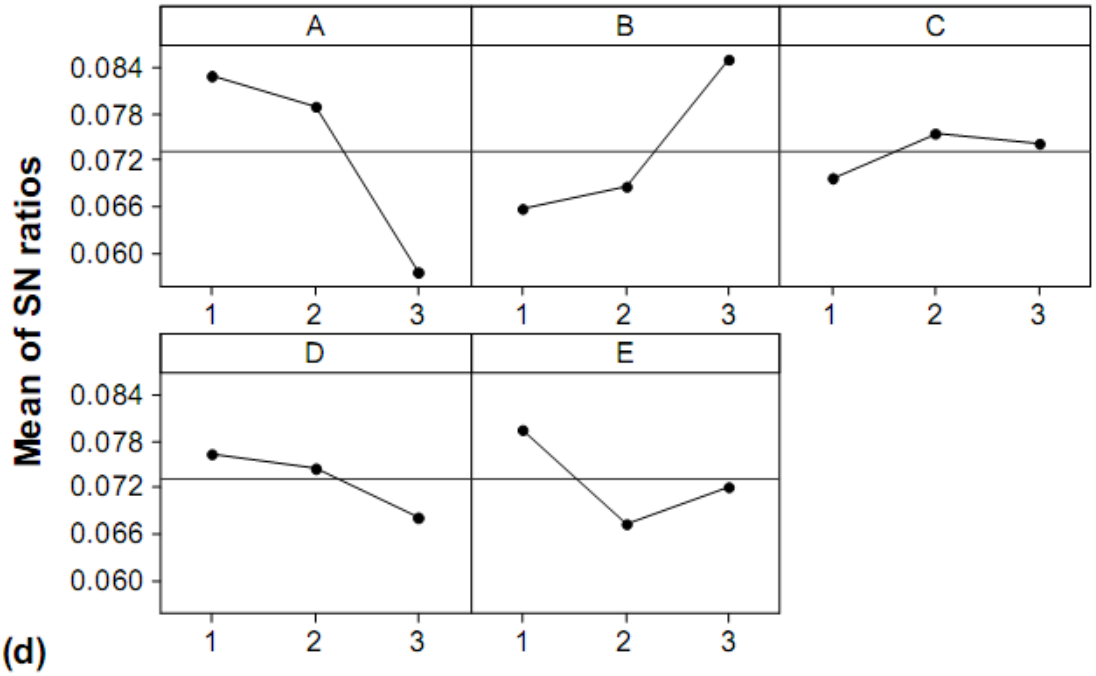

Figure 4.2 Main effect plot of (a) ΔL (b) ΔW (c) ΔT (d) Δd for S/N ratio (smaller the better)

Table 4.7 Optimum factor level with significant factors and interactions

Factor	ΔL	ΔW	ΔT	Δd
A	3	3	1	1
B	1	1	1	3
C	3	2	1	2
D	2	2	3	1
E	3	2	2	1
Significant	A,B,C,BXD,BXE	A,B,AXB,BXE	A,B,AXB,BXC,BXD	A,B,E,AXB,BXD,BXE

For confirming the results of Taguchi analysis, confirmation experiments are conducted for each response at optimum factor levels mentioned in Table 4.7. Table 4.8 presents the comparison of results of confirmation experiments and those predicted by Taguchi model given by equation 4.7. The small error between the predicted and experimental values for ΔL, ΔW, ΔT and Δd respectively proves the suitability of resulting model.

Table 4.8 Confirmation experiment result

Response	S/N ratio		Error
	Predicted	Experimental	
ΔL	40.75	39.81	2.3%
ΔW	14.91	14.61	2.0%
ΔT	-9.07	-8.88	2.1%
Δd	0.094	0.093	1.5%

From Table 4.3 to Table 4.6, it is observed that significant factor and interactions are different for different dimensions. Further, optimum factor levels are different for each dimension (Table 4.7). Therefore, all the responses are converted into grey relational grade using Grey based Taguchi method for overall dimensional accuracy improvement of the part. To achieve this, ΔL, ΔW, ΔT and Δd is taken as input to the grey Taguchi method. Grey relational generation is calculated using equation 4.9 as all the four performance characteristics considered are smaller the better type and results are shown in Table 4.9. Grey relation coefficient is calculated using equation 4.11 taking distinguishing coefficient as 0.5. For grey relation grade calculation using equation 4.12, equal weights for all the performance characteristics are considered. Results of grey Taguchi method are shown in Table 4.10.

Table 4.9 Result of Grey relational generation

Exp. No.	Grey relation generation			
	ΔL	ΔW	ΔT	Δd
1	0.747663	0.327102	0.957886	0.804003
2	0.397195	0.560748	0.831571	0.431385
3	0.471960	0.000000	1.000000	0.647078
4	0.799067	0.140187	0.989465	0.853028
5	0.000000	0.467289	0.842106	0.725540
6	0.079436	0.560748	0.989465	0.921643
7	0.911217	0.420561	0.926308	0.853028
8	0.299064	0.233644	0.821049	0.872618
9	0.411214	0.280374	0.852628	1.000000
10	1.000000	0.88785	0.989465	0.686362
11	0.883179	0.093457	0.778948	0.872618
12	0.677569	0.467289	0.757892	0.735282
13	0.528035	0.654205	0.86315	0.872618
14	0.280374	0.560748	0.715791	0.902054
15	0.327102	0.654205	0.757892	0.705951
16	0.644861	0.654205	0.947364	0.568615
17	0.556072	0.233644	0.78947	0.725540
18	0.803738	0.654205	0.86315	0.607899
19	0.668222	1.000000	0.494739	0.000000
20	0.714955	0.579439	0.115793	0.529437
21	0.233642	0.831776	0.136837	0.960822
22	0.836446	0.915888	0.231574	0.117641
23	0.869161	0.607476	0.000000	0.382359
24	0.387847	0.747663	0.515783	0.823592
25	0.929906	0.775701	0.494739	0.460822
26	0.728973	0.607476	0.242108	0.107899
27	0.925235	0.607476	0.357889	0.951080

Table 4.10 Result of Grey relational grade calculations

Exp. No.	Grey relation coefficient				GRG
	ΔL	ΔW	ΔT	Δd	
1	0.664596	0.426295	0.922316	0.718393	0.682900
2	0.453389	0.532338	0.748023	0.467895	0.550412
3	0.486362	0.333333	1.000000	0.586220	0.601479
4	0.713335	0.367698	0.979365	0.772831	0.708307
5	0.333333	0.484163	0.760001	0.645611	0.555777
6	0.351973	0.532338	0.979365	0.864518	0.682049
7	0.849209	0.463204	0.871547	0.772831	0.739198
8	0.416342	0.394834	0.736430	0.796962	0.586142
9	0.459227	0.409962	0.772353	1.000000	0.660386
10	1.000000	0.816794	0.979365	0.614524	0.852671
11	0.810608	0.355482	0.693432	0.796962	0.664121
12	0.607954	0.484163	0.673756	0.653836	0.604927
13	0.514422	0.591160	0.785114	0.796962	0.671914
14	0.409962	0.532338	0.637585	0.836196	0.604020
15	0.426294	0.591160	0.673756	0.629684	0.580224
16	0.584700	0.591160	0.904755	0.536835	0.654363
17	0.529701	0.394834	0.703700	0.645611	0.568462
18	0.718120	0.591160	0.785114	0.560475	0.663717
19	0.601122	1.000000	0.497383	0.333333	0.607960
20	0.636906	0.543147	0.361218	0.515165	0.514109
21	0.394833	0.748252	0.366794	0.927337	0.609304
22	0.753519	0.856000	0.394189	0.361700	0.591352
23	0.792595	0.560209	0.333333	0.447371	0.533377
24	0.449579	0.664596	0.508018	0.739198	0.590348
25	0.877049	0.690322	0.497383	0.481149	0.636476
26	0.648486	0.560209	0.397491	0.359169	0.491339
27	0.869921	0.560209	0.437786	0.91088	0.694699

The main factor plot for grey relation grade (Figure 4.3) gives factor level as A_2, B_1, C_3, D_2, E_1. ANOVA on grey relation grade shows that factor A, B and interactions BXC, BXD, BXE are significant (Table 4.11). Result of sensitivity analysis (Figure 4.4) shows that different values of distinguishing coefficient give same factor level. ANOVA shows that factor B is most significant followed by factor A whereas factor C, D, E are insignificant but their interactions with B is significant. Therefore, optimum factor level of these factors is selected as per the interaction plot given in Figure 4.5. The optimal factor levels which will minimize all the four responses simultaneously or maximize the grey relational grade are A_2, B_1, C_1, D_2, E_3.

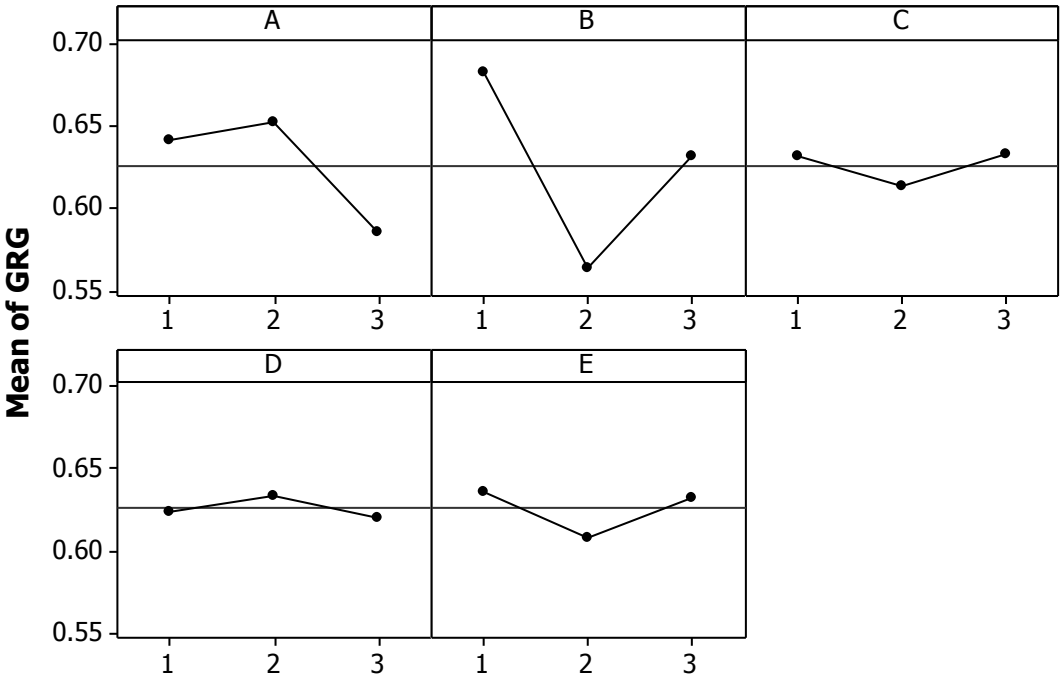

Figure 4.3 Factor effect plot for GRG

Table 4.11 ANOVA for GRG

Source	DOF	SS	V	F	P
A	2	4.4196	2.2098	10.52286	16.03367
B	2	12.5657	6.2829	29.91857	45.58653
C		0.3427[a]			
D		0.0933[a]			
E		0.824[a]			
AXB	4	3.0896	0.7724	3.678095	11.20862
BXC	4	2.0314	0.5079	2.418571	7.369624
BXD	4	2.5176	0.6294	2.997143	9.133487
BXE	4	1.6806	0.4202	2.000952	6.096973
Error	6	1.2600	0.2100		
Total	26	27.5645			[a]pooled

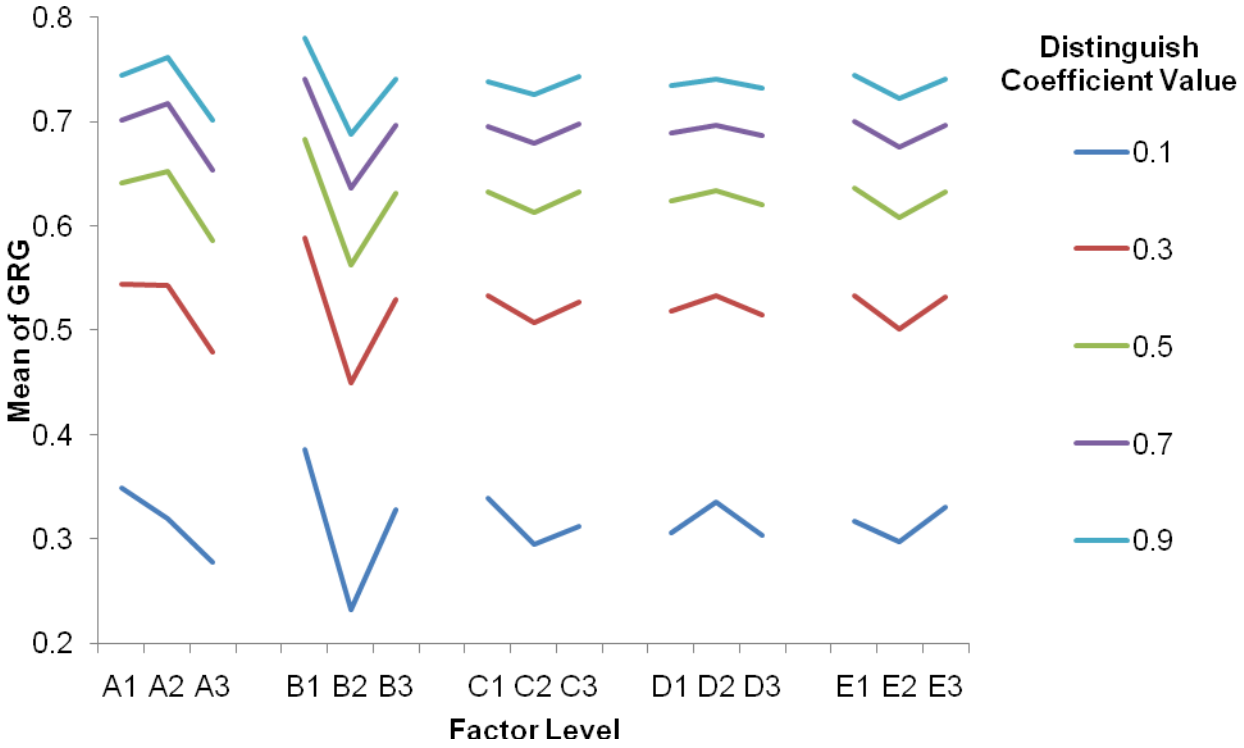

Figure 4.4 Sensitivity analyses for different distinguishing coefficients

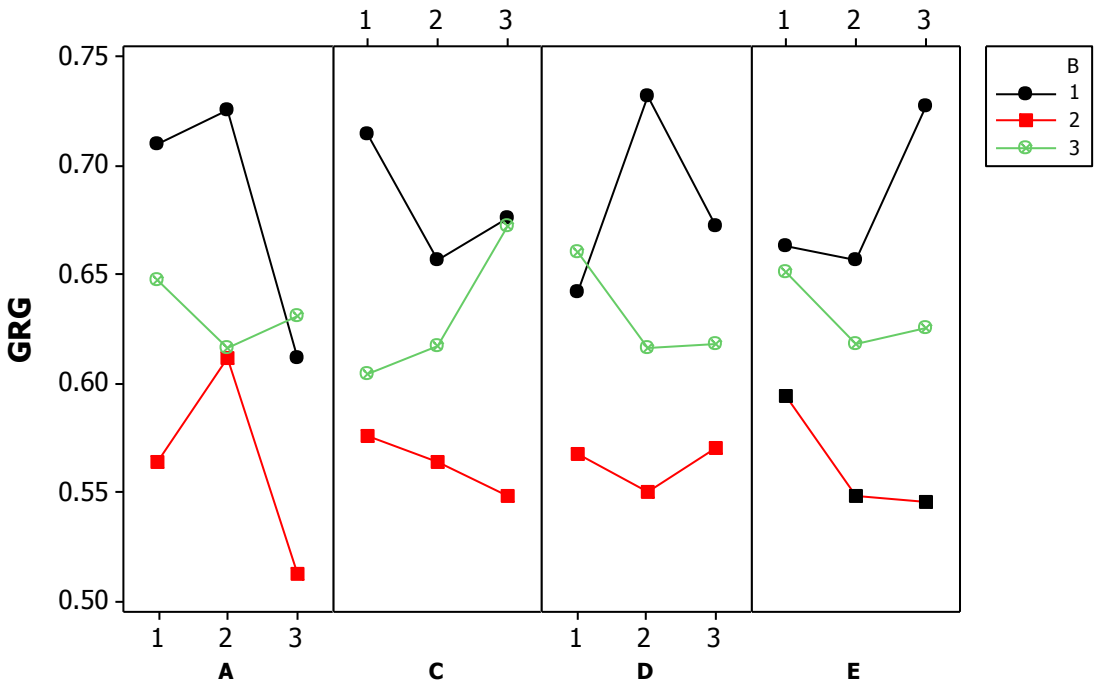

Figure 4.5 Factor interaction plot for GRG

4.4 Discussions

From Table 4.1, it is observed that shrinkage is predominant in length, width, and diameter of hole but dimension increases from its desired value in thickness direction. Shrinkage may be attributed to contraction of deposited fibre. Contraction will take place in two stages. First is related with the contraction of depositing fibre when cooling from extrusion temperature to glass transition temperature. At this stage depositing fibre is free to contract. In second stage, contraction will take place in deposited fibre when cooling from glass transition temperature to build chamber temperature. During this stage deposited fibre will bound with already deposited fibre by local re-melting of previously solidified material and diffusion. As a result of constraint offer by bounded surface it is not free to contract or expand. This may lead to distortion and dimensional inaccuracy within the part [185, 187].

For the case of thickness, it seems that increase is mainly due to prevention of shape error and irregular layer surface generated at the time of deposition [102, 150]. For example, consider Figure 4.6, which shows that height of test part (H) is function of its inclination (θ) with respect to base (build platform), length (L) and thickness (T). Height of part considered in this work at maximum orientation of 30° will be 43.48mm. If we slice it with minimum thickness of 0.127mm, total 342.36 slices will be required by simple arithmetic. Material flow rate is constant, so 0.36 has no meaning and it will be rounded off to nearest whole number. But to prevent shape error it will round off to one and machine will deposit 343 slices. This argument is true for any orientation of part.

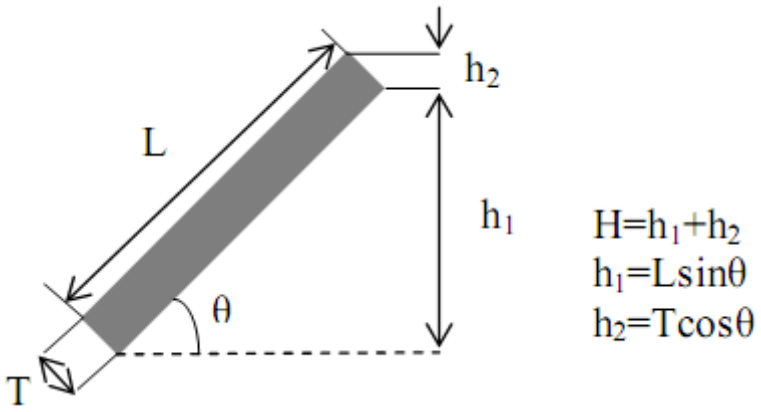

Figure 4.6 Orientation of part with respect to the base (H is height of part)

The material extruded out of circular cross section nozzle tip will spread sideward and forward while the layer is being deposited. This cause there cross section to change from circular to approximately elliptical and as a result surface of generated layer will not be flat as can be seen in Figure 4.7. Deposition of next layer

on this not so flat layer will results in its irregular deposition and may increase the dimension along the thickness. Diffusion of material between neighbouring rasters also produces the bump (Figure 4.8) because of overfilling at contact area which results in uneven layer. As a result, the next layer which will be deposited on this layer will not get the even planer surface and may result in increase in dimension along the part build direction. Further if the rasters are deposited with positive air gap as shown in Figure 4.9, the material from bottom layer will extrude upward at the spacing between two rasters and presence of voids will also results in uneven layer surface.

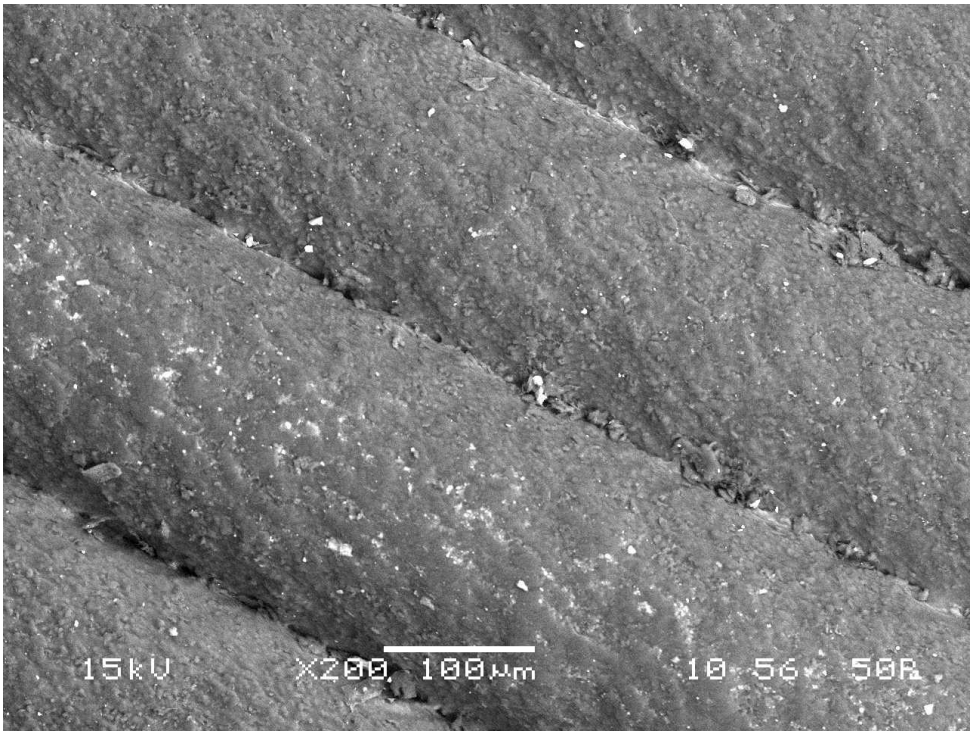

Figure 4.7 SEM image of part showing not so flat layer surface. (The surfaces of the test part were examined by scanning electron microscope (SEM) JEOL JSM-6480LV in the LV mode)

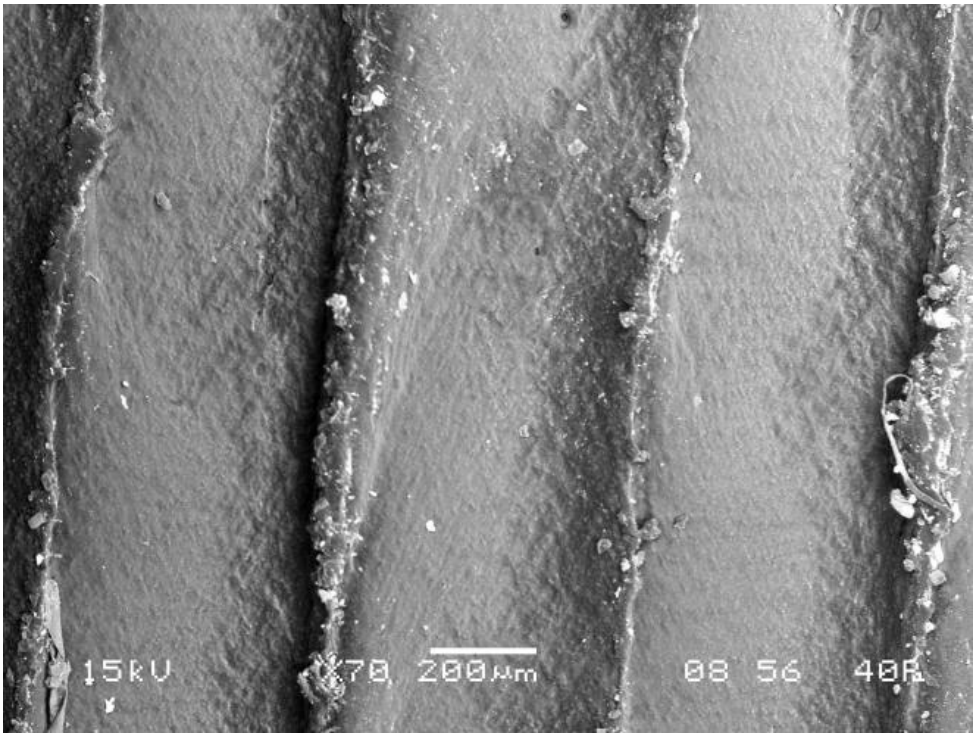

Figure 4.8 SEM image of part showing overfilling at the contact of two raster. (The surfaces of the test part were examined by scanning electron microscope (SEM) JEOL JSM-6480LV in the LV mode)

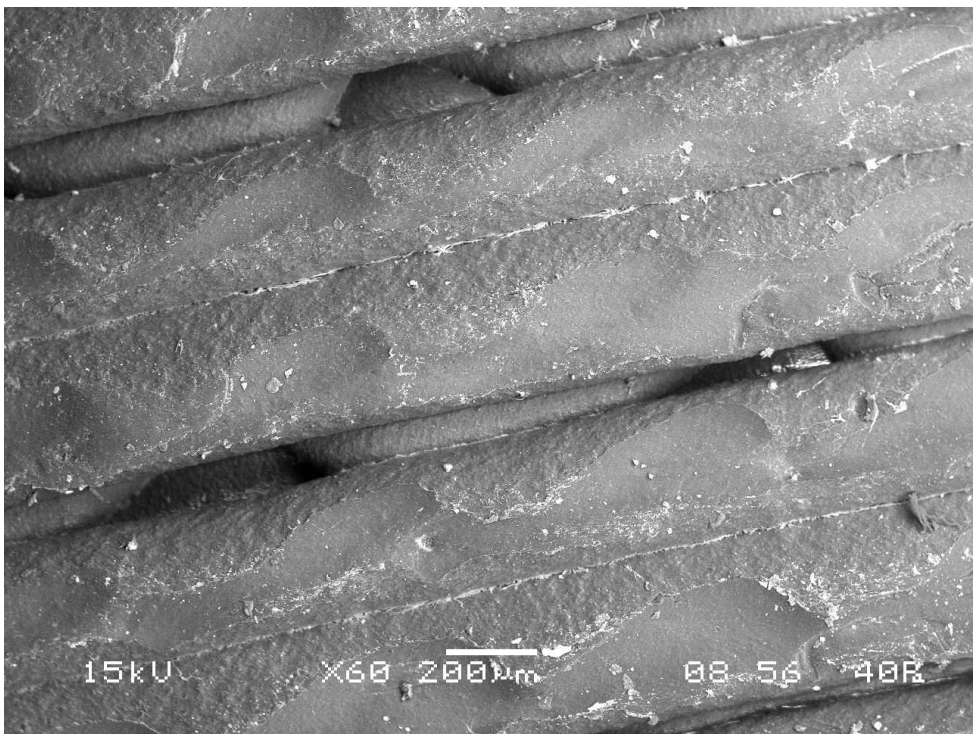

Figure 4.9 SEM image showing air gap (The surfaces of the test part were examined by scanning electron microscope (SEM) JEOL JSM-6480LV in the LV mode)

4.5 Predictive models

To predict the dimensional accuracy of FDM built part two commonly used prediction tools known as ANN and FIS are employed.

4.5.1 Prediction using ANN

ANN prediction is an alternative to structured modeling which allows complex systems to be built without requiring explicit formulation of possible relationships that may exist between variables. It is well suitable for the cases where there are large numbers of conflicting parameters and there interrelationship is difficult to understand as in FDM process. One of the advantages of using the neural network approach is that a model can be constructed very easily based on the given input and output and trained to accurately predict process dynamics. The details of this methodology are described by Rajasekaran and Pai [211]. In the present analysis factors A, B, C, D and E are taken as five input parameters. Each of these parameters is characterized by one neuron and consequently the input layer in the ANN structure has five neurons. The database is built considering experiments at the limit ranges of each parameter. GRG values are used to train the ANN in order to understand the input-output correlations. The database is then divided into two categories, namely: (i) A training category, which is exclusively used to adjust the network weights (ii) A test category, which corresponds to the set that validates the results of the training protocol. A software package NEUNET PRO for neural computing using back propagation algorithm is used as the prediction tool for grey relation grade under various test conditions. The architecture of network is decided by considering one input layer, one hidden layer and one output layer. ANN is trained using gradient descent back propagation algorithm. To determine the number of neurons in hidden layer different ANN structures with varying number of neurons in the hidden layer is tested at constant cycles of 50000, learning rate of 1%, error tolerance of ± 0.01, momentum parameter of 5%. The network performance is evaluated using normalized root mean square (NRMS) value. Figure 4.10 shows the results for different network architectures. Based on these results, neural network having six numbers of neurons in hidden layer is selected.

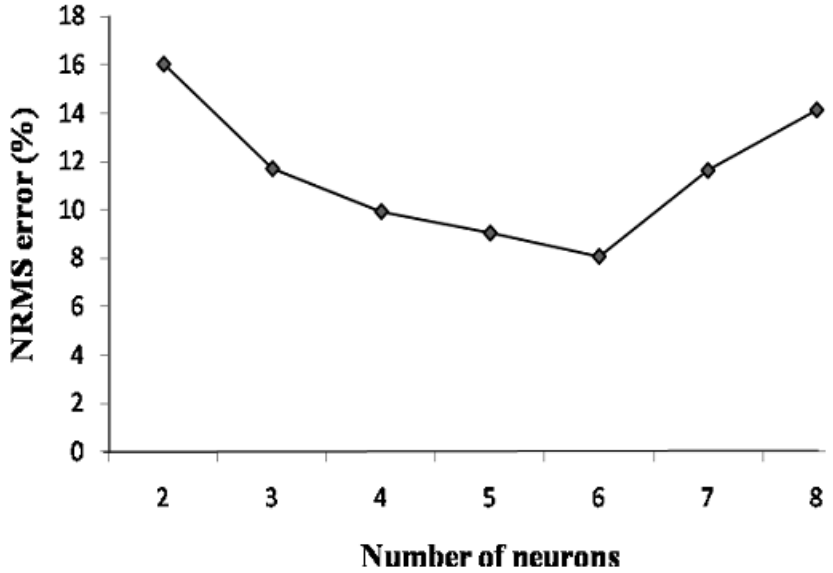

Figure 4.10 Plot between number of neurons in hidden layer and NRMS error

For prediction of GRG using three layer network having five neurons in input layer, six neurons in hidden layer and one output layer neuron is used with seventy five percent of data for training and twenty five percent data is used for testing. For rigorous training the number of cycles selected during training is 200000 and other parameters are kept same as those used for determining the hidden layer neuron.

4.5.2 Prediction using fuzzy inference system

Fuzzy inference is the process of formulating the mapping from a given input to an output using fuzzy logic. The mapping then provides a basis from which decisions can be made. The process of fuzzy inference involves fuzification of crisp input by defining membership function, fuzzy logic operators, and if-then rules. Block diagram of a typical fuzzy logic system is presented in Figure 4.11.

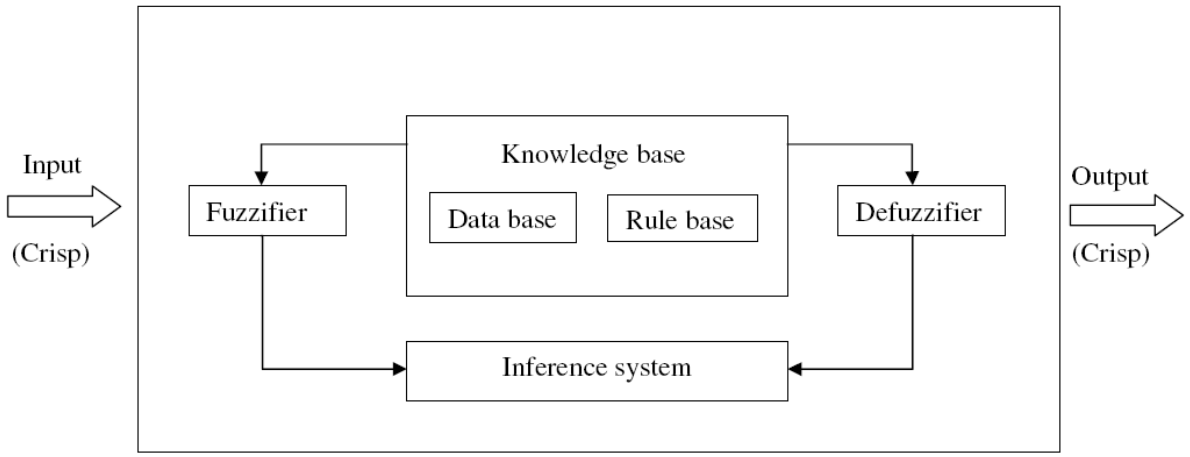

Figure 4.11 Structure of fuzzy rule based system

As outlined in Figure 4.11, a fuzzy rule based system consists of four parts: fuzzifier, knowledge base, inference engine and defuzzifier. These four parts are described below:

- Fuzzifier:

The real world input to the fuzzy system is applied to the fuzzzifier. In fuzzy literature, this input is called crisp input since it contains precise information about the specific information about the parameter. The fuzzifier converts this precise quantity to the form of imprecise quantity like 'large', 'medium', 'high' etc. with a degree of belongingness to it. Typically, the value ranges from 0 to 1.

- Knowledge base:

The main part of the fuzzy system is the knowledge base in which both rule base and database are jointly referred. The database defines the membership functions of the fuzzy sets used in the fuzzy rules where as the rule base contains a number of fuzzy if-then rules.

- Inference engine:

The inference system or the decision-making unit performs the inference operations on the rules. It handles the way in which the rules are combined.

- Defuzzifier:

The output generated by the inference block is always fuzzy in nature. A real world system will always require the output of the fuzzy system to the crisp or in the form of real world input. The job of the defuzzifier is to receive the fuzzy input and provide real world output. In operation, it works opposite to the input block.

In general two most popular fuzzy inference systems are available: Mamdani fuzzy model and Sugeno fuzzy model. The selection depends on the fuzzy reasoning and formulation of fuzzy IF-THEN rules. Mamdani fuzzy model is based on the collections of IF-THEN rules with both fuzzy antecedent and consequent predicts. The benefit of this model is that the rule base is generally provided by an expert and hence to a certain degree it is translucent to explanation and study. Because of its ease, Mamdani model is still most commonly used technique for solving many real world problems [206, 207].

In present study a fuzzy set $\tilde{A}$ is represented by triangular fuzzy number which is defined by the triplet (a, b, c) shown in Figure 4.12. Membership function, $\mu_{\tilde{A}}(x)$ is defined as:

$\forall \quad x,a,b,c \in R$

$$\mu_{\tilde{A}}(x) = \begin{cases} 0 & if \quad x < a \\ \dfrac{(x - a)}{(b - a)} & if \quad a \le x < b \\ \dfrac{(c - x)}{(c - b)} & if \quad b \le x \le c \\ 0 & if \quad x > c \end{cases} \tag{4.13}$$

The Mamdani implication method is employed for the rules definition.

For a i^{th} rule

R_i : *if* x_1 *is* A_{1i} *and* x_2 *is* A_{2i} *.....* x_s *is* A_{si} *then* y_i *is* C_i

$\forall \quad i = 1,2,...M$

where M is total number of fuzzy rule; x_j (j=1,2,…,s) are input variables; y_i are the output variables; and A_{ij} and C_i are fuzzy sets modeled by membership functions $\mu_{\tilde{A}_{ij}}(x)$ and $\mu_{\tilde{C}_i}(y_i)$ respectively.

The aggregated output for the M rules is:

$$\mu_{\tilde{C}_i}(y_i) = \max\{\min_i [\mu_{\tilde{A}_{1i}}(x_1), \ \mu_{\tilde{A}_{2i}}(x_2), ..., \mu_{\tilde{A}_{si}}(x_s)]\} \tag{4.14}$$

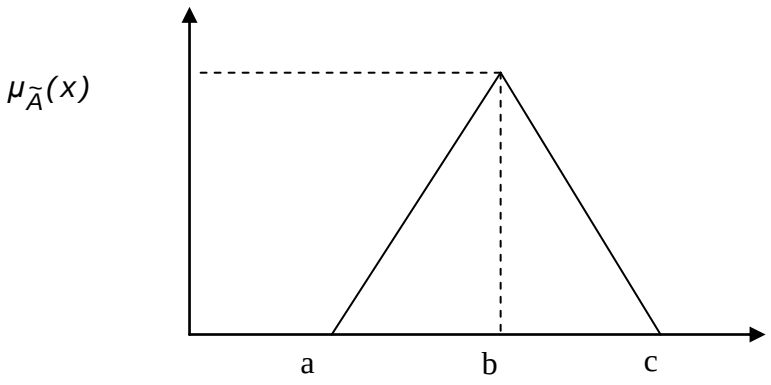

Figure 4.12 Triangular Fuzzy Number

Using a defuzzification method, fuzzy values can be combined into one single crisp output value. The center of gravity, one of the most popular methods for defuzzifying fuzzy output functions, is employed in the study. The formula to find the centroid of the combined outputs $\hat{y}_i$ is given by:

$$\hat{y}_i = \frac{\int y_i \mu_{\tilde{C}_i}(y_i) dy}{\int \mu_{\tilde{C}_i}(y_i) dy} \tag{4.15}$$

For the above stated problem the fuzzy rule-based prediction model has been developed using five input variables (corresponding to factors under study) and one output variable. The range of inputs has been partitioned into three sets while the range of output has been partitioned into six sets as shown in Table 4.12. Figure 4.13 gives the membership function of plot of input variables and Figure 4.14 gives the

membership function plot of output. Total 27 rules derived using Taguchi's orthogonal array and are given as follows:

R1: if A is Low and B is Low and C is Low and D is Low and E is Low then GRG is Average.

R2: if A is Low and B is Medium and C is Low and D is Medium and E is Medium then GRG is Poor.

R3: if A is Low and B is High and C is Low and D is High and E is High then GRG is Slightly average.

R4: if A is Low and B is Low and C is Medium and D is Medium and E is Medium then GRG is Average.

R5: if A is Low and B is Medium and C is Medium and D is High and E is High then GRG is Very poor.

R6: if A is Low and B is High and C is Medium and D is Low and E is Low then GRG is Slightly average.

R7: if A is Low and B is Low and C is High and D is High and E is High then GRG is Slightly good.

R8: if A is Low and B is Medium and C is High and D is Low and E is Low then GRG is Very poor.

R9: if A is Low and B is High and C is High and D is Medium and E is Medium then GRG is Poor.

R10: if A is Medium and B is Low and C is Low and D is Medium and E is High then GRG is Very good.

R11: if A is Medium and B is Medium and C is Low and D is High and E is Low then GRG is Slightly average.

R12: if A is Medium and B is High and C is Low and D is Low and E is Medium then GRG is Slightly average.

R13: if A is Medium and B is Low and C is Medium and D is High and E is Low then GRG is Slightly average.

R14: if A is Medium and B is Medium and C is Medium and D is Low and E is Medium then GRG is Very poor.

R15: if A is Medium and B is High and C is Medium and D is Medium and E is High then GRG is Poor.

R16: if A is Medium and B is Low and C is High and D is Low and E is Medium then GRG is Average.

R17: if A is Medium and B is Medium and C is High and D is Medium and E is High then GRG is Poor.

R18: if A is Medium and B is High and C is High and D is High and E is Low then GRG is Average.

R19: if A is Medium and B is Low and C is Low and D is High and E is Medium then GRG is Average.

R20: if A is High and B is Medium and C is Low and D is Low and E is High then GRG is Very poor.

R21: if A is High and B is High and C is Low and D is Medium and E is Low then GRG is Very poor.

R22: if A is High and B is Low and C is Medium and D is Low and E is High then GRG is Average.

R23: if A is High and B is Medium and C is Medium and D is Medium and E is Low then GRG is Slightly average.

R24: if A is High and B is High and C is Medium and D is High and E is Medium then GRG is Poor.

R25: if A is High and B is Low and C is High and D is Medium and E is Low then GRG is Good

R26: if A is High and B is Medium and C is High and D is High and E is Medium then GRG is Poor.

R27: if A is High and B is High and C is High and D is Low and E is High then GRG is Slightly average.

Figure 4.15 gives the fuzzy inference result for factor combination.

Table 4.12 Inputs and output with their fuzzy and fuzzy intervals

S.no	System's Linguistic variable	Variables	unit	Linguistic value	Fuzzy interval (a,b,c)
1	Input	Layer thickness (A)	mm	Low (L)	(0.0635,0.127,0.1905)
				Medium (M)	(0.127,0.1905,0.254)
				High (H)	(0.1905,0.254,0.3175)
2		Orientation (B)	degree	Low (L)	(-15,0,15)
				Medium (M)	(0,15,30)
				High (H)	(15,30,45)
3		Raster angle (C)	degree	Low (L)	(-30,0,30)
				Medium (M)	(0,30,60)
				High (H)	(30,60,90)
4		Raster width (D)	mm	Low (L)	(0.3564,0.4064,0.4564)
				Medium (M)	(0.4064,0.4564,0.5064)
				High (H)	(0.4564,0.5064,0.5564)
5		Air gap (E)	mm	Low (L)	(-0.004,0,0.004)
				Medium (M)	(0,0.004,0.008)
				High (H)	(0.004,0.008,0.012)
6	Output	Grey relational grade (GRG)	-	Slightly average (SA)	(0,0.35,0.4)
				Average (A)	(0.35,0.55,0.552)
				Slightly good (SG)	(0.4,0.6,0.65)
				Good (G)	(0.6,0.65,0.72)
				Very good (VG)	(0.7,0.755,0.85)
				Excellent (Exc)	(0.8,1,1.2)

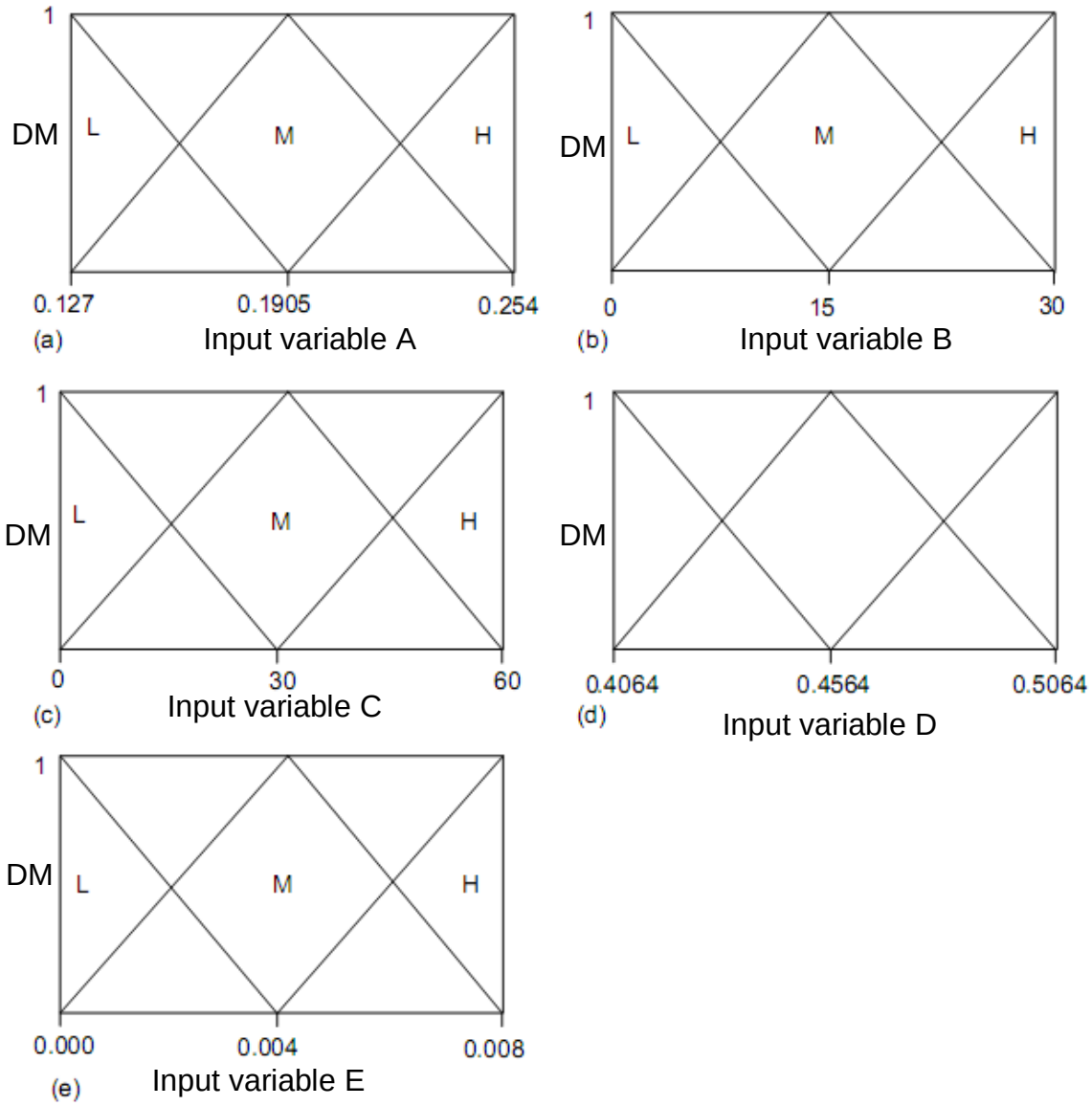

Figure 4.13 Membership function of input variables (a) Layer thickness (A), (b) Orientation (B), (c) Raster angle (C), (d) Raster width (D), (e) Air gap (E) (DM=degree of membership)

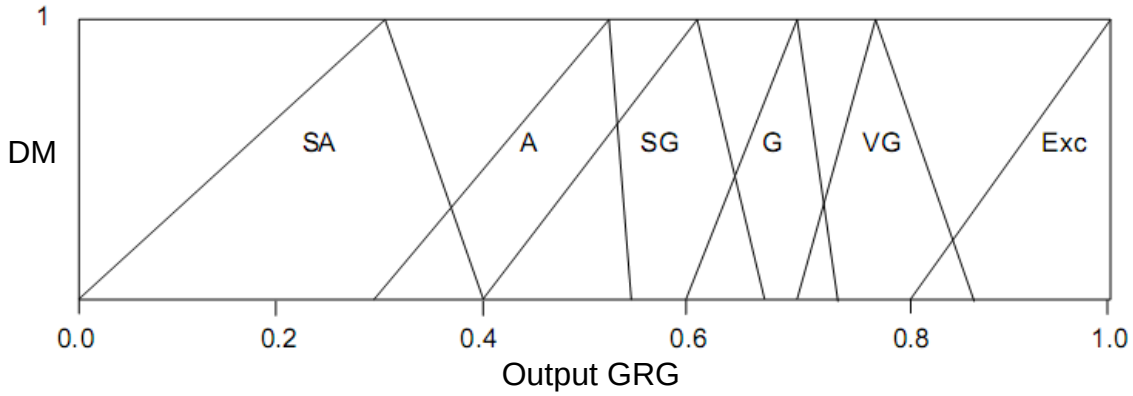

Figure 4.14 Membership function of output variable (GRG) (DM=degree of membership)

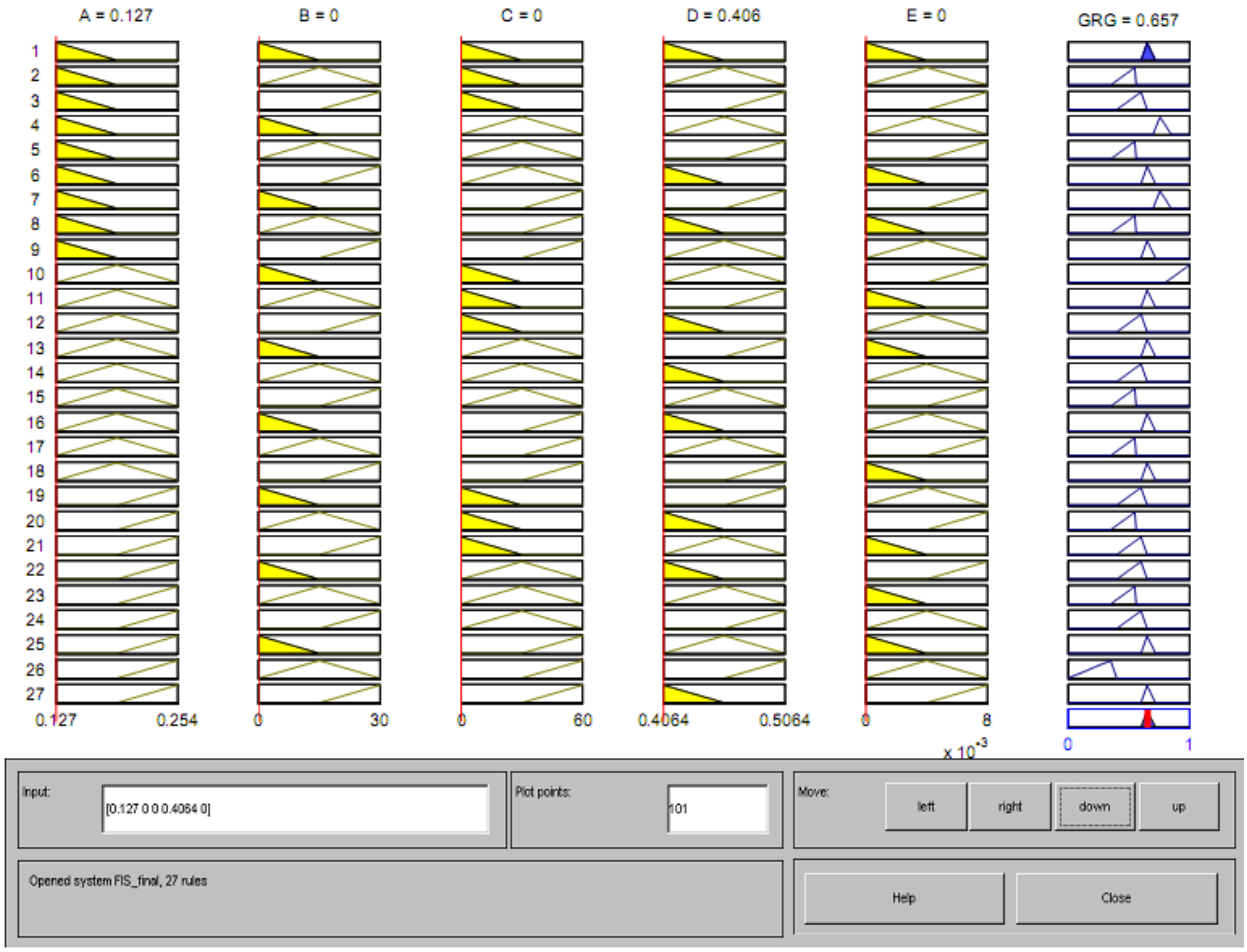

Figure 4.15 MATLAB output for Fuzzy inference system

4.5.3 Comparative evaluation of predictive models

Prediction of GRG using three layer ANN and fuzzy inference system is shown in Table 4.13. Small mean absolute error of 2.56% in case of fuzzy inference prediction, is less than the mean absolute error of 4.07%, proves the superiority of fuzzy inference as compared to neural network prediction model.

Table 4.13 Comparison of experimental, ANN and Fuzzy results of Test data

		Predicted value	
Exp. No.	GRG	Using ANN	Using FIS
1	0.683	0.682	0.657
2	0.55	0.550	0.550
3	0.601	0.601	0.600
4	0.708	0.711	0.700
5	0.556	0.556	0.550
6	0.682	0.682	0.657
7	0.739	0.738	0.768
8	0.586	0.586	0.550
9	0.66	0.660	0.657
10	0.853	0.853	0.834
11	0.664	0.664	0.657
12	0.605	0.605	0.600
13	0.672	0.672	0.657

14	0.604	0.603	0.600
15	0.58	0.580	0.550
16	0.654	0.654	0.657
17	0.568	0.569	0.550
18	0.664	0.664	0.657
19	0.608	0.608	0.657
20	0.514	0.514	0.550
21	0.609	0.511	0.600
22	0.591	0.682	0.600
23	0.533	0.502	0.550
24	0.59	0.485	0.600
25	0.636	0.510	0.657
26	0.491	0.487	0.490
27	0.695	0.464	0.657
Mean absolute relative error		4.07%	2.56%

To verify the results some experiments are conducted by taking random combination of factor levels as shown in Table 4.14. The lower value of mean absolute error of range 5.5% in case of FIS again confirmed the suitability of fuzzy inference as compared to ANN model having mean absolute error of 8.7%.

Table 4.14 Comparison of experimental, ANN and Fuzzy results of GRG

S.No.	Factors					GRG		
	A	B	C	D	E	Experimental	ANN	Fuzzy logic
1	2	1	1	2	1	0.789	0.731	0.769
2	2	1	1	1	2	0.692	0.814	0.657
3	2	3	1	3	3	0.596	0.619	0.548
4	1	1	1	3	1	0.713	0.693	0.768
5	1	2	3	3	3	0.540	0.584	0.571
6	1	3	3	1	3	0.711	0.598	0.720
7	1	3	2	3	2	0.606	0.661	0.500
8	3	1	1	2	1	0.584	0.601	0.550
9	3	3	3	1	1	0.665	0.538	0.657
10	3	2	3	2	3	0.468	0.471	0.471
					Mean absolute relative error		8.70%	5.50%

4.6 Conclusions

In the present work, effect of five factors that is, layer thickness, part build orientation, raster angle, air gap and raster width each at three levels together with the interaction of part build orientation with all the other factors is studied on the dimensional accuracy of FDM build part. Taguchi's design of experiment is used to find the optimum factor levels and significant factors and interactions. It is found that shrinkage is dominant along the length, width and diameter of hole of test part where as thickness is always more than the desired value. To improve the dimensional accuracy, four performance characteristics such as change in length, change in width, change in thickness and change in hole diameter of test part are considered

with the aim to minimize each one of them. It is found that factor optimal settings are different for performance characteristics. To determine the optimum factor level setting which will satisfy all the four performance characteristics simultaneously, grey Taguchi method is adopted. The result of grey Taguchi method shows that layer thickness of 0.254mm, part orientation of 0°, raster angle of 0°, raster width of 0.4564mm and air gap of 0.008mm are optimal factor settings for improving all performance characteristics simultaneously. Two predictive models- one based on fuzzy approach and the other on ANN approach are proposed. It is demonstrated that these models well reflect the effects of various factors on the dimensional accuracy and their predictive results are consistent with experimental observations. Further, it is clear from the study that the Mamdani fuzzy system gives the better result than the ANN result. The main advantage of the fuzzy model lies in the fact that it does not need any training data set as required for ANN system. Hence, this proposed model will be easily implemented in a hardware system as compared to ANN model. The proposed models outperform Taguchi's predictive model because it is of additive in nature and hardly incorporates non-linearity which is a found in real-life situations particularly in FDM processed parts. Moreover the work establishes the application of Taguchi orthogonal array for rules formation.

The next chapter present the effect of process parameters on surface roughness of FDM build part.

CHAPTER 5

IMPROVEMENT OF SURFACE ROUGHNESS

5.1 Introduction

Previous chapter (chapter 4) highlight the influence of five important process parameters i.e. layer thickness (A), orientation (B), raster angle (C), raster width (D) and air gap (E) on the dimensional accuracy of FDM built part. For the application of FDM process in manufacturing as a prototype or end usable product, it is necessary to control these parameters on the dimensional accuracy of manufactured component. In the similar line, surface roughness is an important characteristic of manufactured products for engineering application because it determines the functionality of the part in a specific situation, particularly in bearings, gears, guide ways, and applications subjected to fatigue loading and hence need to be minimized [163-178]. In this direction, present chapter aims at studying the important process parameters responsible for improving the surface roughness of parts built by fused deposition modelling (FDM) process. For this purpose, a face centred centre composite design (FCCCD) is employed to generate experimental data on surface roughness in three faces (top, side and bottom) of sample parts. Surface plots are analysed to assess the influence of various process parameters on surface roughness along three sides. Predictive equations are derived using full quadratic model. Residual analysis has been carried out to establish validity of the model. In order to determine the optimum factor level settings that minimize the roughness on each face in a single setting, weighted principal component analysis is used for combining multiple responses into a single response known as multi-response performance index (*MPI*). The advantage of using weighted principal component analysis lies in the fact that correlated responses (such as surface roughness on three sides) can be converted into uncorrelated components [212]. Finally, empirical relationship between process parameters and *MPI* is derived using response surface methodology. Development of valid model helps to search the optimisation landscape to find out best possible parametric combination resulting in minimum surface roughness which has not been explored during experimentation. In order to follow search procedure in an efficient manner, latest evolutionary technique such as bacteria foraging optimisation algorithm (BFOA) has been adopted due to its superior performance over other similar random search techniques [213]. Bacteria foraging is easier to implement because only few parameters need to be adjusted. Every bacterium remembers its own previous best value as well as the neighbourhood best and hence, it has a more effective memory capability than other techniques. BFOA has been successfully applied to solve different type of problems like forecasting [214], transmission loss reduction [215] and identification of nonlinear dynamic

systems [216]. Rest of this chapter is organised as follows. Section 5.2 accounts a brief description on principal component analysis. Section 5.3 provides an overview of BFOA optimization procedure. Detailed discussion on process parameter selection, experimental design, specimen preparation and roughness measurement is provided in section 5.4. Analysis of experimental results and optimisation procedure are presented in section 5.5. Conclusions from the present study are summarised in section 5.6.

5.2 Weighted principal component method

Principal component analysis (PCA) is a multivariate analysis method widely used for data reduction. It involves a mathematical procedure that reduces the dimensions of a set of variables by re-constructing them into uncorrelated combinations [212]. The analysis combines the variables that account for the largest amount of variance to form the first principal component. The second principal component accounts for the next largest amount of variance, and so on until the total sample variance is combined into component groups. In a multiple response case, the responses need to be converted into an equivalent single response for analysis purpose. While estimating surface roughness of parts in FDM process, the surface roughness of parts in the top, bottom and side faces of the specimen not only depend on process parameters but also they are correlated to each other. The surface quality of top surface depends on layer thickness set for building the part and it affects the surface quality of side surfaces. Similarly, layer thickness and type of support material used influence quality of bottom surface. A part to have functional requirement, surface quality in all directions must be considered. As the responses (surface roughness) along three sides of a specimen are highly correlated, uncorrelated responses need to be extracted to define the equivalent single response. In order to eliminate scaling effect, all the responses must be normalized using the “smaller-the-better” type quality characteristic as shown in the following relation because surface roughness is to be minimized [212].

$$Y_{ij}^{*} = \frac{max(L_j) - L_{ij}}{max(L_j) - min(L_j)} \tag{5.1}$$

L_{ij} and Y^{*}_{ij} represent the observed value and its normalised value for the i^{th} experimental run and the j^{th} response respectively; $max(L_j)$ and $min(L_j)$ represent the maximum and the minimum observed values of the j^{th} response, respectively.

Let Y_m^{*} be the normalized value of the m^{th} response for m =1, 2,…p. To carry out PCA, k ($k \leq p$) components will be obtained to explain variance in the p responses. Principal components are independent (uncorrelated) to each other.

Simultaneously, the explained variance of each principal component for the total variance of the responses is also obtained. The formed n principal component is a linear combination, $Z_n = \sum_{m=1}^{p} a_{nm} Y_m^*$ for $n = 1, 2, \ldots k$ subjected to $\sum_{m=1}^{p} a_{nm}^2 = 1$; the coefficient a_{nm} is called eigenvector [217].

In weighted principal component method, all principal components will be used. Thus, the explained variance can be completely elucidated in all responses [217]. Since different principal components have their own variance to account for the total variance, the variance of each principal component is regarded as the weight. Because principal components are independent to each other, an additive model can be developed by simply adding all principal components to represent multi-response performance index. Therefore, multi-response performance index (*MPI*) is given as [217]:

$$MPI = \sum_{n=1}^{k} W_n Z_n \tag{5.2}$$

where W_n is the weight of n^{th} principal components.

The weighted principal component provides weights (variance explained by each component) for each principal component to be extracted from data rather than resorting arbitrary and ambiguous method of assigning weights for converting multi-responses into an equivalent single response (composite quality index or *MPI*). The larger the *MPI* is the higher the quality. Finally, significant factors affecting *MPI* can be obtained using ANOVA.

5.3 Bacteria foraging optimization algorithm (BFOA)

The use of evolutionary algorithms to solve complex optimization problems is common these days because they provide competitive results while solving engineering design problems [218, 219]. Furthermore, swarm intelligence approaches have been also used to solve this kind of problems [220, 221]. However, most of the work is centered on some algorithms such as Particle Swarm Optimization [222], Ant Colony Optimization [223] and Artificial Bee Colony [224]. Recently, another swarm-intelligence-based model known as Bacterial Foraging Optimization Algorithm (BFOA), inspired by the behavior of bacteria Escherichia coli (E. Coli) in its search for food, has been proposed [225]. The foraging strategy of E. coli bacterium present in the human intestine can be explained by four processes viz., chemotaxis, swarming, reproduction, elimination and dispersal.

a) Chemotaxis: The characteristics of movement of bacteria in search of food can be defined in two ways, i.e. swimming and tumbling together known as

chemotaxis. A bacterium is said to be 'swimming' if it moves in a predefined direction, and 'tumbling' if moving in an altogether different direction. Mathematically, tumble of any bacterium can be represented by [225]:

$$\theta^i(j+1,k,l) = \theta^i(j,k,l) + C(i)\Phi(j) \tag{5.3}$$

were θ^i (j,k,l) is i^{th} bacterium position at the j^{th} chemotactic step, k^{th} reproduction step, and l^{th} elimination-dispersal event. $C(i)>0$, $i=1,2,\ldots,S$ denote a basic chemotactic step size taken in unit random direction $\Phi(j)$. Otherwise $C(i)$ is a basic chemotactic step size that will use to define the lengths of steps during swimming. S is the total number of bacteria.

b) Swarming: For the bacteria to reach at the richest food location (i.e. for the algorithm to converge at the solution point), it is desired that the optimum bacterium till a point of time in the search period should try to attract other bacteria so that together they converge at the solution point more rapidly. To achieve this, a penalty function based upon the relative distances of each bacterium from the fittest bacterium till that search duration, is added to the original cost function. Finally, when all the bacteria have merged into the solution point this penalty function becomes zero. The effect of Swarming is to make the bacteria congregate into groups and move as concentric patterns with high bacterial density. Mathematically, it is defined as [225]:

$$\begin{aligned} J_{cc}(\theta_g(j,k,l),\ \theta(j,k,l)) &= \sum_{i=1}^{S} J_{cc}^i(\theta_{gm}(j,k,l),\ \theta^i(j,k,l)) \\ &= \sum_{i=1}^{S}[\ d_{attract}\, exp(\ \omega_{attract} \sum_{m=1}^{p} (\theta_{gm} - \theta_m^i)^2)] \\ &+ \sum_{i=1}^{S}[\ -h_{repellent}\, exp(-\omega_{repellent} \sum_{m=1}^{p} (\theta_{gm} - \theta_m^i)^2)] \end{aligned} \tag{5.4}$$

J_{cc} is called swarm attractant cost, θ_g is the position of the global optimum bacterium and m represent the m^{th} parameter of bacterium location. $d_{attract}$ is the depth of the attractant released by the cell, $\omega_{attract}$ measure width of the attractant signal, $h_{repellent}$ is the depth of the repellent effect and $\omega_{repellent}$ is the measured of the width of the repellent signal. Since it is not possible for two bacterium to have same location therefore it is assumed that $h_{repellent} = d_{attract}$.

c) Reproduction: The original set of bacteria, after getting evolved through several chemotactic stages, reaches the reproduction stage. Here, the best set of bacteria (chosen out of all the chemotactic stages) gets divided into two groups. The healthier half replaces the other half of bacteria, which gets eliminated, owing to their poorer foraging abilities. This makes the population of bacteria constant in the evolution process. Mathematically, for

reproduction, the population is sorted in terms of accumulated cost (J_{sw}) which is sum of cost function value (J) added with the swarm attractant cost (J_{cc}) [215].

$$J_{sw}(i,j,k,l) = J(i,j,k,l) + J_{cc}(\theta_g(j,k,l), \theta(j,k,l)) \quad (5.5)$$

d) Elimination and Dispersal: In the evolution process, a sudden unforeseen event can occur, which may drastically alter the smooth process of evolution and cause the elimination of the set of bacteria and/or disperse them to a new environment. Instead of disturbing the usual chemotactic growth of the set of bacteria, the unknown event may place a newer set of bacteria nearer to the food location. From a broad perspective, elimination and dispersal are parts of the population-level long-distance motile behaviour. In its application to optimization, it helps in reducing the behaviour of stagnation i.e. being trapped in a premature solution point or local optima.

5.3.1 Pseudo-code for BFOA

Step 1: *Initialize*

(a) Number of parameters (p) to be optimized,
(b) Number of bacteria (S) to be used for searching the total region,
(c) Maximum swimming length (SL_{max}) after which tumbling of bacteria will be undertaken in a chemotaxis step,
(d) Number of iteration (N_c) to be undertaken in a chemotaxis loop,
(e) Maximum number of reproduction (N_R) cycles,
(f) Maximum number of elimination-dispersal (N_e) events imposed on bacteria,
(g) Probability (P_{ed}) with which elimination-dispersal will continue
(h) Location P(p, S, 1) of initial set of bacteria,
(i) Random swim direction ($\Phi(j)$) and step length ($C(i)$),
(j) Swarming coefficients ($d_{attract}$, $w_{attract}$, $h_{repellent}$ and $w_{repellent}$).

Step 2: *Elimination-dispersal loop*

With some probability (P_{ed}), the existing set of bacteria gets eliminated and dispersed in a new random direction. Increment l=l+1. Go to step 2 if l<N_e else go to step 3.

Step 3: *Reproduction loop*

a. For given k and l, and for each i=1,2,…,S, sort accumulated total cost (J_{sw}) in order of ascending cost. Let J_{health} = sort {J_{sw} (i, j, k, l)}. Higher cost of any bacteria means poor health.

b. Out of the total *S* bacteria, the better halves having lower J_{health} values sustain the evolution process and replace the other less healthy bacteria.

c. Increment $k=k+1$. Go to step 3 if $k<N_R$ go to step 4 else go to step 5

Step 4: *Chemotaxis loop*

a. Calculate cost function value $J(i, j, k, l)$.

b. Find the global minimum bacteria (θ_g) from all the cost functions evaluated till that point.

c. Calculate $J_{sw}(i, j, k, l)$.

d. If $j=1$, tumble

e. For $j > 1$

Reorient the set of bacteria in a favourable direction through swimming or tumbling.

If $J_{sw}(i, j, k, l) < J_{sw}(i, j-1, k, l)$ and $SL < SL_{max}$

Swim and increment $SL=SL+1$

Else, tumble and reset $SL=0$.

f. The next bacterium ($i+1$) is taken for swimming or tumbling process till $i=S$.

Step 5: *Stop if stopping condition is met else go to* step 2.

In order to ensure stability of the chemotactic dynamics in BFOA, the step-size parameter $C(i)$ must be adjusted according to the current location of the bacterium and its current fitness. Therefore, the proposed algorithm uses adaptive step size as given by:

$$C(i) = \frac{|J^i(\theta)|}{1+\frac{1}{|J^i(\theta)|}} \tag{5.6}$$

where $J^i(\theta)$=fitness of i^{th} bacterium

If $J^i(\theta)\rightarrow 0$, then $C(i)\rightarrow 0$ and when $J^i(\theta)\rightarrow$large, $C(i)\rightarrow 1$. This implies the bacterium which is in the vicinity of noxious substance associates with higher cost function. Hence, it takes larger steps to migrate to a place with higher nutrient concentration.

5.4 Experimental plan

Review of literature suggests that reason for inferior surface finish of parts built by FDM (and other RP) process may be largely attributed to layer by layer deposition of material during building stage causing staircase effect. It becomes prominent on those surfaces which are inclined to build direction. Therefore, the effect can be minimized by choosing proper orientation or minimum possible layer

thickness [90-112]. The model generated by these studies were suitable for other RP processes but not for FDM processed part [163-166].

In FDM process material extruded out of the circular cross section nozzle will spread in side and forward direction due to shearing effect. The deposited fibres will have a curved profile (Figure 4.7). As a result, the generated layer will not have a flat surface. Generally, FDM process fabricates each layer by depositing material at the outer contour first and then filling the rasters in interior region. While filling interior rasters in each layer, raster gap (air gap) may be created between two adjacent rasters. If the part is fabricated with zero or negative air gap, there is possibility that bumps may be created due to overlapping of rasters (Figure 4.8). On the other hand, material from bottom layer may be extruded upward if positive air gap is used (Figure 4.9). This inherent part build methodology may affect the surface smoothness of build part. Thus, the effect of layer generation procedure cannot be neglected while controlling the surface roughness of part in FDM process. This fact is further fortified by the efforts of Anitha et al. [166], and Campbell et al. [19]. To assess the effect of process parameter on surface roughness of built part, the process parameters listed in Table 3.5 are considered. Experiments were designed in accordance with the procedure explained in sub-section 3.6.2. The average of three readings of surface roughness (R_a) on top, bottom and left side surface of each specimen is taken along the direction shown in Figure 3.6 using Hommel werke Turbo Wave V7.20 roughness tester as per the procedure explained in sub-section 3.4.2.

5.5 Results and discussions

Mean of measured roughness values for all the three surfaces (top, bottom and side) are shown in Table 5.1.

Table 5.1 Roughness data as per FCCCD runs

Run order	Factor					Roughness in µm		
	A	B	C	D	E	TOP	BOTTOM	SIDE
1	-1	-1	-1	-1	1	2.8600	2.5540	0.9034
2	1	-1	-1	-1	-1	1.4170	5.1948	1.8068
3	-1	1	-1	-1	-1	9.1780	11.046	0.4769
4	1	1	-1	-1	1	9.8830	8.7280	0.5057
5	-1	-1	1	-1	-1	4.9418	2.2170	0.4785
6	1	-1	1	-1	1	1.9932	3.6863	0.8619
7	-1	1	1	-1	1	4.2356	5.7563	0.8436
8	1	1	1	-1	-1	4.8067	5.1333	0.8793
9	-1	-1	-1	1	-1	1.1415	4.1950	0.4171
10	1	-1	-1	1	1	3.9056	4.5153	0.9699
11	-1	1	-1	1	1	8.8538	9.7465	0.4402
12	1	1	-1	1	-1	4.6988	6.4857	0.9012
13	-1	-1	1	1	1	5.0050	3.4303	0.5482
14	1	-1	1	1	-1	2.1372	3.5212	0.8429
15	-1	1	1	1	-1	9.4190	11.875	0.4706

16	1	1	1	1	1	6.8732	9.2910	0.6356
17	-1	0	0	0	0	5.5376	6.0323	0.6838
18	1	0	0	0	0	4.0672	6.1970	0.8594
19	0	-1	0	0	0	2.4592	2.4350	0.8544
20	0	1	0	0	0	3.0760	2.5293	0.6870
21	0	0	-1	0	0	5.5603	2.9640	0.7241
22	0	0	1	0	0	5.0454	5.2387	0.6325
23	0	0	0	-1	0	5.0544	3.5520	0.6719
24	0	0	0	1	0	3.0648	4.2115	0.6954
25	0	0	0	0	-1	4.1730	3.6160	0.6072
26	0	0	0	0	1	4.5032	3.6207	0.6297
27	0	0	0	0	0	4.2956	4.1870	0.7523
28	0	0	0	0	0	5.1026	3.7960	0.6432
29	0	0	0	0	0	4.6800	2.7450	0.6638
30	0	0	0	0	0	3.8993	3.4797	0.6615
31	0	0	0	0	0	3.4412	1.8493	0.6285
32	0	0	0	0	0	5.3310	3.8523	0.7580

A close examination of Table 5.1 reveals that surface roughness on side face of the specimen is less as compared to other faces. Usually, staircase effect is observed on the side surface of the FDM parts due to part build orientation and layer thickness but the effect becomes dominant for curved profiles rather than the straight profiles as used in the present study. While building FDM parts, an outer contour is deposited followed by raster filling of interior region. Deposition of outer contour may help to smooth the side surface. However, the profile of outer contour is curved instead of flat and hence outer contour contributes roughness in side surfaces. Further, the irregularities due to crisscross filling (Figure 5.1) and distortion of rasters may affect the smoothness of the surface. Distortion of successive filaments due to melting, stacking and overlapping between layers may cause considerable undulations on surfaces of built parts (Figure 5.2). The geometry of the cross section of the deposited filament further enhances roughness of the surface. Process related errors occurring in one layer may propagate and transfer to other layers resulting in an accumulated error effect on top surface of a built part [150]. The bottom surface is always in contact with support material and hence, affected by the impression of support structure in addition to propagation of irregularities of layers above it. These observations are further supported by the roughness profiles of top, bottom, and side surfaces shown in Figure 5.3. A close examination of Figure 5.3 shows that roughness profile is approximately parabolic in nature for top and side face roughness (Figure 5.3 a, c). This may be due to the approximately elliptical cross section of deposited material. Whatever undulations are observed in top and side roughness profiles, it may be due to process related error. However, the roughness profile of bottom surface deviate considerably from parabolic profile (Figure 5.3 b). The reason for this observation may be attributed to the fact that bottom surface is

always in contact with support material and hence the impression of support surface is overlapping with bottom surface profile.

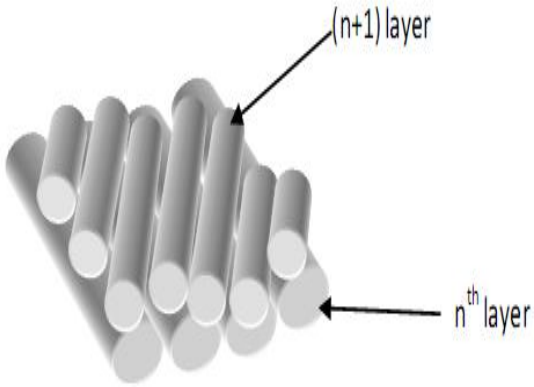

Figure 5.1 Schematic of crisscross built style

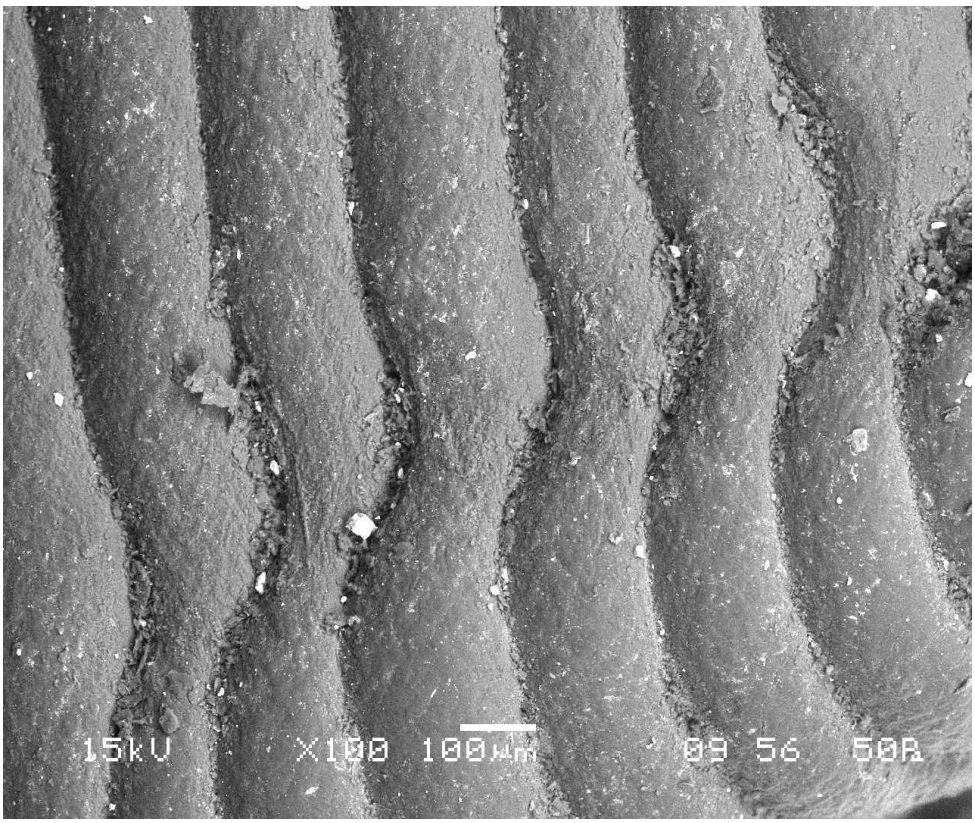

Figure 5.2 SEM image showing distortion of rasters (The surfaces of the test part were examined by scanning electron microscope (SEM) JEOL JSM-6480LV in the LV mode)

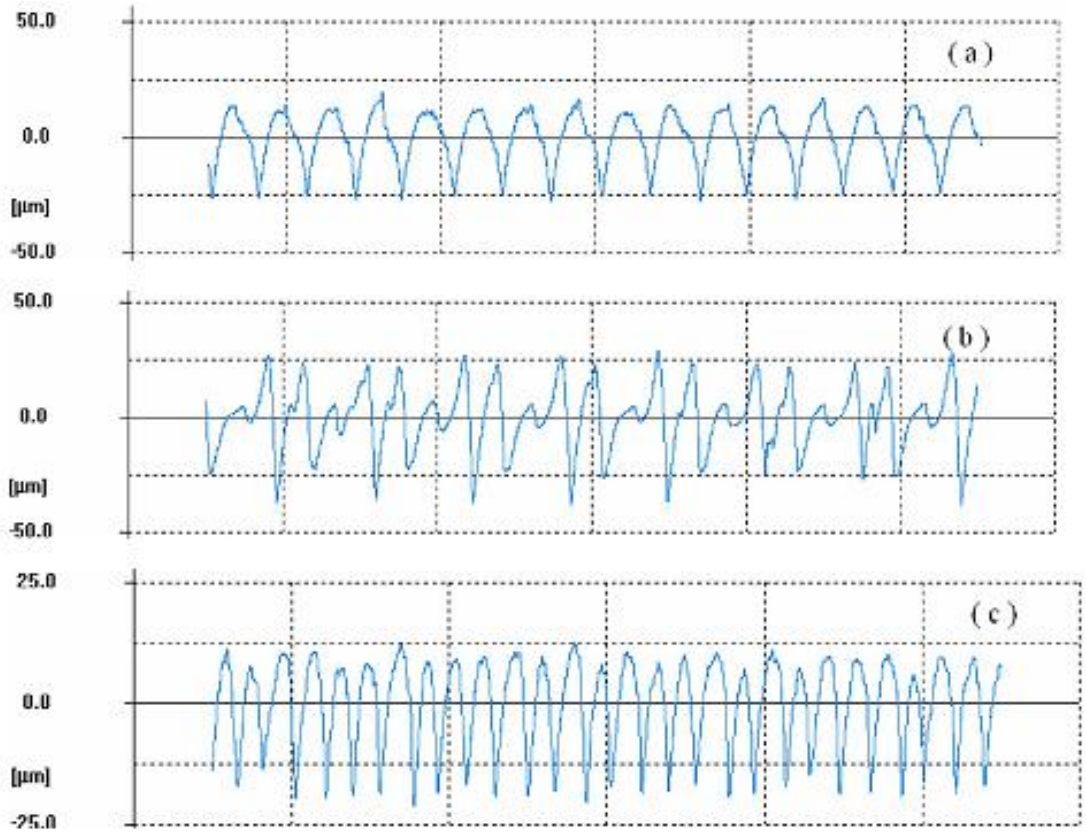

Figure 5.3 Roughness profile of specimen built as per experiment plan 3 (Table 5.1) (a) Top surface (b) Bottom surface (c) Side surface

The experimental data obtained from FCCCD design runs is analysed with the help of MINITAB R14 software using full quadratic response at 95% of confidence level. For significance check, F-value given in ANOVA table is used. Probability of F value greater than calculated F value due to noise is indicated by p-value. If p value is less than 0.05, significance of corresponding term is established. For lack of fit, p-value must be greater than 0.05. An insignificant lack of fit is desirable because it indicates any term left out of model is not significant and developed model fits well [196, 197]. Based on analysis of variance (ANOVA), quadratic model was found to be suitable for predicting average surface roughness of top, bottom and side face of specimen with regression p-value less than 0.05 and lack of fit more than 0.05. The ANOVA results are summarised in Table 5.2 to Table 5.4 for top, bottom and side roughness respectively.

Table 5.2 ANOVA for top surface roughness

Source	Degree of freedom	Sum of square	Variance	F-value	p-value
Regression	20	136.844	6.8422	6.41	0.001
Linear	5	78.58	15.7159	14.73	0
Square	5	11.492	2.2983	2.15	0.134
Interaction	10	46.772	4.6772	4.39	0.011

Residual Error	11	11.733	1.0666		
Lack-of-Fit	6	9.134	1.5223	2.93	0.129
Pure Error	5	2.599	0.5199		
Total	31	148.577			

Table 5.3 ANOVA for bottom surface roughness

Source	Degree of freedom	Sum of square	Variance	F-value	p-value
Regression	20	190.113	9.5057	5.54	0.003
Linear	5	91.426	18.2851	10.66	0.001
Square	5	58.635	11.7271	6.84	0.004
Interaction	10	40.052	4.0052	2.33	0.090
Residual Error	11	18.873	1.7157		
Lack-of-Fit	6	15.092	2.5154	3.33	0.104
Pure Error	5	3.781	0.7561		
Total	31	208.986			

Table 5.4 ANOVA for side surface roughness

Source	Degree of freedom	Sum of square	Variance	F-value	p-value
Regression	20	1.85735	0.092867	18.47	0.000
Linear	5	0.88174	0.176348	35.08	0.000
Square	5	0.05755	0.011511	2.29	0.117
Interaction	10	0.91806	0.091806	18.26	0.000
Residual Error	11	0.05530	0.005027		
Lack-of-Fit	6	0.03950	0.006584	2.08	0.219
Pure Error	5	0.01580	0.003159		
Total	31	1.91265			

Estimated regression coefficients of model terms are given in Table 5.5. The individual significance of each term is calculated by t-test at 95% of confidence and terms having p-value less than 0.05 are considered as significant. equation 5.7 to equation 5.9 gives the response surface equations for top surface roughness (R_a^T), bottom surface roughness (R_a^B) and side surfaces roughness (R_a^S) respectively. The coefficient of determination (R^2) which indicates the percentage of total variation in the response explained by the terms in the model is 92.10%, 90.97% and 97.11% for top, bottom and side surface respectively.

Table 5.5 Estimated regression coefficients

	Top surface		Bottom surface		Side surface	
Term	Coefficient	p-value	Coefficient	p-value	Coefficient	p-value
Constant	4.24832	0.000	3.42523	0.000	0.689109	0.000
A	-0.63280	0.025	-0.22777	0.476	0.166693	0.000
B	1.95353	0.000	2.15790	0.000	-0.102380	0.000
C	-0.16894	0.502	-0.29334	0.362	-0.052906	0.009
D	0.04051	0.871	0.52243	0.119	-0.083729	0.000
E	0.34442	0.185	-0.10864	0.732	-0.030129	0.099
A×A	0.71156	0.303	2.60916	0.010	0.079090	0.108
B×B	-1.32324	0.070	-1.02334	0.246	0.078211	0.111
C×C	1.21199	0.093	0.59586	0.490	-0.014223	0.759

D×D	-0.03124	0.963	0.37626	0.661	-0.008856	0.848
E×E	0.24726	0.714	0.11286	0.895	-0.074026	0.130
A×B	-0.05809	0.826	-0.83169	0.027	-0.090236	0.000
A×C	-0.35389	0.198	0.06068	0.856	-0.066706	0.003
A×D	-0.23056	0.391	-0.41267	0.234	0.007643	0.675
A×E	0.83258	0.008	0.85822	0.024	-0.146837	0.000
B×C	-0.75201	0.014	-0.02164	0.948	0.116943	0.000
B×D	0.04776	0.857	0.29531	0.386	0.063399	0.004
B×E	-0.14895	0.576	-0.00476	0.989	-0.002557	0.888
C×D	0.76221	0.013	0.86906	0.022	0.024883	0.188
C×E	-0.76655	0.013	0.04969	0.882	0.062548	0.005
D×E	0.53830	0.061	0.23579	0.487	0.030557	0.113

$$R_a^T = 4.24832 - 0.06328A + 1.95353B + 0.83258AE - 0.75201BC + 0.76221CD - 0.76655CE \quad (5.7)$$

$$R_a^B = 3.42523 + 2.15790B + 2.60916A^2 - 0.83169AB + 0.85822AE + 0.86906CD \quad (5.8)$$

$$R_a^S = 0.689109 + 0.16693A - 0.102380B - 0.052906C - 0.083729D - 0.090236AB - 0.066706AC - 0.146837AE + 0.116943BC + 0.063399BD + 0.062548CE \quad (5.9)$$

Anderson-Darling (AD) normality test results are shown in Figure 5.4 for respective roughness standardized residue. Since p-value of the normality plots is found to be above 0.05, it signifies that residue follows normal distribution and models given by equation 5.7 to equation 5.9 are suitable for practical engineering applications. It is evident from Table 5.5 that parameters A and B and interactions such as AxE, BxC, CxD and CxD influence the surface roughness in the top surface. Similarly, parameters B, square term AxA and interactions such as AxB, AxE, and CxD are significant for estimating surface roughness of bottom surface. As far as side face is concerned, more parameters like A, B, C and D and interactions such as AxB, AxC, AxE, BxD and CxE are statistically significant. In fact, parameters like layer thickness (A) and orientation (B) have significant influence on surface roughness as suggested in literature but other factors cannot be neglected because they may not contribute significantly as individual factors but their interactions are quite significant. Therefore, estimation of surface roughness using only two factors (layer thickness (A) and orientation (B)) may not be correct one. All significant factors, their interactions and square terms should be included in the model.

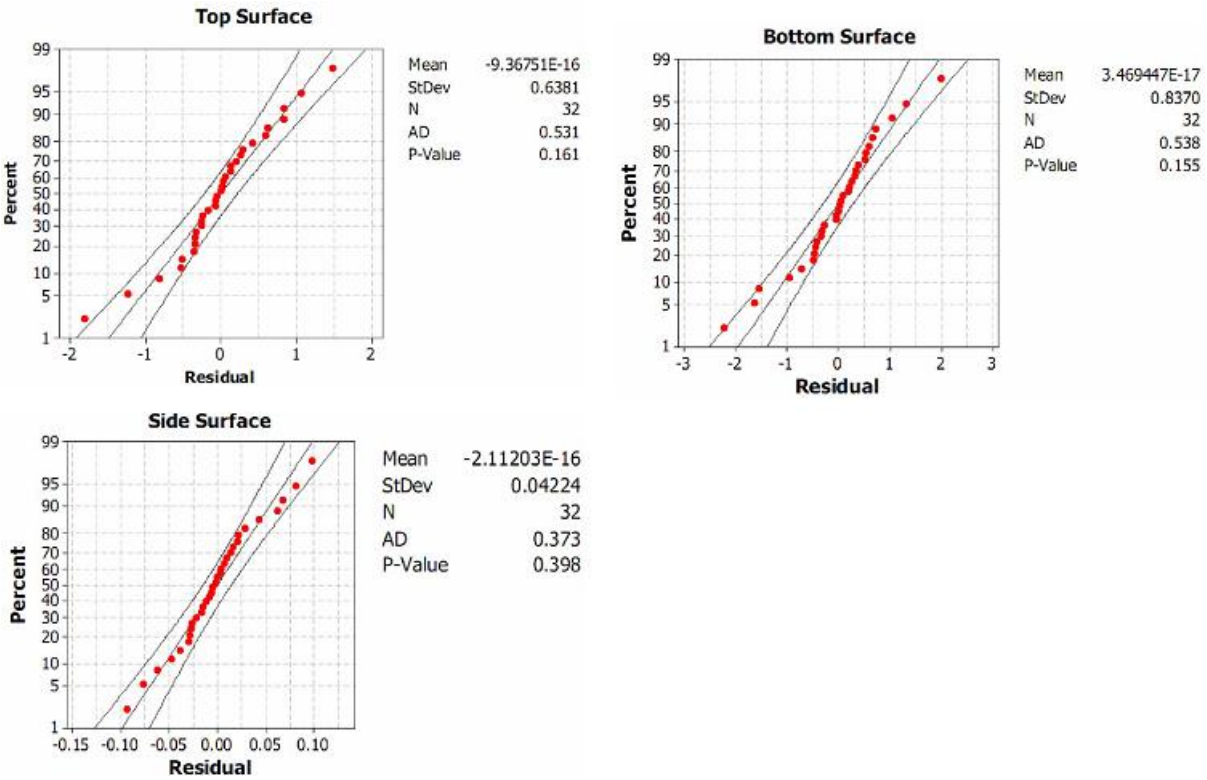

Figure 5.4 Normal probability plot of standardized residuals at 95% of confidence interval

Typical response surface plots for significant interactions are shown in Figure 5.5. It is clearly seen that surface roughness value increases as layer thickness (A) and orientation (B) increases. However, increase of surface roughness with respect to layer thickness is more prominent at low level of orientation than high level of orientation. It can also be noted that surface finish can be improved if raster angle (C) is maintained at low level. It can also be observed that surface roughness increases with raster width (D). As far as air gap (E) is concerned, surface roughness value initially increases and then decreases due to bump formation and extrusion of lower level material upwards at low and high level of air gap. A close examination of Table 5.1 reveals that deterioration in surface finish is mostly pronounced in side surface due to staircase effect. In the bottom surface, roughness increases due to presence of support materials. However, surface quality of top surface seems to be reasonably good. The surface quality is mainly affected by shrinkage of material due to number of heating and cooling cycles as a part of FDM fabrication technique. The heating and cooling cycles are again dependent on process parameters.

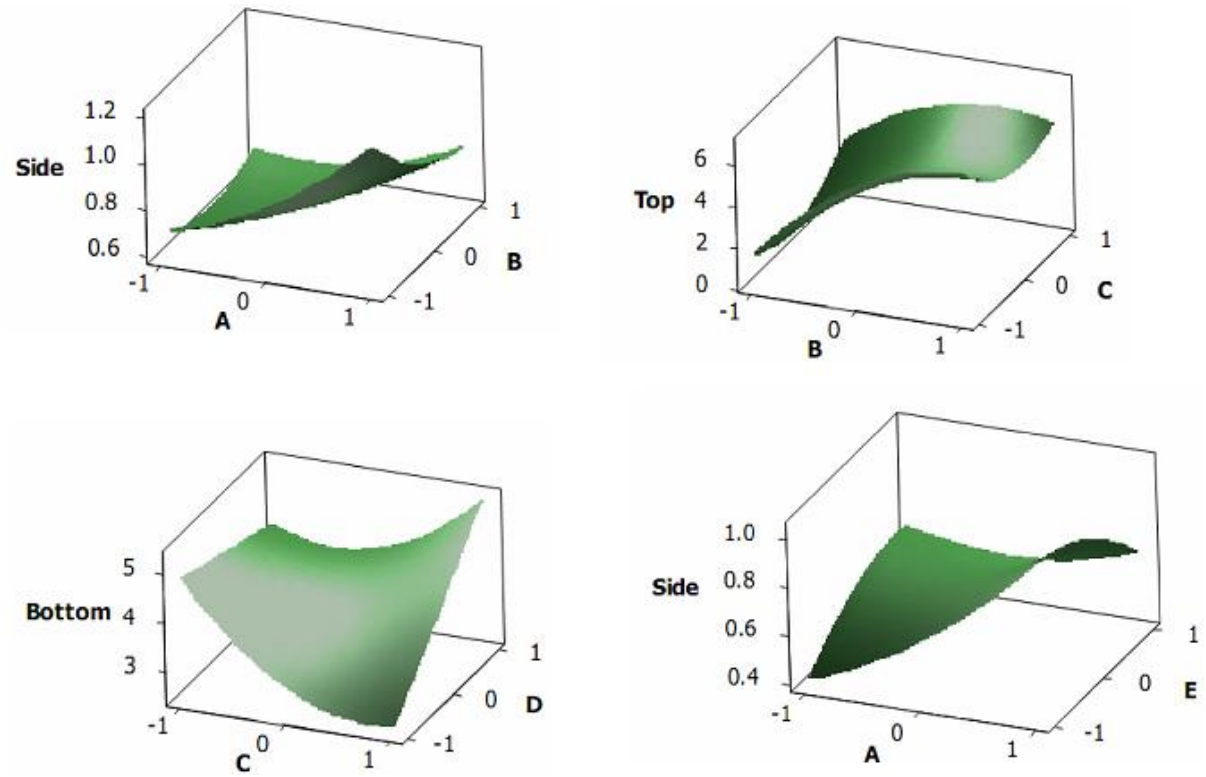

Figure 5.5 Typical Response Surface plots

The final step in this work uses multi-objective optimization to find out best process settings that gives best surface finish in all sides of the part. The common procedure for solving multi-objective optimization problem rests on combining all the objectives into a single objective by assigning weights depending on relative importance of each objective [226]. But this procedure has its own limitations in terms of use of decision-maker's preference of relative weight for each objective, which is highly subjective in nature. To overcome this limitation, this work uses PCA to combine the multiple responses (surface roughness values in three directions) into single response called *MPI*. All normalized individual responses are transformed into uncorrelated linear combinations. For *m* linear combinations there will be *m* principal components. Table 5.6 shows the explained variation in each response and their eigen vectors. The relationship between different principal components (*PC*) and responses are given in equation 5.10 to equation 5.12.

Table 5.6 The explained variation and eigen vector

Principal component (PC)	Eigen Value	Explained variation	Cumulative variation	Eigen vector
PC1	2.0287	0.676	0.676	[0.668, 0.589, -0.454]
PC2	0.8115	0.270	0.947	[0.089, 0.543, 0.835]
PC3	0.1593	0.053	1.000	[-0.738, 0.599, -0.310]

$$PC1 = 0.668\overline{R_a^T} + 0.589\overline{R_a^B} - 0.454\overline{R_a^S} \quad (5.10)$$

$$PC2 = 0.089\overline{R_a^T} + 0.543\overline{R_a^B} - 0.835\overline{R_a^S} \quad (5.11)$$

$$PC3 = 0.738\overline{R_a^T} + 0.599\overline{R_a^B} - 0.310\overline{R_a^S} \quad (5.12)$$

where *PC*1, *PC*2, *PC*3 are three principal components and $\overline{R_a^T}, \overline{R_a^B}, \overline{R_a^S}$ are normalized value of three responses. The values of principal components are shown in Table 5.7.

Table 5.7 Principal components of roughness data

Exp. No.	Principal components		
	*PC*1	*PC*2	*PC*3
1	0.0138640	0.3478388	-0.2114530
2	-0.2364023	1.0189999	-0.1333773
3	1.1349012	0.6158275	-0.1423401
4	1.0431754	0.5147853	-0.3467839
5	0.2919605	0.0954820	-0.3125612
6	0.0277100	0.3753950	-0.0613616
7	0.3266217	0.4994069	-0.1229424
8	0.3220063	0.4929136	-0.2163347
9	0.1378076	0.1270450	0.1401473
10	0.1872494	0.5046956	-0.1973919
11	1.0457778	0.5200828	-0.1844195
12	0.3860770	0.5781913	-0.1313009
13	0.3453206	0.2036800	-0.2609403
14	0.0352218	0.3565027	-0.0791445
15	1.2040789	0.6593951	-0.1117514
16	0.8038243	0.5926653	-0.0880143
17	0.4945655	0.4315422	-0.1807072
18	0.3345071	0.5310085	-0.0859024
19	-0.0077558	0.3078868	-0.1738007
20	0.0996042	0.2186954	-0.1828992
21	0.3028617	0.2898229	-0.3749356
22	0.4271048	0.3526964	-0.1751138
23	0.3158051	0.2851523	-0.2854532
24	0.1948447	0.3147139	-0.0833131
25	0.2733467	0.2407719	-0.1927854
26	0.2915002	0.2579167	-0.2254043
27	0.2688704	0.3601073	-0.2013800
28	0.3432109	0.2815924	-0.2685342
29	0.2424287	0.2327686	-0.3002541
30	0.2266996	0.2632063	-0.1899284
31	0.1066872	0.1504096	-0.2413000
32	0.3264672	0.3559463	-0.3100622

As different principal components have their own variance to account for the total variance, all components are considered to explain the variance in all the responses instead of using only significant principal components. Since these principal components are independent to each other, the *MPI* is calculated by equation 5.13 and is given in Table 5.8.

$$MPI = 0.676PC1 + 0.270PC2 + 0.053PC3 \quad (5.13)$$

Table 5.8 *MPI* value

Exp. No.	Factor A	B	C	D	E	*MPI*
1	-1	-1	-1	-1	1	0.0920815
2	1	-1	-1	-1	-1	0.1082531
3	-1	1	-1	-1	-1	0.9259226
4	1	1	-1	-1	1	0.8257990
5	-1	-1	1	-1	-1	0.2065797
6	1	-1	1	-1	1	0.1168364
7	-1	1	1	-1	1	0.3491202
8	1	1	1	-1	-1	0.3392972
9	-1	-1	-1	1	-1	0.1348879
10	1	-1	-1	1	1	0.2523866
11	-1	1	-1	1	1	0.8375939
12	1	1	-1	1	-1	0.4101408
13	-1	-1	1	1	1	0.2746005
14	1	-1	1	1	-1	0.1158710
15	-1	1	1	1	-1	0.9860712
16	1	1	1	1	1	0.6987401
17	-1	0	0	0	0	0.4412652
18	1	0	0	0	0	0.3649463
19	0	-1	0	0	0	0.0686751
20	0	1	0	0	0	0.1166865
21	0	0	-1	0	0	0.2631151
22	0	0	1	0	0	0.3746698
23	0	0	0	-1	0	0.2753464
24	0	0	0	1	0	0.2122722
25	0	0	0	0	-1	0.2395732
26	0	0	0	0	1	0.2547452
27	0	0	0	0	0	0.2683122
28	0	0	0	0	0	0.2938082
29	0	0	0	0	0	0.2108159
30	0	0	0	0	0	0.2142484
31	0	0	0	0	0	0.0999423
32	0	0	0	0	0	0.3003641

Response surface methodology is used to determine the predictive equation of *MPI* in terms of process parameters. Analysis of variance shows that quadratic model is suitable for *MPI* prediction (Table 5.9). Significance of individual term is established by t-test and the terms having p-value less than 0.05 are considered as significant (Table 5.10). The predictive equation for *MPI* in terms of process parameters is given by equation 5.14.

Table 5.9 ANOVA for *MPI*

Source	Degree of freedom	Sum of square	Variance	F-value	p-value
Regression	20	1.79418	0.089709	6.68	0.001
Linear	5	1.03738	0.207477	15.44	0.000
Square	5	0.33150	0.066300	4.93	0.013
Interaction	10	0.42529	0.042529	3.16	0.036
Residual Error	11	0.14783	0.013439		
Lack-of-Fit	6	0.11981	0.019969	3.56	0.092
Pure Error	5	0.02801	0.005602		
Total	31	1.94200			

Table 5.10 t-test results for *MPI*

Term	Coefficient	p-value
Constant	0.226597	0.000
A	-0.056436	0.063
B	0.228844	0.000
C	-0.021577	0.446
D	0.037963	0.192
E	0.013073	0.642
A×A	0.179997	0.033
B×B	-0.130428	0.105
C×C	0.095784	0.221
D×D	0.020700	0.785
E×E	0.024050	0.751
A×B	-0.044371	0.154
A×C	-0.009483	0.750
A×D	-0.035781	0.243
A×E	0.101267	0.005
B×C	-0.047032	0.133
B×D	0.014901	0.617
B×E	-0.007531	0.800
C×D	0.086281	0.013
C×E	-0.039824	0.197
D×E	0.038285	0.213

$$MPI = 0.226597 + 0.228844B + 0.179997A^2 + 0.101267AE + 0.086281CD \quad (5.14)$$

R^2=92.39%

Anderson-Darling (AD) normality test results (Figure 5.6) signifies that standardized residuals follows normal distribution and model given by equation 5.14 is suitable for navigation in design space for optimal point location.

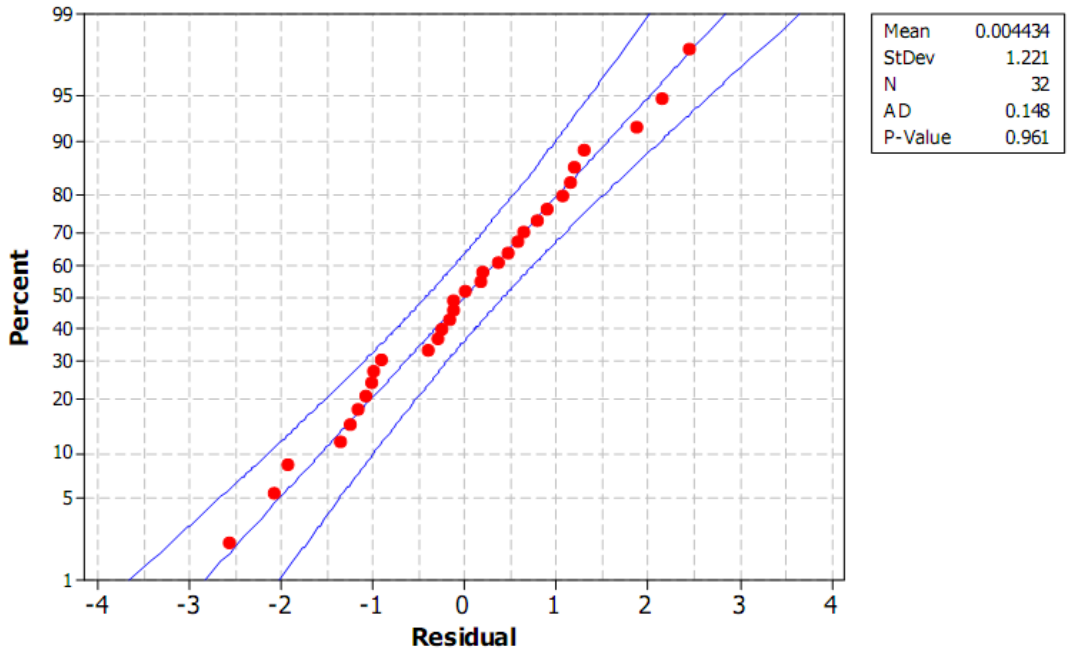

Figure 5.6 Normal probability plot of standardized residual at 95% of confidence interval (Response is *MPI*)

Once the empirical models are validated for *MPI* of FDM built parts, next step is to search the optimization region for finding out suitable parameter settings that maximize responses beyond the experimental domain. Here, the objective function to be maximized is given as:

Maximize *MPI*

Subjected to constraints:

$$A_{min} \le A \le A_{max}$$
$$B_{min} \le B \le B_{max}$$
$$C_{min} \le C \le C_{max}$$
$$D_{min} \le D \le D_{max}$$
$$E_{min} \le E \le E_{max}$$

The min and max in constraints show the lowest and highest control factors settings (control factors) used in this study. To choose the number of reproduction and chemotaxis loop, algorithm is run for fixed number of iterations keeping one of them fixed and increasing the value of other one. It is observed that increase of *MPI* is more pronounced when N_R is increased for fixed value of N_c as compared to change of N_c for fixed value of N_R. Therefore, N_R is fixed at 10,000 whereas N_c is kept at 10. In order to apply BFOA, initial parameters of the are set as: number of bacteria, S =50, chemotactic loop limit, N_c =10, swim length, SL_{max} =100, number of bacteria for reproduction, S_r =50%, elimination-dispersal loop limit, N_{ed} =50, and probability of elimination dispersal, P_{ed} =0.05. The algorithm is coded in MATLAB and run on HP Intel^{R} Core^{TM} 2 DUO processor 2.33GHz, 1.95GB RAM. Algorithm is terminated when error equals to 10^{-3} and the convergence curve is shown in Figure

5.7. A maximum value of *MPI* equals to 0.9456 is obtained after 182 iterations. The optimum process parameter values in coded unit are obtained as: A = -1, B = 0.9983, C = -0.9985, D = -0.9806, and E = -0.9999. In actual parameter settings, the values in uncoded form are described as: layer thickness (A) = 0.127mm, part build orientation (B) = 29.97°, raster angle (C) = 0.045°, raster width (D) = 0.407mm and air gap (E) = 0.0000004 mm. Comparison of these values with nearest possible process parameter values shown in Table 5.1 reveals that experiment number 3 having process parameters A, B, C, D and E values as 0.127 mm, 30°, 0°, 0.4064 mm and 0 mm respectively is closer to optimum parameter value and has a *MPI* of 0.9259 which happens to be less than *MPI* calculated using BFOA (0.9456).

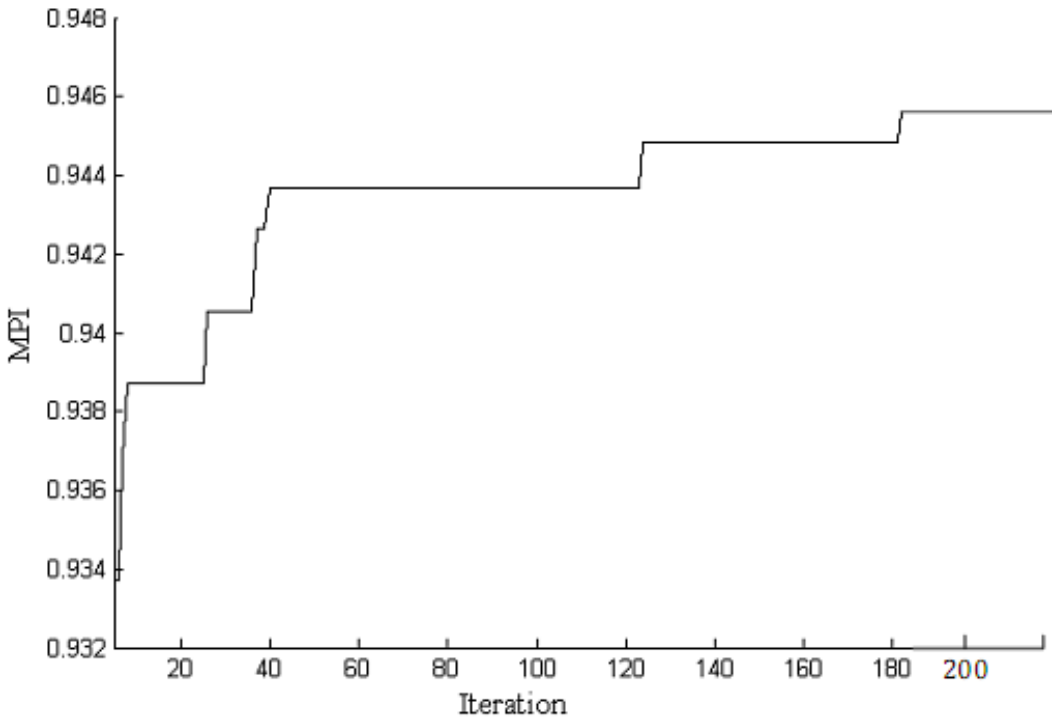

Figure 5.7 Convergence curve

5.6 Conclusions

Surface quality, particularly, surface roughness is an important characteristic of manufactured products for engineering application because it determines the functionality of the part in a specific situation, particularly in bearings, gears, guide ways, and applications subjected to fatigue loading. In FDM process, many process variables interact in a complex manner influencing material deposition making it difficult to develop modelling and analysis approaches for assessment of resultant properties of built parts. Therefore, an attempt has been made in this work to develop valid empirical model using experimental data. For this purpose, a response surface methodology (FCCCD) has been adapted keeping in view of limitations of

adjustments of machine parameters and experimental time and cost. Many variables as much as five process parameters viz., layer thickness, orientation, raster angle, raster width and air gap are considered in this study. Quadratic models involving parameters and their square terms and interactions have been estimated and validated using ANOVA and residual analysis. The response plots are analysed to assess influence of each factor and their interaction on surface roughness. The coefficients of determination (R^2) of predictive models for surface roughness are found to be 92.10%, 90.97% and 97.11% for top, bottom and side surface respectively. The models contain different factors and their square and interaction terms for surface roughness along different surfaces. In an attempt to find a best parameter setting for surface roughness along all the surfaces, the responses along three surfaces are combined into a single response (*MPI*) using weighted principal component analysis. *MPI* involves all the principal components so that total variance can be accounted for. PCA method eases out assignment of relative weight to each objective. The weights are calculated as percentage of variation explained by each component. Therefore, user preference, which is highly subjective in nature, is effectively avoided in a multi-objective optimization situation. Again, a quadratic model suitable for *MPI* prediction is developed and validated by ANOVA and residual analysis. The coefficient of determination for predictive model of *MPI* is found to be 92.39%. Finally, bacteria foraging optimization approach is adopted to find out optimal parameter setting for improving surface finish along three surfaces simultaneously. The rationale for using bacteria foraging lies in the fact that it is more efficient in maintaining the diversity of the swarm as all the particles use the information related to the most successful particle in order to improve themselves. The optimal parameter setting is listed as layer thickness (A) = 0.127mm, part build orientation (B) = 29.97°, raster angle (C) = 0.045°, raster width (D) = 0.407mm and air gap (E) = 0.0000004 mm resulting in *MPI* value of 0.9456. Due to hardware limitations, it is not possible to conduct the experiment at these optimal factor level values. But it is observed that these optimal values are nearer to the factor level setting used in experiment number 3 (Table 5.1). Comparison of these values with nearest possible process parameter values found experimentally in experiment number 3 shows that experimental setting has a *MPI* of 0.9259 which happens to be less than *MPI* produced by BFOA. The study highlights a simple but workable approach for prediction of surface roughness along various surfaces of FDM built parts combining response surface methodology, principal component analysis and bacteria foraging optimization technique. The method is quite general and can be

adapted to any process optimization situation when multiple objectives need to be optimised.

CHAPTER 6

IMPROVEMENT OF MECHANICAL STRENGTH

6.1 Introduction

Reduction of product development cycle time is a major concern in industries to remain competitive in the marketplace and hence, focus has shifted from traditional product development methodology to rapid fabrication techniques like rapid prototyping (RP) [11-16]. The RP process is capable of building parts of any complicated geometry in least possible time without incurring extra cost due of absence of tooling [22-25]. Another advantage with RP is to produce functional assemblies by consolidating sub assemblies into single unit at the computer aided design (CAD) stage and thus reduces part counts, handling time, and storage requirement and avoids mating and fit problem [35-46]. Although RP is an efficient technology, full scale application has not gained much emphasis because of compatibility of presently available materials with RP technologies [130-138]. To overcome this limitation, one approach may be development of new materials having superior characteristics than conventional materials and its compatibility with technology [119-134]. Another convenient approach may be suitably adjusting the process parameters during fabrication stage so that properties may improve. A good number of researchers have devoted towards the second approach [151-155, 160-166, 182-190]. Literature reveals that properties of RP parts are function of various process related parameters and can be significantly improved with proper adjustment. Since mechanical properties are important for functional parts, it is absolutely essential to study influence of various process parameters on mechanical properties so that improvement can be made through selection of best settings. The present chapter focuses on the assessment of mechanical properties namely tensile, flexural, impact and compressive strength of part fabricated using fused deposition modelling (FDM) technology. As the relation between mechanical property and process parameters is difficult to establish, attempt has been made to derive the empirical model between the processing parameters and mechanical properties using central composite design (CCD) methodology. In addition, effect of each process parameter on mechanical property is analyzed.

In actual practice, the parts are subjected to various types of loadings and it is necessary that the fabricated part must withhold more than one mechanical property simultaneously. To address this issue, a desirability function approach is used to combine all the studied responses into single objective known as composite desirability. Advantage of using this approach lies in the fact that composite desirability lies between user defined minimum and maximum limits of each response and hence more realistic. Finally, composite desirability is maximized using quantum

behaved particle swarm optimization (QPSO). QPSO is a stochastic optimization algorithm that was originally motivated by the thinking model of an individual of the social organism. Unlike its predecessor particle swarm optimization (PSO), it is based on the quantum behavior of particle. The experiment results on several benchmark functions indicate that the QPSO is more effective and a promising algorithm in many engineering applications as compared to other conventional algorithms [227-229]. The next section discusses the experiment methodology used in this work. This is followed by analysis of experimental results in section 6.3. Discussion on the effect of process parameters on studied mechanical strengths is presented in section 6.4. Process parameter optimization is presented in section 6.5. This section also presents the comparative evaluation of QPSO with its precursor PSO. Desirability function approach for combining all the studied strengths into composite desirability is also presented in this section. In the end, conclusions from present study are highlighted in section 6.6.

6.2 Experimental methods

Factors and their levels are selected as per the discussion given in section 3.6 in chapter 3 and shown in Table 3.5. For conducting tensile, flexural, impact and compression test three specimens of each shown in Figure 3.8, Figure 3.10, Figure 3.13, and Figure 3.14 respectively is manufactured in FDM vantage SE machine using ABSP400 as material. For specimen fabrication, process parameters are set in accordance to the experiment plan given in Table 3.7. Procedure of testing is explained in sub-section 3.4.3 to section 3.4.6 for respective strength measurement.

6.3 Analysis of experimental results

Mean of each experiment trial is taken as represented value of respective strength and shown in Table 6.1.

Table 6.1 Experimental data obtained from the FCCCD runs

Run order	Factor (Coded units)					Tensile Strength (MPa)	Flexural Strength (MPa)	Impact Strength (MJ/m^2)	Compressive Strength (MPa)
	A	B	C	D	E				
1	-1	-1	-1	-1	+1	15.6659	34.2989	0.367013	15.21
2	+1	-1	-1	-1	-1	16.1392	35.3593	0.429862	12.41
3	-1	+1	-1	-1	-1	9.1229	18.8296	0.363542	10.16
4	+1	+1	-1	-1	+1	13.2081	24.5193	0.426042	10.78
5	-1	-1	+1	-1	-1	16.7010	36.5796	0.375695	14.28
6	+1	-1	+1	-1	+1	17.9122	38.0993	0.462153	15.83
7	-1	+1	+1	-1	+1	18.0913	39.2423	0.395833	7.448
8	+1	+1	+1	-1	-1	14.0295	22.2167	0.466667	16.98
9	-1	-1	-1	+1	-1	14.4981	27.6040	0.342708	13.89
10	+1	-1	-1	+1	+1	14.8892	34.5569	0.429167	16.18

11	-1	+1	-1	+1	+1	11.0262	20.0259	0.379167	11.13
12	+1	+1	-1	+1	-1	14.7661	25.2563	0.450001	10.44
13	-1	-1	+1	+1	+1	15.4510	36.2904	0.375000	13.58
14	+1	-1	+1	+1	-1	15.9244	37.3507	0.437785	16.29
15	-1	+1	+1	+1	-1	11.8476	22.9759	0.419792	11.83
16	+1	+1	+1	+1	+1	15.9328	28.8362	0.482292	10.78
17	-1	0	0	0	0	13.4096	27.7241	0.397222	12.49
18	+1	0	0	0	0	15.8933	33.0710	0.44757	12.34
19	0	-1	0	0	0	14.4153	34.7748	0.402082	14.98
20	0	+1	0	0	0	9.9505	25.2774	0.388539	12.28
21	0	0	-1	0	0	13.7283	27.5715	0.382986	11.95
22	0	0	+1	0	0	14.7224	30.0818	0.401388	11.87
23	0	0	0	-1	0	13.5607	28.9856	0.401041	11.56
24	0	0	0	+1	0	13.8388	28.8622	0.395833	11.25
25	0	0	0	0	-1	13.6996	28.8063	0.405555	12.26
26	0	0	0	0	+1	13.8807	29.0359	0.409028	11.09
27	0	0	0	0	0	14.4088	29.7678	0.407292	11.72
28	0	0	0	0	0	13.0630	31.6717	0.396373	12.48
29	0	0	0	0	0	13.8460	30.1584	0.406558	12.67
30	0	0	0	0	0	13.8727	31.0388	0.397712	11.31
31	0	0	0	0	0	13.5914	29.1475	0.401156	11.01
32	0	0	0	0	0	13.2189	31.9426	0.410686	12.88

Analysis of the experimental data obtained from FCCCD design runs is carried out on MINITAB R14 software at 95% of confidence. Based on analysis of variance (ANOVA), full quadratic model was found to be suitable for tensile strength (Table 6.2), flexural strength (Table 6.3), impact strength (Table 6.4) and compressive strength (Table 6.5) with regression p-value less than 0.05 and lack of fit more then 0.05. For tensile strength, all the terms are significant whereas square terms are insignificant for flexural strength and interaction terms do not impart significant effect on impact strength. Based on p-value, it can be concluded that the compressive stress is mainly influenced by the linear terms and interaction terms followed by square terms.

Table 6.2 ANOVA for Tensile strength

Source	Degree of freedom	Sum of square	Variance	F-value	p-value
Regression	20	112.482	5.6241	11.65	0.000
Linear	5	64.373	12.875	26.66	0.000
Square	5	14.966	2.9932	6.20	0.006
Interaction	10	33.143	3.3143	6.86	0.002
Residual	11	5.312	0.4829		
Lack of fit	6	4.116	0.6861	2.87	0.134
Pure error	5	1.196	0.2392		
Total	31	117.794			

Table 6.3 ANOVA for Flexural strength

Source	Degree of freedom	Sum of square	Variance	F-value	p-value
Regression	20	799.058	39.953	14.96	0.000
Linear	5	611.818	122.36	45.81	0.000
Square	5	4.47	0.894	0.33	0.882
Interaction	10	182.771	18.277	06.84	0.002
Residual	11	29.383	2.671		
Lack of fit	6	23.245	3.874	3.16	0.114
Pure error	5	6.138	1.228		
Total	31	828.442			

Table 6.4 ANOVA for Impact strength

Source	Degree of freedom	Sum of square	Variance	F-value	p-value
Regression	20	0.0293	0.00146	16.72	0.000
Linear	5	0.0258	0.00515	58.88	0.000
Square	5	0.0019	0.00038	4.30	0.021
Interaction	10	0.0016	0.00016	1.85	0.164
Residual	11	0.001	8.8E-05		
Lack of fit	6	0.0008	0.00013	4.03	0.074
Pure error	5	0.0002	3.3E-05		
Total	31	0.0302			

Table 6.5 ANOVA for Compressive strength

Source	Degree of freedom	Sum of square	Variance	F-value	p-value
Regression	20	126.839	6.3420	13.66	0.000
Linear	5	65.700	13.1400	28.30	0.000
Square	5	11.653	2.3306	5.02	0.012
Interaction	10	49.486	4.9486	10.66	0.000
Residual	11	5.107	0.4642		
Lack of fit	6	2.119	0.3532	0.59	0.731
Pure error	5	2.987	0.5975		
Total	31	131.946			

The t-test was performed to determine the individual significant term at 95% of confidence level and results are shown from Table 6.6 to Table 6.9 for respective strength.

Table 6.6 t-test result for Tensile Strength

Term	Coefficient	t-value	p-value
Constant	13.5625	68.289	0.000
A	0.7156	4.369	0.001
B	-1.3123	-8.012	0.000
C	0.9760	5.959	0.000
D	-0.3476	-2.122	0.057
E	0.5183	3.164	0.009
A*A	1.1671	2.635	0.023
B*B	-1.3014	-2.938	0.014
C*C	0.7410	1.673	0.123
D*D	0.2154	0.486	0.636
E*E	0.3058	0.690	0.504
A*B	0.3312	1.906	0.083
A*C	-0.4363	-2.512	0.029
A*D	0.4364	2.512	0.029
A*E	-0.4364	-2.512	0.029
B*C	0.4364	2.512	0.029
B*D	0.2985	1.718	0.114
B*E	0.4898	2.819	0.017
C*D	-0.5389	-3.102	0.010
C*E	0.5389	3.102	0.010
D*E	-0.5389	-3.102	0.010

Table 6.7 t-test result for Flexural Strength

Term	Coefficient	t-value	p-value
Constant	29.9178	64.052	0.000
A	0.8719	2.263	0.045
B	-4.8741	-12.653	0.000
C	2.4251	6.295	0.000
D	-0.9096	-2.361	0.038
E	1.6626	4.316	0.001
A*A	1.0073	0.967	0.354
B*B	0.6358	0.610	0.554
C*C	-0.5636	-0.541	0.599
D*D	-0.4664	-0.448	0.663
E*E	-0.4692	-0.450	0.661
A*B	-0.6774	-1.658	0.126
A*C	-1.7199	-4.209	0.001
A*D	1.7412	4.261	0.001
A*E	-1.1275	-2.759	0.019
B*C	0.5087	1.245	0.239
B*D	0.0513	0.126	0.902
B*E	1.0621	2.599	0.025
C*D	-0.3200	-0.783	0.450
C*E	1.0621	2.599	0.025
D*E	-1.0408	-2.547	0.027

Table 6.8 t-test result for Impact Strength

Term	Coefficient	t-value	p-value
Constant	0.401992	150.343	0.000
A	0.034198	15.508	0.000
B	0.008356	3.789	0.003
C	0.013673	6.200	0.000
D	0.001328	0.602	0.559
E	0.001894	0.859	0.409
A*A	0.021383	3.585	0.004
B*B	-0.005703	-0.956	0.360
C*C	-0.008826	-1.480	0.167
D*D	-0.002576	-0.432	0.674
E*E	0.006278	1.053	0.315
A*B	-0.001993	-0.852	0.412
A*C	-0.000004	-0.002	0.999
A*D	-0.000004	-0.002	0.999
A*E	0.000004	0.002	0.999
B*C	0.003997	1.709	0.116
B*D	0.008077	3.453	0.005
B*E	-0.003997	-1.709	0.116
C*D	-0.000004	-0.002	0.999
C*E	0.000004	0.002	0.999
D*E	0.000004	0.002	0.999

Table 6.9 t-test result for Compressive Strength

Term	Coefficient	t-value	p-value
Constant	12.0164	61.712	0.000
A	0.6673	4.155	0.002
B	-1.7123	-10.662	0.000
C	0.3743	2.331	0.040
D	0.0396	0.246	0.810
E	-0.3618	-2.253	0.046
A*A	0.3950	0.909	0.383
B*B	1.6100	3.707	0.003
C*C	-0.1100	-0.253	0.805
D*D	-0.6150	-1.416	0.185
E*E	-0.3450	-0.794	0.444
A*B	0.2914	1.711	0.115
A*C	0.8326	4.888	0.000
A*D	-0.3526	-2.070	0.063
A*E	0.0151	0.089	0.931
B*C	0.1399	0.821	0.429
B*D	-0.2124	-1.247	0.238
B*E	-0.8251	-4.844	0.001
C*D	-0.3211	-1.885	0.086
C*E	-1.1339	-6.657	0.000
D*E	0.2364	1.388	0.193

Final response surface equations for tensile strength (F_T), flexural strength (F_F), impact strength (F_I) and Compressive Strength (F_C) are given from equations

6.1–6.4 respectively in terms of coded units. The coefficient of determination (R^2) which indicates the percentage of total variation in the response explained by the terms in the model is 95.5%, 96.5%, 96.8% and 96.13% for tensile, flexural, impact strength and compressive strength, respectively.

$$F_T=13.5625 + 0.7156A - 1.3123B + 0.9760C + 0.5183E + 1.1671A^2 - 1.3014B^2 - 0.4363AC + 0.4364AD - 0.4364AE + 0.4364BC + 0.4898BE - 0.5389CD + 0.5389CE - 0.5389DE \quad (6.1)$$

$$F_F=29.9178 + 0.8719A - 4.8741B + 2.4251C - 0.9096D + 1.6626E -1.7199AC+1.7412AD - 1.1275AE + 1.0621BE + 1.0621CE - 1.0408DE \quad (6.2)$$

$$F_I=0.401992 + 0.034198A + 0.008356B + 0.013673C+ 0.021383A^2 + 0.008077BD \quad (6.3)$$

$$F_C=12.0164 + 0.6673A -1.7123B + 0.3743C - 0.3618E + 1.61B^2 + 0.8326AC -0.8251BE-1.1339CE \quad (6.4)$$

The model adequacy is checked by Anderson–Darling (AD) normality test shown in Figure 6.1. Since p-value of the normality plots is found to be above 0.05, it indicates that residuals follows normal distribution and the predictions made by the mathematical models are in good agreement with the experimental values.

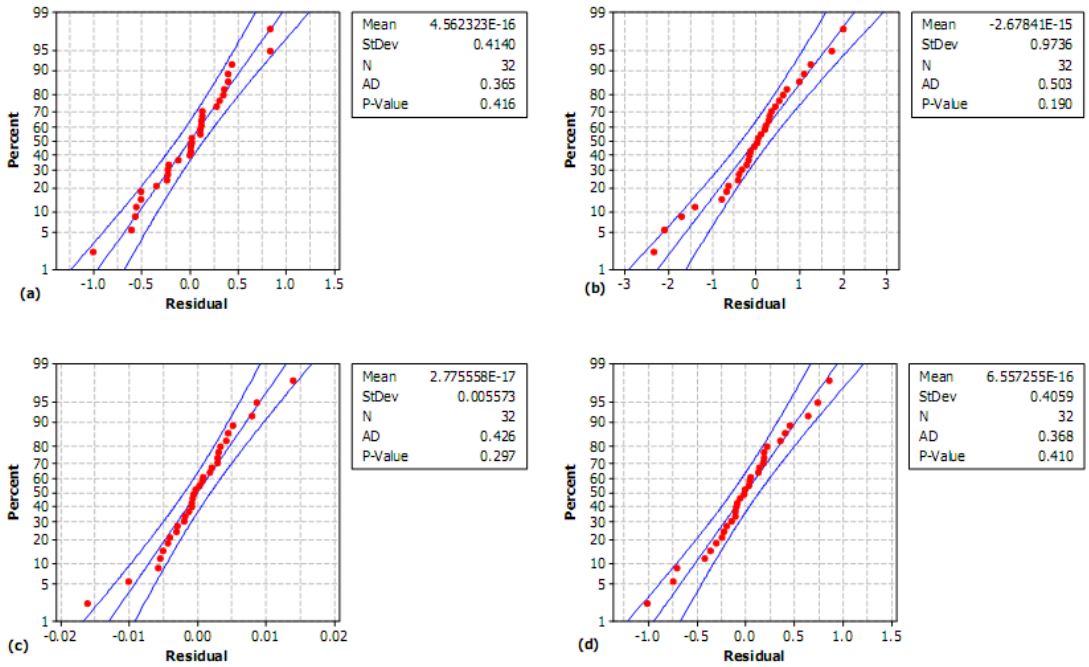

Figure 6.1 Normal probability plot of residual at 95% of confidence interval: (a) response is tensile strength, (b) response is flexural strength, (c) response is impact strength, and (d) response is compressive strength.

6.4 Discussions

In FDM process, build material in the form of a flexible filament is partially melted and extruded from a robotically controlled deposition nozzle onto a table in a temperature-controlled environment for building the 3-D part layer by layer. The 3-D part takes the form of a laminate composite with vertically stacked layers consisting of contiguous material fibres (raster) with interstitial voids (air gap) (Figure 4.9). During part fabrication, uneven heating and rapid cooling cycles of the material result in non-uniform temperature gradients. The reasons attributed to non uniform heating and cooling cycles are explained as follows:

- Material is extruded out from depositing nozzle in a semi molten state. Its temperature is higher than the already deposited material temperature and builds chamber temperature. Part of the heat will go towards the adjacent deposited material and results in localized increase in adjacent material temperature. Due to this phenomenon, local re-melting of previously solidified material takes place and causes to diffuse and bond with extruded material. Part of the heat of extruded material will go towards the bottom layer material and develops a non uniform temperature gradient towards bottom layer. This process will continue until complete part is built [180, 186].

- As the nozzle tip temperature is higher than the build chamber or deposited material temperature, heat transfer will take place from nozzle tip towards the deposited material. Speed at which nozzle is depositing the material may alter the heating and cooling cycle and results in different degree of thermal gradient. It is observed that nozzle deposition speed is slower at lower slice thickness as compared to higher slice thickness. Also during deposition, nozzle stops depositing material if material is trapped or temperature is increased and return to service location for tip cleaning. While depositing the material at the turns near the boundary of part, nozzle speed has to be decreased to avoid jerk to the nozzle and increase to uniform speed on straight deposition path [118, 185].

- If the direction of deposition is long enough then large temperature difference between the start and end point along the deposition length occurs. Thus, temperature gradient will be developed along the direction of deposition. Hence, short deposition length (raster length) is preferred along the long axis of the part to reduce the temperature gradient [187, 189].

- The void created by air gap of two adjacent layers (Figure 4.9) may provide the small pockets for heat dissipation.

The non uniform temperature gradient cause stresses to build up leading to distortion, inner layer cracking (Figure 6.2) or de-lamination [180, 185-187] and hence reduce mechanical strength.

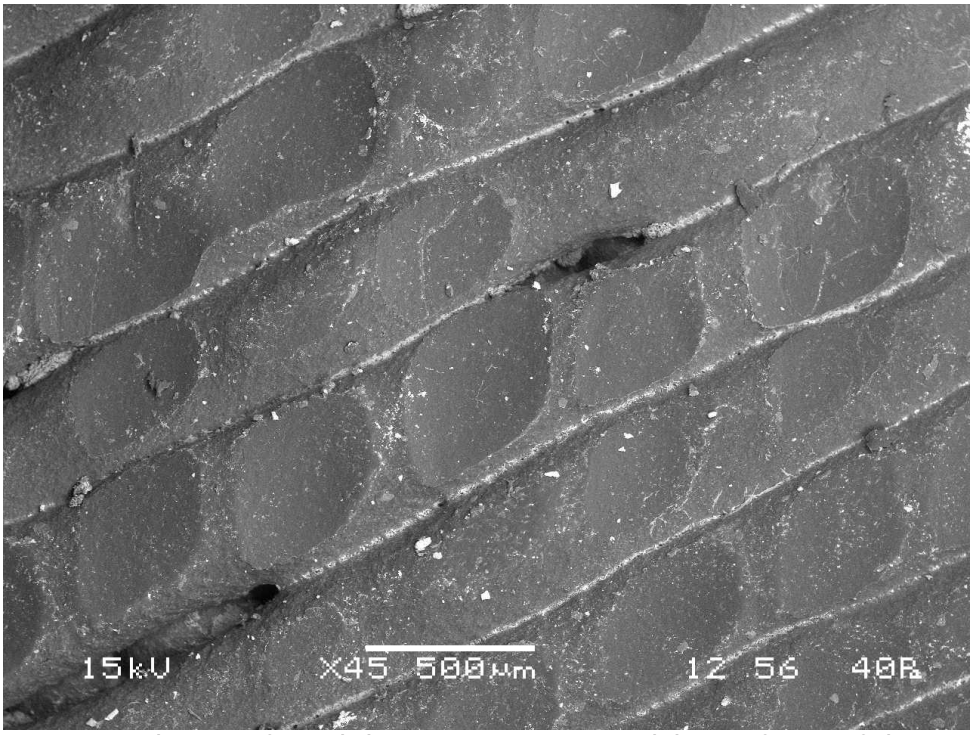

Figure 6.2 SEM image of crack between two rasters (The surfaces of the test part were examined by scanning electron microscope (SEM) JEOL JSM-6480LV in the LV mode)

To understand the effect of process parameters on mechanical strength, response surfaces for respective strength significant interaction terms are analyzed as follows:

6.4.1 Response surface analysis for tensile strength

From response surfaces (Figure 6.3, T1, T2, and T3), it can be noted that tensile strength first decreases and then increases as layer thickness (A) increases. The weak interlayer bonding is responsible for decrease in strength because distortion occurs due to high temperature gradient towards the bottom layers. As the layer thickness increases, less number of layers will be required and distortion effect is minimized and hence, strength increases [15,16]. Similarly number of layers increases with orientation (B) and hence, distortion phenomenon dominates resulting in decrease in strength (Figure 6.3, T4, T5). But for small value of orientation, decrease in strength is relatively small. Strength increases with the increase of raster angle (C) (Figure 6.3, T1, T4, T6 and T7) because higher raster angles produce smaller rasters which are subjected to less distortion [15,17]. From Figure 6.3 T2, T6 and T8, it can be corroborated that effect observed in case of increase in raster length is also seen with increase in raster width. It is expected that small air gap helps to create strong bond between two rasters and thus, improves strength. But, small air gap restricts heat dissipation; thus increases chance of stress accumulation.

Positive air gap causes flow of material towards the adjacent layers through the gap and increases bonding of surfaces (Figure 4.9). Therefore, strength improves with air gap (Figure 6.3, T3 and T5). It is to be noted from Figure 4.9 that gap is present after two rasters and not between each rasters. SEM image of fracture surface (Figure 6.4) shows that failure is caused because of pulling and rupturing of rasters and material separation occurs in a plane approximately normal to a tensile stress. The stress–strain curve shown in Figure 6.5 indicates the brittle nature of failure. The staircase pattern shows that force per unit area has reached a value at which material continues to deform. After that it increases without causing significant deformation. This pattern is repeated in regular steps until the part fractures. It can be concluded that failure will start at weakest raster resulting in increase in stress on surviving rasters and as the load is further increased next weak raster will break and so forth. Thus, to offer resistance against the failure rasters must be strong.

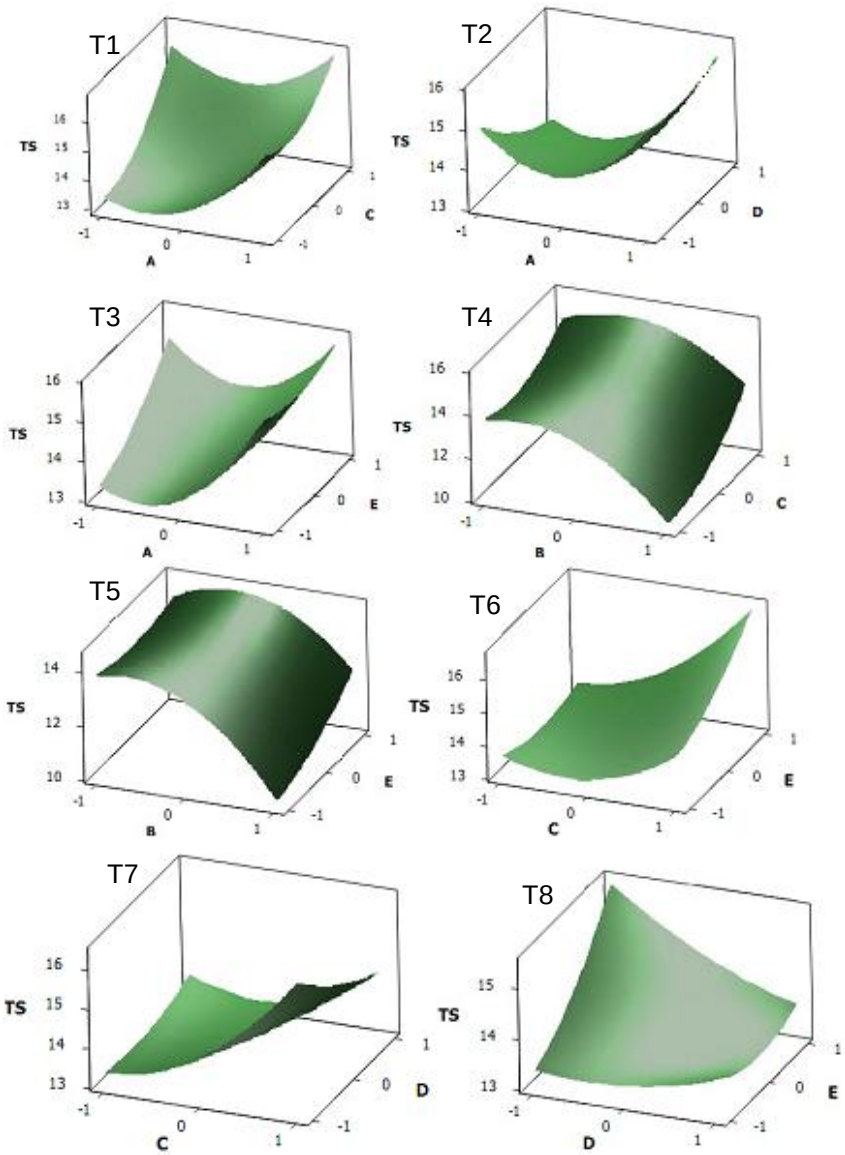

Figure 6.3 Response surface for tensile strength (TS)

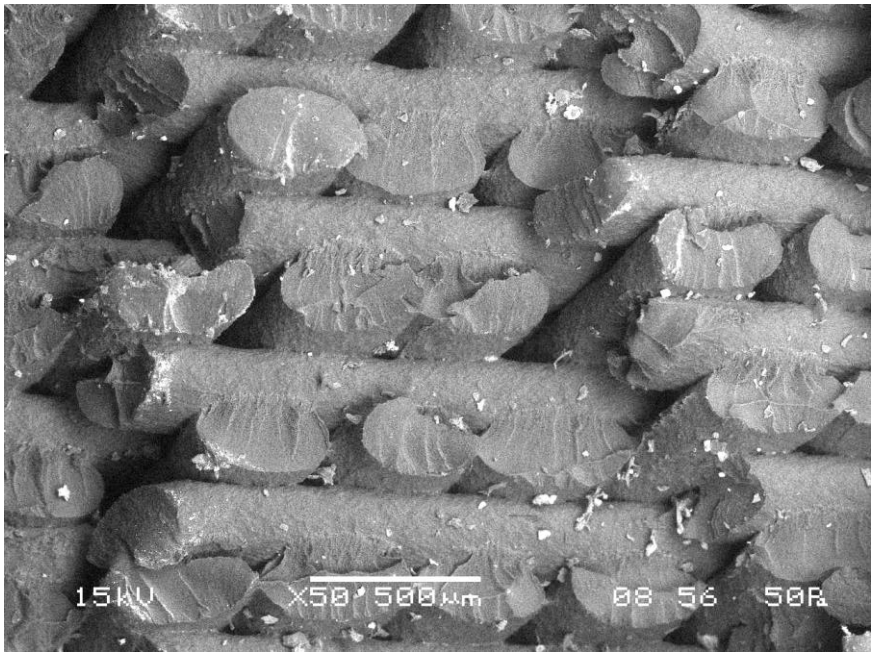

Figure 6.4 SEM image of tensile failure of specimen (The surfaces of the test part were examined by scanning electron microscope (SEM) JEOL JSM-6480LV in the LV mode)

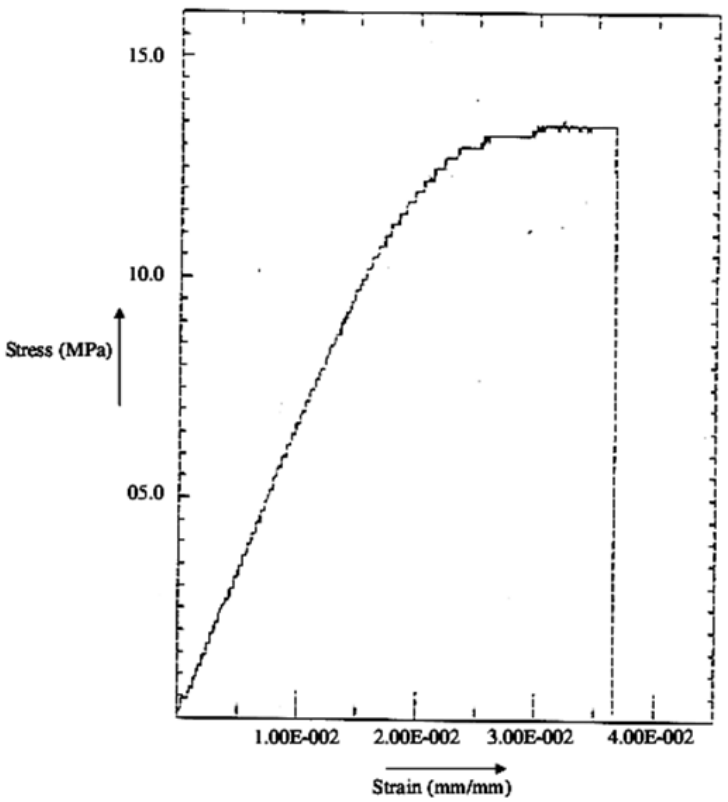

Figure 6.5 Stress–Strain curve for Tensile Strength

6.4.2 Response surface analysis for flexural strength

From response surface plots shown in Figure 6.6, it can be observed that effect of orientation (B), raster angle (C), raster width (D) and air gap (E) on the flexural strength is similar to what is observed for the case of tensile strength (Figure 6.3). The reasons discussed for tensile strength behaviour can be extended here. Flexural strength increases at lower values of raster angle (Figure 6.6, F1) and air gap (Figure 6.6, F3) as layer thickness (A) increases and shows opposite trend at the higher value of raster angle and air gap. As observed (Figure 6.6, F1) maximum strength will be at minimum layer thickness and higher raster angle. It seems strong bonding due to high temperature gradient towards the bottom layers influences more on the flexural strength and reduction in distortion of rasters also contributes to some extent. At zero degree orientation, rasters will offer more resistance to bending because they are parallel to bending plane as length is more. When raster orientation increases, their inclination with respect to plane of bending changes producing rasters of smaller length and net effect is decrease in resistance. It seems that interaction of these two effects results in increase in strength as layer thickness increase at low value of raster angle and decrease in strength at high value of raster angle. Similarly, positive air gap increases the heat dissipation and thus results in higher strength at lower layer thickness (Figure 6.6, F3). Response surface between layer thickness and raster width shows that strength decreases on increasing layer thickness at any fixed value of raster width. This may be due to reduction in bonding strength of bottom layer rasters and also it is easy to bend thin rasters as well as thick rasters which are distorted due to excess heat input.

Examination of fracture specimen reveals that failure starts at tensile side but pieces are held together by unbroken fibres of compression side and also crack propagation along load direction is almost straight for specimen built at zero degree of orientation (Figure 6.7). Stress–strain curve for flexural strength shown in Figure 6.8 show the staircase pattern indicating breaking of individual rasters.

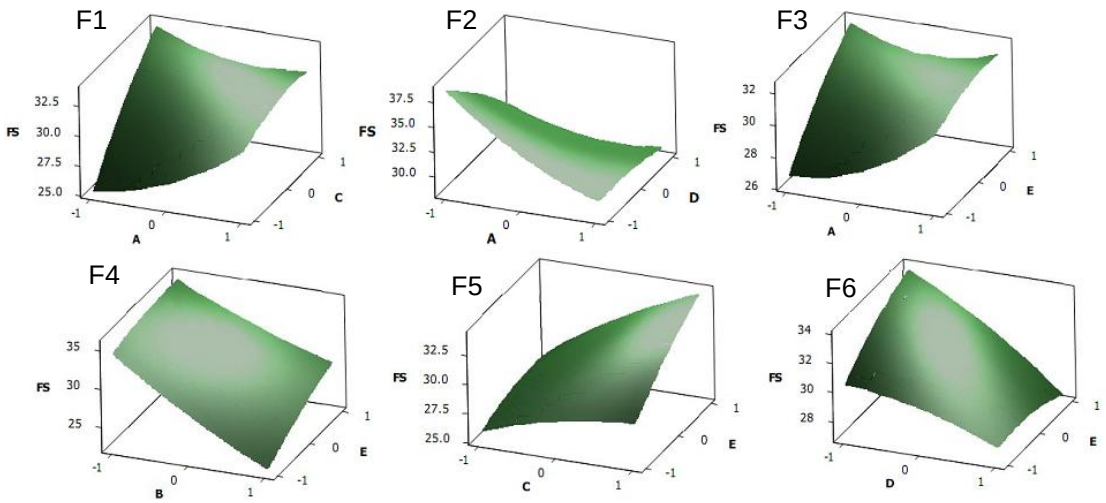

Figure 6.6 Response surface for flexural strength (FS)

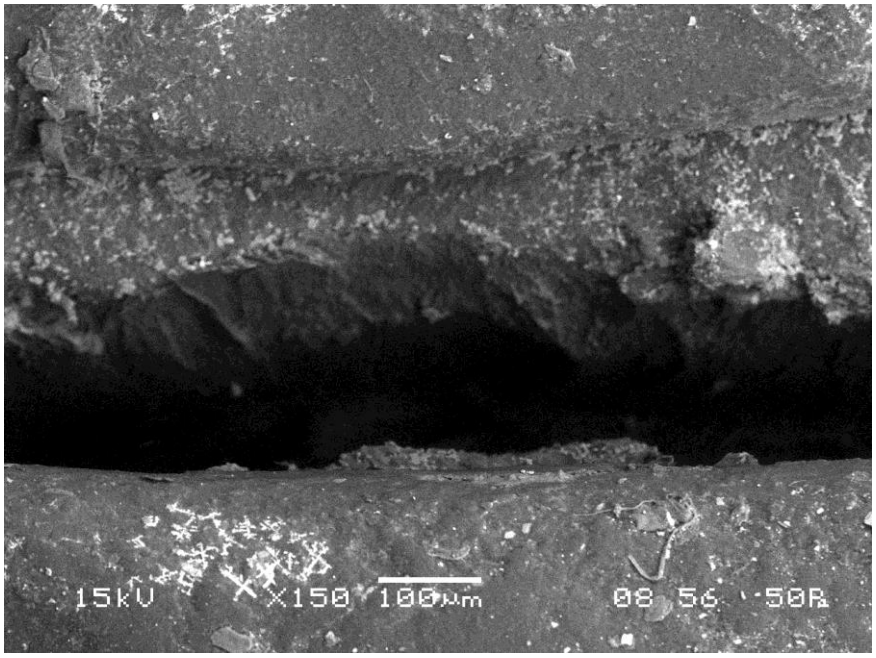

Figure 6.7 Crack surface of flexural specimen (The surfaces of the test part were examined by scanning electron microscope (SEM) JEOL JSM-6480LV in the LV mode)

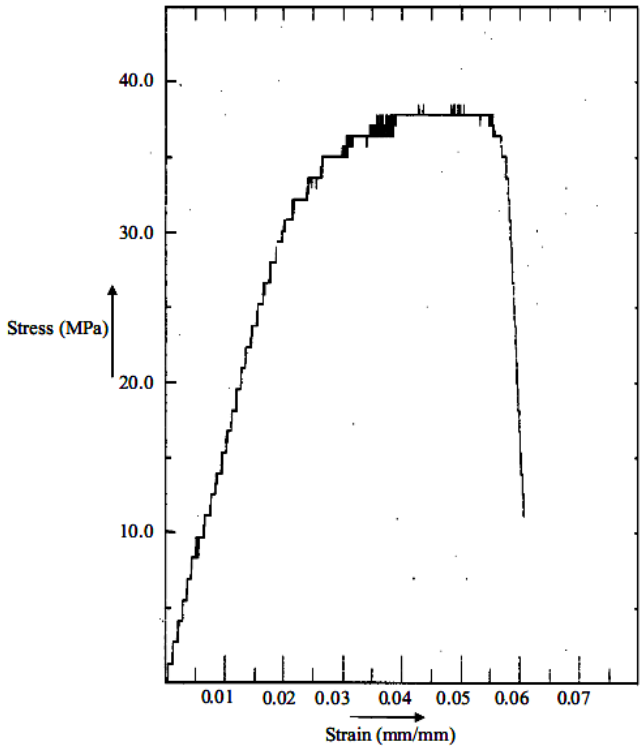

Figure 6.8 Stress-Strain curve for flexural strength

6.4.3 Response surface analysis for impact strength

The response surface of impact strength versus orientation (B) and raster width (D) (Figure 6.9) shows that strength increases and then decreases at lower value of raster width. Increase in orientation causes increase in number of layers. Increase in number of layers increases the heat conduction towards bottom layers resulting in increase in the temperature at bonding interface and hence, proper diffusion takes place between adjacent rasters. Thus, strength increases on increasing the orientation. But this has some adverse effect in causing increase in interlayer distortion and therefore, strength decreases after certain value of orientation. At higher value of raster width (Figure 6.9), strength increases with the increase in orientation. This may be due to the fact that thicker rasters offer more resistance to impact blow. Also excess heat input by thick rasters results in strong bonding between rasters; thus high strength. SEM image of fracture surface for impact specimen is shown in Figure 6.10 indicates failure by sudden rupture of rasters.

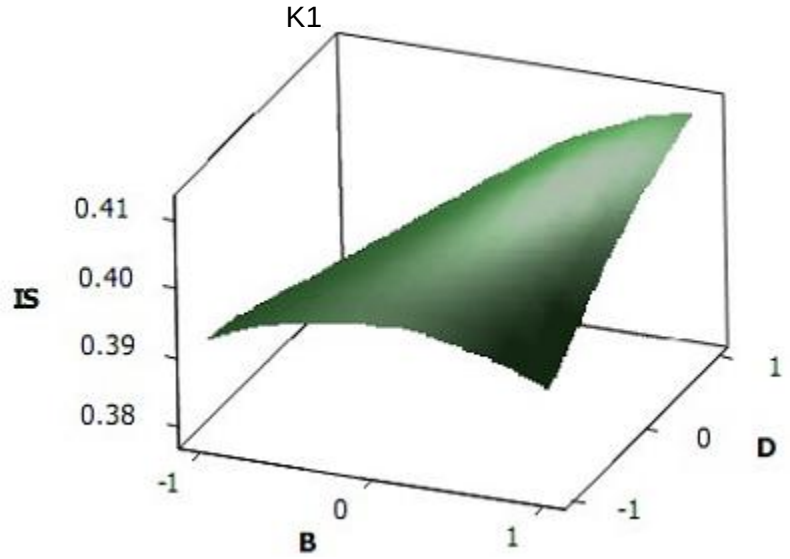

Figure 6.9 Response surface for impact strength (IS)

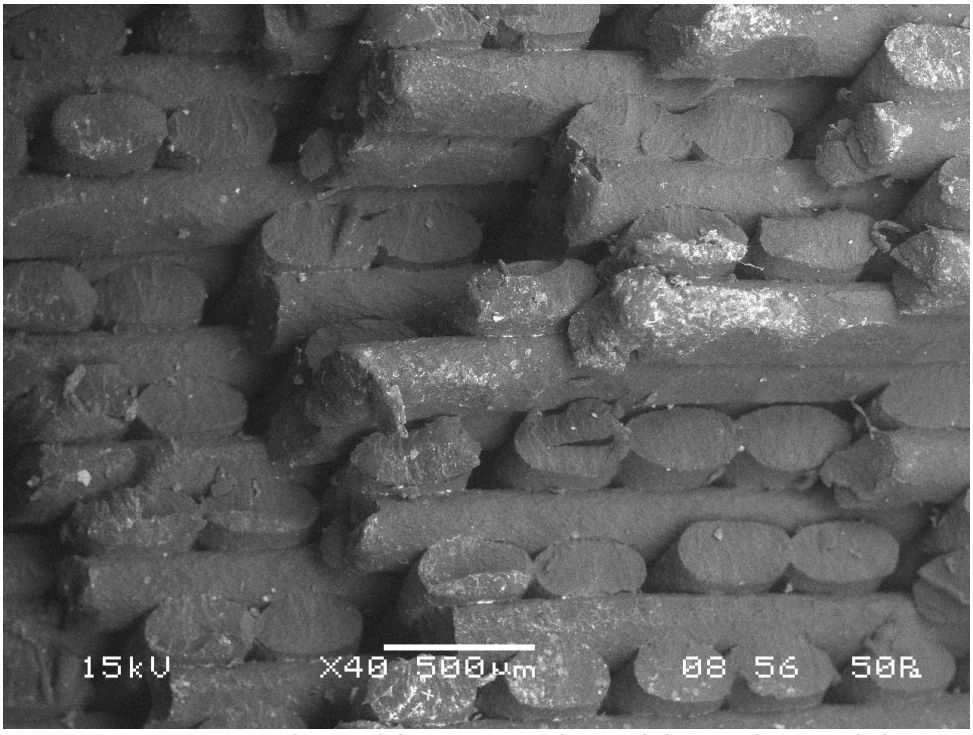

Figure 6.10 Fracture surface of impact specimen (The surfaces of the test part were examined by scanning electron microscope (SEM) JEOL JSM-6480LV in the LV mode)

6.4.4 Response surface analysis for compressive strength

From response surface plot shown in Figure 6.11, decrease in layer thickness (A) (Figure 6.11C1) or increase in part build orientation (B) (Figure 6.11C2), both causes increase in number of layers thus decreases compressive strength. When two similar slices are filled with rasters at different angles for each slice, one with larger raster angle value will have more number of rasters having lengths smaller

than the slice with smaller raster angle. Thus, it can be said that increase in raster angle will decrease the raster length and improve the compressive strength. Figure 6.11C1 and Figure 6.11C3 are in agreement to above conclusion. On the contrary, compressive strength decreases at low level of layer thickness (A) in Figure 6.11C1 and high level of air gap (E) in Figure 6.11C3 on increasing raster angle (C). Further, Figure 6.11C1 shows that the compressive stress decreases with increase in layer thickness (A) at low level of raster angle (C) although numbers of layers are decreasing. It can be believed for Figure 6.11C1 that increase in raster angle minimizes distortion in single layer but if number of layers is increased, accumulated distortion due to raster angle becomes prominent irrespective of raster angle. Similarly, if distortion in single layer is more, it will be accumulated on all the layers deposited above it. As a result, distortion effect is pronounced in spite of less number of layers. In the case of Figure 6.11C3, air gap increases the spacing between two rasters resulting in weak bonding and void structure.

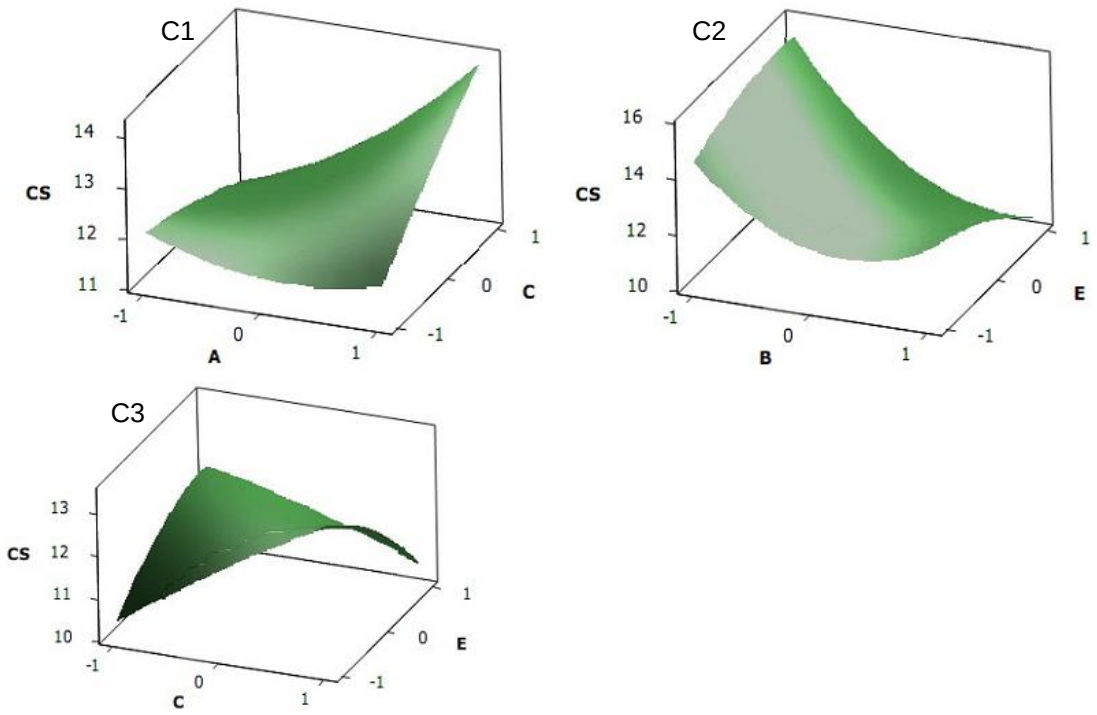

Figure 6.11 Response surface plots for compressive strength (CS)

Figure 6.12a shows the stress-strain curve. The stress versus strain behavior of specimen under compression is initially linear. With the generation of cracks, the behavior becomes nonlinear and inelastic. The resisting stress decreases with increase in strain, after the specimen reaches the peak stress. A non linear region has stair steps as shown in Figure 6.12b which means that force per unit area has reached a value at which material continues to deform. After that, it increases without causing significant deformation. This pattern is repeated in regular steps until the part

fractures. Most of the specimen show buckling of fibres (Figure 6.13a) when the region between the fibre breaks is deformed plastically. This behaviour is similar to unidirectional composites which fail under compression [230]. The progressive interfacial de-bonding (Figure 6.13b) between fibers may occur under increasing deformations and influence the overall stress-strain behavior of specimen. After the interfacial de-bonding, the de-bonded fibers may lose the load carrying capacity in the de-bonded direction. However, they are still able to transmit internal stresses through the bonded portion and are regarded as partially de-bonded fibers. The damage zone creates locally high compressive stress concentrations in the intact fibers surrounding it and buckling can also distort or laterally displace the surrounding fibers. This causes the fibers to bend, so they generate or further strain, resulting in bending to the point where they fracture. It can be regarded that the distortion due to uneven heating and cooling cycles or presence of interlayer porosity are responsible for de-bonding in fibers and hence decrease in strength [180]. Further, the deposited polymer molecules align themselves with the direction of flow when they are extruded through the nozzle resulting in anisotropic properties which is again responsible for less strength.

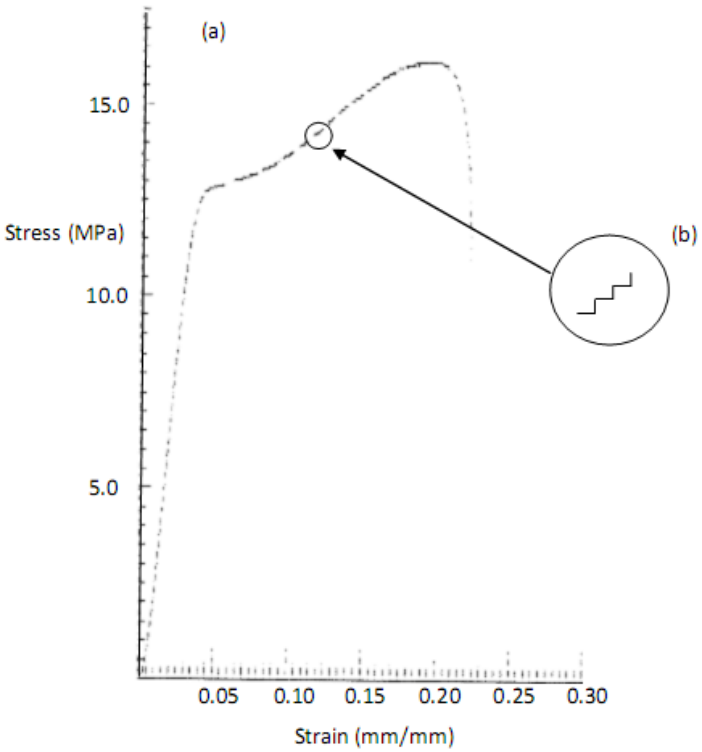

Figure 6.12 (a) Stress Strain curve for compressive strength (b) Presence of stair steps

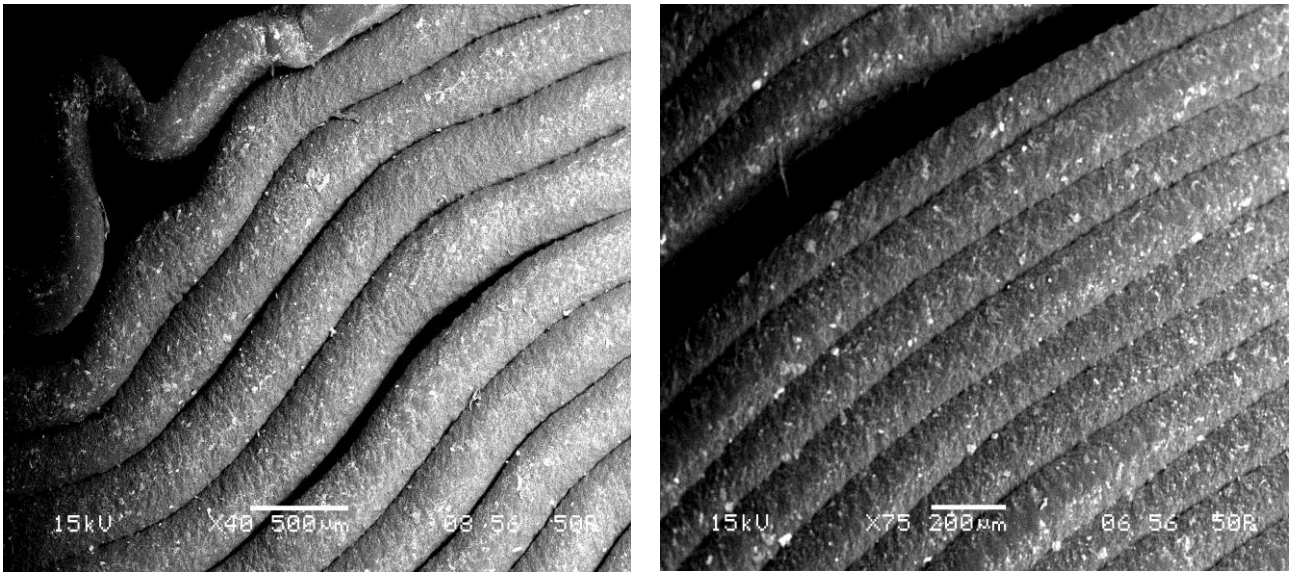

Figure 6.13 Microphotographs of specimens after compressive failure. (a) Failure due to buckling (b) De-bonding between fibres (the surfaces of the test part were examined by scanning electron microscope (SEM) JEOL JSM-6480LV in the LV mode)

6.5 Optimization of process parameters

Above discussion highlights the complex interrelationship between process parameters and studied mechanical strength. For improvement in process part properties, it is necessary to propose the optimum parameter setting. For this purpose, this section discusses the optimization of FDM process parameters by QPSO. QPSO is modification of PSO. As a population based stochastic evolutionary technique, PSO simulates the knowledge evolvement of a social organism, in which individuals (particles) representing the candidate solutions to the problem at hand, fly through a multidimensional search space to find out the optima or sub optima. The particle evaluates its position to a goal (fitness) at every iteration, and particles in a local neighbourhood share memories of their “best” positions. These memories are used to adjust particle velocities and their subsequent positions [222, 227]. In the standard PSO with N particles in the D dimensional search space, the potential solution can be represented by the particle’s position vector $x_i(t)$. The position, $x_i(t)$, of the i^{th} particle is adjusted by a stochastic velocity $v_i(t)$. Thus, the particle moves according to the following equation [227]:

$$v_i(t+1) = w\, v_i(t) + c_1\, r_1(pbest_i(t) - x_i(t)) + c_2\, r_2(gbest_j(t) - x_i(t)) \quad (6.5)$$

$$x_i(t+1) = x_i(t) + v_i(t+1) \quad (6.6)$$

i=1, 2, ….., N

where, $pbest_i$ is the best solution that particle i has obtained until iteration generation t, and $gbest_i$ is the best solution obtained from $pbest_i$ in the whole swarm at iteration t. w is inertia weight, c_1 is the cognition learning factor and c_2 is the social learning factor; r_1 and r_2 are the random numbers uniformly distributed in [0,1]. The procedure for implementing the PSO is given by the following steps [222, 227]:

Step 1: Initialization of swarm positions and velocities: Initialize a population (array) of particles with random positions and velocities in the D dimensional problem space using uniform probability distribution function.

Step 2: Evaluation of particle's fitness: Evaluate each particle's fitness value. Fitness function is maximized rather than minimize in this study.

Step 3: Comparison to *pbest* (personal best): Compare each particle's fitness with the particle's *pbest*. If the current value is better than *pbest*, then set the *pbest* value equal to the current value and the *pbest* location equal to the current location in a D-dimensional space.

Step 4: Comparison to *gbest* (global best): Compare the fitness with the population's overall previous best. If the current value is better than *gbest*, then reset *gbest* to the current particle's array index and value.

Step 5: Updating of each particle's velocity and position: Change the velocity, v_i, and position of the particle, x_i, according to equation 6.5 and 6.6 respectively.

In comparison to other stochastic based search algorithms like genetic algorithm (GA) or simulated annealing (SA) algorithms, PSO has fewer parameters than either GA or SA algorithm and has shown to be comparable in performance with them [231]. The main disadvantage of the PSO algorithm may be that it has still large number of training parameters and cannot guaranteed to be global convergent, as it is prone to trap into local optima[232]. Inspired by the trajectory analysis of the PSO and quantum mechanics, Sun et al. [228] developed and proposed the quantum-behaved particle swarm optimization (QPSO) algorithm. In the quantum model of a particle swarm optimization (PSO), the state of a particle (potential solution point) is depicted by wave function $\psi(x,t)$ (Schrödinger equation) instead of position and velocity [229]. The dynamic behaviour of the particle is widely divergent from that of the particle in traditional PSO systems in that the exact values of position and velocity cannot be determined simultaneously according to uncertainty principle. Only probability of the particle's appearing in position x can be determined from probability

density function $|\psi(x,t)|^2$, the form of which depends on the potential field the particle lies in. Any i^{th} particle move according to the following iterative equation [229]:

$$\begin{aligned} x_i(t+1) &= p + \beta \times \left| Mbest_i - x_i(t) \right| \times ln(\frac{1}{u}) \quad \text{if} \quad k \geq 0.5 \\ x_i(t+1) &= p - \beta \times \left| Mbest_i - x_i(t) \right| \times ln(\frac{1}{u}) \quad \text{if} \quad k < 0.5 \end{aligned} \tag{6.7}$$

where β is a design parameter called contraction-expansion coefficient, u and k are values generated using the uniform probability distribution function in the range [0,1]. The global point called mainstream thought or mean best (*Mbest*) of the population is defined as the mean of the personal best (*pbest)* positions of all particles which are associated with the best solution (fitness) it has achieved so far and is given by [229]:

$$Mbest = \frac{1}{N} \sum_{i=1}^{N} pbest_i(t) \tag{6.8}$$

Here, N is total number of particles and t indicates the iteration. To guarantee convergence, Clerc and Kennedy [227] present the following coordinates of p in equation 6.7 [229]:

$$p = \frac{R_1 pbest_i + R_2 gbest_i}{R_1 + R_2} \tag{6.9}$$

where R_1 and R_2 are two random number generated using uniform probability distribution in the range [0, 1] and *gbest* is the location of overall best value particle has achieved so far.

The procedure for implementing the QPSO is given by the following steps [229].

Step 1: Initialization of swarm positions: Initialize a population (array) of particles with random positions in the D-dimensional problem space using a uniform probability distribution function.

Step 2: Evaluation of particle's fitness: Evaluate the fitness value of each particle.

Step 3: Updating of global point: Calculate the *Mbest* using equation 6.8.

Step 4: Comparison to *pbest* (personal best): Compare each particle's fitness with the particle's *pbest*. If the current value is better than *pbest*, then set the *pbest* value equal to the current value and the *pbest* location equal to the current location in the D-dimensional space.

Step 5: Comparison to *gbest* (global best): Compare the fitness with the population's overall previous best. If the current value is better than *gbest*, then reset *gbest* to the current particle's value.

Step 6: Updating of particles' position: Change the position of the particles using equation 6.7.

Step 7: Repeating the evolutionary cycle: Loop to Step 2 until a stop criterion is met, usually a sufficiently good fitness or a maximum number of iterations.

6.5.1 Fitness function

For evaluating the fitness (objective value), the desirability function concept is used. Desirability represents the closeness of a response to its ideal value (Target) and lies between 0 to 1. If a response reaches its target value or a value more than the target value, desirability is assigned to unity. If a response lies within the unacceptable intervals, the desirability is 0, and if a response falls within the acceptable limit but less than the target value, the desirability lies between 0 and 1. Individual desirability function values corresponding to individual response can be combined to form a composite desirability which converts a multiple responses into an equivalent single response [196, 197]. In the present problem, it is desired to maximize tensile, flexural, impact and compressive strength. Therefore, "higher the better" quality characteristic has been adopted to convert each response into corresponding desirability value. The desirability can be measured as [197]:

$$d_{ij} = \begin{cases} 0 & if \quad y_{ij} \le low_j \\ \dfrac{y_{ij} - low_j}{high_j - low_j} & if \quad low_j < y_{ij} < high_j \\ 1 & if \quad y_{ij} \ge high_j \end{cases} \tag{6.10}$$

where d_{ij} is the desirability of i^{th} alternative of j^{th} response. y_{ij} is the found value of i^{th} alternative of j^{th} response. low_j and $high_j$ are the minimum and the maximum values respectively of the experiment data for j^{th} response. These desirability values are combined to single unit known as composite desirability as [197]:

$$C_d^i = \left(\prod_{j=1}^{m} d_{ij}^{w_j}\right)^{\frac{1}{\sum_{j=1}^{m} w_j}} \tag{6.11}$$

where C_d^i is the composite desirability of i^{th} alternative. w_j is the weight or importance of j^{th} response, usually decided by the designer. For present study $w_j = 1, \forall j$.

For calculating the respective strength values for each particle position equation 6.1-6.4 are used. These strength values are converted to desirability using equation 6.10 and combine to composite desirability using equation 6.11.

The fitness function is formulated as follows:

$$\text{Maximize } F(X) = C_d\,[d_{iT}\{F_T(X)\}, d_{iF}\{F_F(X)\}, d_{iI}\{F_I(X)\}, d_{iC}\{F_C(X)\}] \quad (6.12)$$

Subjected to:

$$0.127 \le A \le 0.254$$

$$0 \le B \le 30$$

$$0 \le C \le 60$$

$$0.4064 \le D \le 0.5064$$

$$0.000 \le E \le 0.008$$

where X=[A, B, C, D, E] are the process variables, input to calculate respective strength (F_T, F_F, F_I, F_C) value whose outputs are converted to respective desirability (d_T, d_F, d_I, d_C)which are combined to form composite desirability C_d.

Whenever a generated particle lies beyond each parameter low value (l_v) and high value (h_v), a repair rule is applied according to equation 6.13 and equation 6.14, respectively.

$$x_i = x_i + rand[0,1].\{h_V(x_i) - l_V(x_i)\} \quad (6.13)$$

$$x_i = x_i - rand[0,1].\{h_V(x_i) - l_V(x_i)\} \quad (6.14)$$

where *rand*[0,1] is a uniformly distributed random value between 0 and 1.

6.5.2 Parameter configuration

PSO and QPSO are tested, each with maximum number of generation fixed to 1000 and population size 50. For PSO inertia weight w is varied linearly between 0.7 to 0.4 and c_1=c_2=2 is considered. For the case of QPSO contraction-expansion coefficient (β) is varied from 1 to 0.05 with a linear decreasing rate.

6.5.3 Simulation result

For calculating the composite desirability high and low value of each objective function depend upon user choice but for present analysis low value of each strength is set as 0 and high value of strength is taken from maximum values given in Table 6.1. PSO and QPSO algorithms are coded in Matlab 7.0 and run on HP Intel^{R} Core^{TM} 2 DUO processor 2.33GHz, 1.95GB RAM. A solution quality of both the algorithms is compared graphically and is shown in Figure 6.14.

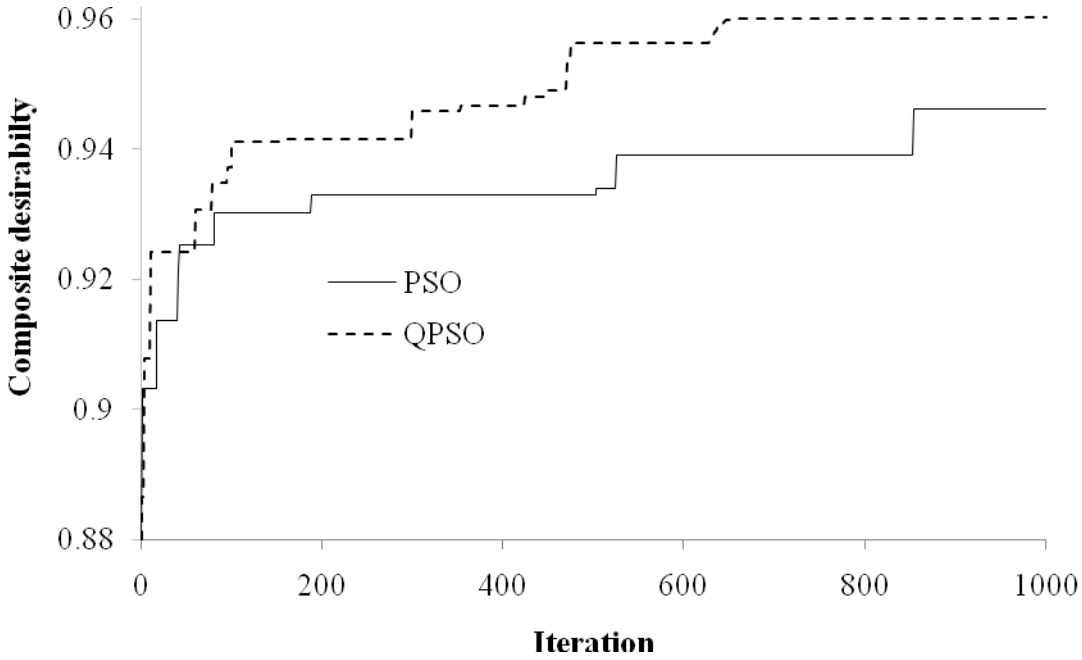

Figure 6.14 Convergence curve

The Figure 6.14 shows that in the all iterative process, the convergence speed of QPSO is faster than PSO. In addition, when the end of maximum iterations reached, the optimal found by traditional PSO is still less than the optimum value found by QPSO. It is obvious that the global search capability of QPSO is better than traditional PSO. As the movement of the aggregation of particles in the quantum space is dependent on a probability density function $|\psi(x,t)|^2$, there is not an assured moving track. Particles will move in a feasible solution space in a more random manner to find the global optimal solution. Thus, the QPSO with the global search capability is much better than traditional PSO. Table 6.10 gives the optimal parameter setting obtained by modified QPSO after 1000 iterations.

Table 6.10 Optimum parameter setting

Fitness function	Optimum parameter	Tensile Strength	Flexural strength	Impact strength	Compressive strength
0.9602	A=0.254 mm B=0.081degree C=60degree D=0.40661mm E=0.00799mm	16.34 MPa	42.73MPa	0.47MJ/m^2	13.63MPa

6.6 Conclusions

Functional relationship between process parameters and strength (tensile, flexural, impact and compressive) are determined using response surface

methodology. The process parameters considered are layer thickness, orientation, raster angle, raster width and air gap. The response surface plots involving interaction terms are studied and the reasons behind the observed response can be summarized as follows.

6.6.1. Number of layers in a part depends upon the layer thickness and part orientation. If number of layers are more (due to decrease in layer thickness or increase in orientation), high temperature gradient towards the bottom of part is resulted. This will increase the diffusion between adjacent rasters, increase the boding of rasters and improve the strength. But high temperature gradient is also responsible for distortion within the layers or between the layers. Moreover, increase in number of layers also increases the number of heating and cooling cycles and thus accumulation of residual stress increases. This may results in distortion, interlayer cracking and part de-lamination or fabrication failure. Hence, strength will reduce.

6.6.2. Small raster angles are not preferable as they will results in long rasters which will increase the stress accumulation along the direction of deposition resulting in more distortion and hence weak bonding.

6.6.3. Thick rasters results in stress accumulation along the width of part and have the same effect as the long rasters. But this stress accumulation results in high temperature near the boding surfaces which may improve the diffusion and may result in strong bond formation.

6.6.4. Zero air gap will improve the diffusion between the adjacent rasters but may also decreases the heat dissipation as well as total bonding area.

Part build mechanism in FDM is a complex phenomenon. Therefore, effect of various factors and their interactions can be observed but difficult to assign exact reasons. However, some of the possible reasons have been outlined. To summarize, it can be said that reduction in distortion is a necessary requirement for good strength. Further, factor levels cannot be selected independent of each other because interactions play an important role. To find the optimum factor setting which will maximize all the studied responses, the responses are combined into a single response known as composite desirability. Optimum factor setting is obtained using QPSO which is having better search ability in comparison to PSO.

CHAPTER 7

A STUDY ON SLIDING WEAR

7.1 Introduction

Amongst many RP techniques, fused deposition modelling (FDM) is considered as most appropriate process for RP due to its ease of operation, inexpensive machinery and durability of built parts [38, 46, 54]. The process offers time and cost advantages over conventional technologies [4, 12, 16]. However, the major limitation of this process is that performance of prototypes is sensitive to process parameter variation. This makes it essential to understand the performance of FDM processed parts in relation to variation of process parameters so that the process can be made reliable enough for industrial applications. Previous chapters in this direction mainly focus on dimensional accuracy of the built part [chapter 4], surface roughness improvement [chapter 5] and mechanical strength characterization [chapter 6]. These works demonstrate that properties of built part depend on process parameters and can be improved by their suitable selection without incurring additional expenses on changing existing hardware and software. Wear is important characteristic for the durability of part and very little work is done to understand the wear characteristic of RP processed part [191-193]. To fill this gap, the present chapter focuses on sliding wear behaviour of FDM processed part and its relationship with process parameters. Moreover, it is vital to develop predictive equation relating process parameters and wear rate so that tool engineers can build wear resistant parts at ease. The study may be useful where sliding contact of mating surfaces occurs e.g. gears, journal bearings, seals, cams etc. [16, 24, 25] when conventional parts is replaced with FDM processed parts due to easiness of fabrication, economic production of prototypes, light weight and high specific mechanical properties.

Comprehensive investigation on the effect of process parameters on sliding wear of FDM processed part is made using face centred central composite design (FCCCD). Response surfaces are analyzed to understand effect of parameters on wear rate. Sliding wear test (Pin on disc) is used to measure the wear volume. Wear volume divided by sliding distance is used as measure of amount of wear. For parametric analysis and empirical modeling of the process, a central composite design (CCD) methodology is used to reduce the experimental runs and study the effect of parameters including their interactions [197]. The cylindrical specimens of length 30mm and diameter 6mm are prepared using FDM Vantage SE machine as per factor setting in the CCD and are subjected to pin on disc test as per ASTM G99-04 (standard test method for wear testing with pin on disk apparatus). The material used to fabricate test specimen is acrylonitrile butadiene styrene (ABS P400). In

order to optimize process parameters for minimum wear, quantum-behaved particle swarm optimization (QPSO) and bacteria foraging optimisation algorithm (BFOA) are used and compared to each other.

Sometimes traditional approaches become unsuitable for developing good functional relationship particularly when a process behaves in a non-linear fashion and involve large number of interacting parameters. However, neural networks can be easily applied to situations where relationship between the predictor variables (inputs) and predicted variables (outputs) is quite involved and complex and difficult to easily articulate in the usual terms of correlations [233]. Inspired by this characteristic, present study uses resilient back propagation algorithm (RBPA) based artificial neural network (ANN) for predicting wear rate of FDM built parts. As both the QPSO and BFOA algorithms assume a continuous search space and hence the optimum factor setting generated by them cannot be confirmed on present FDM setup because of hardware limitations. Therefore, proposed ANN model is used for confirmation purpose.

7.2 Experimental methods

In order to build empirical model for wear prediction, experiments were conducted based on face central composite design (FCCD) as explained in chapter 3, sub-section 3.6.2. Wear testing is done using pin on disk apparatus (Ducom, TR-20LE-M5) shown in Figure 3.15 as per ASTM G99-04 standard, (a standard test method for wear testing with pin on disk apparatus). Test specimen, shown in Figure 3.16, having flat end contact geometry is positioned perpendicular to the flat circular disc (EN 31 hardened steel). Due to surface roughness and foreign materials present at the specimen surface, initial wear rate is not uniform. The initial period is known as “break in period” during which surface roughness and foreign material is removed so that complete contact between the disc and specimen is established. Wear rate after “break in period” is the true wear rate of the specimen under operating conditions. Wear volume (in cubic millimeter) is determined by multiplying the cross sectional area with decrease in height while sliding distance (in meter) is determined by multiplying time with speed of rotation. Wear results are plotted as wear volume versus sliding distance. Initial data (10-15% of total readings) having non linear relationship between wear volume and sliding distance is regarded as break in period data.

7.3 Experimental results

Figure 7.1 shows the plot of wear results for experiment number one. The slope of the fitted straight line at each experiment trial is taken as represented value of wear and shown in Table 7.1.

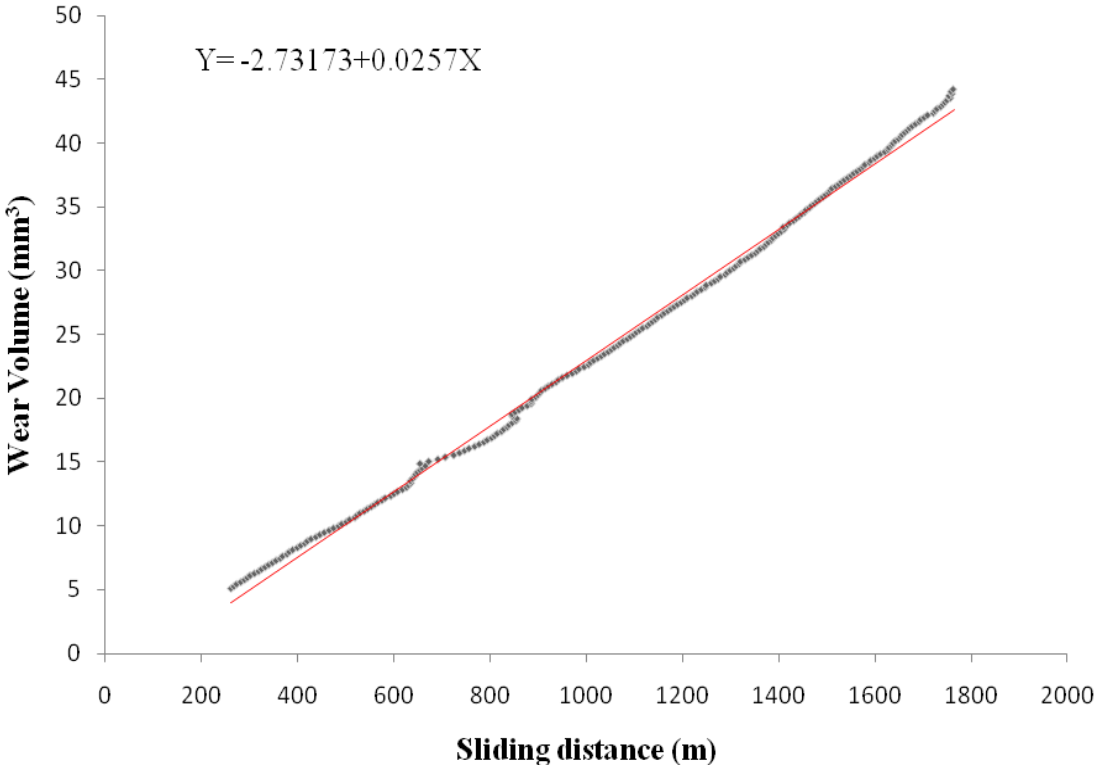

Figure 7.1 Wear result for experiment 1 (Y=wear volume, X=sliding distance)

Table 7.1 Experimental data obtained from the FCCCD runs

Exp. No.	Factors					Wear (mm^3/m)
	A	B	C	D	E	
1	-1	-1	-1	-1	1	0.02570
2	1	-1	-1	-1	-1	0.03046
3	-1	1	-1	-1	-1	0.03260
4	1	1	-1	-1	1	0.01630
5	-1	-1	1	-1	-1	0.02686
6	1	-1	1	-1	1	0.04880
7	-1	1	1	-1	1	0.02018
8	1	1	1	-1	-1	0.01477
9	-1	-1	-1	1	-1	0.01443
10	1	-1	-1	1	1	0.01660
11	-1	1	-1	1	1	0.01131
12	1	1	-1	1	-1	0.01152
13	-1	-1	1	1	1	0.01541
14	1	-1	1	1	-1	0.01540
15	-1	1	1	1	-1	0.01621
16	1	1	1	1	1	0.03217
17	-1	0	0	0	0	0.02452

18	1	0	0	0	0	0.03083
19	0	-1	0	0	0	0.02467
20	0	1	0	0	0	0.02485
21	0	0	-1	0	0	0.03403
22	0	0	1	0	0	0.03424
23	0	0	0	-1	0	0.03905
24	0	0	0	1	0	0.02695
25	0	0	0	0	-1	0.02663
26	0	0	0	0	1	0.04188
27	0	0	0	0	0	0.03220
28	0	0	0	0	0	0.03135
29	0	0	0	0	0	0.03256
30	0	0	0	0	0	0.02896
31	0	0	0	0	0	0.03620
32	0	0	0	0	0	0.03660

From the plot of variation of coefficient of friction with respect to sliding direction (Figure 7.2) for experiment number one, it is observed that the friction coefficient was unstable and increase rapidly at the beginning of sliding process. After a certain sliding distance, the surface asperities were removed and the variation of friction coefficient becomes stable. The similar trend is observed for the remaining experiments mentioned in Table 7.1.

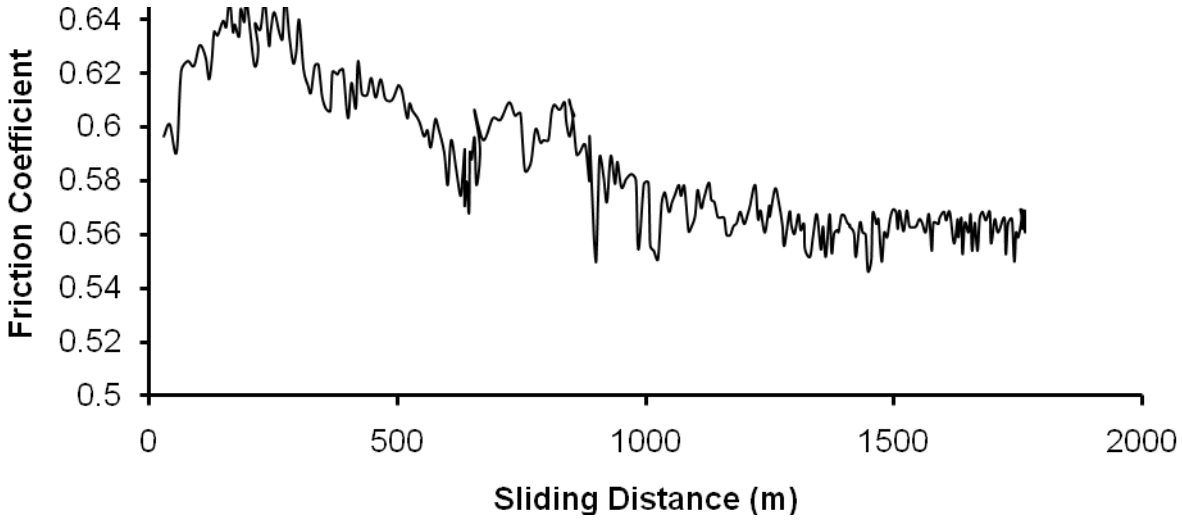

Figure 7.2 Variation of friction coefficient with sliding distance

Based on ANOVA, full quadratic model was found to be suitable for wear strength (Table 7.2) with regression p-value less than 0.05 and lack of fit more than 0.05. In the developed model linear, square and interaction terms are significant as their p value is less than 0.05.

Table 7.2 ANOVA Table

Source	Degree of freedom	Sum of square	Mean sum of square	F	P
Regression	20	0.002616	0.000131	10.81	0.000
Linear	5	0.000769	0.000154	12.72	0.000
Square	5	0.000935	0.000187	15.46	0.000
Interaction	10	0.000911	0.000091	7.54	0.001
Residual Error	11	0.000133	0.000012		
Lack-of-Fit	6	0.000090	0.000015	1.74	0.280
Pure Error	5	0.000043	0.000009		
Total	31	0.002749			

Estimated regression coefficients of model terms are given in Table 7.3. The individual significance of each term is calculated by t-test at 95% of confidence and terms having p-value less than 0.05 are considered as significant. The final response surface equation is given by equation 7.1. The coefficient of determination (R^2) which indicates the percentage of total variation of the response explained by model terms is found to be 95.16%.

Table 7.3 Estimated coefficient of each term

Term	Coefficient	t	p
Constant	0.032993	33.198	0.000
A	0.001645	2.007	0.070
B	-0.002136	-2.605	0.024
C	0.001727	2.107	0.059
D	-0.005261	-6.419	0.000
E	0.002193	2.675	0.022
AXA	-0.005330	-2.404	0.035
BXB	-0.008242	-3.718	0.003
CXC	0.001130	0.510	0.620
DXD	-0.000005	-0.002	0.998
EXE	0.001250	0.564	0.584
AXB	-0.002150	-2.473	0.031
AXC	0.002602	2.993	0.012
AXD	0.000833	0.959	0.358
AXE	0.003702	4.258	0.001
BXC	-0.000480	-0.552	0.592
BXD	0.003583	4.122	0.002
BXE	-0.000906	-1.042	0.320
CXD	0.001237	1.422	0.183
CXE	0.003902	4.488	0.001
DXE	0.000727	0.836	0.421

Wear = 0.032993-0.002136xB-0.005261xD+0.002193xE-0.005330x(AXA) -

0.008242x(BXB) -0.002150x(AXB)+ 0.002602x(AXC)+ 0.003702x(AXE)+

0.003583x(BXD)+ 0.003902x(CXE) (7.1)

Anderson-Darling (AD) normality test results are shown in Figure 7.3. Since p-value of the normality plots is found to be above 0.05, it signifies that residue

follows normal distribution and model given by equation 7.3 is suitable for practical engineering applications.

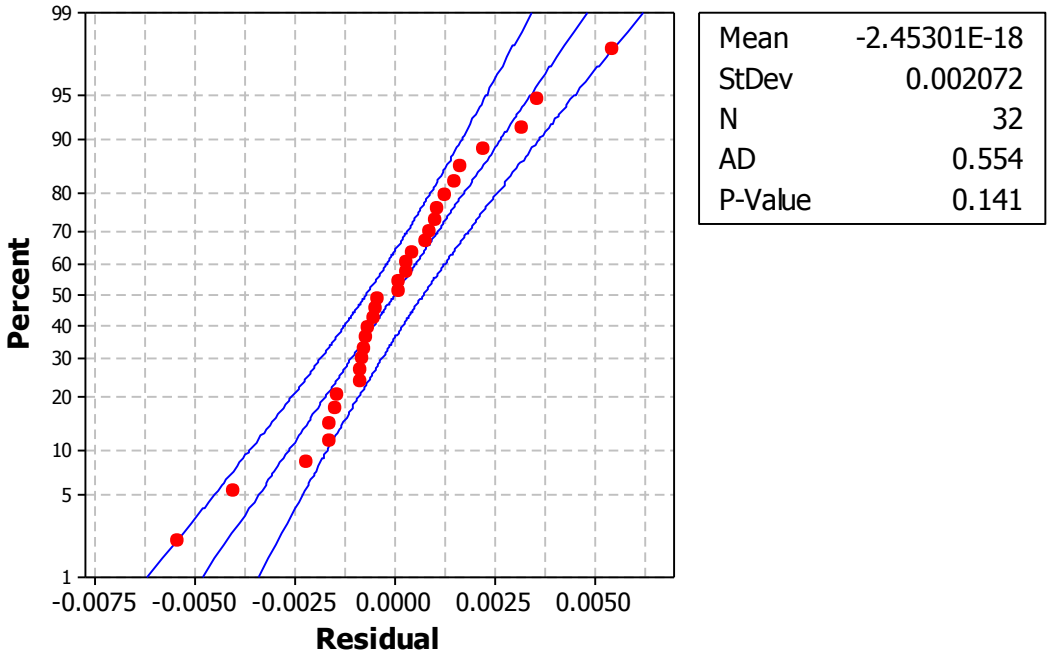

Figure 7.3 Probability plot for residue at 95% of confidence

7.4 Discussions

Figure 4.7 shows that the surface of FDM processed part is not flat but has multiple bumps due to rasters and this type of uneven surface exists for each constituting layer. When the surface of a FDM built part comes in contact with a comparatively very flat surface, 100% surface contact is hardly possible. Surface crack (Figure 6.2) may also be developed due to distortion taking place during part building stage. Depositing rasters with positive air gap gives rise to void formation resulting in internal porous structure (Figure 4.9). Due to relative sliding motion, wearing will take place and wear debris come in between the spacing between two rasters. As shown in Figure 7.4, contact pressure will force the test specimen against the rotating disc and particles in between the raster spacing will cause the deformation, abrasion, surface fatigue, adhesion at the surface of part (Figure 7.5). Adhesion is the phenomena which results in attractive forces between two surfaces in close contact. The junction formed by the asperities on the contacting surfaces increase in size by plastic deformation as the motion continues; eventually plastic shearing of the junction occurs.

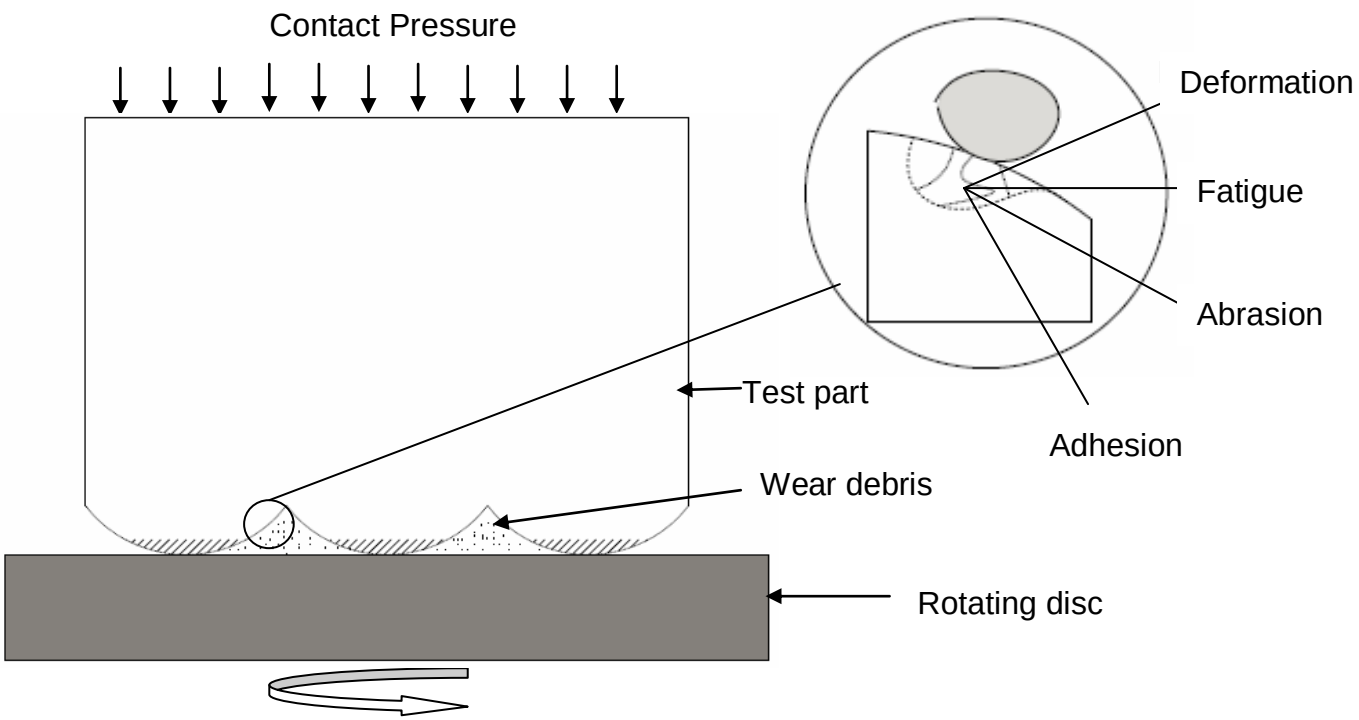

Figure 7.4 Mechanism of wear

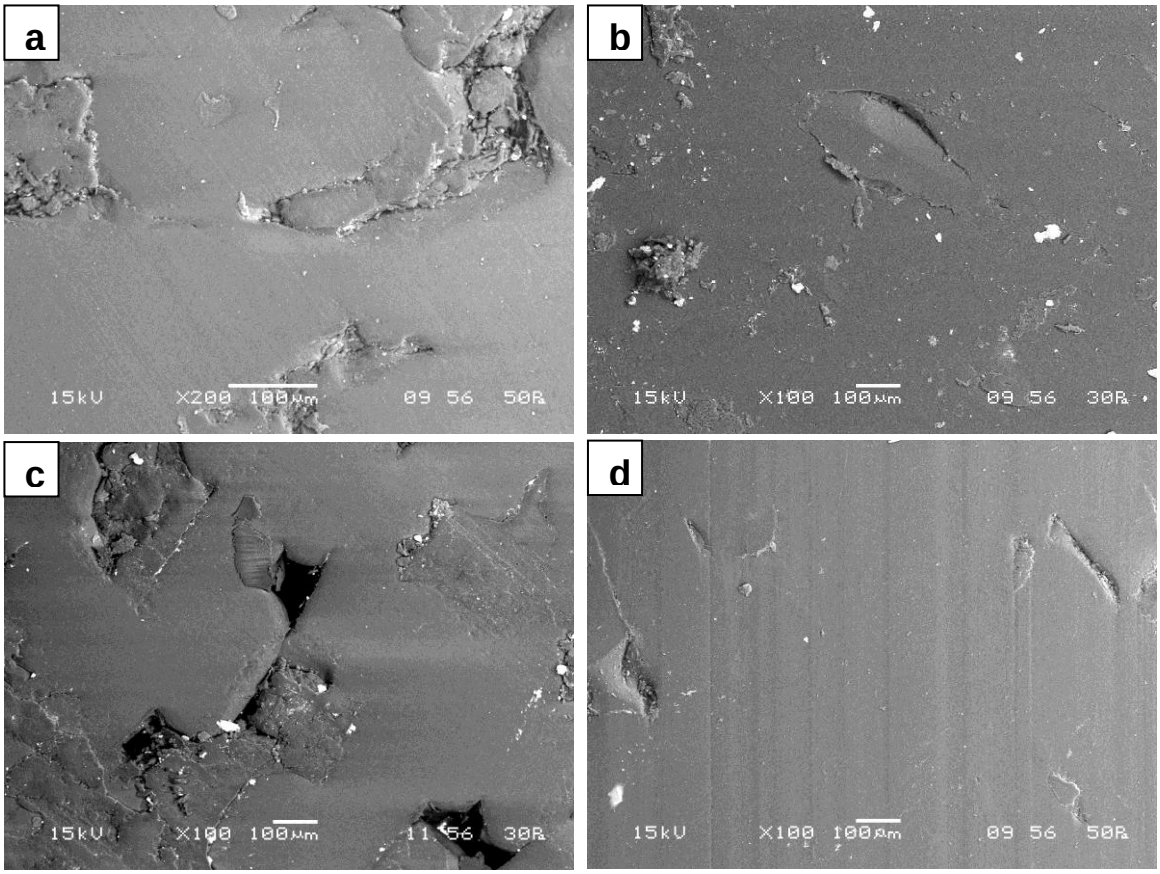

Figure 7.5 SEM image of wear surface (a) Adhesive wear and crushing (b) Crack development (c) Pit formation (d) Abrasion (The surfaces of the test part were examined by scanning electron microscope (SEM) JEOL JSM-6480LV in the LV mode)

Microphotograph shown in Figure 7.5.a indicates material removal due to adhesive junction. Relative motion and constant compressive force maintained for contact, crushing may also take place. Wear due to surface fatigue can be characterized by the crack formation and flanking of material due to repeated sliding contact of asperities on the surface because of relative motion (Figure 7.5.b) or the repeated impact of wear debris. Depending on the angle of propagation of cracks, shallow or deep pits may be formed. When rasters are deposited with positive air gap, the void between them may also be responsible for pit formation. Figure 7.5.c shows the micro-photograph for experiment number 26 in Table 7.1 for which air gap (E) is maintained at its high level and other factors at their centre level. Wear surface having pits can be clearly visible in this microphotograph. Abrasion of material by soft abrasive occurs by rubbing. Abrasive particles are called soft when the hardness is equal to or less then the wearing material [234]. The attack of soft abrasives may result in elastic and plastic deformation, surface fatigue, surface cracking and adhesion. Protuberances due to plastic deformation of the rubbed surface may be cut or repeatedly pushed aside by soft abrasive particles (Figure 7.5.d). Wear mechanism shown in Figure 7.5.a, 7.5.b and 7.5.d corresponds to specimen of experiment number 17, 21 and 19 respectively (Table 7.1). As already mentioned, the main reasons of wearing in these specimen is attributed to flanking of material due to repeated sliding contact of asperities on the surface because of relative motion or the impact contact of wear debris. At low level of layer thickness (experiment no. 17), orientation (experiment no. 19) and raster angle (experiment no. 21), weak inter-layer and intra-layer bonding is resulted because chances of distortion within the part are high [185-187]. This may result in increased wear debris formation responsible for flanking of material. The debris may form the adhesive bond or may result in abrasion, crack development or may get crushed due to loading condition.

Like other mechanical properties, wear is also dependent on internal resistance of part against the external forces. In the context of sliding wear, it is the resistance to sliding contact of two mating surface. If internal structure is strong, it may resist the wearing. As mentioned in Chapter 6, strength of FDM built part depends upon the internal distortion in part; hence it may be corroborated that wear strength will also be improved by controlling the distortion that affect the inter and intra layer bonding. Study on the effects of process parameters for improving wear strength is carried out using response surface plots (Figure 7.6) of significant interaction terms in equation 7.1 and are explained as follows.

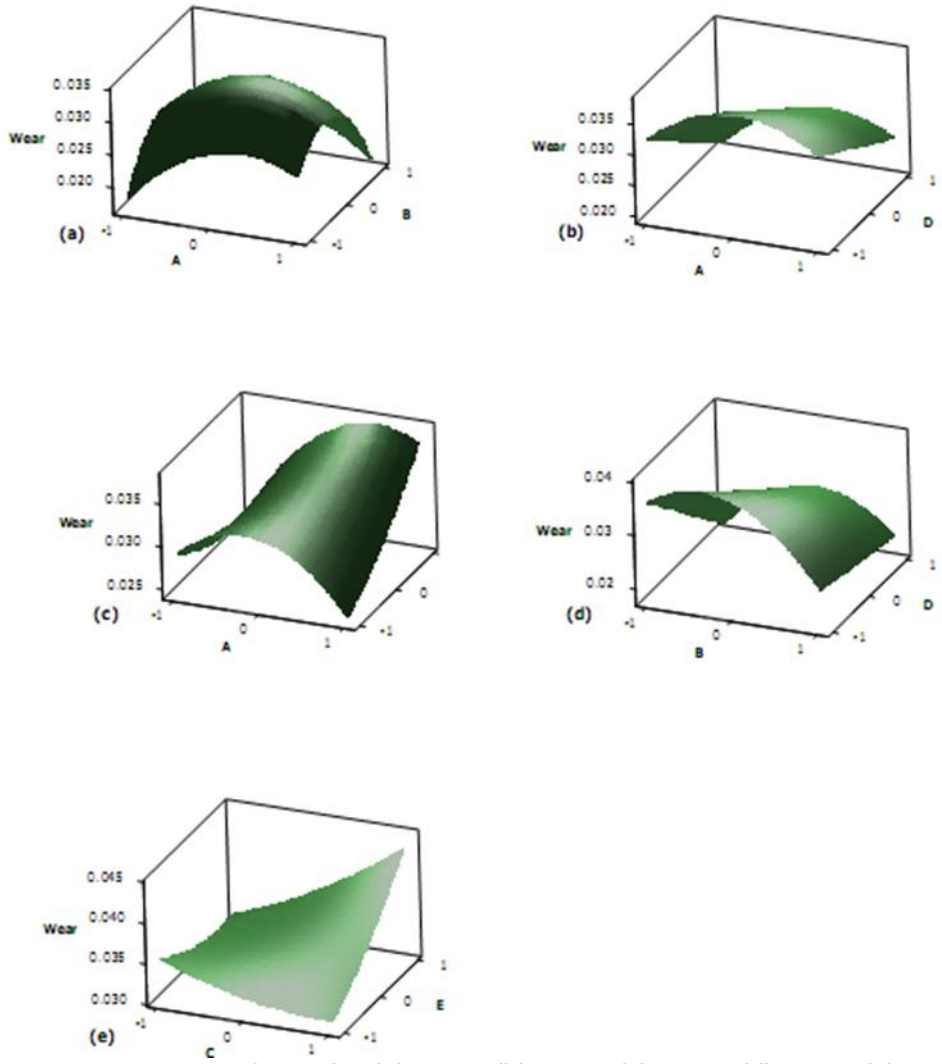

Figure 7.6 Response surface plot (a) AXB, (b) AXD, (c) AXD, (d) BXD, (e) CXE (for each plot other factors are kept at their centre point value)

From response surfaces (Figure7.6.a-7.6.c), it can be noted that wear rate first increases and then decreases as layer thickness (A) increases. When a part is built by layer by layer deposition method, the temperature of the depositing material is essentially higher than already deposited substrate and chamber temperature; therefore, heat transfer to the surroundings occurs [180, 185]. Part of this heat is transferred to the already deposited layers causing increase in their temperature. So local re-melting and diffusion between the adjacent filaments of same layers as well as neighbouring layers occurs and hence, results in strong bond formation [186]. The strong bonding is responsible for increase in strength and reduces wear. But this phenomenon is also responsible for uneven heating and cooling of material and develops non-uniform temperature gradients. As a result, uniform stress will not be developed in the deposited material and distorts them [185, 187]. The distortions

arising during part build stage are primarily responsible for weak strength of FDM part. It may be presumed that strong bonding occurs at low level of layer thickness due to sufficient heat transfer in spite of distortion phenomenon. As layer thickness increases from its low level, it seems that distortion effect dominates the bonding effect and increases the wear. Further increase of layer thickness causes reduction in distortion effect and again wears starts decreasing. From response surfaces (Figure 7.6.a), it can be noted that wear first increases and then decreases as orientation (B) increases. Number of layers increases with orientation. When orientation is small, number of layers is less and it increases with orientation. In fact, layer thickness is inversely related to number of layers. Therefore, same reasoning explained for effect of layer thickness on wear is equally applicable here. Increase in raster angle results in deposition of small rasters that potentially decreases the distortion phenomenon and ultimately increases the strength of built parts [180, 187]. From response surfaces (Figure 7.6.e), it can be noted that wear decreases with increase in raster angle (C) as expected at the low level of air gap (E). However, wear increases with increase in raster angle for high level of air gap. This is caused because spacing between rasters increases as air gap increases resulting in weak bond formation between adjacent rasters. Figure 7.6.b and Figure 7.6.d shows that wear decreases with increase in raster width (D). This is due to the fact that smaller number of rasters is required for unit cross sectional area when raster width is increased and possibly distortion effect is minimized with less number of rasters. Ultimately, wear characteristic of the built parts improves. From response surfaces (Figiure 7.6.c, Figure 7.6.e), it can be observed that wear increases with increase in air gap (E) at high level of layer thickness because spacing between adjacent rasters increase with increase in air gap causing a weak bonding of rasters. Weak bonding may be responsible for reduction in strength and increase in wear. However, wear decreases with increase in air gap when layer thickness (A) is maintained at low level (Figure 7.6.c). Phenomenon of re-melting of rasters due to heat transfer towards the bottom layers dominates at the low values of layer thickness [18]. The melted material will flow towards the voids created by air gap, diffuse together and assist in strong bond formation causing decrease in wear. At low level of raster angle, Figure 7.6.e shows that wear slightly decreases with increase in air gap. As spacing between adjacent rasters increases with increase in air gap, heat can be easily dissipated and chance of distortion due to thermal stress is less. Hence, both increase of air gap and reduction in raster angle are decreasing the wear although not appreciably.

7.5 Optimization of process parameters

Over the past several decades, population-based random optimization techniques motivated by natural evolution such as genetic algorithms (GA), evolutionary programming (EP) etc. has been widely employed to solve optimization problems [235]. Recently natural swarm inspired algorithms like Particle Swarm Optimization (PSO) [227], Ant Colony Optimization (ACO) [223] have found their way into this domain and proved their effectiveness. PSO method is a kind of swarm intelligence algorithm for global optimization over a continuous search space and is inspired by exploring simple analogy of social interaction of a group of organisms such as bees, birds and fishes, rather than purely individual cognitive abilities. However, PSO is not a global optimization algorithm; hence, many attempts have been made to improve the performance of the PSO [220, 229]. Recently, quantum behaved particle swarm optimization (QPSO) [228] has emerged as a novel optimization algorithm which keeps to the philosophy of PSO and is based on quantum mechanics such as use of Schrödinger equation and potential field distribution. QPSO algorithm has attracted the considerable interest of practitioners. The reason lies in the fact that QPSO is very simple and easy to implement. It outperforms the PSO in global search ability and is a promising optimizer for complex problems [231, 232]. Following the same trend of swarm based algorithms, Passino proposed the bacteria foraging optimization algorithm (BFOA) in 2002 [225]. Application of group foraging strategy of a swarm of E.coli bacteria in function optimization is the key idea of the new algorithm. Bacteria search for nutrients in a manner to maximize energy obtained per unit time. Individual bacterium also communicates with others by sending signals. A bacterium takes foraging decisions after considering two previous factors. The process, in which a bacterium moves by taking small steps while searching for nutrients, is called chemotaxis provides the exploring ability to algorithm in a given problem domain. Whereas getting replaced by better bacteria, owing to their poorer foraging abilities (reproduction) or eliminated by sudden unforeseen event, which may drastically alter the smooth process of evolution (elimination-dispersal) not only maintain the population diversity but also helps in reducing the behaviour of stagnation. Since its inception, BFOA has drawn the attention of researchers from diverse fields of knowledge especially due to its biological motivation and graceful structure [213-216].

Previous chapters, that is chapter 5 and chapter 6 present the relevant background of BFOA and QPSO algorithms respectively and shown there suitability for real life industrial problems. In this part of chapter, these two methods are compared in terms of optimizing FDM process parameters for minimum wear. To

achive this, empirical model between wear and process parameters presented in equation 7.1 is taken as fitness function with each parameter is varied between its given low and high level. The number of individuals in the population (population size) is maintained at 50 and the maximum number of iterations is fixed at 3000. Respective parameters of each algorithm are tuned on the basis of faster convergence and are given in Table 7.4. Both the algorithms are coded in Matlab 7.0 and run on HP Intel^{R} Core^{TM} 2 DUO processor 2.33GHz, 1.95GB RAM. Graphical comparison of BFOA and QPSO is given in Figure 7.7.

Table 7.4 Algorithm parameter configuration

QPSO		BFOA	
Parameter	Value	Parameter	Value
Contraction- expansion coefficient	linearly decrease from 1 to 0.5	Elimination dispersal loop	3
		Chemotaxis loop	5
		Reproduction loop	5
		Maximum swim length	10
		Depth of attraction	1.9
		Depth of repulsion	1.9
		Width of attraction	0.2
		Width of repulsion	10

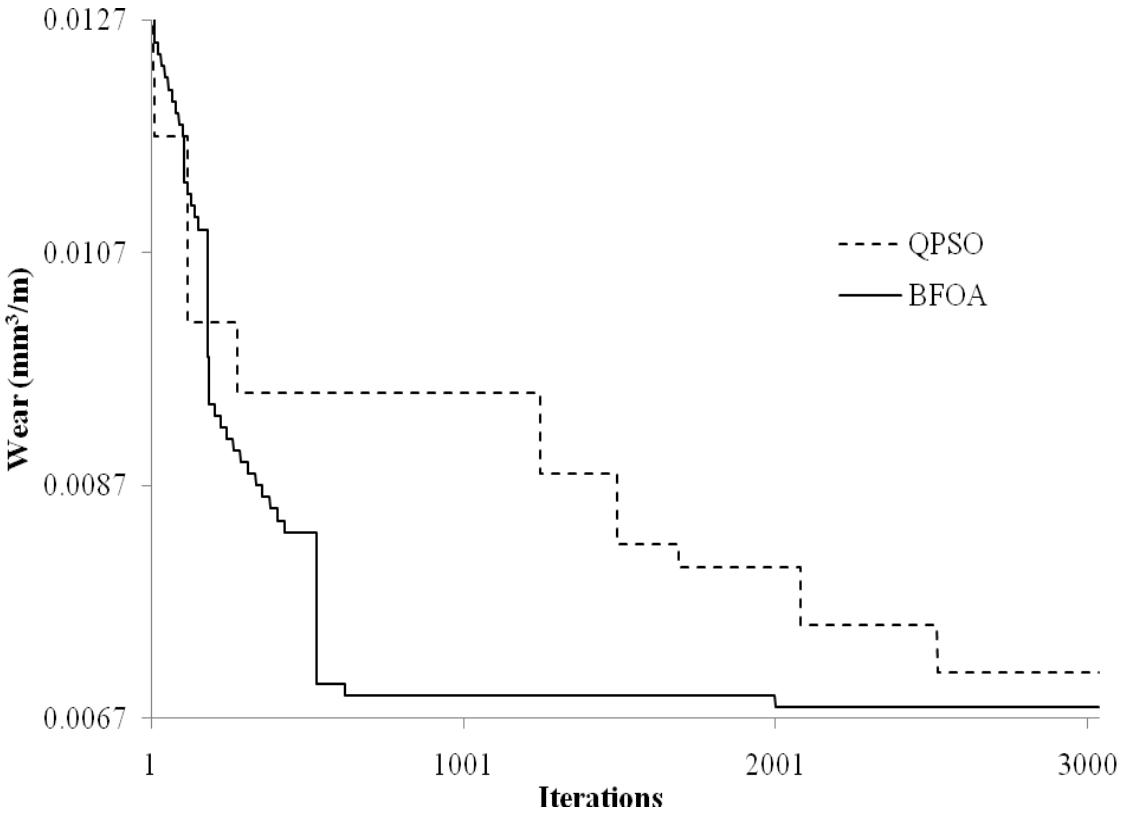

Figure 7.7 Convergence curve

Figure 7.7 shows that BFOA converges faster as compared to QPSO when bacteria are further from optimum point. The reason lies on their better exploration and exploitation capabilities. Table 7.5 gives the optimal parameter settings generated from both the algorithms.

Table 7.5 Optimal Parameter level and Predictive response

	Wear (mm^3/m)	A (mm)	B (degree)	C (degree)	D (mm)	E (mm)
QPSO	0.0071	0.254	29.99	46.41	0.4988	0.000002
BFOA	0.0068	0.1278	0.15	59.91	0.5037	0.000697

Optimal parameter levels in QPSO show that wear is least near the high level of layer thickness (A) and orientation (B) or near the low level of both the factors as in BFOA results. This is in agreement to response surface plot presented in section 7.4 as both the conditions are responsible for minimum distortion and improvement in the strength of part. Similarly at higher level of raster angle (C), raster width (D) and lower level of air gap (E), minimum wear is accepted as discussed in section 7.4.

7.6 Neural network prediction

As FDM process involves large number of conflicting factors and complex phenomena for part building, it is difficult to predict the output characteristics accurately by conventional methods. So, an ANN with back propagation algorithm has been adapted to model FDM process. The details of this methodology are described by Rajasekaran and Pai [211]. In the present analysis, factors such as A, B, C, D and E are taken as five input parameters. Each of these parameters is characterized by one neuron and consequently the input layer in the ANN structure has five neurons. The database is built considering experiments at the limit ranges of each parameter. Wear values are used to train the ANN in order to understand the input-output correlations. The database is then divided into two categories, namely: (i) A training category, which is exclusively used to adjust the network weights (ii) A test category, which corresponds to the set that validates the results of the training protocol. Experimental runs in Table 7.1 corresponding to half factorial experimental runs are used for training purpose and experimental runs corresponding to axial runs are used for testing the train network. The training of neural network involves updating the weights of the connections in such a manner that the error between the outputs of the neural network and the actual output is minimized. The standard BPA with a fixed learning rate and momentum usually suffers from extremely slow convergence [236]. To achieve faster convergence, the learning rate of an algorithm that defines the shift of the weight vector has to be dynamically varied in accordance with the region that the weight vector currently stands. Out of the different training

algorithms, resilient back propagation algorithm (RBP) is chosen in the present work. Advantage of using RBP is that only the sign of the derivative of error function is used to determine the direction of the weight update; the magnitude of the derivative has no effect on the weight update further weight update is performed after the gradient of the whole pattern set (one epoch) has been computed [237]. ANN algorithm is coded in Matlab 7.0 and run on HP Intel^{R} Core^{TM} 2 DUO processor 2.33GHz, 1.95GB RAM. To determine the number of neurons in hidden layer, different ANN structures with varying number of neurons in the hidden layer is tested. After training, the topology 5-8-1 is selected as the optimum based on minimum value of performance function which is 2.99018×10^{-10} and can be considered as equivalent to zero. The activation level of neurons is determined by tan-sigmoid transfer function except for output layer neurons for which linear output transfer function is used so that output is not limited to small values [238]. In order to evaluate the competence of this trained network, the training data set was presented to the trained network. Figure 7.8 shows the regression analysis results between the network response and the corresponding targets. High correlation coefficient (R^2-value) between the predicted (outputs) and targets establish the performance of network. Wear value predicted by ANN at optimum factor levels found in section 7.5 is compared with QPSO and BFOA results and shown in Table 7.6 for confirmation purpose. The small error on comparing BFOA result with ANN prediction indicates the better convergence quality of BFOA algorithm.

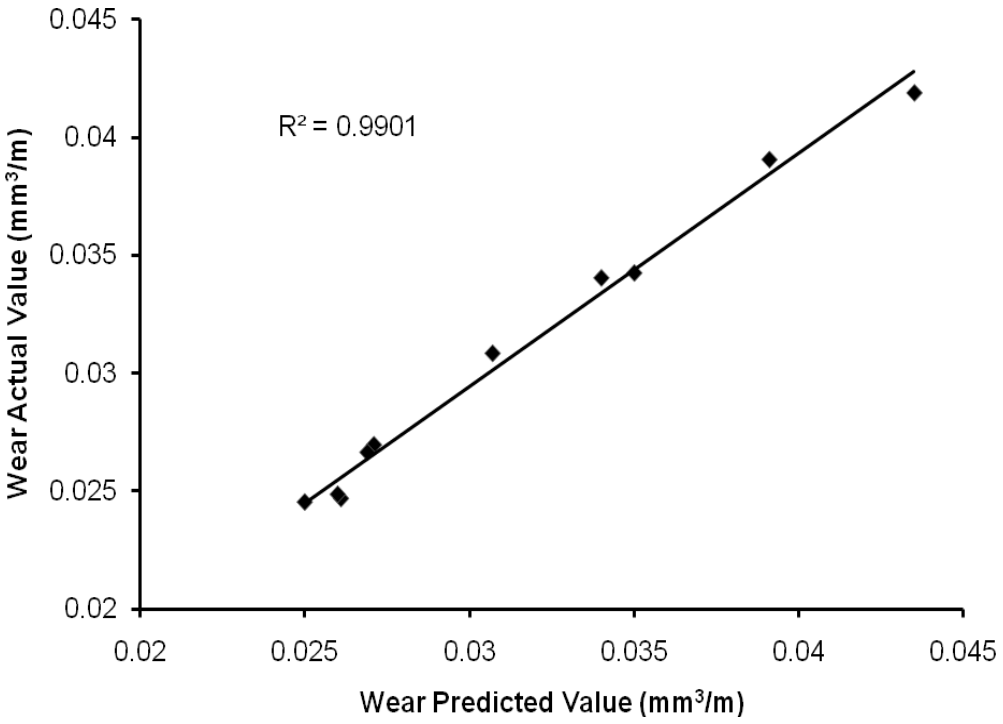

Figure 7.8 Performance of neural model

Table 7.6 Confirmation result

Algorithm	A	B	C	D	E	Optimum wear	ANN predicted wear	Error
QPSO	0.254	29.99	46.41	0.4988	0.000002	0.0071	0.0098	0.001
BFOA	0.1278	0.15	59.91	0.5037	0.000697	0.0068	0.0038	0.0009

7.7 Conclusions

Functional relationship between process parameters and wear was determined using response surface methodology. The process parameters considered are layer thickness, orientation, raster angle, raster width and air gap. Central composite design is used for experimentation and model building. Wear model is validated using ANOVA and Anderson-Darling (AD) normality test. Microphotographs shows that wearing of FDM processed ABS part is a complex phenomena and may result due to formation and breaking of interfacial adhesive bonds, removal of material due to scratching and fatigue and formation of cracks in surface regions due to tribological stress cycles that result in the formation of pits or separation of material. Response surface plots indicate that reduction of distortion during part building stage is a necessary requirement for minimum wear. Hence factor levels which minimize the distortion must be used. Curvature present in response plots shows high amount of non linearity indicating the complex relationship between process parameters and output response. This is further substantiated by ANN prediction. Optimization of process is achieved using BFOA and QPSO. Optimization results establish the superiority of BFOA in comparison to QPSO as the chemotaxis provides the exploring ability to algorithm in a given problem domain. Whereas getting replaced by better bacteria, owing to their poorer foraging abilities (reproduction) or eliminated by sudden unforeseen event, which may drastically alter the smooth process of evolution (elimination-dispersal) not only maintain the population diversity but also helps in reducing the behaviour of stagnation. The optimization results are further verified using ANN.

CHAPTER 8

EXECUTIVE SUMMARY AND CONCLUSIONS

8.1 Introduction

Fused deposition modelling (FDM) process build parts of any geometry by sequential deposition of the material extruded out from the tip of a nozzle in a temperature controlled environment. FDM has significant advantages in terms of elimination of expensive tooling, flexibility, and possibility of producing complex parts and shapes [22-34]. Existing examples tend to prove that this process offer time and cost advantages over conventional technologies [5, 45, 46, 52, 121-126]. One of the current challenges faced by FDM users relates to the quality of parts produced. This drawback is partly attributed to processable material constraints but major limitation arise due to building principle of FDM [11, 13, 15, 18, 19, 21, 97-102, 147, 166, 178, 181, 182, 185-187]. In this direction the present work emphasises on the improvement of part quality by proper control of process parameters.

8.2 Summary of findings

The understandings generated in this work not only properly explain the complex build mechanism but also present in detail the effect of process parameters on output responses. For example,

- As the material is extruded out in a temperature controlled environment there is a shearing effect that causes material to spread forward and sideward when the nozzle moves.
- The material will have sufficient residual heat energy to activate the surfaces of the adjacent regions so that bonding between neighbouring filaments can take place via thermally driven diffusion welding.
- The part of heat goes to the already deposited materials at bottom layer and increases their temperature. This results in more diffusion phenomenon for adjacent filaments in bottom layers as compared to upper layers.
- As the number of layers (due to decrease in layer thickness or increase in orientation) increases this effect becomes more prominent.
- Further, increase in temperature of bottom and adjacent materials will not be uniform. This is due to the fact that nozzle is not moving with uniform speed. Its speed has to be non-uniform at turns to prevent jerk to nozzle movement. In addition, it is observed that deposition speed of the nozzle is slow at lower slice thickness as compared to higher slice thickness. While in operation, the nozzle frequently stops depositing material and return to service location for tip cleaning. This not only results in non uniform deposition rate (although material extrusion rate is constant) but also varies the convective conditions

within the building part as the nozzle tip temperature is always higher than that of the build chamber and deposited material.

- This phenomenon results in development of non uniform temperature gradient along the direction of deposition as well as towards bottom layers.
- Further, the constraint offered by the bonding will not allow deposited material to expand or contract resulting in generation of non-uniform thermal stresses.
- To keep the direction of deposition small, it is advisable to keep the raster length as small as possible. But the raster length depends upon the cross section of the slice and it cannot be kept smaller than a certain permissible value. Figure 8.1 shows two slices of same cross sectional area. Slice 1, which deposit rasters at smaller angle, require more number of rasters with longer length as compared to rasters in slice 2, which deposits at larger angle. Therefore, raster angle must be large in order to reduce the non-uniform temperature gradient.

Figure 8.1 Layer filling strategy

- But large raster angles also mean more number of rasters, more turns at the layer boundary and more time required to fill the layer resulting in overall increase in non uniform thermal stresses.
- Same reasoning is also true with increase or decrease in road width. Stress accumulation increases with increase in road width. A small road width causes less heat input into the system in a specified period of time but requires more loops to fill a certain area. More loops means more time required for deposition of single layer and more non-uniform thermal stresses.
- The accumulated stresses may lead to inner layer cracking (Figure 6.2) or de-lamination.
- Smaller air gap means that adjacent rasters are placed nearer to each other and helps to create strong bonding. This will be deteriorate if diffusion is in excess, resulting in unevenness in a layer due to bump formations (Figure 4.8) and also restricts heat dissipation giving rise to increased chance of stress accumulation. Increasing the spacing between rasters will provide the small pockets for heat dissipation but also increases the voids (Figure 4.9) and thus reduces the load bearing capacity.

The work not only highlights the important contribution of each factor on the output response but also emphasises on the interaction involved among them (Table

8.1). For example, for the case of wear, it can be noted that wear decreases with increase in raster angle (C) as expected at the low level of air gap (E). However, wear increases with increase in raster angle for high level of air gap (Figure 7.6.e). This is caused because spacing between rasters increases as air gap increases resulting in weak bond formation between adjacent rasters. Similarly, for the case of bottom surface roughness (Table 8.1) layer thickness (A) is not only significant but also effect of its square term and interaction with orientation (B) and air gap (E) are important.

Table 8.1 Significant factors and interactions for each response

Response	Significant terms
Dimensional accuracy along length	A, B, C, BXD, BXE
Dimensional accuracy along width	A, B, AXB, BXE
Dimensional accuracy along thickness	A, B, AXB, BXC, BXD
Dimensional accuracy along diameter	A, B, E, AXB, BXD, BXE
Top surface roughness	A, B, AXE, BXC, CXD, CXE
Bottom surface roughness	B, A^2, AXB, AXE, CXD
Side surface roughness	A, B, C, D, AXB, AXC, AXE, BXC, BXD, CXE
Tensile strength	A, B, C, E, A^2, B^2, AXC, AXD, AXE, BXC, BXE
Flexural strength	A, B, C, D, E, AXC, AXD, AXE, BXE, CXE, DXE
Impact strength	A, B, C, A^2, BXD
Compressive strength	A, B, C, E, B^2, AXC, BXE, CXE
Wear	B, D, E, A^2, B^2, AXB, AXC, AXE, BXD, CXE

As highlighted in Table 8.1, different factors and their interactions are significant for each studied response and thus demands the suitable methods for optimum factor level determination. To achieve this, present work utilizes the latest techniques of optimization such as grey Taguchi method, QPSO, and BFOA. The suitability of grey Taguchi method lies in the fact that it translates all the responses into an equivalent single response known as grey relational grade (GRG), which can be used for determining optimal factor setting for all the responses simultaneously. The primary drawback of this method is that GRG has no physical meaning rather it only represents the level of correlation between the reference sequence and the comparability sequence. Also, it requires the assignment of importance to each studied response which usually depends on decision makers' judgment or the structure of the proposed problem. On the other hand, QPSO and BFOA methods are a kind of swarm intelligence algorithms inspired by exploring simple analogy of social interaction of a group of organisms rather than purely individual cognitive abilities. There major limitation with respect to FDM process is that they assume a continuous search space for optimality determination which may not be suitable for some of the FDM process parameters due to hardware limitations. But it can be said

that the optimal conditions achieved using these methods (Table 8.2) are as per the understanding generated for part build mechanism in this work. It can be proposed that advancement in FDM hardware will further enhance the effectiveness of the process for industrial applications. The present work also compares QPSO and BFOA algorithms and shows that QPSO is simple, fast and require less parameters to be tuned but its exploration and exploitation capabilities are not better than the BFOA.

Table 8.2 Optimum factor level setting for each quality characteristic

Quality characteristic	Factors				
	Layer thickness in mm (A)	Orientation in degree (B)	Raster angle in degree (C)	Raster width in mm (D)	Air gap in mm (E)
Dimensional accuracy	0.254	0	0	0.4564	0.008
Surface roughness	0.127	29.97	0.045	0.4070	$4x10^{-7}$
Strength	0.254	0.081	60	0.40661	0.00799
Wear	0.1278	0.15	59.91	0.5037	0.000697

8.3 Contribution of the research work

- Unlike other RP processed parts which have shrinkage in all the directions, this work demonstrates that FDM built parts are always oversize along the direction of build due to slicing error and uneven layer deposition.
- Surface roughness study demonstrates that layer thickness and part build orientation are important factors but other studied factors effect cannot be neglected.
- The mechanical strength study demonstrates anisotropic and brittle characteristics of FDM built part.
- The work can be seen as the first attempt to study the wear mechanism of FDM built parts.
- The understandings generated in this work properly explain the complex build mechanism and also present in detail the processing parameter effect on output responses using microphotographs and experiments.
- The main reason identified for poor quality of FDM built part is uneven heating and cooling cycles generated during part building stages. The study proposes that proper parameter level setting can minimize this negative effect.
- Complex inter relationship among factors makes it difficult to ascertain the factor setting by simple analysis of factor variation effect. In this direction, design of experiment (DOE) related methodologies adopted, in this work, are shown to be suitable enough for asserting the effect of every single condition

possible in an experiment under the influence of numerous factors considered with better precision in less experimental runs.

- The results validated by standard statistical tests help the practitioners to predict the output response with greater confidence and accuracy.
- The findings will not only contribute for manufacturing prototypes with greater accuracy and better surface finish but also helps in generating tools and end useable parts with greater precision, better service performance and life because of good mechanical strength and wear properties.

8.4 Limitations of the study

In spite of several advantages obtained through proposed study, the followings may be treated as limitations of the study since they have not been addressed in this study

- The work extensively studies the static mechanical properties and sliding wear characteristic of FDM built parts but the response under dynamic loading like fatigue, creep, and vibration and abrasive, fretting, and erosive wear characteristics need to be analyzed to test the functionality of parts.
- Effect of process parameters on dimensional accuracy is studied on flat and circular profiles but the study needs to be extended to other types of profiles like helical surfaces.
- The study on surface roughness can also be extended to concave or convex shaped surfaces instead of flat surfaces.
- The parametric study has been carried out on test parts recommended by International standards. The behaviour should be appraised on real working model where intricate part geometries are encountered.
- Present study mainly develops empirical models but mathematical or numerical approaches must be developed to study effect of process parameters on various responses.
- In this work, only FDM process has been considered limiting the scope of improvement in other RP processes.

8.5 Scope for future work

The present work leaves a wide scope for future investigators to explore many aspects of FDM and other RP processes on similar lines. Some recommendations for future research include:

- Based on the results generated in this work, expert based control algorithms like fuzzy controller can be developed for process control.

- The study may be extended to dynamic loading condition.
- The effects of environmental variables like temperature and humidity on the part quality need to be explored.
- Comparative evaluation of various RP process based on their part build mechanism strengths and weakness can be carried out.
- Applicability of FDM from small size batch production to medium or large batch sizes can be extended by increasing the build space and providing multiple nozzles for material deposition.
- FDM process specific CAD modelling and analysis tools need to be developed.
- Option of depositing multiple materials in a single setting and necessary changes in hardware need to be explored.
- Possibility of using different materials or modifications in the present material composition can be explored.

Bibliography

[1] T. Tolio, D. Ceglarek, H. A. ElMaraghy, A Fischer, S.J. Hu, L. Laperrière, S.T. Newman, and J. Váncza, "SPECIES-Co-evolution of Products, Processes and Production Systems," *CIRP Annals-Manufacturing Technology*, vol. 59, 2010, pp. 672-693.

[2] Y. Yan, S. Li, R. Zhang, F. Lin, R. Wu, Q. Lu, Z. Xiong, and X. Wang, "Rapid Prototyping and Manufacturing Technology: Principle, Representative Technics, Applications, and Development Trends," *Tsinghua Science & Technology*, vol. 14, 2009, pp. 1-12.

[3] T.Wohler, "Additive Manufacturing State of the Industry Annual Worldwide Progress Report," *Wohler associates*, Colorado, USA, 2010.

[4] C.K. Chua, S.H. The and R.K.L. Gay, "Rapid Prototyping and Virtual Manufacturing in Product Design and Manufacturing," *International Journal of Advanced Manufacturing Technology*, vol. 15, 1999, pp. 597-603.

[5] Q. Liu, M.C. Leu, and S.M. Schmitt, "Rapid Prototyping in Dentistry: Technology and Application," *International Journal of Advanced Manufacturing Technology*, vol. 29, 2005, pp. 317-335.

[6] V. Raja, S. Zhang, J. Garside, C. Ryall, and D. Wimpenny, "Rapid and Cost-Effective Manufacturing of High Integrity Aerospace Components," *International Journal of Advanced Manufacturing Technology*, vol. 27, 2005, pp. 759-773.

[7] B. Dong, G. Qi, X. Gu, and X. Wei, "Web Service Oriented Manufacturing Resource Applications for Networked Product Development," *Advanced Engineering Informatics*, vol. 22, 2008, pp. 282-295.

[8] H. Lan, "Web Based Rapid Prototyping and Manufacturing Systems: A Review," *Computers in Industry*, vol. 60, 2009, pp. 643-656.

[9] Graham Tromans, "Developments in Rapid Casting," *Professional Engineering Publishing*, London, UK, 2003.

[10] A. Gosh and A.K. Mallik, "Manufacturing Science," *Affiliated East-West Press Private Limited*, New Delhi, India, 1985.

[11] S. O. Onuh and Y. Y. Yusuf, “Rapid Prototyping Technology: Applications and Benefits for Rapid Product Development,” *Journal of Intelligent Manufacturing*, vol. 10, 1999, pp. 301-311.

[12] S. Upcraft and R. Fletcher, “The Rapid Prototyping Technologies,” *Assembly Automation*, vol. 23(4), 2003, pp. 318-330.

[13] C. C. Kai and L. K Fai, “Rapid Prototyping: Principles and Applications in Manufacturing,” *John Wiley and Sons*, Singapore, 1997.

[14] W. L. Wang, J. G. Conley, Y. N. Yan and J. Y. H. Fuh, “Towards Intelligent Setting of Process Parameters for Layered Manufacturing,” *Journal of Intelligent Manufacturing*, vol. 11, 2000, pp. 65-74.

[15] Rafiq Noorani, “Rapid Prototyping-Principles and Application,” *John Wiley & Sons*, New Jersey, USA; 2005.

[16] N Hopkinson, R. J. M Hagur and P.H. Dickens, “Rapid Manufacturing: An Industrial Revolution for the Digital Age,” *John Wiley & Sons*, England, UK, 2006.

[17] T. Wohlers, “CAD Meets Rapid Prototyping,” *Computer Aided Engineering*, vol. 11(4), 1992, pp. 62-73.

[18] G.D. Kim and Y.T. Oh, “A Benchmark Study on Rapid Prototyping Processes and Machines: Quantitative Comparisons of Mechanical Properties, Accuracy, Roughness, Speed, and Material Cost,” *Proceedings of the Institution of Mechanical Engineers, Part B: Journal of Engineering Manufacture*, vol. 222(2), 2008, pp. 201-215.

[19] R. Campbell, M. Martorelli and H.S Lee, “Surface Roughness Visualisation for Rapid Prototyping Models,” *Computer Aided Design*, vol. 34, 2002, pp. 717-725.

[20] K. Chockalingam, N. Jawahar, K.N. Ramanathan, and P.S. Banerjee, “Optimization of Stereolithography Process Parameters for Part Strength Using Design of Experiments,” *International Journal of Advanced Manufacturing Technology*, vol. 29, Mar. 2005, pp. 79-88.

[21] R. Ippolito, L. Iuliano, P. di Torino and A. Gatto,, “Benchmarking of Rapid Prototyping Techniques in Terms of Dimensional Accuracy and Surface Finish,” *CIRP Annals-Manufacturing Technology*, vol. 44 (1), 1995, pp. 157-160.

[22] I. Gibson, D. W. Rosen and B. Stucker, “Additive Manufacturing Technologies:Rapid Prototyping to Direct Digital Manufacturing,” *Springer*, New York, USA, 2010.

[23] F.L. Krause, M. Chiesla, Ch. Stiel and A. Ulbrich, “Enhanced Rapid Prototyping for Faster Product Development Processes,” *CIRP Annals-Manufacturing Technology*, vol. 46 (1), 1997, pp. 93-96.

[24] A Bernard and A Fischer, “New Trends in Rapid Product Development,” *CIRP Annals- Manufacturing Technology*, vol. 51, 2002, pp. 635-652.

[25] J. P. Kruth, M. C. Leu and T. Nakagawa, “Progress in Additive Manufacturing and Rapid Prototyping,” *CIRP Annals-Manufacturing Technology*, vol. 47(2), 1998, pp. 525-540.

[26] B. Wiedemann and H. A. Jantzen, “Strategies and Applications for Rapid Product and Process Development in Daimler-Benz AG” *Computers in Industries*, vol. 39(1), 1999; pp. 11–25.

[27] E. Berry, J. M. Brown, M. Connell, C. M. Craven, N. D. Efford, A. Radjenovic and M. A. Smith, “Preliminary Experience with Medical Applications of Rapid Prototyping by Selective Laser Sintering,” *Medical Engineering & Physics*, vol. 19(1), 1997, pp. 90-96.

[28] J. Giannatsis and V. Dedoussis, “Additive Fabrication Technologies Applied to Medicine and Health Care: A Review,” *International Journal of Advanced Manufacturing Technology*, vol. 40, 2009, pp. 116-127.

[29] S. Girod, M. Teschner, U. Schrell, B. Kevekordes and B. Girod, “Computer Aided 3-D Simulation and Prediction of Craniofacial Surgery: A New Approach,” *Journal of Cranio-Maxillofacial Surgery*, vol. 29(30), 2001, pp. 156-158.

[30] E. Heissler, F.S. Fischer, S. Bolouri, T. Lehmann, W. Mathar, A. Gebhardt, W.Lanksch and J. Bier, “Custom-Made Cast Titanium Implants Produced with CAD/CAM for the Reconstruction of Cranium Defects,” *International Journal of Oral and Maxillofacial Surgery*, vol. 27(5), 1998, pp. 334-338.

[31] S. Lohfeld, P. Mchugh, D. Serban, D.Boyle, G. O’Donnell and N. Peckitt, “Engineering Assisted SurgeryTM: A Route for Digital Design and Manufacturing of Customised Maxillofacial Implants,” *Journal of Materials Processing Technology*, vol. 183, 2007, pp. 333–338.

[32] G. Colombo, S. Filippi, C. Rizzi and F. Rotini, “A New Design Paradigm for the Development of Custom-Fit Soft Sockets for Lowe Limb Prostheses,” *Computers in Industry*, vol. 61(6), 2010, pp. 513-523.

[33] M.H. Too, K.F. Leong, C.K. Chua, Z.H. Du, S.F. Yang, C.M. Cheah and S.L. Ho, “Investigation of 3D Non Random Porous Structures by Fused Deposition Modeling,” *The International Journal of Advance Manufacturing Technology*, vol. 19, 2002, pp. 217-223.

[34] G.N. Levy, R. Schindel, and J.P. Kruth “Rapid Manufacturing and Rapid Tooling with Layer Manufacturing (LM) Technologies: State of The Art and Future Perspective,” *CIRP Annals-Manufacturing Technology*, vol. 2, 2003, pp. 589-609.

[35] K. K. B. Hon, “Digital Additive Manufacturing: From Rapid Prototyping to Rapid Manufacturing,” *Proceedings of the 35th International MATADOR Conference*, 2007, S. Hinduja and K.C. Fan (Eds.), Taipai, Taiwan, 2007, pp. 337-340.

[36] Y. Im, B. Cho, S. Seo, J. Son, S. Chung, and H. Jeong, “Functional Prototype Development of Multi-Layer Board (MLB) Using Rapid Prototyping Technology,” *Journal of Materials Processing Technology*, vol. 187-188, 2007, pp. 619-622.

[37] Y. Ding, H. Lan, J Hong and D. Wu, “An Integrated Manufacturing System for Rapid Tooling Based on Rapid Prototyping,” *Robotics and Computer-Integrated Manufacturing*, vol. 20, 2004, pp. 281-288.

[38] P. Dunne, S.P. Soe, G. Byrne, A. Venus and A.R. Wheatley, “Some Demands on Rapid Prototypes Used as Master Patterns in Rapid Tooling for Injection Moulding,” *Journal of Materials Processing Technology*, vol. 150, 2004, pp. 201-207.

[39] C. K. Chua, K. H. Hong and S. L. Ho, “Rapid Tooling Technology. Part 1. A Comparative Study” *International Journal of Advanced Manufacturing Technology*, vol. 15, 1999, pp. 604-608.

[40] Z. Shan, Y. Yan, R. Zhang, Q. Lu, and L. Guan, “Rapid Manufacture of Metal Tooling by Rapid Prototyping,” *International Journal of Advanced Manufacturing Technology*, vol. 21, May. 2003, pp. 469-475.

[41] S. Rahmati and P. Dickens, “Rapid Tooling Analysis of Stereolithography Injection Mould Tooling,” *International Journal of Machine Tools and Manufacture*, vol. 47, 2007, pp. 740-747.

[42] B. Mueller and D. Kochan, “Laminated Object Manufacturing for Rapid Tooling and Patternmaking in Foundry Industry,” *Computers in Industry*, vol. 39(1), 1999, pp. 47-53.

[43] J. Czyżewski, P. Burzyński, K. Gaweł, and J. Meisner, “Rapid Prototyping of Electrically Conductive Components Using 3D Printing Technology,” *Journal of Materials Processing Technology*, vol. 209, 2009, pp. 5281-5285.

[44] C.M. Cheah, C.K. Chua, C.W. Lee, S.T. Lim, K.H. Eu, and L.T. Lin, “Rapid Sheet Metal Manufacturing. Part 2: Direct Rapid Tooling,” *International Journal of Advanced Manufacturing Technology*, vol. 19, 2002, pp. 510-515.

[45] N.P. Karapatis, J.P.S. Van Griethuysen and R. Glardon, “Direct Rapid Tooling: A Review of Current Research,” *Rapid Prototyping Journal*, vol. 4(2), 1998, pp. 77-89.

[46] C.M. Cheah, C.K. Chua, C.W. Lee, C. Feng, and K. Totong, “Rapid Prototyping and Tooling Techniques: A Review of Applications for Rapid Investment Casting,” *International Journal of Advanced Manufacturing Technology*, vol. 25, 2004, pp. 308-320.

[47] R. Mustafizur, E. A.Haider and E.H. Tay, “Integration of powder metal based rapid prototyping and plating techniques for EDM tooling,” *Proceedings of the 24 International Conference on Manufacturing*, ICM 2000 Bangladesh, 2000, pp.161-168.

[48] M. Monzon, A.N. Benıtez, M.D. Marrero, N. Hernandez, P. Hernandez and J. Aisa, “Validation Of Electrical Discharge Machining Electrodes Made with Rapid Tooling Technologies,” *Journal of Materials Processing Technology*, vol. 196, 2008, pp. 109–114.

[49] C.Y. Hsu, D.Y. Chen, M.Y. Lai, and G.J. Tzou, “EDM Electrode Manufacturing Using RP Combining Electroless Plating with Electroforming,” *International Journal of Advanced Manufacturing Technology*, vol. 38, 2007, pp. 915-924.

[50] Yu Zhang and Hongwu Liu, “Application of Rapid Prototyping Technology in Die Making of Diesel Engine,” *Tsinghua Science and Technology*, vol. 14 (S1), 2009, pp. 127-131.

[51] S. Ma, I. Gibson, G. Balaji, and Q. Hu, “Development of Epoxy Matrix Composites for Rapid Tooling Applications,” *Journal of Materials Processing Technology*, vol. 192-193, 2007, pp. 75-82.

[52] S. Kumar and J. P. Kruth, “Composites by Rapid Prototyping Technology,” *Materials and Design*, vol. 31, 2010, pp. 850–856.

[53] R.I. Campbell, and M. R. N. Bernie, “Creating a Database of Rapid Prototyping System Capabilities,” *Journal of Materials Processing Technology*, vol. 61, 1996, pp. 163-167.

[54] D.T. Pham and R.S. Gault, “A Comparison of Rapid Prototyping Technologies,” *International Journal of Machine Tools and Manufactures*, vol. 38, 1998, pp. 1257-1287.

[55] R. Bibb, Z Taha, R. Brown,and D. Wright, “Development of a Rapid Prototyping Design Advice System,” *Journal of Intelligent Manufacturing*, vol. 10, 1999, pp. 331-339.

[56] M. Mahesh, J.Y.H. Fuh, Y.S. Wong, and H.T. Loh, “Benchmarking for Decision Making in Rapid Prototyping Systems,” *Proceedings of IEEE International Conference on Automation Science and Engineering*, 2005, N. Vishwanandam and M.Y. Wang (Eds.), Alberta, Canada, 2005, pp. 19-24.

[57] O.S. Vaidya and S. Kumar, “Analytic hierarchy process: An Overview of Applications,” *European Journal of Operational Research*, vol. 169, 2006, pp. 1-29.

[58] B.M. Braglia and A. Petroni, “A Management-Support Technique for the Selection of Rapid Prototyping Technologies,” *Journal of Industrial Technology*, vol. 15, 1999, pp. 1-6.

[59] A. Kengpol and C. O’Brien “The Development of A Decision Support Tool for the Selection of Advanced Technology to Achieve Rapid Product Development,” *International Journal of Production Economics*, vol. 69, 2001, pp. 177-191.

[60] S.H. Masood and M. Al-Alawi, “The IRIS Rapid Prototyping System Selector for Educational and Manufacturing Users,” *International Journal of Engineering Education*, vol. 18 (1), 2002, pp. 66-77.

[61] S. Masood and A. Soo, “A Rule Based Expert System for Rapid Prototyping System Selection,” *Robotics and Computer-Integrated Manufacturing*, vol. 18, 2002, pp. 267-274.

[62] H.S. Byun and K.H. Lee, “A Decision Support System for the Selection of a Rapid Prototyping Process using the Modified TOPSIS Method,” *International*

Journal of Advanced Manufacturing Technology, vol. 26, Apr. 2004, pp. 1338-1347.

[63] H. Lan, Y. Ding, and J. Hong, "Decision Support System for Rapid Prototyping Process Selection Through Integration of Fuzzy Synthetic Evaluation and An Expert System," *International Journal of Production Research*, vol. 43,. 2005, pp. 169-194.

[64] B. V. Chowdary, "Back-propagation Artificial Neural Network Approach for Machining Centre Selection," *Journal of Manufacturing Technology Management*, vol. 18(3), 2007, pp. 315-332.

[65] R.V. Rao and K.K. Padmanabhan, "Rapid Prototyping Process Selection Using Graph Theory and Matrix Approach," *Journal of Materials Processing Technology*, vol. 194, 2007, pp. 81-88.

[66] K. Subburaj and B. Ravi, "Computer Aided Rapid Tooling Process Selection and Manufacturability Evaluation for Injection Mold Development," *Computers in Industry*, vol. 59, Mar. 2008, pp. 262-276.

[67] S.J. Rock and M.J. Wozny, "A Flexible File Format for Solid Freeform Fabrication," *Proceedings of Solid Freeform Fabrication Symposium*-1991, University of Texas, Austin, USA, 1991, pp. 1-12.

[68] A. Dolenc and I. Makela, "Some Efficient Procedures for Correcting Triangulated Models," *Proceedings of Solid Freeform Fabrication Symposium*-1993, University of Texas, Austin, USA, 1993, pp. 126-134.

[69] G. Barequet and Y. Kaplan "A Data Front-End For Layered Manufacturing," *Computer Aided Design*, Vol. 30, 1998, Pp. 231-243.

[70] D. Ma, F. Lin, and C.K. Chua, "Rapid Prototyping Applications in Medicine. Part 2: STL File Generation and Case Studies," *International Journal of Advanced Manufacturing Technology*, vol. 18, 2001, pp. 118-127.

[71] C. C. Kai, G. K Gan, Jacob and T. Mei, "Interface Between CAD and Rapid Prototyping Systems. Part 1: A Study of Existing Interfaces," *International Journal of Advanced Manufacturing Technology*, vol.13, 1997 pp. 566-570.

[72] D. Dutta, V. Kumar, M.J. Pratt and R.D. Sriram, "Towards STEP-Based Data Transfer in Layered Manufacturing," *Proceedings of the Tenth International IFIP WG5.2/5.3 Conference PROLAMAT*-98, G. Jacucci,; G.J. Olling, K. Preiss, and M.J. Wozny. (Eds.), 1998

[73] G. Jacob, Chua Chee Kai and Tong Mei “Development of A New Rapid Prototyping Interface,” *Computers in Industry*, vol. 39, 1999, pp. 61-70.

[74] M. Pratt, A.D. Bhatt, D. Dutta, K.W. Lyons, L. Patil and R.D. Sriram, “Progress Towards an International Standard for Data Transfer in Rapid Prototyping and Layered Manufacturing,” *Computer Aided Design*, vol. 34, 2002, pp. 1111-1121.

[75] T. Wu and E.H.M. Cheung, “Enhanced STL,” *International Journal of Advanced Manufacturing Technology*, vol. 29, 2005, pp. 1143-1150.

[76] C.C. Kai, G.G.K. Jacob, and T. Mei, “Interface Between CAD and Rapid Prototyping Systems. Part 2: LMI- An Improved Interface,” *International Journal of Advanced Manufacturing Technology*, vol 13, 1997, pp. 571-576.

[77] S. Guduri, R.H. Crawford, and J.J. Beaman, “A Method to Generate Exact Contour Files for Solid Freeform Fabrication,” *Proceedings of Solid Freeform Fabrication Symposium*-1992, University of Texas, Austin, USA, 1992, pp. 95-105.

[78] P Vuyyuru, C.F. Kirschman, G.M. Fadel, A. Bagchi, and C.C. Jara-Almonte, “A NURBS-Based Approach for Rapid Product Realization,” 5th *International Conference of Rapid Prototyping*, Dayton, Ohio, 1994, pp 229–239.

[79] R. Jamieson and H. Hacker, “Direct Slicing of CAD Models for Rapid Prototyping,” *Rapid Prototyping Journal*, vol. 1(2), 1995, pp. 4-12.

[80] X. Chen, C. Wang, X. Ye, Y. Xiao, and S. Huang, “Direct Slicing from Powershape Models for Rapid Prototyping,” *International Journal of Advanced Manufacturing Technology*, vol. 17, 2001, pp. 543-547.

[81] W. Cao and Y. Miyamoto, “Direct Slicing from AutoCAD Solid Models for Rapid Prototyping,” *International Journal of Advanced Manufacturing Technology*, vol. 21, 2003, pp. 739-742.

[82] W. Ma, “NURBS-Based Adaptive Slicing for Efficient Rapid Prototyping,” *Computer Aided Design*, vol. 36, 2004, pp. 1309-1325.

[83] G. S. Xu, J. P. Zhang, S. Luo and J. Jin, “Direct Slicing CAD Models with Solidworks for Integral Stereolithography System,” *Advanced Materials Research*, vol. 148-149, 2010, pp. 818-821.

[84] L. Li, N. Schemenauer, X. Peng, Y. Zeng and P. Gu “A Reverse Engineering System for Rapid Manufacturing of Complex Objects,” *Robotics and Computer Integrated Manufacturing*, vol. 18, 2002, pp. 53-67.

[85] M. Sokovic and J. Kopac, “RE (Reverse Engineering) as Necessary Phase by Rapid Product Development,” *Journal of Materials Processing Technology*, vol. 175, 2006, pp. 398-403.

[86] A. Willis, J. Speicher and D.B. Cooper, “Rapid Prototyping 3D Objects from Scanned Measurement Data,” *Image and Vision Computing*, vol. 25, 2007, pp. 1174-1184.

[87] C.C. Ng, C. Lee and A. Seah, “An Integrated Experimental Approach to Link a Laser Digitizer, a CAD/CAM System and a Rapid Prototyping System for Biomedical Applications,” *International Journal of Advanced Manufacturing Technology*, vol. 14, 1997, pp. 110-115

[88] Y. Zhongwei and J. Shouwei,”STL File Generation from Digitized Data Points Based on Triangulation of 3D Parametric Surfaces,” *International Journal of Advanced Manufacturing Technology*, vol. 23, 2004, 882–888.

[89] Y. Qiu, X. Zhou, and X. Qian, “Direct Slicing of Cloud Data With Guaranteed Topology for Rapid Prototyping,” *International Journal of Advanced Manufacturing Technology*, vol. 53(1), 2011, pp. 255-265.

[90] W. Cheng, J.Y.H. Fuh, A.Y.C. Nee, Y.S. Wong, H.T. Loh, T. Miyazawa, “Multi Objective Optimization of Part Building Orientation in Stereolithography,” *Rapid Prototyping Journal*, vol. 1, 1995, pp. 12-23.

[91] P. Lan, S. Chou, L. Chent and D. Gemmill “Determining Fabrication Orientations for Rapid Prototyping with Stereolithography Apparatus,” *Computer Aided Design*, vol. 29, 1997, pp. 53-62.

[92] P. Alexander, S. Allen and D. Dutta “Part Orientation and Build Cost Determination in Layered Manufacturing,” *Computer Aided Design*, vol. 30, 1998, pp. 343-356.

[93] J. Har and K. Lee, “The Development of a CAD Environment to Determine the Preferred Build-up Direction for Layered Manufacturing,” *International Journal of Advanced Manufacturing Technology*, vol. 14, 1998, pp. 247-254.

[94] D. Cormier, K. Unnanon and E. Sanii., “Specifying Non-Uniform Cusp Heights as a Potential Aid for Adaptive Slicing” *Rapid Prototyping Journal*, vol. 6 (3), 2000, pp.204 - 212.

[95] J.Q. Yan and M.Y. Zhou, and J.T. Xi, “Adaptive Direct Slicing with Non-Uniform Cusp Heights for Rapid Prototyping,” *International Journal of Advanced Manufacturing Technology*, vol. 23, Jan. 2004, pp. 20-27.

[97] J. Tyberg and J. H. Bohn “FDM systems and local adaptive slicing,” *Materials & Design*, vol. 20, Jun. 1999, pp. 77-82.

[98] S.H. Masood, W. Rattanawong, and P. Iovenitti, “Part Build Orientations Based on Volumetric Error in Fused Deposition Modelling,” *International Journal of Advanced Manufacturing Technology*, vol. 16, 2000, pp. 162-168.

[99] S.H. Masood and W. Rattanawong, “A Generic Part Orientation System Based on Volumetric Error in Rapid Prototyping,” *Mathematica*, 2002, pp. 209-216.

[100] W. Rattanawong, “Computational Intelligence for Part Orientation in Rapid Prototyping,” *International Conference on Computational Intelligence Robotics and Autonomous Systems*, Singapore, 2001.

[101] Y. Yang, J.Y.H. Fuh, H.T. Loh, and Y.S. Wong, “A Volumetric Difference-based Adaptive Slicing and Deposition Method for Layered Manufacturing,” *Journal of Manufacturing Science and Engineering*, vol. 125, 2003, p. 586.

[102] Y.-S. Liao and Y.-Y. Chiu, “A New Slicing Procedure for Rapid Prototyping Systems,” *International Journal of Advanced Manufacturing Technology*, vol. 18, 2001, pp. 579-585.

[103] S. S. Pande and S. Kumar, “A Generative Process Planning System for Parts Produced by Rapid Prototyping,” *International Journal of Production Research*, vol. 46, Nov. 2008, pp. 6431-6460.

[104] R. L Hope, R. N. Roth and P. A Jacobs, “Adaptive Slicing with Sloping Layer Surfaces,” *Rapid Prototyping Journal*, vol. 3(3), 1997, pp. 89-98.

[105] K. Thrimurthulu, P. M. Pandey and N. Venkata Reddy “Optimum Part Deposition Orientation in Fused Deposition Modeling,” *International Journal of Machine Tools and Manufacture*, vol. 44, May. 2004, pp. 585-594.

[106] H.S. Byun and K.H. Lee, “Determination of Optimal Build Direction In Rapid Prototyping with Variable Slicing,” *International Journal of Advanced Manufacturing Technology*, vol. 28, Apr. 2005, pp. 307-313.

[107] H. Byun and K. Lee, “Determination of the Optimal Build Direction for Different Rapid Prototyping Processes Using Multi-Criterion Decision Making,” *Robotics and Computer Integrated Manufacturing*, vol. 22, Feb. 2006, pp. 69-80.

[108] J. Zhao, R. Xia, W. Liu, and H. Wang, “A computing Method for Accurate Slice Contours Based on an STL model,” *Virtual and Physical Prototyping*, vol. 4, 2009, pp. 29-37.

[109] J. Giannatsis and V. Dedoussis, “Decision Support Tool for Selecting Fabrication Parameters in Stereolithography,” *International Journal of Advanced Manufacturing Technology*, vol. 33, 2006, pp. 706-718.

[110] V. Canellidis, J. Giannatsis, and V. Dedoussis, “Genetic Algorithm Based Multi-Objective Optimization of the Build Orientation in Stereolithography,” *International Journal of Advanced Manufacturing Technology*, vol. 45, 2009, pp. 714-730.

[111] Z. Hu, K. Lee and , J. Hur “Determination of Optimal Build Orientation for Hybrid Rapid Prototyping,” *Journal of Materials Processing Technology*, vol. 130-131, 2002, pp. 378-383.

[112] Y.H. Chen, Z.Y. Yang, and R.H. Ye, “A Fuzzy Decision Making Approach to Determine Build Orientation in Automated Layer Based Machining,” *2008 IEEE International Conference on Automation and Logistics*, vol. 1, Sep. 2008, pp. 1-6.

[113] “A. Nyaluke , B. Nasser, H, R Leep and H. R . Parsaei, “ Rapid Prototyping Work Space Optimization,” *Industrial Engineering*, vol. 31, 1996, pp. 103 - 106.

[114] S. Hur, K. Choi, S. Lee, and P. Chang, “Determination of Fabrication Orientation and Packing in SLS Process,” *Journal of Materials Processing Technology*, vol. 112, 2001, pp. 236-243.

[115] X. Zhang, B. Zhou, Y. Zeng and P. Gu, “Model Layout Optimization for Solid Ground Curing Rapid Prototyping Processes,” *Robotics and Computer-Integrated Manufacturing*, vol. 18, Feb. 2002, pp. 41-51.

[116] A. S. Gogate and S.S. Pande, “Intelligent Layout Planning for Rapid Prototyping,” *International Journal of Production Research*, vol. 46, 2008, pp. 5607-5631.

[117] C.L. Li, K.M. Yu, and T.W. Lam, “Implementation and Evaluation of Thin-Shell Rapid Prototype,” *Computers in Industry*, vol. 35, 1998, pp. 185-193.

[118] W. Han, M. A. Jafari, S. C. Danforth and A. Safari, “Tool Path-Based Deposition Planning in Fused Deposition Processes,” *Journal of Manufacturing Science and Engineering*, vol. 124, 2002, pp. 462-472.

[119] Todd Grimm, “Breakthroughs in Rapid Prototyping Materials,” *Desktop Engineering* (Magazine), February 1, 2008.

[120] J. Stampfl and R. Liska, “New Materials for Rapid Prototyping Applications,” *Macromolecular Chemistry and Physics*, vol. 206, Jul. 2005, pp. 1253-1256.

[121] W. Zhong, F. Li, Z. Zhang, L. Song, and Z. Li, “Short Fiber Reinforced Composites for Fused Deposition Modeling,” *Materials Science and Engineering A*, vol. 301, 2001, pp. 125 - 130.

[122] S. H. Masood and W. Q. Song, “Development of New Metal / Polymer Materials for Rapid Tooling using Fused Deposition Modelling,” *Materials & Design*, vol. 25, 2004, pp. 587-594.

[123] N. Mostafa, H. M. Syed, S. Igor, and G. Andrew, “A Study of Melt Flow Analysis of An ABS-Iron Composite in Fused Deposition Modelling Process,” *Tsinghua Science & Technology*, vol. 14, 2009, pp. 29-37.

[124] Robert W. Gray IV, Donald G. Baird and Jan Helge Bøhn, “Effects of Processing Conditions on Short TLCP Fiber Reinforced FDM Parts", *Rapid Prototyping Journal*, vol. 4 (1), 1998, pp.14 - 25.

[125] David Espalin, Karina Arcaute, David Rodriguez, Francisco Medina, Matthew Posner and Ryan Wicker, “Fused Deposition Modeling of Patient-Specific Polymethylmethacrylate Implants", *Rapid Prototyping Journal*, vol. 16 (3), pp.164-173.

[126] E. Y. Teo, Shin-Yeu Ong, Mark Seow Khoon Chong, Z. Zhang, J. Liu, Shabbir Moochhala,Bow Ho and Swee-Hin Teoh, “Polycaprolactone-Based Fused Deposition Modeled Mesh for Delivery of Antibacterial Agents to Infected Wounds,” *Biomaterials*, Vol 32, 2011, Pp. 297-287.

[127] A Woesz, M. Rumpler, J. Stampfl, F. Varga, N. Fratzlzelman, P. Roschger, K. Klaushofer, and P. Fratzl, “Towards Bone Replacement Materials from Calcium Phosphates via Rapid Prototyping and Ceramic Gelcasting,” *Materials Science and Engineering: C*, vol. 25, 2005, pp. 181-186.

[128] C. Hinczewski, S. Corbel and T. Chartie “Ceramic Suspensions Suitable for Stereolithography,” *Journal of the European Ceramic Society*, vol. 18, 1998, pp. 583-590.

[129] A. Greco, A. Licciulli and A. Maffezzoli, “Stereolitography of Ceramic Suspensions,” *Journal of Materials Science*, vol. 6, 2001, pp. 99-105.

[130] M. Lejeune, T. Chartier, C. Dossou-Yovo, and R. Noguera, “Ink-Jet Printing of Ceramic Micro-Pillar Arrays,” *Journal of the European Ceramic Society*, vol. 29, 2009, pp. 905-911.

[131] H.C. Yen, M. L. Chiu, and H. H. Tang, “Laser Scanning Parameters on Fabrication of Ceramic Parts by Liquid Phase Sintering,” *Journal of The European Ceramic Society*, vol. 29, 2009, pp. 1331-1336.

[132] F.-Hsing Liu, Y.-Kang Shen, and Y.-Shiuan Liao, “Selective Laser Gelation of Ceramic Matrix Composites,” *Composites Part B*, 2011, pp. 57-61.

[133] Y. Zhang, X. He, S. Du, and J. Zhang, “Al2O3 Ceramics Preparation by LOM (Laminated Object Manufacturing),” *International Journal of Advanced Manufacturing Technology*, vol. 17, 2001, pp. 531-534.

[134] A. Hattiangadi and A. Bandyopadhyay, “Modeling of Multiple Pore Ceramic Materials Fabricated via Fused Deposition Process,” *Scripta materialia*, vol. 42, 2000, pp. 581-588.

[135] I. Grida, and J. R. G. Evans, “Extrusion Free forming of Ceramics through Fine Nozzles,” *Journal of the European Ceramic Society*, vol. 23, 2003, pp. 629–635.

[136] S. Bose, S. Suguira, and A. Bandyopadhyay, “Processing of Controlled Porosity Ceramic,” *Acta Metallurgica*, vol. 41, 1999, pp. 1009 -1014.

[137] S. Kumar, “Manufacturing of WC–Co Moulds using SLS Machine,” *Journal of Materials Processing Technology*, vol. 209, 2009, pp. 3840-3848.

[138] R.C Luo, C. L. Chang;Y. L. Pan and J. H. Tzou, “Rapid Tooling using Laser Powered Direct Metallic Manufacturing Process,” *Industrial Electronics Society, 2005. IECON 2005*. 31st Annual Conference of IEEE, 2005.

[139] http://www.sandia.gov/mst/technologies/net-shaping.html

[140] www.osti.gov/bridge/purl.cover.jsp;jsessionid=aaf11d7ba8e8f1a

70f6ea16785395bbd?purl=/650377-9wh64y/webviewable

[141] G. Lewis and E. Schlienger, “Practical Considerations and Capabilities for Laser Assisted Direct Metal Deposition,” *Materials & Design*, vol. 21, 2000, pp. 417-423.

[142] Y. Zhang, P. Li, Y. Chen and A. T. Male, “Automated System for Welding-Based Rapid Prototyping,” *Mechatronics*, vol. 12, 2002, pp. 37-53.

[143] Y. Zang, P. Li, Y. Chen, and A. T. Male, “Weld Deposition-Based Rapid Prototyping: A Preliminary Study,” *Journal of Materials Processing Technology*, vol. 135, 2003, pp. 347–335.

[144] G. WU, A. L. Noshir, R. SADANJI and S. Danforth, “Solid Freeform Fabrication of Metal Components using Fused Deposition of Metals,” *Materials and Design*, vol. 23(1), 2002, pp. 97-105.

[145] Xinhong Xiong, Zhang Haiou and Wang Guilan, (2008) "A new method of direct metal prototyping: hybrid plasma deposition and milling", *Rapid Prototyping Journal*, vol. 14 (1), 2008, pp.53 – 56.

[146] J. Fessler, A. Nickel, G. Link, F. Prinz and P. Fussell, “Functional Gradient Metallic Prototypes through Shape Deposition Manufacturing,” *Proceedings of the SFF Symposium*, 1997.

[147] Q. Dao, J.C. Frimodig, H.N. Le, X. Li, S.B. Putnam, K. Golda, J.,Foyos, R. Noorani, and B. Fritz, “Calculation of Shrinkage Compensation Factors for Rapid Prototyping (FDM 1650),” *Computer Applications in Engineering Education*, vol. 7(3), 1999, pp. 186-195.

[148] F. Xu, Y.S. Wong, and H.T. Loh, “Toward Generic Models for Comparative Rapid Prototyping and Manufacturing,” *Journal of Manufacturing Systems*, vol. 19, 2000, pp. 283-296.

[149] A. Nizam, R.N. Gopal, L. Naing, A.B. Hakim, and A.R. Samsudin, “Dimensional Accuracy of the Skull Models Produced by Rapid Prototyping Technology Using Stereolithography Apparatus,” *Archives of Orofacial Sciences*, 2006, pp. 60-66.

[150] W. Liu, L. Li, and A.K. Kochhar, “A Method for Assessing Geometrical Errors in Layered Manufacturing. Part 1: Error Interaction and Transfer Mechanisms,” *The International Journal of Advance Manufacturing Technology*, 1998, pp. 637-643.

[151] Y. Ning, Y.S. Wong, J.Y.H. Fuh, “Effect of control of hatch length on material properties in the direct metal laser sintering process,” *Proceedings of the Institution of Mechanical Engineers, Part B: Journal of Engineering Manufacture*, vol. 219(1), 2005, pp. 15-25.

[152] K. Senthilkumaran, P.M. Pandey, and P.V.M. Rao, “Influence of Building Strategies on The Accuracy of Parts in Selective Laser Sintering,” *Materials & Design*, vol. 30, Sep. 2009, pp. 2946-2954.

[153] K. Senthilkumaran, P. Pandey, and P.V.M. Rao, “New Model for Shrinkage Compensation in Selective Laser Sintering,” *Virtual and Physical Prototyping*, vol. 4, Jun. 2009, pp. 49-62.

[154] K. Senthilkumaran, P.M. Pandey, and P.V.M. Rao, “Shrinkage Compensation Along Single Direction Dexel Space for Improving Accuracy in Selective Laser Sintering,” 2008 *IEEE International Conference on Automation Science and Engineering*, 2008, pp. 827-832.

[155] J. Zhou, D. Herscovici and C. C. Chen, “Parametric Process Optimization to Improve the Accuracy of Rapid Prototyped Stereolithography Parts,” *International Journal of Machine Tools and Manufacture*, vol. 40, 2000, pp. 363-379.

[156] E. Lehtihet, K. Tong, and S. Joshi, “Software Compensation of Rapid Prototyping Machines,” *Precision Engineering*, vol. 28, Jul. 2004, pp. 280-292.

[157] Y. Huang and H. Lan, “CAD/CAE/CAM Integration for Increasing the Accuracy of Mask Rapid Prototyping System,” *Computers in Industry*, vol. 56, Jun. 2005, pp. 442-456.

[158] Y. Huang and H. Lan, “Dynamic Reverse Compensation to Increase the Accuracy of The Rapid Prototyping System,” *Journal of Materials Processing Technology*, vol. 167, 2005, pp. 167-176.

[159] H.H. Zhu, L. Lu, J.Y.H. Fuh, “Study on Shrinkage Behavior of Direct Laser Sintering Metallic Powder,” *Proceedings of the Institution of Mechanical Engineers, Part B: Journal of Engineering Manufacture*, vol. 220, 2006, 183-190.

[160] R.J. Wang, L. Wang, L. Zhao and Z. Liu, “Influence of Process Parameters on Part Shrinkage in SLS,” *The International Journal of Advance Manufacturing Technology*, vol. 33, 2007, 498–504.

[161] P. Pandey and N. Raghunath, “Improving Accuracy Through Shrinkage Modelling by using Taguchi Method in Selective Laser Sintering,” *International Journal of Machine Tools and Manufacture*, vol. 47, May. 2007, pp. 985-995.

[162] S.L. Campanelli, G. Cardano, R. Giannoccaro, A.D. Ludovic and E.L.J. Bohez, “Statistical Analysis of Stereolithographic Process to Improve the Accuracy,” *Computer Aided Design*, vol. 39(1), 2007, pp. 80–86.

[163] C. Luis Perez, J. Vivancos and M.A. Sebastian, “Surface Roughness Analysis in Layered Forming Processes,” *Precision Engineering*, vol. 25, Jan. 2001, pp. 1-12.

[164] C. Luis Pérez, J. Vivancos and M.A. Sebastian, “Geometric Roughness Analysis in Solid Free-Form Manufacturing Processes,” *Journal of Materials Processing Technology*, vol. 119, Dec. 2001, pp. 52-57.

[165] B. Paul and V. Voorakarnam, “Effect of Layer Thickness and Orientation Angle on Surface Roughness in Laminated Object Manufacturing,” *Journal of Manufacturing Processes*, vol. 3, 2001, pp. 94-101.

[166] R. Anitha, S Arunachalam and P Radhakrishnan, “Critical Parameters Influencing the Quality of Prototypes in Fused Deposition Modelling,” *Journal of Materials Processing Technology*, vol. 118, 2001, pp. 385-388.

[167] F. E. H. Tay and E.A. Haider, “Laser Sintered Rapid Tools with Improved Surface Finish and Strength using Plating Technology,” *Journal of Materials Processing Technology*, vol. 121, 2002, pp. 318-322.

[168] G. Sui and M.C. Leu, “Investigation of Layer Thickness and Surface Roughness in Rapid Freeze Prototyping,” *Journal of Manufacturing Science and Engineering*, vol. 125, 2003, p. 556.

[169] C. Luis, J. Vivancos, I. Puertas, L. Costa and M.A. Sebastián “Comparative Analysis of Injection Systems for Manufacturing Parts,” *Journal of Materials Processing Technology*, vol. 143-144, Dec. 2003, pp. 112-117.

[170] P.M. Pandey, N.V. Reddy and S.G. Dhande, “Improvement of Surface Finish by Staircase Machining in Fused Deposition Modeling,” *Journal of Materials Processing Technology*, vol. 132, Jan. 2003, pp. 323-331.

[171] S. Rossi, F. Deflorian and F. Venturini “Improvement of Surface Finishing and Corrosion Resistance of Prototypes Produced by Direct Metal Laser Sintering,” *Journal of Materials Processing Technology*, vol. 148, May. 2004, pp. 301-309.

[172] H.C. Kim and S. H. Lee, “Reduction of Post-Processing for Stereolithography Systems by Fabrication-Direction Optimization,” *Computer Aided Design*, vol. 37, Jun. 2005, pp. 711-725.

[173] D. Keon Ahn and S. Hee Lee, “Improving the Surface Roughness of SL Parts Using a Coating and Grinding Process,” *Precision Engineering*, vol. 8, 2007, pp. 14-19.

[174] D. Ahn, H. Kim, and S. Lee, “Fabrication Direction Optimization to Minimize Post-Machining in Layered Manufacturing,” *International Journal of Machine Tools and Manufacture*, vol. 47, 2007, pp. 593-606.

[175] D. Ahn, H. Kim, and S. Lee, “Surface Roughness Prediction Using Measured Data and Interpolation in Layered Manufacturing,” *Journal of Materials Processing Technology*, vol. 209, Jan. 2009, pp. 664-671.

[176] D. Ahn, H. Kim, and S. Lee, “Expression for Surface Roughness Distribution of FDM Processed Parts,” *International Conference on Smart Manufacturing Application*- 2008 KINTEX, Gyeonggi-do, Korea, 490-493.

[177] D. Ahn, J.-H. Kweon, S. Kwon, J. Song, and S. Lee, “Representation of Surface Roughness in Fused Deposition Modeling,” *Journal of Materials Processing Technology*, vol. 209, 2009, pp. 5593-5600.

[178] L.M. Galantucci, F. Lavecchia, and G. Percoco, “Experimental Study Aiming to Enhance the Surface Finish of Fused Deposition Modeled Parts,” *CIRP Annals-Manufacturing Technology*, vol. 58, 2009, pp. 189-192.

[179] C. M. Cheah,J. Y. H. Fuh, A. Y. C. Nee, L. Lu, Y. S. Choo and T. Miyazawa, “Characteristics of Photopolymeric Material Used in Rapid Prototypes Part II. Mechanical Properties at Post-Cured State,” *Journal of Materials Processing Technology*, vol. 67(1-3), 1997, pp. 46-49.

[180] O. S. Es-Said, J. Foyos, R. Noorani, M. Mendelson, R. Marloth and B. A. Pregger, “Effect of Layer Orientation on Mechanical Properties of Rapid Prototyped Samples,” *Materials and Manufacturing Processes*, vol. 15(1), 2000, pp. 107 - 122.

[181] S.H Ahn,, M.Montero, D. Odell, S Roundy and P.K Wright, “Anisotropic Material Properties of Fused Deposition Modelling ABS,” *Rapid Prototyping Journal*, vol. 8(4), 2002, 248-257.

[182] Z.A. Khan, B.H. Lee and J. Abdullah, “Optimization of Rapid Prototyping Parameters for Production of Flexible ABS Object,” *Journal of Materials Processing Technology*, vol. 169 (1), 2005, pp.54-61.

[183] U. Ajoku, N. Saleh, N. Hopkinson, R. Hague, and P. Erasenthiran, “Investigating Mechanical Anisotropy and End-of-Vector Effect in Laser-Sintered Nylon Parts,” *Proceedings of the Institution of Mechanical Engineers, Part B: Journal of Engineering Manufacture*, vol. 220, 2006, pp. 1077-1086.

[184] C. Lee, S. Kim, H. Kim, and S. Ahn, “Measurement of Anisotropic Compressive Strength of Rapid Prototyping Parts,” *Journal of Materials Processing Technology*, vol. 187-188, Jun. 2007, pp. 627-630.

[185] Tian-Ming Wang, Jun-Tong Xi and Ye Jin, “A Model Research for Prototype Warp Deformation in the FDM Process,” *The International Journal of Advance Manufacturing Technology*, vol. 33, 2007, pp. 1087-1096.

[186] C.T. Bellehumeur, Q. Sun, G.M. Rizvi and P. Gu, "Effect of Processing Conditions on the Bonding Quality of FDM Polymer Filaments", *Rapid Prototyping Journal*, vol. 14 (2), 2008, pp.72 - 80.

[187] K. Chou and Y. Zhang, “A Parametric Study of Part Distortion in Fused Deposition Modeling using Three Dimensional Element Analysis,” *Proceedings of the Institution of Mechanical Engineers, Part B: Journal of Engineering Manufacture*, vol. 222, 2008, pp. 959-967.

[188] K. Chockalingam, N. Jawahar, U. Chandrasekar, and K. Ramanathan, “Establishment of Process Model for Part Strength in Stereolithography,” *Journal of Materials Processing Technology*, vol. 208, Nov. 2008, pp. 348-365.

[189] A.H. Nickel, D.M. Barnett and F.B. Prinz, “Thermal Stresses and Deposition Patterns in Layered Manufacturing,” *Materials Science and Engineering*, vol 317, 2001, pp. 59–64.

[190] P.M. Pandey, P.K. Jain, and P.V.M. Rao, “Effect of Delay Time on Part Strength in Selective Laser Sintering,” *International Journal of Advanced Manufacturing Technology*, vol. 43, Aug. 2008, pp. 117-126.

[191] C.S. Ramesh and C.K. Srinivas “Friction and Wear Behaviour of Laser-Sintered Iron–Silicon Carbide Composites,” *Journal of Materials Processing Technology*, vol. 209, 2009, pp. 5429-5436.

[192] C.S. Ramesh, C.K. Srinivas, and B.H. Channabasappa, “Abrasive Wear Behaviour of Laser Sintered Iron–Sic Composites,” *Wear*, vol. 267, Oct. 2009, pp. 1777-1783.

[193] S. Kumar and J.-P. Kruth, “Wear Performance of SLS/SLM Materials,” *Advanced Engineering Materials*, vol. 10, Aug. 2008, pp. 750-753.

[194] www.matweb.com

[195] Stratasys, “FDM Vantage User Guide Version 1.1,” www.stratasys.com, 2004.

[196] C. F. Jeff Wu and Michael Hamada," Experiments: Planning, Analysis, and Parameter Design Optimization," *John Wiley & Sons*, New Delhi, India, 2002.

[197] D.C. Montgomery, "Design and Analysis of Experiments," *John Wiley & Sons*, Singapore, 2003.

[198] Glen Stuart Peace,"Taguchi Methods: A hand on approach," *Addison Wesley Publishing Company*, New York, USA; 1993.

[199] P. J. Ross, "Taguchi Techniques for Quality Engineering," *Tata McGraw-Hill Education*, New Delhi, India, 2005.

[200] S. Datta, G. Nandi and A. Bandyopadhaya, " Application of PCA Based Hybrid Taguchi Method for Correlated Multi Criteria Optimization of Submerged Arc Welding: A Case Study," *International Journal of Advanced Manufacturing Technology*, vol. 45, 2009, pp. 276-286.

[201] Ken Jones, Mark Johnson and J.J. Liou, "The Comparison of Response Surface and Taguchi Methods for Multiple-Response Optimization Using Simulation," *IEEE-lCHMT International Electronics Manufacturing Technology Symposium*, 1992, pp. 15-18.

[202] Yiyo Kuo, Taho Yang and Guan-wei Huang, "The Use of Grey-Based Taguchi Method to Optimize Multi Response Simulation Problems," *Engineering Optimization*, vol. 40(6), 2008, pp. 517–528.

[203] R. Rao and V. Yadavagrey, "Multi-Objective Optimization of Nd:YAG Laser Cutting of Thin Superalloy Sheet Using Grey Relational Analysis with Entropy Measurement," *Optics & Laser Technology*, vol. 41, 2009, pp. 922–930.

[204] M.S. Khan and S.S. Mahapatra, "A Neural Network Approach for Assessing Quality in Technical Education: An Empirical Study," *International Journal of Productivity and Quality Management*, vol. 2 (3), 2007, pp. 287–306.

[205] N. Roy, "A Hybrid Model using AHP and Neural Network for Vendor Selection," *International Conference on Industrial Engineering and Management*, Yogyakarta, 2010, pp. 45-50.

[206] M.F. Shipley and S. P. Coy,(2009) "A Fuzzy Logic Model for Competitive Assessment of Airline Service Quality," *International Journal of Productivity and Quality Management*, vol. 4 (1), 2009, pp. 84–102.

[207] M. Assadi and H. Cheraghi, "A Fuzzy Rule Based in Process Inspection and Control System for a Gear Hobbing Process," *International Journal of Industrial and Systems Engineering*, vol. 4(3), 2009, pp. 283–302.

[208] M. Shah, ”Fuzzy Logic: A Realistic Tool for Management of Customer Relation,” *International Journal of Electronic Customer Relationship Management*, vol. 2 (2), 2008, pp. 158–170.

[209] Meng Lu and Kees Wevers, “Grey System Analysis and Applications: A Way Forward,” *Journal of Grey System*, vol. 10(1), 2007, pp. 47–54.

[210] Jyh-Horng Chou, Shinn-Horng Chen and Jin-Jeng Li, “Application of the Taguchi-Genetic Method to Design an Optimal Grey-Fuzzy Controller of a Constant Turning Force System,” *Journal of Materials Processing Technology*, vol. 105, 2000, pp. 333-343.

[211] S Rajasekaran, V. Pai, “Neural Networks, Fuzzy Logic and Genetic Algorithm: Synthesis and Applications,” *Prentice Hall of India*, New Delhi, India, 2003.

[212] J. F Hair, W. C. Black, B. J. Babin, R. E. Anderson and R.L. Tatham, “Multivariate Data Analysis,” *Prentice Hall*, New Jersey, USA 2006.

[213] Y. Liu, K.M. Passino and M.A. Simaan, “Biomimicry of Social Foraging Bacteria for Distributed Optimization: Models, Principles, and Emergent Behaviors,” *Journal of Optimization Theory and Application*, vol 115(3), 2002, pp. 603-628.

[214] R. Majhi, G. Panda, G. Sahoo, P. Dash and D. Das, “Stock Market Prediction of S&P 500 and DJIA Using Bacterial Foraging Optimization Technique,” *Procceeding of the IEEE Congress on Evolutionary Computation*, Singapore, IEEE Press, 2007 ,pp. 2569-2575.

[215] S. Mishra, G.D. Reddy, P.E. Rao and K. Santosh, “Implementation of New Evolutionary Techniques for Transmission Loss Reduction,” *Procceeding of the IEEE Congress on Evolutionary Computation*, Singapore, IEEE Press, 2007, pp. 2331–2336.

[216] G. Panda and B. Majhi, “Bacteria Foraging Based Identificacion of Nonlinear Dynamic System. *Procceeding of the IEEE Congress on Evolutionary Computation*, Singapore, IEEE Press, 2007, pp. 1636–1641.

[217] Hung-Chang Liao, “Multi-response optimization using weighted principal component,” *The International Journal of Advanced Manufacturing Technology*, vol. 27, 2006, 720-725.

[218] S.Marimuthu, N.Jawahar and S.G Ponnamblam, “Evolutionary Algorithms for scheduling M-machine Flow Shop with Lot Streaming,” *Robotics and Computer Integrated Manufacturing*, vol. 24(1), 2008, pp.125-139.

[219] Z. Michalewicz and M. Schoenauer, “Evolutionary Algorithms for Constrained Parameter Optimization Problems,” *Evolutionary Computation*, vol. 4(1), 1996, pp. 1-32.

[220] S. He, E. Prempain and Q.H. Wu, “An Improved Particle Swarm Optimizer for Mechanical Design Optimization Problems,” *Engineering Optimization*, vol. 36(5), 2004, pp. 585-605.

[221] T. Ray, and K. Liew, “Society and civilization: an optimization algorithm based on the simulation of social behavior,” *IEEE Transaction on Evolutionary Computation*, vol 7(4), 2003, pp. 386-396.

[222] K. V. Subbaiah, K.V.V. Mouli and J. C. Srinivas, “Particles Swarm Optimization for production planning problems,” *Journal of Decision and Mathematical Sciences*, vol. 10, 2005, pp. 101-112.

[223] G. Leguizam´on and C.A. Coello-Coello, “A Boundary Search Based ACO Algorithm Coupled with Stochastic Ranking,” *Proceedings of 2007 IEEE Congress. on Evolutionary Computation*, Singapore, 2007, pp.165-172.

[224] D. Karaboga and B. Basturk, “On the Performance of Artificial Bee Colony (ABC) Algorithm,” *Applied Soft Computing*, vol. 8(1), 2008, pp. 687-697.

[225] K. Passino, “Biomimicry of Bacterial Foraging for Distributed Optimization and Control,” *IEEE Control System Magazine*, vol. 22(3), 2002, pp. 52-67.

[226] K.T. Chiang and F.P. Chang, “Optimization of WEDM Process of Particle Reinforced Material with Multiple Performance Characteristics using Grey Relational Analysis,” *Journal of Materials Processing Technology*, vol. 180, 2006, pp. 96-101.

[227] M. Clerc and J.F. Kennedy, “The Particle Swarm: Explosion, Stability and Convergence in a Multi-Dimensional Complex Space,” *IEEE Transaction on Evolutionary Computation*, vol. 6(1), 2002, pp. 58-73.

[228] J. Sun, M. Xi, and W. Xu, “An Improved Quantum-Behaved Particle Swarm Optimization Algorithm with Weighted Mean Best Position,” *Applied Mathematics and Computation*, vol. 205 (2), 2008, pp. 751-59.

[229] Leandro Dos Santos Coelho, “Gaussian Quantum-Behaved Particle Swarm Optimization Approaches for Constrained Engineering Design Problems,” *Expert System with Application*, vol. 37, 2010, pp.1676-683.

[230] N. K. Naik and Rajesh S. Kumar, “Compressive Strength of Unidirectional Composites: Evaluation and Comparison of Prediction Models,” *Composite Structures*, vol. 46(3), 1999, pp. 299-308.

[231] X. Wang, J. Sun and W. Xu, “A Parallel QPSO Algorithm Using Neighborhood Topology Model,” 2009 *World Congress on Computer Science and Information Engineering*, 2009, pp. 831-835.

[232] J. Sun, W. Fang, D. Wang, and W. Xu, “Solving the Economic Dispatch Problem with A Modified Quantum-Behaved Particle Swarm Optimization Method,” *Energy Conversion and Management*, vol. 50, 2009, pp. 2967-2975.

[233] Manukid Parnichkun, Theerayuth Chatchanayuenyong, “Neural Network Based-Time Optimal Sliding Mode Control for an Autonomous Underwater Robot,” *International Journal of Mechatronics*, vol. 16(8), 2006, pp. 471-478.

[234] R.C.O. Richardson, “The Wear of Metals by Relatively Soft Abrasives,” *Wear*, vol. 11, 1968, pp. 245-275.

[235] K. Deb, “Multi-Objective Optimization Using Evolutionary Algorithms,” *John Wiley & Sons*, New Delhi, India, 2008.

[236] D.A. Fadare and U.I. Ofidhe, “Artificial Neural Network Model for Prediction of Friction Factor in Pipe Flow,” Journal *of Applied Science Research*, vol. 5(6), 2009, pp. 662-670.

[237] Heiermann, K., Riesch-Oppermann, H., Huber, N., 2005. Reliability Confidence Intervals for Ceramic Components as Obtained from Bootstrap Methods and Neural Networks. *Computational Matererial Science* 34(1), 1-13.

[238] Demuth, Howard, Hagan, Martin, Mark, Beale, 2010. “Neural Network Toolbox™ User’s Guide,” *The MathWorks Inc*., Natick, MA., 2010

APPENDIX A1

List of publications

List of Publications in International Journals

1. **A. K. Sood**, R.K. Ohdar and S.S. Mahapatra, “Improving Dimensional Accuracy of Fused Deposition Modelling Processed Part Using Grey Taguchi Method,” *Materials and Design*, vol 30, 2009, pp. 4243–4252.
2. S. K. Panda, S. K. Padhee, **A. K. Sood** and S. S. Mahapatra, “Optimization of Fused Deposition Modelling (FDM) Process Parameters Using Bacterial Foraging Technique,” *Intelligent Information Management*, vol. 1, 2009, pp. 89-97.
3. **A. K. Sood**, R.K. Ohdar and S.S. Mahapatra, “Parametric Appraisal of Mechanical Property of Fused Deposition Modelling Processed Parts,” *Materials and Design*, vol. 31, 2010, pp. 287-295.
4. **A. K. Sood**, R.K. Ohdar and S.S. Mahapatra, “Parametric Appraisal of Fused Deposition Modelling Process Using the Grey Taguchi Method,” *Proceedings of the Institution of Mechanical Engineers, Part B: Journal of Engineering Manufacture,* vol. 223, 2010, pp. 135-145.
5. **A. K. Sood**, A. Equbal, V. Toppo, R. K. Ohdar and S.S. Mahapatra, “Prediction and Analysis of Sliding Wear Performance of Fused Deposition Modeling (FDM) Processed ABS Plastic Parts,” *Proceedings of the Institution of Mechanical Engineers, Part J: Journal of Engineering Tribology*, vol. 224, 2010, pp. 1261-1271.
6. **A. K. Sood**, A. Equbal, R. K. Ohdar and S.S. Mahapatra, “Prediction of Dimensional Accuracy in Fused Deposition Modelling: A Fuzzy Logic Approach,” *International Journal of Productivity and Quality Management*, vol. 7(1), 2011, pp. 22-43.

Papers Accepted for Publication

7. **A. K. Sood**, R.K. Ohdar and S.S. Mahapatra, “Experimental Investigation and Empirical Modelling of FDM Process for Compressive Strength Improvement,” *Journal of Advanced Research*.

8. **A. K. Sood**, A. Equbal, V. Toppo, R. K. Ohdar and S.S. Mahapatra, "An investigation on Sliding Wear of FDM Built Parts," *CIRP Journal of Manufacturing Science and Technology*.
9. **A. K. Sood**, R.K. Ohdar and S.S. Mahapatra, "Weighted Principal Component Approach for Improving Surface Finish of ABS Plastic Parts Built Through Fused Deposition Modelling (FDM) Process," *Journal of Rapid manufacturing*.
10. **A. K. Sood**, R.K. Ohdar and S.S. Mahapatra, "Optimization of FDM Process," *International Journal of Applied Engineering Research*.
11. R. K. Sahu, S.S. Mahapatra and **A. K. Sood, "**Improvement in Dimensional Accuracy of FDM Built Parts Using Fuzzy Logic," *International Journal of Applied Engineering Research*.

Communicated Papers

12. **A. K. Sood**, R.K. Ohdar and S.S. Mahapatra, "Bayesian Regularization based Levenberg-Marquardt Neural Model Combined with BFOA for Improving Surface Finish of FDM Processed Part," *International Journal of Advanced Manufacturing Technology*.
13. R. K. Sahu, S.S. Mahapatra and **A. K. Sood**, "A Study on Dimensional Accuracy of Fused Deposition Modelling (FDM) Processed Parts Using Fuzzy Inference System," *Sadhana*.

List of Publications in International Conferences

1. **A. K. Sood**, R.K. Ohdar and S.S. Mahapatra, "Grey Taguchi Method for Improving Dimensional Accuracy of FDM Process," *AIMS International Conference on Value-based Management*, Haridwar, August 11-13, 2010, pp. 608-613.
2. R. K. Sahu**,** S.S. Mahapatra and **A. K. Sood**, "Improving Dimensional Accuracy of Fused Deposition Modelling (FDM) Processed Part Using Desirability Function Approach," *3rd International and 24th AIMTDR-2010*, 13-15 December, 2010, Visakhapatnam, Beela Satyanarayana et al. (Eds), pages 247-252
3. S. S. Mahapatra, **A.K. Sood**, S.K. Patel and S. Sahu, "Optimization of Process Parameters in Fused Deposition Modeling Using Weighted Principal Component Analysis," *The 3rd International Conference on Global*

Interdependence and Decision Sciences, December 28-30, 2009, Hyderabad, India, 2009.

Chapters contributed in book

1. **A. K. Sood**, R.K. Ohdar and S.S. Mahapatra, "A Hybrid ANN-BFOA Approach for Optimization of FDM Process Parameters," *Lecture Note in Computer Science* (LNCS), 2010, pp. 396-403. Panigrahi B.K. et al. (Eds.), Springer-Verlag Berlin Heidelberg.